UNIVERSITÉ DE GRENOBLE

THÈSE

Pour obtenir le grade de

DOCTEUR DE L'UNIVERSITÉ DE GRENOBLE

Spécialité : **Signal, image, parole, télécommunication (SIPT)**

Arrêté ministériel : 7 août 2006

Présentée par

Mohammad NIKNAZAR

Thèse dirigée par **Christian JUTTEN** et
codirigée par **Bertrand RIVET**

préparée au sein du **laboratoire Grenoble, images, parole, signal, automatique (GIPSA-lab)**
dans **l'école doctorale d'électronique, électrotechnique, automatique et traitement du signal (EEATS)**

Extraction et débruitage de signaux ECG du fœtus

Thèse soutenue publiquement le **7 Novembre 2013**,
devant le jury composé de :

M. Pierre-Yves GUMERY
Professeur, TIMC, Université Joseph Fourier, Président
M. Vicente ZARZOSO
Professeur, Laboratoire I3S, Université Nice Sophia Antipolis, Rapporteur
M. Laurent ALBERA
Maître de conférences (HDR), Université de Rennes 1, Rapporteur
M. Mohammad Bagher SHAMSOLLAHI
Professeur, BiSIPL, Université de technologie de Sharif, Examinateur
M. Christian JUTTEN
Professeur, Université Joseph Fourier, Directeur de thèse
M. Bertrand RIVET
Maître de conférences, Grenoble INP, Co-encadrant de thèse

Extraction and Denoising of Fetal ECG Signals

Mohammad Niknazar

Submitted in partial fulfillment of the requirements
for the degree of Doctor of Philosophy in
Signal, Image and Speech Processing and Telecommunications

in the

University of Grenoble, Grenoble, France
Grenoble Images Signal Parole et Automatique Laboratory (GIPSA-lab)

under the co-supervision of

Prof. Christian Jutten and **Dr. Bertrand Rivet**

November 2013

Dedicated to my family,

especially my beloved mother

Acknowledgments

First and foremost, praises and thanks to God, the Almighty, for the wisdom and perseverance that he has been bestowed upon me during this research project, and indeed, throughout my life.

My deepest gratitude is to my supervisor, Prof. Christian Jutten. I have been amazingly fortunate to have such a supervisor who is a well-known leading scholar in the domain and has an exceptional character. He gave me the freedom to explore on my own, and at the same time the guidance to recover when my steps faltered. Christian taught me how to question thoughts and express ideas. His patience and support helped me overcome critical situations and finish this dissertation.

My co-supervisor, Dr. Bertrand Rivet, was always there to listen and give advice. I am deeply grateful to him for the long discussions that helped me sort out the technical details of my work. During this research project, I appreciated a lot his creative mind and his perseverance in covering myriad studies that are somehow related to my thesis. The thesis would not have come to a successful completion, without the help I received from him.

It is a pleasure to thank my committee members: the president of the jury Prof. Pierre-Yves Gumery, the reviewers Prof. Vicente Zarzoso and Dr. Laurent Albera for the evaluation of this work and their invaluable comments, and the examiner Prof. Mohammad Bagher Shamsollahi for his insightful feedbacks.

I owe much of my signal processing insights to Prof. Mohammad Bagher Shamsollahi, who also recommended me to Christian and Bertrand for this project.

It is an honor for me that I had a chance to collaborate with Prof. Pierre Comon during my thesis. The contributions of one of the chapters of this thesis have been obtained based on our collaboration with him and his Ph.D. student Hanna Becker.

I would like to thank my dear friends and colleagues at GIPSA-lab, with whom I shared many of the ideas of this research and who gave me invaluable feedbacks.

My sincere thanks also go to many friends who have helped me stay happy through these years. Their support and care helped me overcome setbacks and stay focused on my studies. We shared excellent moments together. I greatly value their friendship and I deeply appreciate their belief in me.

Finally, none of this would have been possible without the love and patience of my family. My beloved family, to whom this dissertation is dedicated, has been a constant source of love, concern, support and strength all these years. I would like to express my gratitude and appreciation to my family from the deep core of my heart. My family has aided and encouraged me throughout this endeavor. I have to give a special mention for my dearest mother who has always devoted her love and support to me throughout my life and taught me how to be resolute for achieving my goals.

Contents

List of Figures

List of Tables

Abbreviations

BCI	brain-computer interface
BPM	beats per minute
BSS	blind source separation
CP	canonical polyadic
DTW	dynamic time warping
ECG	electrocardiogram
EEG	electroencephalogram
EKF	extended Kalman filter
EKS	extended Kalman smoother
EMG	electromyogram
ERPs	event-related potentials
fECG	fetal electrocardiogram
GCP	Gaussian canonical polyadic
GP	Gaussian process
ICA	independent component analysis
IEI	inter-event intervals
KF	Kalman filter
MAD	median absolute deviation
MCG	magnetocardiogram
mECG	maternal electrocardiogram
MICA	multidimensional independent component analysis
MMSE	minimum mean square error
par-EKF	parallel extended Kalman filter
par-EKS	parallel extended Kalman smoother
πCA	periodic component analysis
PCA	principal component analysis
PVC	premature ventricular contraction
seq-EKF	sequential extended Kalman filter
seq-EKS	sequential extended Kalman smoother
SIR	signal to interference ratio
SNR	signal to noise ratio
SQUID	superconducting quantum interference device
SVD	singular value decomposition
WCP	weighted canonical polyadic

Chapter 1

Introduction

Congenital[1] heart disease is the most common type of birth defect [1] and the leading cause of birth defect-related deaths [2]. Approximately, one out of 125 babies born each year have some form of congenital heart defects [3]. Some of these defects are so slight that the baby appears healthy for many years after birth and some other can be so dangerous that they may lead to birth defect-related death [4]. Genetic syndrome, inherited disorder, or environmental factors such as infections and drug misuse are among the causes of cardiac anomalies [5,6]. Advances in medical and surgical treatments over the past decades have led to more than 85% of these infants surviving to adulthood [7, 8]. Most interventions, however, have not been curative and about half of adults with congenital heart disease face the prospect of further surgery, arrhythmia, heart failure, and if not managed appropriately premature death [9].

Since heart defects originate in the early weeks of pregnancy when the heart is forming [3], the regular monitoring of the fetal heart and the early detection of cardiac abnormalities may help obstetrics and pediatric cardiologist to prescribe proper medications in time, or to consider the necessary precautions during delivery.

The electrocardiogram (ECG) signal may provide useful information about the fetus' heart condition for detecting the fetus at risk of damage or death in the uterus. Although fetal echocardiography can be used for detecting R-peaks and monitoring the heart status, extracted fetal ECG (fECG) can provide more information for medical groups. Nevertheless, except for during labor, fetal electrocardiography has not proved an effective tool for imaging specific structural defects and hence the medical analysis of fECG signals is still in its infancy. This is, partly due to a lack of availability of gold standard databases, partly due to the less complete clinical knowledge concerning fetal cardiac function and development, and in part, due to the relatively low signal to noise ratio (SNR) of the fetal ECG compared to the maternal ECG (mECG) [10]. Indeed, despite of the rich literature in the field of ECG processing, the extraction of fECG from maternal abdominal ECG sensors remains a difficult problem for the biomedical engineering community. As a result, since the technology to reliably extract fECG is still unavailable, fetal monitoring today is based only on the fetal heart rate and does not incorporate characteristics of the fECG waveform characteristics that are the cornerstone of cardiac evaluation [10]. This

[1] A congenital defect is an abnormality that is present at birth.

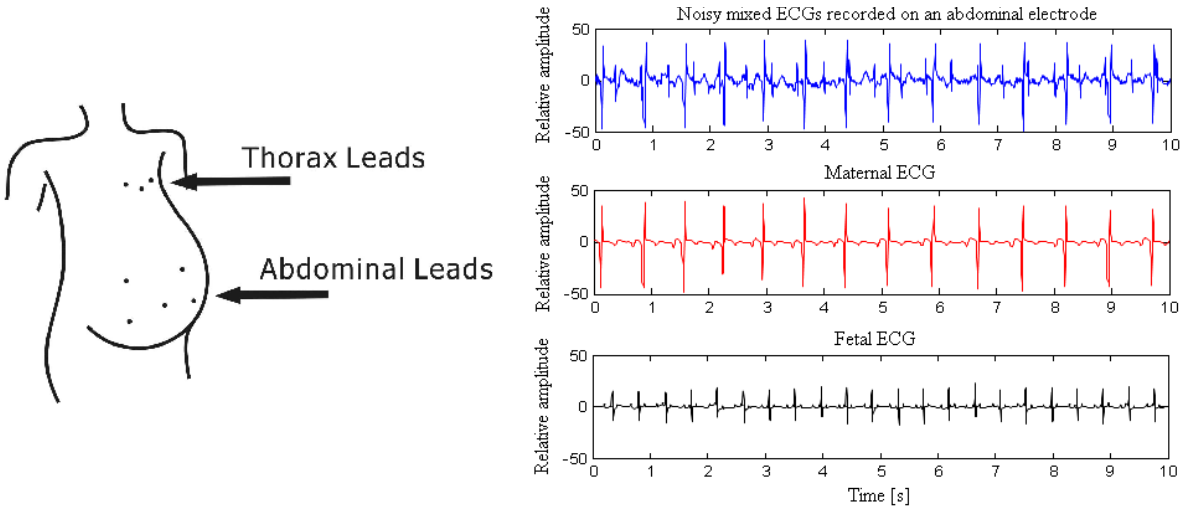

Figure 1.1: A typical example of noisy mixed ECGs recorded on an abdominal electrode and corresponding maternal and fetal ECGs.

means that the most critical source of information from clinical practice is excluded since most cardiac defects have some manifestation in the morphology of ECG, which is believed to contain much more information as compared with conventional sonographic methods [11].

The fECG can be measured by placing electrodes on the mother's abdomen (see Figure 1.1). However, this signal has very low power and is mixed with several sources of noise and interference. These include fetal brain activity, electromyogram (EMG) signals (from both the mother and fetus), respiratory activity, and power line interference. Moreover, its variability is increased by factors related to gestational age, position of the electrodes, skin impedance, etc. Nevertheless, the main contamination is the maternal ECG [12], since its amplitude is much higher than that of the fetus [12]. As a result, the basic problem is to extract the fECG signal from the mixture of mECG and fECG signals, where the interfering mECG is a much stronger signal.

In spite of the rich literature devoted to the filtering of fetal cardiac signals, due to the complexity of the problem there are still many open issues that need improved signal processing techniques. One of the such complexities from the signal processing perspective is that there is no specific domain (time, space, frequency, or feature) in which the fetal ECG can be totally separated from the interfering signals [13]. Therefore, sophisticated signal processing techniques are required to address this problem.

In this study, the objective is to improve the signal processing aspects of fetal cardiography and to obtain better insights of this problem, by developing new techniques for the modeling and filtering of fetal ECG signals recorded from electrodes placed on the maternal abdomen. The basic idea behind the developed methods is to refine currently existing models or design novel techniques to capture weak traces of fetal ECG signal using a minimal number of electrodes. The lower number of observations, the less available information about fetal ECG. Therefore, mECG, fECG and noise should be modeled accurately to obtain good results. Moreover, since

fECG can change from an observation to another due to the factors related to gestational age, position of the electrodes, etc, the proposed method should be robust enough to cover various possible scenarios.

The hereby proposed methods are based on the cardiac signal morphology and its quasi-periodic nature. We do not go into the procedure of fetal ECG generation or the medical interpretation of the obtained results. We will show that the same methods are applicable to other cardiac monitoring modalities such as the magnetocardiogram (MCG), which are morphologically similar to the ECG. Therefore, throughout the manuscript, unless specifically noted, all the methods developed for the ECG are also applicable to MCG recordings. Moreover, due to the generality of the proposed methods, the same procedures are also applicable to single or multichannel adult ECG recordings and can be used in real-time cardiac monitoring systems.

1.1 Overview of the Thesis and Contributions

A practical clinical monitoring system of fetal cardiac activity can be based on a small number of electrodes located on mother's abdomen, and on a sound sensitive sensor. In such a context, in the present study, we first concentrate on a refined model of the signal recorded on a unique electrode to see what performance can be obtained with only one electrode via this parametric method. Then, we go a step further and add more channels to assess possible performance improvement using multichannel recordings. However, we limit our methods to utilize a minimal number of electrodes (usually only 2). Finally, the performance of a novel nonparametric method which is applicable to single-channel recordings is evaluated. In what follows, we will have a brief overview of each chapter.

Chapter 2

In this chapter, a selection of the related literature are reviewed according to their methodologies, which include linear or nonlinear decomposition and adaptive filtering. Each of these methodologies has merits and flaws that have been explained. Moreover, the number of utilized electrodes in each approach is highlighted. Then the current modalities used in fetal cardiac activity monitoring are recalled and the advantages of electrocardiography modality over them are described to clarify the reasons behind the attempts in extraction of fetal ECG.

At the end of this chapter, we will define the problem of interest and the objectives of this research regarding the limiting factors of the currently existing methods and the number of utilized electrodes.

Chapter 3

In this chapter, we present an extended nonlinear Bayesian filtering framework, based on Kalman filter, for extracting ECGs from a single-channel as encountered in the fetal ECG extraction from abdominal sensor. The recorded signals are modeled as the summation of several ECGs. Each of them is described by a nonlinear dynamic model, previously presented in [14] for the generation

of a highly realistic synthetic ECG. As a result, each ECG has a corresponding term in this model and can thus be efficiently discriminated even if the ECG waves overlap in time. This is the main advantage of the proposed method over the method in [13, p. 50] for fetal ECG extraction. The parameter sensitivity analysis for different values of noise level, amplitude and heart rate ratios between fetal and maternal ECGs has been performed to present the conditions in which, the proposed method is efficient. This framework is finally validated on the extractions of fetal ECG from actual abdominal recordings, as well as of actual twin MCGs.

The full version of the idea with quantitative results on synthetic data and qualitative results on actual data has been also presented in [15].

Chapter 4

Tensor decomposition is an important topic in signal processing, which has found numerous applications in many other areas. This chapter is devoted to customize this method to event-related source extraction with a focus on our problem of interest, i.e. fetal ECG extraction. The deterministic blind separation of sources having different symbol rates, proposed in [16] has been adopted in this chapter for fetal ECG extraction. However, using the classic optimization used in this method to determine the dominant components of the fECG tensor, one fails to find fetal components. Since in the mixture of maternal and fetal ECGs, the mECG signal is much more powerful, it prevents the algorithms to capture the signal of interest, fECG, which has much lower power. In order to overcome this problem, two robust criteria for deterministic tensor decomposition are proposed to cope with interference from other sources that impede on the extraction of weak signals.

The influence of different parameters on the robustness of the proposed method is examined by means of simulations. Then its performance in fetal cardiac signal extraction from dual-channel actual recordings is assessed. Finally, its application on fully automatic fetal R-peak detection is presented. The latter can be found in [17].

Chapter 5

Although the robust tensor decomposition methods presented in Chapter 4 succeed to capture weak event-related sources, e.g. fECG, the dynamics of the sources, i.e., slight variations from one event to another, are lost. The reason is that the tensor decomposition model assumes identical temporal patterns for each source. In the case of ECG signal, valuable inter-beat dynamics of ECG signal are lost, since all extacted ECG beats have exactly identical shapes up to their amplitudes. In this chapter, a generic nonlinear Bayesian filtering framework is developed to recover such dynamics of event-related sources from multichannel recordings. This model is used within a Kalman filtering framework, whose mixing matrix and state parameters are obtained from the loading matrices of the tensor decomposition. Therefore, the proposed method in this chapter can be considered as the second step of the proposed method in Chapter 4. The method is applied to actual electroencephalogram (EEG), ECG and MCG and its performance is compared with the performance of other source separation methods. A preliminary version of

this method is reported in [18].

In the case of fetal ECG extraction, the proposed method in this chapter can be considered as the multichannel extension of the single-channel extended nonlinear Bayesian filtering framework, proposed in Chapter 3. Thereby, the performances of these two methods are compared via simulation to check possible improvement obtained by adding another channel to the single-channel recording.

In the last section of this chapter, a new method based on dynamic time warping is proposed to enhance the phase state estimate of ECG signal. This method does not assume a linear phase for ECG signal and exploits information of all available channels for phase state estimation. Although it is not expected to be used in the fetal ECG extraction application, it can be employed to simultaneously filter normal and abnormal ECG beats. The material of this section has been published in [19].

Chapter 6

In this chapter, we pursue a different approach for analyzing ECG signal. Instead of explicitly considering the shape of ECG signal and assigning a parametric model to extract ECG, we rely on exploiting statistical characteristics of ECG.

Gaussian processes are widely used in statistical modeling because of properties inherited from the normal distribution. Assuming ECG signal as a Gaussian process, it can be fully described by its second-order statistics. In this chapter, we present suitable covariance functions for maternal and fetal ECGs for ECG denoising and fetal ECG extraction. The proposed method is fairly general and can be used in other applications, in which the second-order statistics of desired source can be described.

The primary and simplified versions of the proposed method have been published in [20] and [21], respectively.

Chapter 7

In the last chapter, we summarize the findings of this research and their points of strength and weakness, as compared with previous methods. We will also present some of the possible directions of research that are left as open challenges for future studies in this field.

Chapter 2

State of the Art

2.1 Introduction

In this chapter, the state of the art in fetal cardiac signal extraction is reviewed and limiting factors and challenging issues are clarified. Since the history of the problem is old and there are many methods in the literature, it is not possible to cover all the existing methods in their details. Moreover, a number of the existing methods have employed a combination of techniques to overcome the complexity of the problem. Therefore, we will review a selection of the available literature which had a significant role in the evolution of the problem of interest. The significant works are categorized according to their methodologies and then the number of utilized electrodes is highlighted. The more detailed literature of each proposed method is presented separately in the corresponding chapter.

2.2 Fetal ECG Extraction Methodologies

Since the first demonstration of the fetal ECG carried out in 1906 by Cremer [22], various methods for fECG monitoring have been proposed to obtain information about the heart status. These methods aimed at fetal heart rate analysis or fetal ECG morphology analysis. Although fetal ECG morphology contains much more clinical information compared to the heart rate analysis alone, most of the previous studies have been only directed to fetal R-R intervals extraction using the R-peaks or ensemble averages of the fetal ECG waveforms [13]. This is due to the very low SNR of fetal ECG signals, which leaves the complete morphologic study of the fetal ECG as a challenging problem. According to the review [10], existing fECG extraction approaches in literature can be categorized by their methodologies, which include linear or nonlinear decomposition and adaptive filtering.

Linear or nonlinear decomposition methods are common approaches in which, single or multi-channel recordings are decomposed into different components using suitable basis functions. The basis functions can be selected based on the coherence with the time, frequency, or scale characteristics of the fetal components. In [23], a wavelet transform-based method was developed to extract fECG from an abdominal electrode. This method is based on the detection of the

singularities obtained from the composite abdominal signal, using the modulus maxima in the wavelet domain. A reconstruction method was then used to obtain the fetal ECG signal from the detected fetal modulus maxima. The obtained result from synthetic and real data presented good detection of singular points locations, but the amplitude of the extracted fECG was not accurate [23]. In another study [24], a new mother wavelet was designed to achieve optimal denoising and compression results in fetal electrocardiography. This mother wavelet, which is called abdominal ECG mother wavelet uses Gaussian functions to model ECG waves and has a more similar shape to an ECG signal compared to more common mother wavelets. Singular value decomposition (SVD) was also used by assuming that the mixed signals can be configured to be algebraically orthogonal to each other and this orthogonality can be exploited for extracting fECG [25]. Nevertheless, linear decomposition methods using either fixed basis functions (e.g., wavelets), or data-driven basis functions (e.g., singular vectors) have limited performance in decomposition of nonlinear or degenerate mixtures of signal and noise [10]. Therefore, they are not expected to estimate well fetal ECG where fetal signals and other interferences and noises are not linearly separable [13].

Blind or semi-blind source separation methods, which are categorized as linear decomposition approach, have also been used for fECG extraction. These methods are based on the assumption of independent components for the maternal and fetal signals, or of the existence of some temporal structure for the desired signals [26–28]. For instance, assuming an ECG signal as a multidimensional signal, a blind source subspace separation method was proposed in [29] to separate mECG and fECG subspaces in multichannel recordings. They also compared the performance of their method with that of a class of SVD-based methods and concluded that their method is more efficient. Nonetheless, most of these methods are rather generic and are not fully customized to the characteristics of the ECG signal. In [30], quasi-periodic nature of ECG has been exploited to extract an independent subspace based on periodicity of fECG signal. This method was then combined with a model-based signal processing tool to better cancel mECG according to a deflation procedure [31]. However, since the deflation procedure is iterative and a filter is applied several times to the mixture, some parts of the fECG signal can be corrupted during this procedure. Another attempt to customize the existing generic methods to the ECG signal was using multidimensional independent component analysis (MICA) for separating out the fECG from the mECG and the rest of the interferences [32, 33]. MICA is an extension of independent component analysis (ICA), based on a linear model such as that used in ICA: however, in contrast to ICA, the components are not assumed to be all mutually independent. Instead, it is assumed that the components can be partitioned into groups, which are statistically independent but components belonging to the same group may be dependent. This method was then refined in [34] to more efficiently work in a larger number of scenarios.

Wavelet decomposition was also combined with blind source separation methods for extracting and denoising fECG signals. In [35], the problem of fetal ECG extraction was addressed using BSS in the wavelet domain. They showed that this method can be particularly advantageous when mixing environment is noisy and time-varying. In BSS methods it is usually assumed that signals and noises are mixed in a stationary and linear manner. However, fECG and other

interferences and noises are not necessarily stationary mixed and linearly separable [13]. An algorithm based on non-stationary ICA and wavelet denoising was proposed in [36] for fetal ECG extraction. In their study, they maintained that according to the low amplitude and poor SNR of the fetal ECG recorded at the abdominal region of a pregnant woman, the signal processing algorithm needs to remove the maternal ECG, reduce motion artifact and enhance extracted fetal ECG signal. To do so and because of non-stationary nature of the ECG signal, they employed a non-stationary ICA method to eliminate maternal signal from the composite ECG signal recorded at abdomen. Wavelet transform was then used to remove baseline wander and enhance fECG signal. The wavelet-ICA method proposed in [37,38] was adopted and fitted to the problem of fECG extraction in [39]. In this method, a multichannel ECG recording is first decomposed by biorthogonal wavelets [40], since the wavelet functions belonging to this family have a shape that is close to the ECG shape. Then, the wavelet components (approximations and details) related to fECG are selected by visual inspection and a new dataset is built with them. Finally, this new dataset is processed by ICA to extract fECG components. This method was compared with the non-stationary ICA and wavelet denoising method in [36]. They showed that the Q, R, and S waves of fECG are better visible using their method. However, P and T waves are not visible in the fECG extracted by this method. The performance of four major BSS algorithms (the joint approximate diagonalization of eigen matrices algorithm [41], the original fixed-point algorithm [42], Infomax algorithm [43], and a specific contrast function based on minimization of mutual information between the components at the output of separator [44]) in fECG extraction has been investigated in [45]. The four algorithms are exerted on dual-channel simulated data to observe the ability of each in extracting fECG. As discussed in the paper, these methods are able to recover fECG if the input SNR is high. In another work, a new technique was proposed to accelerate the traditional ICA method used in fECG extraction [46].

Some theoretical problems that arise in noninvasive extracting fECG especially the diagnostically important fetal P-waves and T-waves early in pregnancy for beat-to-beat diagnosis were discussed in [47] by some well-known extraction methods such as averaging/subtraction approach and ICA. They reported that these methods are not accurate in an extraction problem in which the number of sources exceeds the number of observations especially when the signal of interest has very low amplitude and it is surrounded by noise. For example, averaging/subtraction method, in which fECG is extracted by a large number of synchronized maternal ECG beats and removing this average from abdominal mixed signal and finally extracting averaged fECG, is unable to well present the valuable temporal variations in R-R, P-R and Q-T intervals. In ICA extraction method some theoretical conditions are required. For instance, in this method, it is considered that the abdominal noise is negligible although this noise can be strong or as mentioned before it is considered that signals and noises are linearly mixed which in reality is not true. These assumptions reduce the precision of extracted P and T waves and also the duration of intervals in the fECG signal.

Nonlinear transforms have been also used for mECG cancellation and fECG extraction. These transforms are rather ad hoc and require some prior information about the desired and undesired parts of the signal [13]. In these methods, a state-space representation of noisy signal and of its

delayed versions is constructed and the state-space trajectory is smoothed using conventional or principal component analysis (PCA) smoothers [48–50]. The samples are then transferred back to the time-domain representation. Although these methods are interesting since they are applicable to as few as one single maternal abdominal channel, the selection of the required time-lags for constructing phase space representation is empirical and the important inter-beat variations of the cardiac signals can be wiped-out during the state-space smoothing. Moreover, they demand higher computational complexity in comparison to linear methods, and the correct embedding dimension can vary as the noise statistics change [10].

Adaptive filtering is another common approach for mECG cancellation and fECG extraction [51]. The conventional adaptive filtering is based on training an adaptive filter for either removing the mECG using one or several maternal reference channels [51, 52], or directly training the filter for extracting the fetal QRS waves [53, 54]. However, existing adaptive filtering methods for mECG artifact removal, either require a reference mECG channel that is morphologically similar to the contaminating waveform or require several linearly independent channels to roughly reconstruct any morphologic shape from the references [51]. Both of these approaches are practically inconvenient and with limiting performance, because the morphology of the mECG contaminants highly depends on the electrode locations and it is not always possible to reconstruct the complete mECG morphology from a linear combination of the reference electrodes [10]. Therefore, an adaptive filter that does not require any excess reference electrodes or at most a single reference without the morphological similarity constraint is of great interest. The Kalman filtering framework, which can be considered as a member of the general class of adaptive filters, is a promising approach that uses only arbitrary mECG and fECG references for mECG cancellation and fECG enhancement. In [14], a set of state-space equations was used to model the temporal dynamics of ECG signals, for designing a Bayesian filter to denoise ECG. This Bayesian filtering framework was then used in [13] to extract fECG from single channel mixture of mECG and fECG. However, as it has been mentioned in [13], the filter fails to discriminate between the maternal and fetal components when the mECG and fECG waves fully overlap in time. Practically, it has been shown that for fECG extraction, blind source separation methods outperform adaptive filters [55]. An important advantage of spatial filtering over conventional adaptive filters is their ability to separate mECG and fECG with temporal overlap but it often requires more than two sensors.

2.3 Current Challenges

Besides electrocardiography, the fetus' heart status has been also monitored using other modalities [11], including echocardiography [56], phonocardiography [57, 58], pulse oximetry [59], cardiotocography [60], and magnetocardiography [61, 62]. Among these modalities, echocardiography which is based on standard ultrasound techniques and is also known as sonography of the heart, is commercially the most available means for fetal cardiac monitoring [10]. Nevertheless, the electrocardiography and magnetocardiography modalities can provide more information about fetus' heart status, since most cardiac abnormalities have some manifestation in the ECG

or MCG morphology or R-R interval timing [11]. Due to the morphological similarity of the ECG and its magnetic counterpart, MCG, the ECG-based methods are also applicable to MCG signals. In fact, although using the current superconducting quantum interference device (SQUID) technology for magnetic recordings, the SNR of the fetal MCG is usually higher than that of ECG, ECG recording devices are simpler and currently more affordable as compared with MCG systems [10]. Thereby, the current study is focused on the ECG and partially the MCG to retrieve the fetal ECG (or MCG) morphology with the highest possible fidelity, as required for morphological studies.

In such a context, the proposed methods encounter a number of limiting factors and challenging signal-processing issues. In addition to the weakness of fetal cardiac potentials and high interference of maternal ECG, possible movements of the fetus and the variation of fetal heart rate should be also considered. Indeed, the ratio of fetal and maternal heart rates, the ratio of fetal and maternal ECG powers, noise and fetus' position can change the configuration of mixtures. The methods should be robust enough to the variation of these factors. Moreover, the methods should be as automatic as possible to be applied to long datasets with minimal interaction with an expert operator.

Another important factor in this context is the number of channels utilized for fECG extraction. Current single-channel methods either fail to recover valuable inter-beat variations of fECG (e.g. averaging and nonlinear methods) or fail to discriminate between the maternal and fetal components when the mECG and fECG waves fully overlap in time (e.g. Kalman filtering method). Figure 2.1 shows an example of this kind of failure on an actual recording by the Bayesian filtering framework used in [13]. Current multichannel fECG extraction methods (e.g. blind source separation [29], semi-blind source separation [63], adaptive filtering [51, 53], and periodic component analysis (πCA) [30]) exploit the redundancy of the multichannel ECG recordings to reduce mECG and other interference sources. Nevertheless, even if this reduction has been successful, the exogenous noise cannot be totally canceled in this way [49]. Moreover, they demand several channels to recover weak traces of fetal signal. Figure 2.2 shows an example of performance of two classical methods in extraction of maternal and fetal ECGs where only two electrodes have been utilized. As it is seen, both FastICA [64] and πCA methods completely failed to extract fetal ECG. This can be explained by revising the inherent limitations of these methods. As mentioned above, since maternal and fetal ECGs are not linearly mixed, linear methods are not able to separate them. Moreover, the cardiac signals are multidimensional [13], so these methods which are not applicable to underdetermined mixtures fail to capture fetal components that are dominated by the maternal signal and noise.

Thereby, the current challenge is the development of single-channel methods which do not fail to discriminate between the maternal and fetal ECG waves and also preserve inter-beat dynamics of fECG. The performance of such methods should be evaluated over different possible scenarios and configurations of mixtures. The next step is to develop multichannel methods that outperform single-channel ones in extracting and denoising of fECG signal. In this case, the methods that utilize a minimal number of electrodes are of great interest since this leads to a less expensive and more convenient and portable device for a long-term fetal cardiac activity

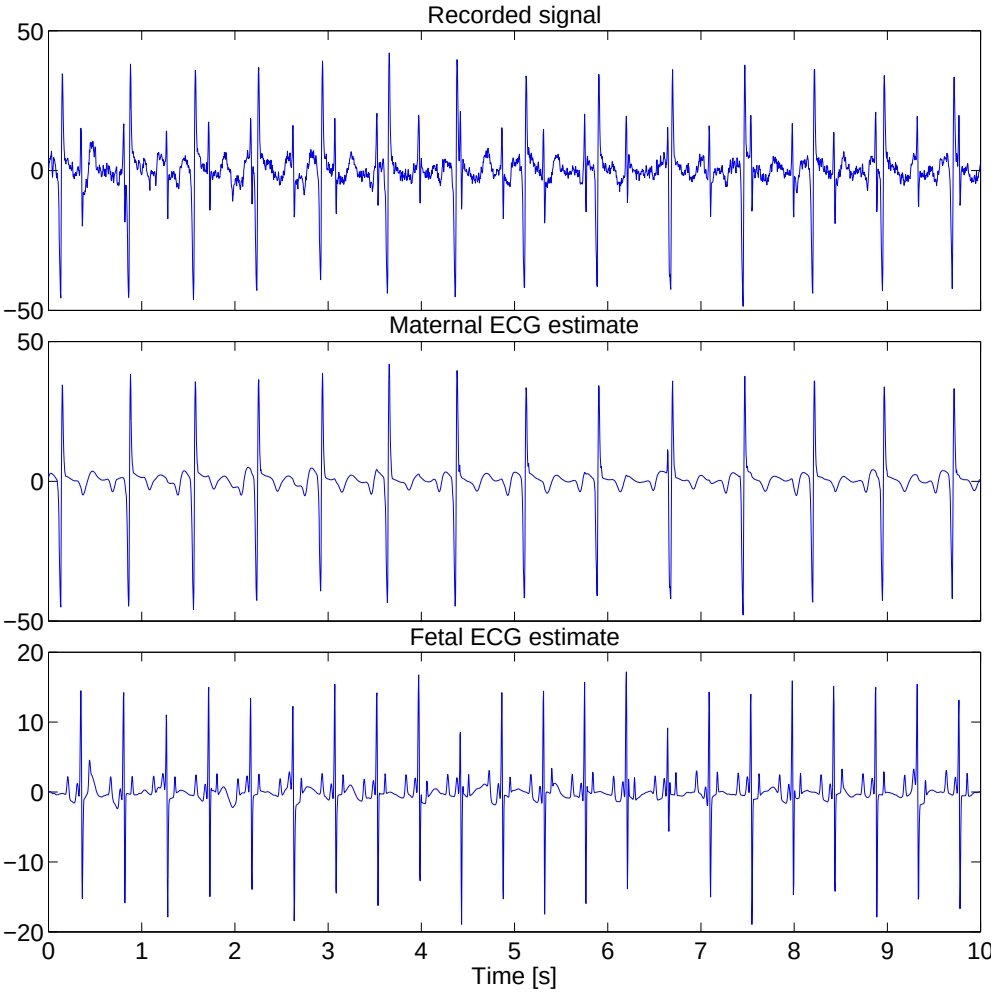

Figure 2.1: A typical example of failure of method in [13] in discriminating maternal and fetal components when the mECG and fECG waves fully overlap in time. It is particularly noticed between t = 6s and t = 7s.

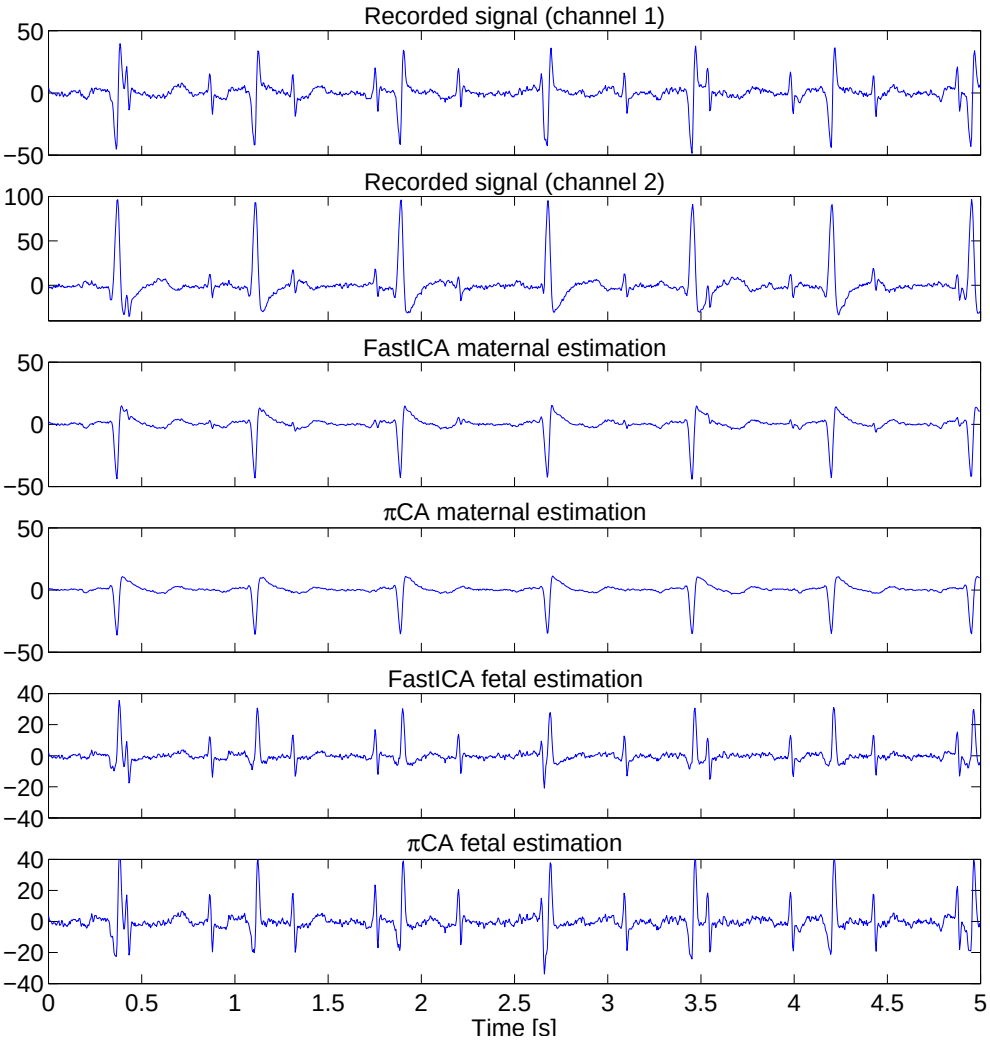

Figure 2.2: A typical example of performance of current multichannel fECG extraction methods in maternal and fetal ECG extraction using only two electrodes. Both FastICA and πCA methods completely fail to extract fetal ECG.

monitoring system.

In Table 2.1, a general comparison between the currently existing methods is provided. Comparison of the benefits and drawbacks of these methods could point the directions of this thesis in this field. Therefore, this thesis aims at filling the blank cells of this table.

2.4 Summary and Conclusions

In this chapter, we briefly reviewed the current approaches and methods for fetal ECG extraction in the literature and their limiting factors and challenging issues. It was noted that in the present study we are interested in improving these methods to retrieve the fECG morphology with the highest possible fidelity using a minimal number of electrodes. In the following chapters, several methods are proposed for achieving these objectives, together with additional byproducts of this work that are not limited to fetal ECG extraction.

Table 2.1: Comparison of existing methods for fetal ECG extraction.

	Method	Benefit	Drawback
Single-channel	Wavelet filtering	Suitable for mixtures having different scales	Limited performance in nonlinear mixtures
	SVD-based filtering	Robust to low SNR mixtures	Limited performance in nonlinear mixtures
	Nonlinear filtering	Applicable to nonlinear or degenerate mixtures	Lose inter-beat dynamics, computationally massive
	Bayesian filtering	Preserve inter-beat dynamics	Failure when ECG waves overlap, require good state estimate
	?	Preserve inter-beat dynamics, not fail when ECG waves overlap	
	?	Preserve inter-beat dynamics, not fail when ECG waves overlap, not require good state estimate	
Multichannel	SVD/PCA	Applicable to noisy high dimensional data	Limited performance in nonlinear mixtures
	ICA	Generality	Limited separation performance, require several channels
	πCA	Adapted to ECG	Limited noise cancellation, require several channels
	Deflation procedure	Adapted to ECG, applicable to a few channels	Limited noise cancellation, iterative, lose fECG features during mECG cancellation
	?	Adapted to ECG, good noise cancellation, applicable to a few channels	
	?	Adapted to ECG, good noise cancellation, applicable to a few channels, preserve fECG features and dynamics during filtering	

Chapter 3

Extended State Kalman Filtering Based on Single-Channel Recordings

3.1 Introduction

So far, many methods have been developed for fECG extraction from the mixtures of maternal and fetal ECGs. Among the methods which are applicable to single-channel recordings one can name nonlinear methods based on construction of phase space of noisy signal and its delayed versions. However, besides computational complexity of these methods, they are unable to recover valuable inter-beat dynamics of ECG signal. The well-known Kalman filter (KF) is one of the methods that can be employed to preserve the important inter-beat dynamics of ECG signal. This filter which is used in estimating hidden states that are observable through a set of measurements of a system with an underlying dynamic model, has been also proven to be the optimal filter in the minimum mean square error (MMSE) sense under certain general constraints [65].

An important advantage of KF over some conventional filters such as Wiener filter is its applicability to non-stationary signals. Although for stationary signals Wiener filter is the optimal linear filtering method in the MMSE sense, applied either in a causal sense in the time domain or as the noncausal filter applied in the frequency domain, it does not give good results for a noisy ECG signal, due to the non-stationary nature of the cardiac signal [13]. In [14], it has been shown that KF outperforms conventional ECG denoising schemes including wavelet denoising, adaptive filtering, and conventional finite impulse response filtering. The KF framework in [14] is designed based on a realistic model to describe the quasi-periodic behavior of the ECG to extend the idea of model-based filtering to a general Bayesian filtering framework for ECG denoising.

This Bayesian filter framework that can be considered as a parametric model for ECG processing was then used in [13, p. 50] to extract fECG from single-channel mixture of mECG and fECG according to a deflation procedure. However, as it has been mentioned in [13], the filter fails to discriminate between maternal and fetal components when mECG and fECG waves fully overlap in time. The reason is that when mECG is being estimated, fECG and other compo-

nents are supposed to be Gaussian noise. However, this assumption is not true, especially when mECG and fECG waves fully overlap in time it is difficult for the filter to follow the desired ECG.

In this chapter, we wonder what performance can be obtained with only one electrode, by using a refined model of the signal recorded on the unique electrode: the model will explicitly take into account that the signal is the superposition of a few ECG signals. The rest of this chapter is organized as follows. In Section 3.2, the Bayesian filtering theory is briefly reviewed. The existing EKF framework for denoising an ECG signal is recalled in Section 3.3. Section 3.4 is devoted to present the proposed method, in which the EKF framework for one ECG is extended to multiple ECGs for simultaneously extracting several ECGs from a mixture. The results of the proposed method on both synthetic and actual data are presented in Section 3.5. In this section, first, considering different possible scenarios in the problem of fECG extraction, the performance of the proposed method in these scenarios is assessed using synthetic data. Then, the performance of the proposed method on actual cardiac recordings is presented and the results are compared with the results of two other methods. Finally, a summary of the chapter and our conclusions are stated in Section 3.6.

3.2 Review of the Bayesian Filtering Theory

The goal of the Kalman filter consists in estimating the state of a discrete-time controlled process that is governed by a linear stochastic difference equation. Therefore, if the process to be estimated and (or) the measurement relationship to the process is nonlinear, it should be modified. The extended Kalman filter (EKF) is an extension of the standard KF to nonlinear systems, which linearizes about the current mean and covariance. Consider a state vector $\mathbf{x}_{k+1}$ governed by a nonlinear stochastic difference equation with measurement vector $\mathbf{y}_{k+1}$ at time instant $k+1$:

$$\begin{cases} \mathbf{x}_{k+1} = f(\mathbf{x}_k, \mathbf{w}_k, k+1) \\ \mathbf{y}_{k+1} = h(\mathbf{x}_{k+1}, \mathbf{v}_{k+1}, k+1) \end{cases} \tag{3.1}$$

where the random variables $\mathbf{w}_k$ and $\mathbf{v}_k$ represent the process and measurement noises, with associated covariance matrices $\mathbf{Q}_k = E\left\{\mathbf{w}_k \mathbf{w}_k^T\right\}$ and $\mathbf{R}_k = E\left\{\mathbf{v}_k \mathbf{v}_k^T\right\}$. The initial estimate of the state vector, $\overline{\mathbf{x}}_0 = E\left\{\mathbf{x}_0\right\}$, is also assumed to be known, with $\mathbf{P}_0 = E\left\{(\mathbf{x}_0 - \overline{\mathbf{x}}_0)(\mathbf{x}_0 - \overline{\mathbf{x}}_0)^T\right\}$. The process and observation models are linearized at the current estimate $\hat{\mathbf{x}}_k$ using the first order Taylor series expansion:

$$\begin{cases} \mathbf{x}_{k+1} \approx f(\hat{\mathbf{x}}_k, \hat{\mathbf{w}}_k, k) + \mathbf{A}_k(\mathbf{x}_k - \hat{\mathbf{x}}_k) + \mathbf{F}_k(\mathbf{w}_k - \hat{\mathbf{w}}_k) \\ \mathbf{y}_k \approx h(\hat{\mathbf{x}}_k, \hat{\mathbf{v}}_k, k) + \mathbf{C}_k(\mathbf{x}_k - \hat{\mathbf{x}}_k) + \mathbf{G}_k(\mathbf{v}_k - \hat{\mathbf{v}}_k) \end{cases} \tag{3.2}$$

where $\mathbf{A}_k$ is the Jacobian matrix of partial derivatives of f with respect to $\mathbf{x}$, $\mathbf{F}_k$ is the Jacobian matrix of partial derivatives of f with respect to $\mathbf{w}$, $\mathbf{C}_k$ is the Jacobian matrix of partial derivatives of h with respect to $\mathbf{x}$ and $\mathbf{G}_k$ is the Jacobian matrix of partial derivatives of h with

respect to $\mathbf{v}$. To simplify the matrix notations, the $\mathbf{F}_k$ and $\mathbf{G}_k$ matrices are usually absorbed into the noise covariance matrices as:

$$\mathbf{F}_k\mathbf{Q}_k\mathbf{F}_k^T \rightarrow \mathbf{Q}_k, \qquad \mathbf{G}_k\mathbf{R}_k\mathbf{G}_k^T \rightarrow \mathbf{R}_k.$$

Finally, the EKF algorithm may be summarized as [14]:

$$\begin{cases} \hat{\mathbf{x}}_{k+1}^- = f(\hat{\mathbf{x}}_k^+, \mathbf{w}, k)|_{\mathbf{w}=\overline{\mathbf{w}}_k} \\ \mathbf{r}_k = \mathbf{y}_k - h(\hat{\mathbf{x}}_k^-, \mathbf{v}, k)|_{\mathbf{v}=\overline{\mathbf{v}}_k} \\ \mathbf{K}_k = \mathbf{P}_k^-\mathbf{C}_k^T[\mathbf{C}_k\mathbf{P}_k^-\mathbf{C}_k^T + \mathbf{R}_k]^{-1} \\ \hat{\mathbf{x}}_k^+ = \hat{\mathbf{x}}_k^- + \mathbf{K}_k\mathbf{r}_k \\ \mathbf{P}_{k+1}^- = \mathbf{A}_k\mathbf{P}_k^+\mathbf{A}_k^T + \mathbf{Q}_k \\ \mathbf{P}_k^+ = \mathbf{P}_k^- - \mathbf{K}_k\mathbf{C}_k\mathbf{P}_k^- \end{cases} \tag{3.3}$$

where $\overline{\mathbf{w}}_k = E\{\mathbf{w}_k\}$, $\overline{\mathbf{v}}_k = E\{\mathbf{v}_k\}$, $\hat{\mathbf{x}}_k^- = \hat{E}\{\mathbf{x}_k|\mathbf{y}_{k-1}, ..., \mathbf{y}_1\}$ and $\hat{\mathbf{x}}_k^+ = \hat{E}\{\mathbf{x}_k|\mathbf{y}_k, ..., \mathbf{y}_1\}$. $\mathbf{P}_k^-$ and $\mathbf{P}_k^+$ are the a priori and a posteriori estimates of the state vector covariance matrices before and after using the $k-th$ observation, respectively.

In the EKF algorithm, the state estimate is updated immediately after a new observation is available. However, immediate updating is not always necessary. Instead, if a small lag in the processing is allowed or if the measured data is processed offline, the future observations can also be used in the state estimation. In this case, it is reasonable to expect to have a better estimation compared with the EKF. The extended Kalman smoother (EKS), which uses the information of future observations, consists of a forward EKF stage followed by a backward recursive smoothing stage. In this study, since the filtering procedure is carried out offline on the entirety of each ECG signal, the fixed interval EKS is used. However, for real-time application of the EKS methods, the fixed lag smoother is usually more appropriate [14].

3.3 EKF Framework for ECG Extraction

In [14], Bayesian filters such as the EKF and EKS have been proposed for single-channel ECG denoising. The state-space model used for these filters is inspired from [66], which suggests the use of Gaussian mixtures to model realistic synthetic ECGs. The basic idea is to approximate the PQRST waves by the sum of 5 weighted Gaussian-shape functions. In [14], the synthetic ECG generator proposed in [66], was transferred into polar coordinates from Cartesian coordinates. This modification and some other modifications make it simpler and more straightforward in interpretation [14]. This modified state-space model was then further developed in [67]. The developed state-space model of one ECG signal, in its discrete form with a small sampling period

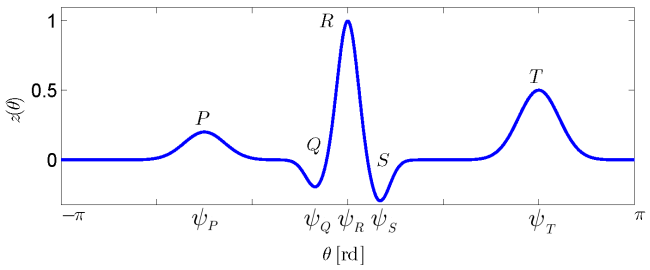

Figure 3.1: Illustration of the ψ_i, which corresponds to the center of the ith Gaussian function.

δ, is:

$$\begin{cases} \theta_{k+1} = (\theta_k + \omega\delta)\text{mod}(2\pi) \\ z_{k+1} = -\sum\limits_{i\in\mathscr{W}} \delta\dfrac{\alpha_{i,k}\omega}{b_{i,k}^2}\Delta\theta_{i,k}\exp(-\dfrac{\Delta\theta_{i,k}^2}{2b_{i,k}^2}) + z_k + \eta_k^z \\ \alpha_{i,k+1} = \alpha_{i,k} + \eta_k^{\alpha_i} \\ b_{i,k+1} = b_{i,k} + \eta_k^{b_i} \\ \psi_{i,k+1} = \psi_{i,k} + \eta_k^{\psi_i} \end{cases} \tag{3.4}$$

where θ, z, α_i, b_i, and ψ_i are the state variables in polar coordinates and k denotes the discrete time index. $\mathscr{W} = \{P, Q, R, S, T\}$ is the set of the PQRST waves. α_i and b_i correspond to the peak amplitude and width parameters of the Gaussian functions used for modeling each of the ECG waves. We define $\Delta\theta_{i,k} = (\theta_k - \psi_i)\text{mod}(2\pi)$, in which ψ_i corresponds to the phase of the maximum of the ith Gaussian function (see Figure 3.1). ω is the phase increment and η_k^z, $\eta_k^{\alpha_i}$, $\eta_k^{b_i}$, and $\eta_k^{\psi_i}$ are random additive noises.

The system state and process noise vectors are defined as:

$$\begin{cases} \boldsymbol{x}_k = & [\theta_k, z_k, \alpha_{P,k}, ..., \alpha_{T,k}, b_{P,k}, ..., b_{T,k}, \psi_{P,k}, ..., \psi_{T,k}]^T \\ \boldsymbol{w}_k = & [\omega_k, \eta_k^z, \eta_k^{\alpha_P}, ..., \eta_k^{\alpha_T}, \eta_k^{b_P}, ..., \eta_k^{b_T}, \eta_k^{\psi_P}, ..., \eta_k^{\psi_T}]^T \end{cases} \tag{3.5}$$

with $\mathbf{Q}_k = E\left\{\boldsymbol{w}_k\boldsymbol{w}_k^T\right\}$ as process noise covariance matrix.

The state vector associated with this ECG signal is thus defined by its phase θ_k, amplitude z_k and Gaussian function parameters α_i, b_i, and ψ_i. In addition to the noisy ECG recording, s_k, an observed phase, ϕ_k, is obtained by a linear time warping of the R-R intervals into $[0, 2\pi)$ (Figure 3.2), leading to the following system:

$$\begin{bmatrix} \phi_k \\ s_k \end{bmatrix} = \begin{bmatrix} 1 & 0 \\ 0 & 1 \end{bmatrix} . \begin{bmatrix} \theta_k \\ z_k \end{bmatrix} + \begin{bmatrix} u_k \\ v_k \end{bmatrix}, \tag{3.6}$$

where u_k and v_k are the corresponding observation noises, with zero-mean random variable entries and the observation noise covariance matrix is given as $\mathbf{R}_k = E\left\{[u_k, v_k]^T[u_k, v_k]\right\}$.

The ECGs composing the observed mixture can be estimated by recursively applying the described EKF: at each step, one ECG is extracted according to a deflation procedure. In the

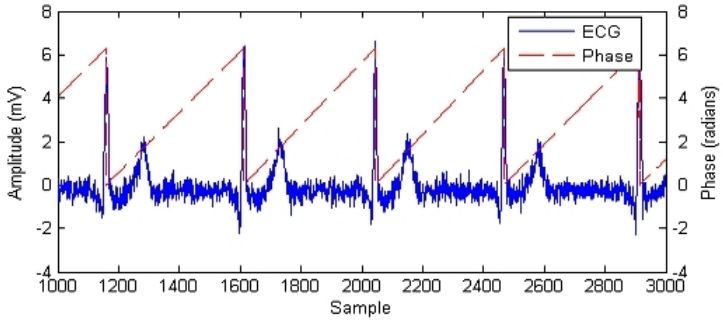

Figure 3.2: Illustration of the phase assignment approach on an ECG.

case of a mixture of mECG and one fECG, the first step extracts, from the raw recording, the dominant ECG (often the mECG) considering the concurrent ECG (here fECG) and other noises as a unique Gaussian noise. After subtracting the dominant ECG from the original signal, the second step is the extraction of fECG from the residual signal. This procedure is referred to as *sequential* EKF or EKS (seq-EKF or seq-EKS). In this recursive extraction, during the first step, the concurrent ECG (i.e. fECG) and additional noise are modeled by Gaussian noises $\mathbf{v}_k$ and $\mathbf{w}_k$, which is not a very relevant assumption. In fact, although this assumption may be acceptable when there are no strong artifacts interfering with the ECG, it is no longer accurate when other ECG artifacts are considerable (i.e. at the first step) since the noise is no longer normally distributed. In addition, concurrent ECGs can be confused with dominant ECG when their waves (especially QRS complexes) fully overlap in time. Meanwhile, resultant inaccuracies, which are generated by the previous steps of the ECG extraction, will be propagated to the next steps while the residuals are computed.

3.4 Methods

In this section, the proposed method is presented. The existing EKF framework for one ECG extraction is extended to multiple ECGs. Therefore, each ECG mixed in the measured signal would have a corresponding term in the state equations. The new state equations are related to the extended observation equations so that each ECG has an independent phase observation and the noisy ECG mixture observation is assumed to be the summation of all ECGs. The model parameter estimation procedure is then extended for the case of multiple ECGs.

3.4.1 Extension to Multiple ECGs: Extended State EKF

The dynamic equations (3.4) are extended for simultaneously modeling N ECGs mixed in a single observation. In this case, the dynamic equations may be written as:

$$\begin{cases} \theta_{k+1}^{(1)} &= (\theta_k^{(1)} + \omega^{(1)}\delta)\text{mod}(2\pi) \\ z_{k+1}^{(1)} &= -\sum_{i\in\mathscr{W}^{(1)}} \delta \frac{\alpha_{i,k}^{(1)}\omega^{(1)}}{b_{i,k}^{(1)^2}} \Delta\theta_{i,k}^{(1)} \exp\left(-\frac{\Delta\theta_{i,k}^{(1)^2}}{2b_{i,k}^{(1)^2}}\right) + z_k^{(1)} + \eta_k^{z^{(1)}} \\ \alpha_{i,k+1}^{(1)} &= \alpha_{i,k}^{(1)} + \eta_k^{\alpha_i^{(1)}} \\ b_{i,k+1}^{(1)} &= b_{i,k}^{(1)} + \eta_k^{b_i^{(1)}} \\ \psi_{i,k+1}^{(1)} &= \psi_{i,k}^{(1)} + \eta_k^{\psi_i^{(1)}} \\ &\vdots \\ \theta_{k+1}^{(N)} &= (\theta_k^{(N)} + \omega^{(N)}\delta)\text{mod}(2\pi) \\ z_{k+1}^{(N)} &= -\sum_{i\in\mathscr{W}^{(N)}} \delta \frac{\alpha_{i,k}^{(N)}\omega^{(N)}}{b_{i,k}^{(N)^2}} \Delta\theta_{i,k}^{(N)} \exp\left(-\frac{\Delta\theta_{i,k}^{(N)^2}}{2b_{i,k}^{(N)^2}}\right) + z_k^{(N)} + \eta_k^{z^{(N)}} \\ \alpha_{i,k+1}^{(N)} &= \alpha_{i,k}^{(N)} + \eta_k^{\alpha_i^{(N)}} \\ b_{i,k+1}^{(N)} &= b_{i,k}^{(N)} + \eta_k^{b_i^{(N)}} \\ \psi_{i,k+1}^{(N)} &= \psi_{i,k}^{(N)} + \eta_k^{\psi_i^{(N)}} \end{cases} \tag{3.7}$$

Therefore, the system state and process vectors are:

$$\begin{cases} \boldsymbol{x}_k = & [\theta_k^{(1)}, z_k^{(1)}, \alpha_{P,k}^{(1)}, ..., \alpha_{T,k}^{(1)}, b_{P,k}^{(1)}, ..., b_{T,k}^{(1)}, \psi_{P,k}^{(1)}, ..., \psi_{T,k}^{(1)}, \dots, \\ & \theta_k^{(N)}, z_k^{(N)}, \alpha_{P,k}^{(N)}, ..., \alpha_{T,k}^{(N)}, b_{P,k}^{(N)}, ..., b_{T,k}^{(N)}, \psi_{P,k}^{(N)}, ..., \psi_{T,k}^{(N)}]^T \\ \boldsymbol{w}_k = & [\omega_k^{(1)}, \eta_k^{z^{(1)}}, \eta_k^{\alpha_P^{(1)}}, ..., \eta_k^{\alpha_T^{(1)}}, \eta_k^{b_P^{(1)}}, ..., \eta_k^{b_T^{(1)}}, \eta_k^{\psi_P^{(1)}}, ..., \eta_k^{\psi_T^{(1)}}, \dots, \\ & \omega_k^{(N)}, \eta_k^{z^{(N)}}, \eta_k^{\alpha_P^{(N)}}, ..., \eta_k^{\alpha_T^{(N)}}, \eta_k^{b_P^{(N)}}, ..., \eta_k^{b_T^{(N)}}, \eta_k^{\psi_P^{(N)}}, ..., \eta_k^{\psi_T^{(N)}}]^T \end{cases} \tag{3.8}$$

with $\mathbf{Q}_k = E\left\{\boldsymbol{w}_k \boldsymbol{w}_k^T\right\}$ as process noise covariance matrix.

In this model, each $[\theta_k^{(n)}, z_k^{(n)}, \alpha_{P,k}^{(n)}, ..., \alpha_{T,k}^{(n)}, b_{P,k}^{(n)}, ..., b_{T,k}^{(n)}, \psi_{P,k}^{(n)}, ..., \psi_{T,k}^{(n)}]^T, \forall n \in \{1, \dots, N\}$ is related to one of the ECGs. Here also, by detecting the R-peaks of the N ECGs, N additional observations are achieved. In order to do so, a phase value between 0 and 2π is assigned to the intermediate samples of R-R intervals for each of the N ECGs, separately. These additional phase observations are employed to synchronize the dynamical KF trajectories with the reference noisy signals, without the need for manual synchronization. This way the quasi-periodic nature of each ECG signal is exploited. Hence, the phase observations of N ECGs, $\phi^{(1)}$,...,$\phi^{(N)}$, and the noisy mixture of the N ECG measurements, s, are related to the state vector at time k as follows:

$$\begin{bmatrix} \phi_k^{(1)} \\ \phi_k^{(2)} \\ \vdots \\ \phi_k^{(N)} \\ s_k \end{bmatrix} = \left[\begin{array}{ccc:ccc} 1 & 0 & \dots & 0 & \dots & 0 \\ 0 & 1 & \dots & 0 & \dots & 0 \\ \vdots & \vdots & \ddots & 0 & \dots & 0 \\ \hdashline 0 & 0 & \dots & 1 & \dots & 1 \end{array}\right] \cdot \begin{bmatrix} \theta_k^{(1)} \\ \theta_k^{(2)} \\ \vdots \\ \theta_k^{(N)} \\ z_k^{(1)} \\ z_k^{(2)} \\ \vdots \\ z_k^{(N)} \end{bmatrix} + \begin{bmatrix} u_k^{(1)} \\ u_k^{(2)} \\ \vdots \\ u_k^{(N)} \\ v_k \end{bmatrix} \tag{3.9}$$

where $u_k^{(1)}$,...,$u_k^{(N)}$ and v_k are the corresponding observation noises with zero-mean random variable entries, and $\mathbf{R}_k = E\left\{[u_k^{(1)}, ..., u_k^{(N)}, v_k]^T[u_k^{(1)}, ..., u_k^{(N)}, v_k]\right\}$ is the observation noise covariance matrix.

This extended state Kalman filtering procedure is referred to as *parallel* EKF or EKS (par-EKF, or par-EKS, respectively). As shown in the results section (Section 3.5), the par-EKF or par-EKS are more accurate to extract fECG from abdominal sensors than the seq-EKF or seq-EKF. Indeed, in the proposed method all ECGs are jointly modeled by dynamic states so that only the state and measurement noise vectors are assumed to be normally distributed. Moreover, the extended state par-EKF fully models overlapping waves of several ECGs. Finally, the state and observation noises allow the filter to fit some variabilities of the ECG shapes. Although the model do not fit too large variations (for example due to arrythmia), an inspection of the residue will reveal the abnormal beats.

3.4.2 Model Parameters Estimation

The proposed par-EKF and par-EKS lie on several state parameters $\{\alpha_i^{(n)}, b_i^{(n)}, \psi_i^{(n)}, \omega^{(n)}\}_{i \in \mathscr{W}_n}$. The procedure described below is an extension of the single ECG parameter estimation [14].

The parameters estimation procedure first needs the R-peaks detection for all ECGs to perform the time warping of the R-R intervals into $[0, 2\pi)$ to define $\phi_k^{(n)}$. The R-peaks are found from a peak search in windows of length $T^{(n)}$, where $T^{(n)}$ corresponds to the R-peak period calculated from approximate $n-th$ ECG beat-rate. R-peaks with periods smaller than $\frac{T^{(n)}}{2}$ or larger than $T^{(n)}$ are not detected to make sure that only one R-peak is detected in each beat. Although maternal R-peaks are easily detectable from the mixture, fetal R-peaks detection is more complex due to its lower amplitude than mECG. Therefore, a rough estimation of fECG is obtained by using the seq-EKF algorithm, which now allows us to easily detect the fetal R-peaks.[1] Then, for each ECG, each beat (defined by the signals between two consecutive R-peaks) is time-warped into $[0, 2\pi)$. The average of the ECG waveform is obtained by the mean of all time-warped beats, for all phases between 0 and 2π. Finally, by using a nonlinear least-squares approach [68], the best estimate of the parameters in the MMSE sense is found. Also, $\omega^{(n)}$ can be set as $\frac{2\pi}{T^{(n)}}$.

[1] In practice, one could also use a sound sensor to have a reliable R-peak detector. In this case, even if there exists a delay, it does not impact the method, because the delay is constant and it can be synchronized.

The process covariance Q_k is estimated by assuming that the noise sources are uncorrelated, i.e. Q_k is a diagonal matrix. The measurement noise covariance matrix, R_k, is similarly considered to be diagonal.

In order to find estimates for $\eta_k^{\alpha_i^{(n)}}$, $\eta_k^{b_i^{(b)}}$ and $\eta_k^{\psi_i^{(n)}}$, for $n-th$ ECG the standard deviation of different ECG cycles around the average ECG cycle can be used. Again, this nonlinear least-squares problem is solved by finding the optimal solutions that generate the best fit of the average ECG within the range of the average ECG plus and minus the standard deviation of ECG. A simple estimate for $\eta_k^{z^{(n)}}$ would be a zero mean Gaussian random variable with an appropriate variance. As mentioned in [14], an intuitive value for this variance may be found from the deviations of the inactive segment of the ECG between the end of the T-wave and the beginning of the next P-wave or the isoelectric segment between the end of the P-wave and the Q point, since no late potentials or baseline wander should manifest during this period.

Assuming a rather reliable R-peak detector, a possible noise source for phase observation is the sampling error that occurs when the actual R-peak is located between two sample times. This can be easily modeled by assuming that the R-peak is uniformly distributed between two consecutive samples. Considering that each ECG cycle is equivalent to 2π in the phase domain, $u_k^{(n)}$ would be uniformly distributed in the range of $\pm\omega^{(n)}\delta/2$ and $E\left\{(u_k^{(n)})^2\right\} = (\omega^{(n)}\delta)^2/12$. There are also several possible ways to estimate the variance of the amplitude measurement noise, v_k. One method is to estimate the noise power from the deviations of all time-warped beats of the strongest ECG, or from the portions of the strongest ECG between two successive T and P waves.

3.5 Results and Discussions

Both synthetic and actual data have been used to study the performance of the proposed method. In the first subsection, quantitative results coming from simulations and influence of the main parameters of mixed ECGs on the performance of the method have been studied. They will present the conditions in which the proposed method is efficient. In the second subsection, the effectiveness of the method on actual data has been examined.

3.5.1 Numerical Performance Analysis on Synthetic Data

Since there is neither ground truth nor golden standard on single-channel recordings, it is important to provide quantitative performance with simulations to validate the behavior of the proposed method. In order to do so, realistic synthetic mixtures of mECG and fECG with white Gaussian noise have been generated for different situations and the proposed method has been applied on them to extract mECG and fECG. Synthetic mECG and fECG used in this study are based on a three-dimensional canonical model of the single dipole vector of the heart, proposed in [69] and inspired by the single-channel ECG dynamic model presented in [66]. Sampling frequency is set to 500 Hz and signals include 20,000 samples. The main parameters that can affect the mixtures are input noise power, ratio between amplitudes of fECG and mECG, and ratio

between fetal and maternal heart rates. In order to investigate the performance of the proposed method one hundred trials were carried out under each value of these parameters. In the output, estimated mECG and fECG signals, $\hat{\mathbf{s}}_m$ and $\hat{\mathbf{s}}_f$, are assumed to be the sum of mECG, fECG and noise, such that:

$$\begin{aligned} \hat{\mathbf{s}}_m &= \alpha_1 \mathbf{s}_m + \alpha_2 \mathbf{s}_f + \alpha_3 \mathbf{n}, \\ \hat{\mathbf{s}}_f &= \beta_1 \mathbf{s}_m + \beta_2 \mathbf{s}_f + \beta_3 \mathbf{n}, \end{aligned} \tag{3.10}$$

where coefficients α_1, α_2, α_3, β_1, β_2, and β_3, have to be estimated and $\mathbf{s}_m$, $\mathbf{s}_f$, and $\mathbf{n}$ denote mECG, fECG and noise, respectively. In order to estimate the coefficients, $\mathbf{s}_m$, $\mathbf{s}_f$, and $\mathbf{n}$ are assumed to be orthogonal, i.e., decorrelated. The orthogonality principle states that an estimator $\hat{\mathbf{s}}$ achieves MMSE if and only if $E\left\{(\hat{\mathbf{s}} - \mathbf{s})^T \hat{\mathbf{s}}\right\} = 0$. Satisfaction of this criteria leads to:

$$\begin{aligned} \hat{\alpha}_1 &= \frac{E(\hat{\mathbf{s}}_m^T \mathbf{s}_m)}{E(\mathbf{s}_m^T \mathbf{s}_m)}, \quad \hat{\alpha}_2 = \frac{E(\hat{\mathbf{s}}_m^T \mathbf{s}_f)}{E(\mathbf{s}_m^T \mathbf{s}_f)}, \quad \hat{\alpha}_3 = \frac{E(\hat{\mathbf{s}}_m^T \mathbf{n})}{E(\mathbf{s}_m^T \mathbf{n})}, \\ \hat{\beta}_1 &= \frac{E(\hat{\mathbf{s}}_f^T \mathbf{s}_m)}{E(\mathbf{s}_f^T \mathbf{s}_m)}, \quad \hat{\beta}_2 = \frac{E(\hat{\mathbf{s}}_f^T \mathbf{s}_f)}{E(\mathbf{s}_f^T \mathbf{s}_f)}, \quad \hat{\beta}_3 = \frac{E(\hat{\mathbf{s}}_f^T \mathbf{n})}{E(\mathbf{s}_f^T \mathbf{n})}. \end{aligned} \tag{3.11}$$

In a successful estimation, contribution of desired ECG in output should be much more than contribution of undesired ECG and noise. In other words, in extraction of fECG the power of $\beta_2 \mathbf{s}_f$ should be much larger than power of $\beta_1 \mathbf{s}_m + \beta_3 \mathbf{n}$, which means the contribution of mECG and noise is very low in the fECG estimate. In the same manner, the power of $\alpha_1 \mathbf{s}_m$ should be much larger than power of $\alpha_2 \mathbf{s}_f + \alpha_3 \mathbf{n}$ in mECG extraction. In order to quantify contribution of the desired ECG in the output, output SNR for maternal and fetal ECGs are defined as:

$$\begin{aligned} SNR_{m_{out}} &= \frac{\hat{\alpha}_1^2 P_{\mathbf{s}_m}}{\hat{\alpha}_2^2 P_{\mathbf{s}_f} + \hat{\alpha}_3^2 P_{\mathbf{n}}}, \\ SNR_{f_{out}} &= \frac{\hat{\beta}_2^2 P_{\mathbf{s}_f}}{\hat{\beta}_1^2 P_{\mathbf{s}_m} + \hat{\beta}_3^2 P_{\mathbf{n}}}. \end{aligned} \tag{3.12}$$

where $P_{\mathbf{s}_m}$, $P_{\mathbf{s}_f}$, and $P_{\mathbf{n}}$ denote power of mECG, fECG, and noise, respectively. Output SNR is now compared with input SNR to investigate performance of desired ECG extraction. Input SNRs are defined as:

$$SNR_{m_{in}} = \frac{P_{\mathbf{s}_m}}{P_{\mathbf{s}_f} + P_{\mathbf{n}}} \quad \text{and} \quad SNR_{f_{in}} = \frac{P_{\mathbf{s}_f}}{P_{\mathbf{s}_m} + P_{\mathbf{n}}} \tag{3.13}$$

Input signal to interference ratio (SIR) and output SIR are also defined as:

$$\begin{aligned} SIR_{m_{in}} &= \frac{P_{\mathbf{s}_m}}{P_{\mathbf{s}_f}}, \qquad SIR_{f_{in}} = \frac{P_{\mathbf{s}_f}}{P_{\mathbf{s}_m}}, \\ SIR_{m_{out}} &= \frac{\hat{\alpha}_1^2 P_{\mathbf{s}_m}}{\hat{\alpha}_2^2 P_{\mathbf{s}_f}}, \quad SIR_{f_{out}} = \frac{\hat{\beta}_2^2 P_{\mathbf{s}_f}}{\hat{\beta}_1^2 P_{\mathbf{s}_m}}. \end{aligned} \tag{3.14}$$

The performance of the proposed method for different values of input noise power, ratio

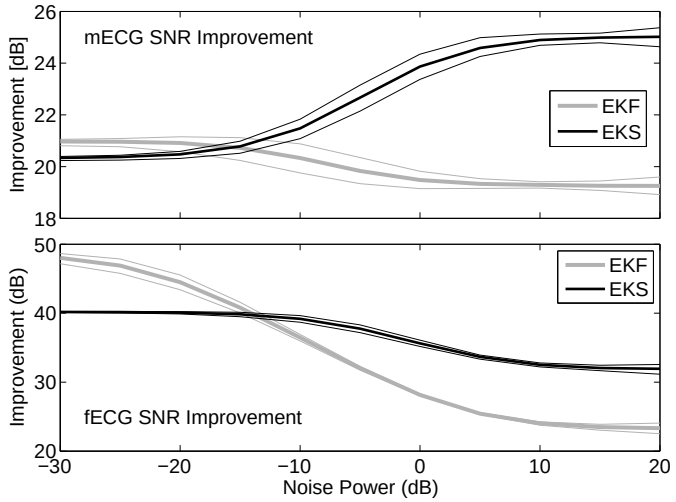

Figure 3.3: Mean SNR improvement results of the EKF and EKS against input noise power (bold lines) . Upper and lower borders (thin lines) present maximum and minimum, respectively.

between amplitudes of fECG and mECG, and ratio between fetal and maternal heart rates is presented in this subsection.

SNR Analysis

Figure 3.3 shows SNR improvement results of par-EKF and par-EKS over a wide range of input noise power. The SNR improvement in dB is defined as the output SNR of the filter minus the input SNR. In all trials, power of mECG signals is normalized to 1 (0 dB) and the ratio of amplitudes of fECG and mECG is 0.3. Maternal and fetal heart rates are set to 1.1 Hz and 2 Hz, respectively. Moreover, in order to have more realistic signals, mECG and fECG are allowed to have slight Gaussian random fluctuations (5%) in amplitude and duration at each beat. Moreover, initial phases of ECGs are random. As it can be seen in Figure 3.3, both EKF and EKS successfully improved the SNR for all ranges of the input SNRs. When the mixture is rather noise free (noise power -30 dB) the minimum SNR improvement of fECG is 40 dB, which means efficient cancellation of mECG. Nevertheless, even for very noisy mixtures (noise power 20 dB), the SNR improvement of fECG remains over 20 dB. According to this figure, EKF is more effective when a rather clean signal is available. On the contrary, as power of noise increases, EKS significantly outperforms EKF. The reason of this difference can be explained by revising the EKS algorithm. As it has been explained in Section 3.2, the EKS algorithm consists of a forward EKF stage followed by a backward recursive-smoothing stage. Therefore, if a rather clean signal is available, the recursive smoothing stage will deteriorate EKF output, because the output is already smooth enough and recursive smoothing leads to over-filtering. Conversely, if the signal is very noisy, the EKF output is not denoised enough yet. Therefore, the recursive smoothing stage can be successfully used to cancel more noise from the signal.

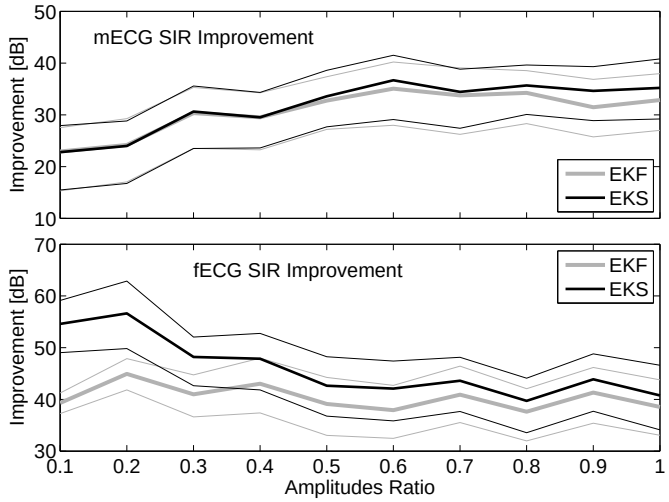

Figure 3.4: Mean SIR improvement results of the EKF and EKS against amplitude ratio (bold lines). Upper and lower borders (thin lines) present maximum and minimum, respectively.

Amplitude Ratio Analysis

The basic problem of fECG monitoring is to extract the fECG signal from the mixture of mECG and fECG signals, where the interfering mECG is a stronger signal. Therefore, it is necessary to evaluate the performance of the method for different ratios of fECG and mECG amplitudes. For this purpose, SIR improvement of output signals have been calculated in the range of 0.1 to 1 of amplitude ratio of fECG and mECG [2]. Figure 3.4 shows SIR improvement results of the EKF and EKS for different values of amplitude ratios. Power of mECG signals is normalized to 1 (0 dB) with 5% Gaussian random fluctuation, input SNR with respect to mECG is 10 dB, and average maternal and fetal heart rates are 1.1 Hz and 2 Hz, respectively. As it is seen in Figure 3.4, although the fetal SIR improvements of both EKF and EKS remain over 30 dB for all ranges of the amplitude ratios, results of EKS are slightly better.

Heart Rate Ratio Analysis

Another important parameter that may affect performance of the method, is the ratio of heart rates. At about five weeks gestation, fetus' heart begins to beat. At this point, a normal fetal heart rate is about the same heart rate as the mother's, about 80-85 beats per minute (BPM). From this point, it will increase its rate about 3 beats per minute per day during that first month. By the beginning of the ninth week of pregnancy, the normal fetal heart rate is an average of 175 BPM. At this point it begins a rapid deceleration to the normal fetal heart rate for the middle of the pregnancy of about 120-180 BPM. There is also a slowing of the normal fetal heart rate in the last ten weeks of pregnancy, though the normal fetal heart rate is still about twice the normal adult's resting heart rate [70]. Therefore, since fetal heart rate may vary in a wide range,

[2]The large range of tested ratio values does not only include usual ratios encountered between fetal and maternal signals, but also ratio values encountered between two fetal signals.

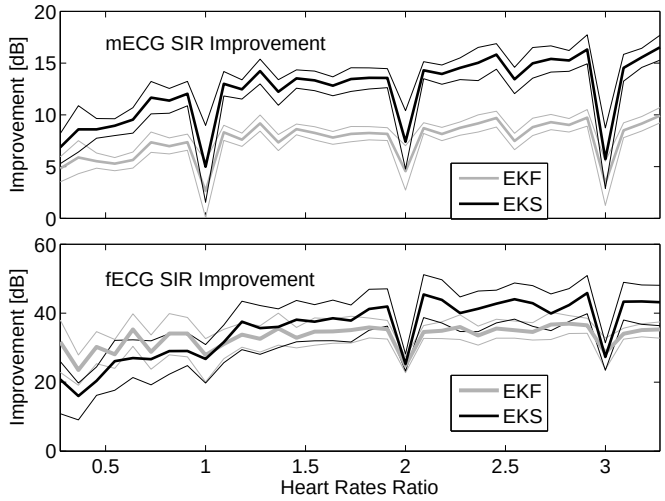

Figure 3.5: Mean SIR improvement results of the EKF and EKS against heart rate ratio (bold lines). Upper and lower borders (thin lines) present maximum and minimum, respectively.

the performance of the method was studied on a wide range of 0.3 Hz to 3.6 Hz of fetal heart rate. Figure 3.5 shows SIR improvement results of EKF and EKS. Power of mECG signals is normalized to 1 (0 dB) with 5% Gaussian random fluctuation and the ratio of amplitudes of fECG and mECG is 0.3. Input SNR with respect to mECG is 10 dB, and maternal heart rate is set to 1.1 Hz. In this section, heart rate fluctuations are slighter (1%) to study harmonic issues more accurately. As expected, SIR improvement diagram has three deep local minima at ratios 1, 2 and 3. The reason is that when main frequencies of mECG and fECG are proportional, the signals overlap more closely in the frequency domain. Therefore, discrimination of mECG and fECG is more difficult for these ratios. Nevertheless, these situations are unlikely to happen because the heart rates ratio is usually more than 1 and less than 2. Even in these cases, fetal SIR improvement remains over 20 dB. As it is seen in Figure 3.5, both EKF and EKS improved input SIR for all values of heart rate ratios. Here again, EKS slightly outperforms EKF.

3.5.2 Fetal ECG Extraction on Actual Data

In the previous subsection, efficiency of the proposed method in fECG extraction for a wide range of possible configurations has been examined using synthetic data. In this subsection, the results of application of the proposed method on actual data are presented. As mentioned before, there is no golden standard on actual single-channel recordings. Nevertheless, in order to better compare the performance of single-channel methods, we adopted the πCA method [30] as the golden standard. Please note that the πCA method is a multichannel method and we used all channels available on each dataset to provide the πCA output. Results of πCA method are then post-processed via EKS on the best ECG estimate [14] to improve the πCA output.

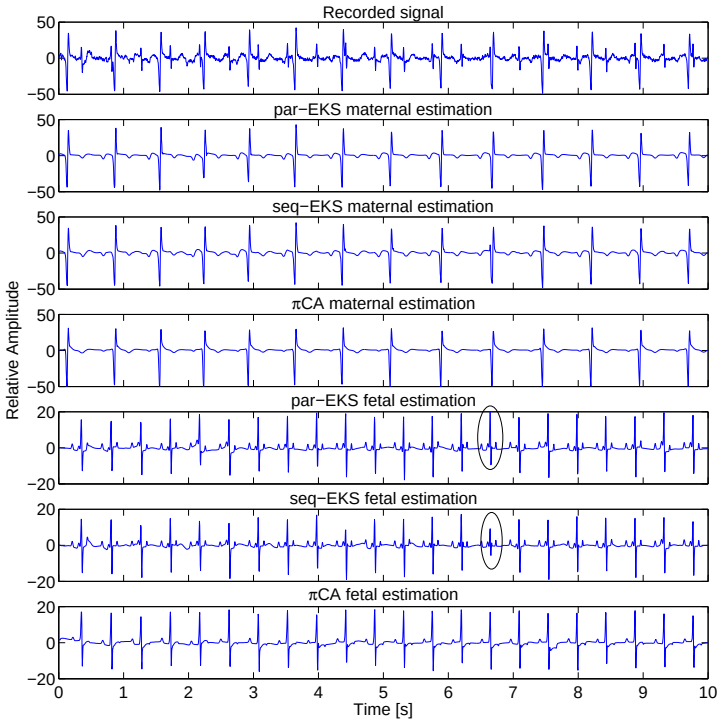

Figure 3.6: Comparison of fECG extraction by par-EKS, seq-EKS and πCA on the first channel of DaISy data. Unlike seq-EKS, par-EKS does not fail when mECG and fECG fully overlap in time. This is particularly noticed between t = 6s and t = 7s.

DaISy Database

The first ECG data used in this subsection is the DaISy fetal ECG database [71], as described in Appendix A, Section A.1.

Figure 3.6 presents the results of par-EKS and seq-EKS using the first channel of the dataset. The πCA method [30], using the eight channels is also included as the golden standard. As already mentioned, unlike seq-EKS, par-EKS does not fail when mECG and fECG fully overlap in time. This is particularly noticed between t = 6s and t = 7s in Figure 3.6 in which, some parts of fECG signal have been corrupted during mECG extraction by the seq-EKS method. On the contrary, the proposed par-EKS jointly models the fECG and mECG, resulting in a better estimate of fECG than seq-EKS. Since par-EKS estimates a single component while πCA can estimate several components, the cosine between the subspace of the par-EKS estimate and the subspace of the πCA estimate (in this experiment it has two components) is used. The achieved cosine value is equal to 0.92 in this experiment, which is close to 1. This means that the two estimates are quite similar.

Finally, Figure 3.7 shows the results of fECG extraction using par-EKS applied on the other abdominal channels of the DaISy dataset. It experimentally proves that par-EKS is able to extract fECG even in ill-conditioned mixtures, such as the recordings observed on channels 4 or 5.

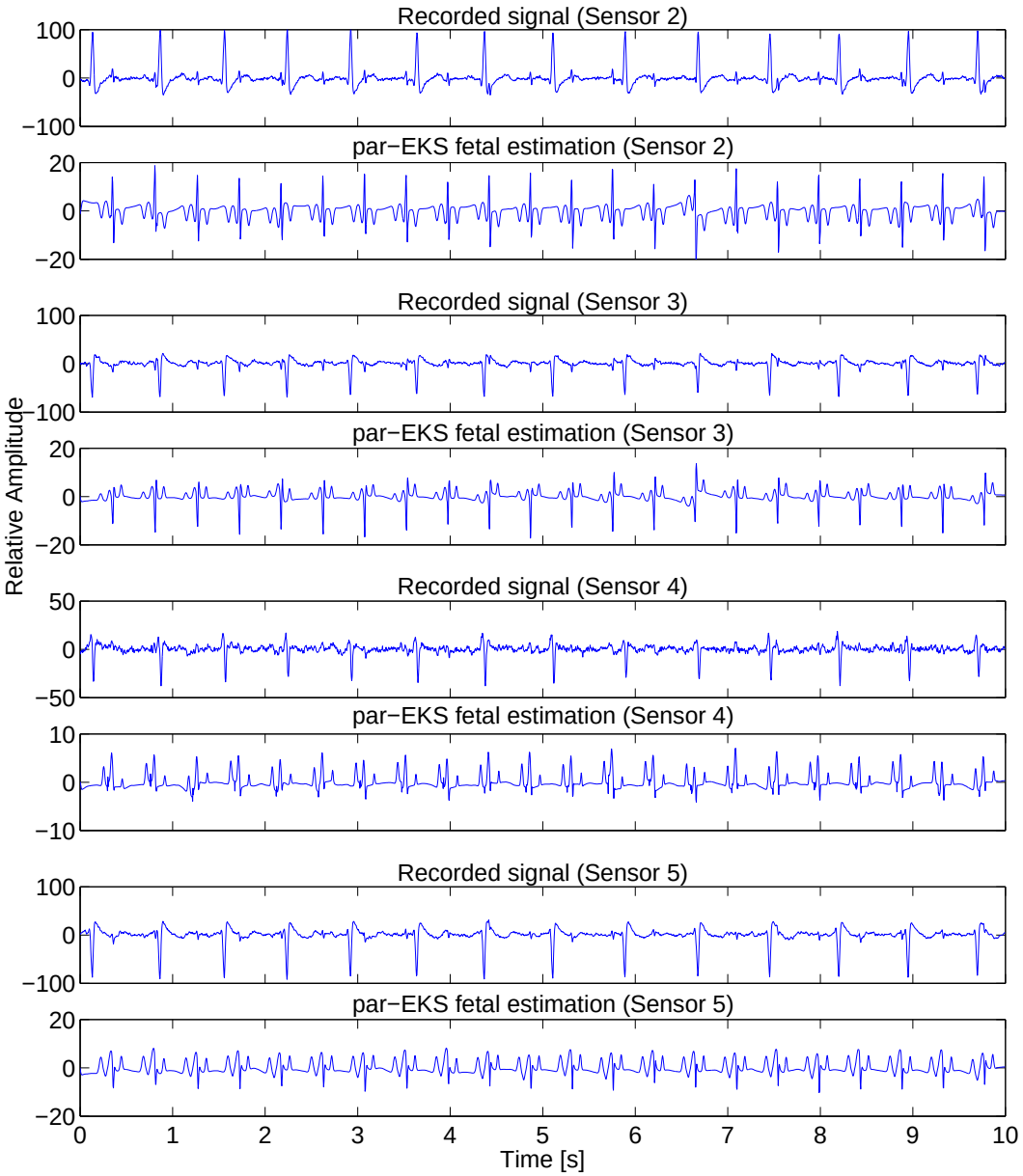

Figure 3.7: Results of fECG extraction using par-EKS applied on channels 2 to 5 of the DaISy dataset (top to bottom). Note differences of scales, according to the channels and the fetal estimates.

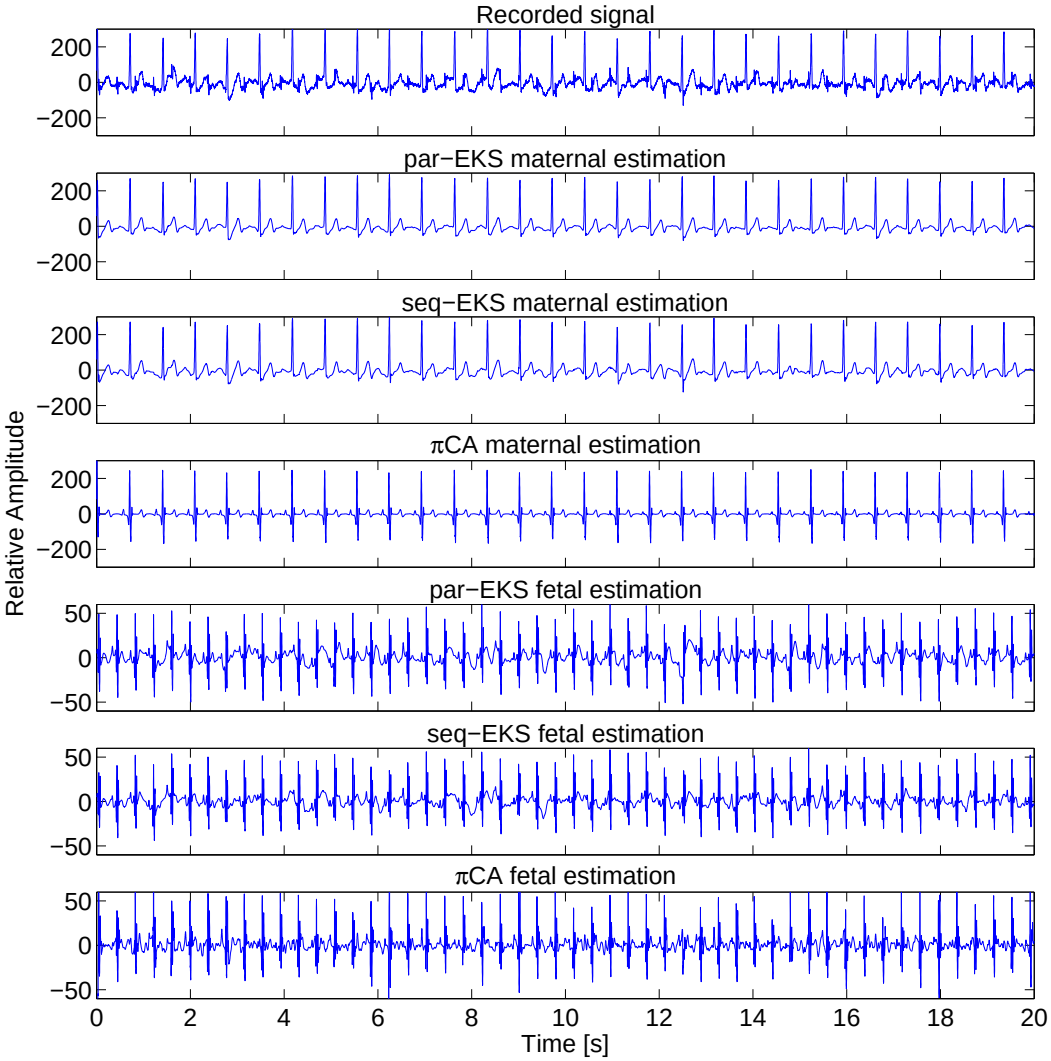

Figure 3.8: Comparison of fECG extraction by par-EKS, seq-EKS and πCA on ecgca771 of the PhysioNet database.

Noninvasive Fetal Electrocardiogram Database

The PhysioNet noninvasive fetal electrocardiogram database [72] described in Appendix A, Section A.2 was also used to show the effectiveness of the proposed method in fECG extraction at different periods of pregnancy, and different channel locations. Figure 3.8 shows the results of seq-EKS and par-EKS using channel 3, and πCA using all channels of the first 20s of namely the ecgca771 dataset.

To show the effectiveness of the proposed method in extraction of the fECG at different periods of pregnancy, and from different channel locations, the first 20s of the mixtures and fetal par-EKS outputs of the datasets ecgca274 channel 5, ecgca748 channel 4, and ecgca997 channel 3 are plotted in Figure 3.9.

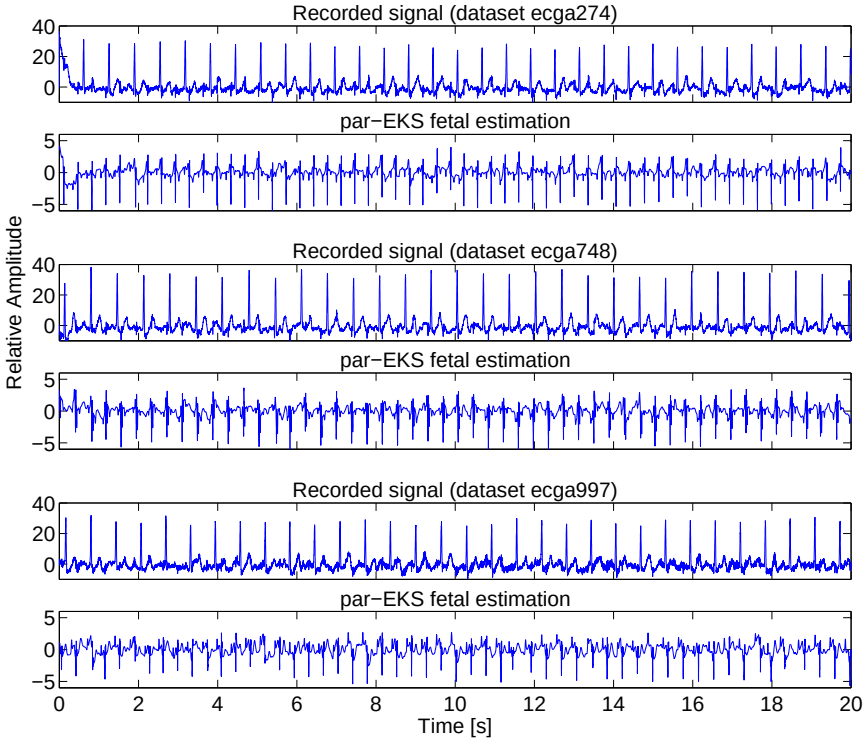

Figure 3.9: ECG mixtures of the datasets ecgca274 channel 5, ecgca748 channel 4, and ecgca997 channel 3 and their fetal par-EKS outputs.

Twin MCGs Extraction

The proposed method has been principally designed for ECG signals. Nevertheless, due to the morphological similarity of the ECG and the MCG, it is also directly applicable to MCG recordings. In this section, the twin fetal cardiac magnetic signal dataset described in Appendix A, Section A.3 was employed to assess the performance of the proposed method in extraction of cardiac signals of twins.

Figure 3.10 presents the results of the proposed par-EKS to extract the two fetal MCG signals from a single sensor. A typical channel (indexed 92) of namely the q00002252 dataset has been selected. Even though the multichannel πCA method provides better results in this case than single channel methods (par-EKS or seq-EKS), the proposed par-EKS succeeds to extract the two fetal MCG while seq-EKS fails to correctly discriminate the two fetal MCGs when they overlap (see highlighted signal parts, Figure 3.10).

In order to show the good behavior of par-EKS in several configurations, par-EKS has been applied on other sensors (Figure 3.11). One can note that the proposed par-EKS succeeds to extract the two fetal MCGs.

Finally, it is worth noting that an important part of the proposed par-EKS is the R-peaks detection. Although this detection is quite direct when a single fetus is present (Section 3.4.2), some words should be added on twin data. Indeed, on such data the detection of the mother's R-peaks is still direct since it is the dominant signal. On the contrary, the discrimination between

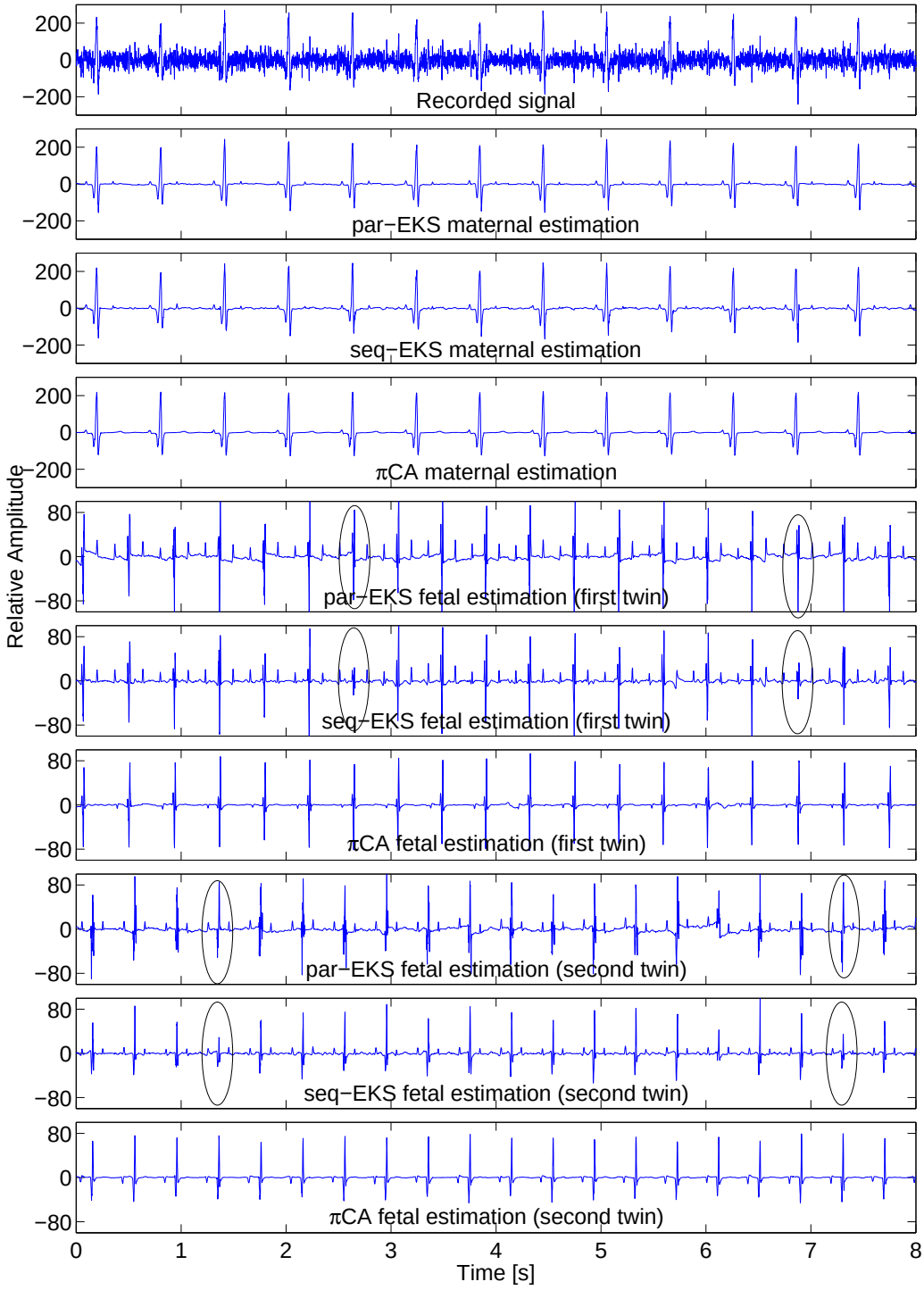

Figure 3.10: Results of the par-EKS, seq-EKS, and πCA on twin MCG data. Unlike seq-EKS, par-EKS does not fail when maternal MCG and fetal MCG fully overlap in time. This is particularly noticed between t = 2s and t = 3s and between t = 6s and t = 7s for the first fetus and between t = 1s and t = 2s and between t = 7s and t = 8s for the second fetus.

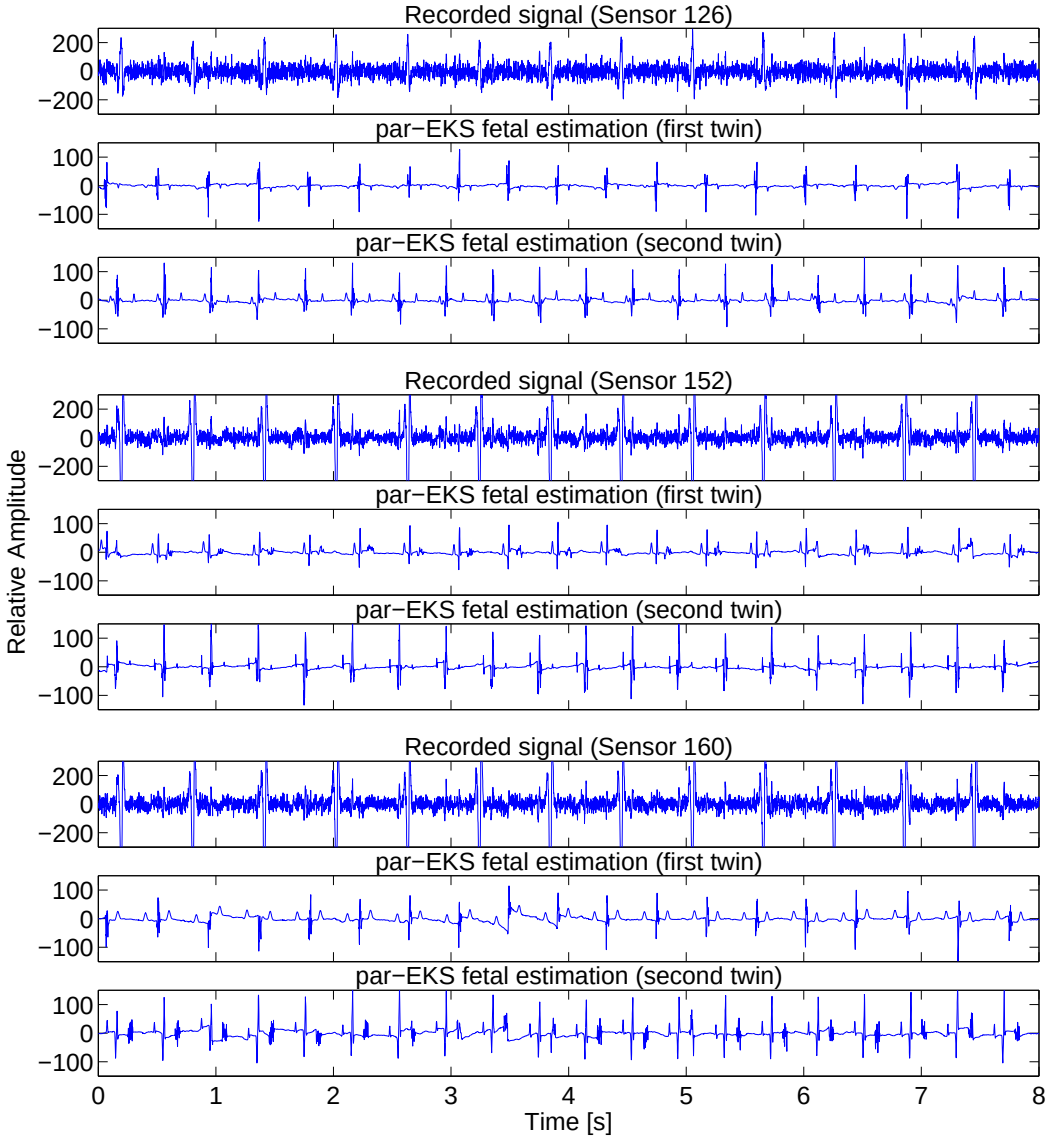

Figure 3.11: MCG mixtures of the channels 126, 152, and 160 and their fetal par-EKS outputs.

the two fetal R-peaks is much more difficult. Even though in this study, the oracle is obtained using several sensors and applying an ICA algorithm (here, we used Fast-ICA), it can be replaced in practice by a sound sensor located on mother's abdomen.

3.6 Summary and Conclusions

In this chapter, a synthetic dynamic ECG model within a KF framework has been extended to jointly model several ECGs to extract desired ECGs from a unique mixture (i.e. one channel recording) of maternal and fetal ECGs and noise. Although the proposed method only uses a single channel to separate different ECGs, since each ECG has a corresponding term in the model, the proposed model can efficiently discriminate ECGs even if desired and undesired ECG waves overlap in time. As proved on synthetic data and illustrated on actual data (single and multiple fetal pregnancy), the main merit of the proposed algorithm relies on its performance in a large class of situations. The performance of the proposed method on extraction of fECG from one mixture of mECG and fECG was examined according to noise level, amplitude ratio and heart rate ratio parameters: results show that the proposed method can be successfully employed in many scenarios. According to the obtained results, as long as R-peaks are correctly detected, the proposed model achieves good results. Although a reliable R-peaks detection is a straightforward procedure in a single fetal pregnancy (which is most likely to happen) even with a single sensor, it is much more difficult in multiple fetal pregnancy (twin or more). Nonetheless, in these situations, the R-peaks detection could be provided by other modalities such as echocardiography.

Finally, the proposed method compares favorably with efficient multi-sensor methods such as πCA (which also requires reliable R-peaks detection), while it requires only one sensor. The latter criterion is of high interest, since applicability a single channel does not only mean less electronic components (such as analog to digital converters or amplifiers) and thus a cheaper device, but also a more convenient and portable device for a long term monitoring system or at home since only a single electrode has to be placed on mother's abdomen.

Chapter 4

Extraction of Event-Related Sources via Robust Tensor Decomposition

4.1 Introduction

In this chapter,[1] a general blind source separation approach based on robust tensor decomposition is presented for extraction of event-related sources in underdetermined mixtures. An event-related source is characterized by typical patterns which are elicited after some events: such patterns may vary in amplitudes and/or in inter-event intervals (IEI). In this context, an event-related source is referred to as: (i) quasi-periodic source (e.g., ECG) in which IEI and amplitudes can only slightly change from a period to another; (ii) source with synchronized stimuli (e.g., event-related potentials (ERP)) in which a pattern is repeated with no assumption on IEI but with quasi-constant amplitudes; (iii) amplitude-variant source whose amplitude (even sign) can largely change from a period to another but with quasi-constant IEI (e.g., telecommunication); (iv) general source without any assumptions on amplitudes and IEI, which can thus largely vary from an event to another one (e.g., digital communications).

The proposed method, which is based on robust deterministic tensor decomposition, is applicable to all of the above-mentioned types of event-related sources. Nonetheless, a special case for the hereby proposed method is the problem of separating fetal cardiac signals from interferences and noise. It will be shown that the robust tensor decompositions proposed in this chapter can be efficiently applied to underdetermined mixtures of maternal and fetal cardiac signals to recover weak fetal cardiac components.

The rest of this chapter is organized as follows. In Section 4.2 the background of the blind separation of sources from underdetermined mixtures is first reviewed briefly and then application of tensor decomposition methods for extraction of event-related sources is recalled. Section 4.3 is dedicated to present the proposed method. In this section, a tensor construction and decomposition method is adapted for extraction of event-related sources. Considering the limitations of this method, two robust tensor decompositions are then proposed to better track

[1] The contributions of this chapter have been partly obtained based on the collaboration of the author and his supervisors with Hanna Becker and her supervisor, Pierre Comon.

weak sources mixed with strong ones. The performance of the proposed method is assessed in Section 4.4 by means of simulated and actual data. First, robustness of the proposed method to the percentage of outliers, initialization, amplitude variability and synchronization errors are investigated using synthetic data. Then, actual fetal ECG and MCG mixtures are used to show the performance of the proposed method in extraction of fetal cardiac signal. The application of the proposed method in fully automatic fetal R-peak detection is presented in Section 4.5. Finally, the summary and the conclusions of the chapter are stated in Section 4.6.

4.2 Background

4.2.1 Blind Separation of Sources from Underdetermined Mixtures

In the recent years, a lot of attention has been paid to blind source separation (BSS) due to its wide-ranging applications in many areas [73] such as audio and speech processing [74], telecommunications [75], biomedical engineering [76], hyperspectral imaging [77], etc. Assuming an M-dimensional observation vector, $\mathbf{y}(k)$, this problem is mathematically expressed as:

$$\mathbf{y}(k) = \mathbf{A}\mathbf{x}(k) + \mathbf{b}(k), \tag{4.1}$$

where $\mathbf{x}(k)$ denotes the N-dimensional source vector, $\mathbf{b}(k)$ denotes the M-dimensional additive noise vector, and $\mathbf{A}$ is the $M \times N$ mixing matrix. The BSS framework aims at identifying the mixing matrix $\mathbf{A}$, or estimating the sources $\mathbf{x}(k)$, or both, from the observation $\mathbf{y}(k)$. Unlike the determined or overdetermined cases, when the number of sources exceeds the number of mixtures ($N > M$), i.e. in the underdetermined case, the estimation of the mixing matrix $\mathbf{A}$ does not permit to directly recover the original sources. In fact, the mixing matrix does not admit a left inverse in that case, which makes it more difficult to recover the sources even if the mixing matrix is known and full rank [73, 78]. It is then necessary to rely on a prior on the sources.

Sparsity of the sources in a transformed domain is a possible prior to address underdetermined BSS [79]. Indeed, most of the proposed methods in the literature of underdetermined BSS are based on the sparsity of sources in a domain, (e.g., the frequency domain [80] or the time-frequency domain [81]). In this case, even if several sources are active at the same time so that the mixture is locally overdetermined, the mixing matrix can usually be estimated by clustering methods. However, this kind of search usually requires massive computations that limit the applicability of these methods to a smaller number of observation channels and sources [82].

Separation of underdetermined sources consists of two steps: estimation of the mixing matrix and extraction of the sources. Many algebraic and geometric (clustering) methods have been developed for the first step. They employ various decompositions of different data structures such as cumulant, correlation and cross-correlation matrices or tensors [73, 82]. Then, a second step is required for recovering the original sources.

4.2.2 Tensor Decomposition for Event-Related Source Extraction

Higher-order tensors have gained increasing importance as they can be used to represent higher order cumulants that are exploited in independent component analysis [83] and have been used successfully in BSS [83]. In addition, they are natural representations of multidimensional (higher than 2) data than matrices in many practical applications (e.g., in chemistry, biomedical engineering, and wireless communications). A fundamental challenge in these applications is to find informative and sparse representations of tensors, i.e., tensor decompositions. Tensor decompositions take into account information about different variables of the data, such as, for example, spatial, temporal and spectral information, and may provide links among the various extracted factors or latent variables with physical or physiological meaning and interpretation [84].

There are many applications, in which the sources are known to be event-related. These properties are observed in digital communication, speech and some physiological signals such as electrocardiograms. The behavior of second- and fourth-order BSS algorithms in a cyclostationary context has been studied in [85]. In a recent study [82], an underdetermined separation method has been developed, which is suitable for separation of signals that are piecewise stationary, having time-varying variances. These algorithms that exploit the cyclostationarity property, resort to statistical tools.

In [16], a parallel deflation procedure based on a deterministic tensor decomposition has been proposed to address the problem of underdetermined BSS in the cyclostationary context. The basic approach consists in constructing a tensor by synchronizing on the symbol rate of a certain source, and decomposing the tensor using the canonical polyadic (CP) decomposition [86] to extract the characteristics of the source.

In this chapter, the method described in [16] has been adapted for the estimation of the mixing matrix, temporal patterns, and amplitudes of event-related sources. The method described in [16] fails to extract a source which has very little power compared with the other sources because the latter act as interferers with high amplitudes that can be considered as outliers and impede on the accurate tensor decomposition. To overcome this problem, we propose to apply robust tensor decomposition. In the literature, one can find several methods that have been developed to this end [87, 88]. In general, these techniques are based on a modification of the classical quadratic cost function that is optimized during the tensor decomposition. For example, the authors of [88] suggested to minimize the mean absolute error, which reduces the impact of outliers in the data, but does not prevent them from influencing the results since high outliers still lead to high errors. It is also possible to introduce weights that account for different uncertainties of the tensor elements (see, e.g., [87]). In this chapter, we present two robust CP decomposition methods. The first one, which we subsequently refer to as Gaussian CP (GCP) decomposition, goes a step further compared with the approach taken in [88] and optimizes a cost function that limits the maximal error to 1. The second method exploits the particular structure of the data to compute weights that discriminate outliers and employs a weighted CP (WCP) decomposition.

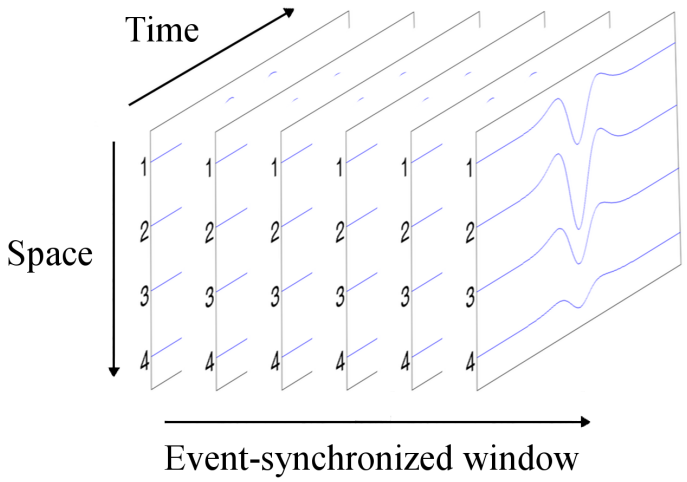

Figure 4.1: Illustration of a tensor with event-synchronized windows.

4.3 Methodology

4.3.1 Tensor Construction and CP Model

In the style of [16], we exploit the event-related nature of the signals of interest to construct a data tensor with dimensions space, event-synchronized window, and time from the M-dimensional measurements for each of Q event-related sources. To this end, for the q-th source, we identify L_q event-synchronized windows of length T_q of the corresponding time signal. This can, for instance, be achieved based on a characteristic pattern within each event-synchronized window that can be recognized in the measurements. This pattern also serves as a reference point to synchronize the signals of different patterns of the event-related source, such as the maximum amplitude in the case of impulsive signals. As an example, for ECG signals, one can use the R-peak to identify and synchronize the signals of different heartbeats (each beat corresponds to the recognized pattern of the event-related source). For each of the L_q event-synchronized windows, one can thus extract a $M \times T_q$ data matrix from the measurements. These matrices are then stacked along the second dimension of the tensor $\boldsymbol{Y}^{(q)} \in \mathbb{R}^{M \times L_q \times T_q}$ (see Figure 4.1).

Assuming that the q-th source can be described by $R_q \in \mathbb{N}$ components that are identical for all event-synchronized windows except for changes of amplitude, the elements of the tensor can be written as

$$Y^{(q)}_{ijk} = \sum_{r=1}^{R_q} a^{(q)}_{ir} s^{(q)}_{jr} h^{(q)}_{kr} + b_{ijk}. \tag{4.2}$$

The first term in the right-hand side of (4.2) corresponds to the CP decomposition of a tensor where $a^{(q)}_{ir}$, $s^{(q)}_{jr}$, and $h^{(q)}_{kr}$ are the elements of three loading matrices $\mathbf{A}^{(q)} \in \mathbb{R}^{M \times R_q}$, $\mathbf{S}^{(q)} \in \mathbb{R}^{L_q \times R_q}$, and $\mathbf{H}^{(q)} \in \mathbb{R}^{T_q \times R_q}$, respectively [86]. The loading matrices correspond to the mixing matrix ($\mathbf{A}^{(q)}$), the matrix of pattern amplitudes ($\mathbf{S}^{(q)}$), and the matrix containing the temporal patterns of the event's components ($\mathbf{H}^{(q)}$) that characterize the mixture of the q-th source. The

second term contains noise and interference from the desynchronized signals of other sources.

Since we assume that each event-related source may consist of more than one component, the number of sources N in the model (4.1) corresponds to the total number of components, i.e., $N = \sum_{q=1}^{Q} R_q \geqslant Q$, while the full mixing matrix $\mathbf{A}$ in the model (4.1) can be obtained as $\mathbf{A} = [\mathbf{A}^{(1)}, \ldots, \mathbf{A}^{(Q)}]$.

In practice, one can obtain estimates for the mixing matrix, the pattern amplitudes, and the signal patterns by decomposing the tensor using the following criterion that optimizes the classical CP cost function:

$$\left\{\hat{\mathbf{A}}^{(q)}, \hat{\mathbf{S}}^{(q)}, \hat{\mathbf{H}}^{(q)}\right\} = \underset{\left\{\mathbf{A}^{(q)}, \mathbf{S}^{(q)}, \mathbf{H}^{(q)}\right\}}{\arg\min} \sum_{i,j,k} \left\| y_{ijk}^{(q)} - \sum_{r=1}^{R_q} a_{ir}^{(q)} s_{jr}^{(q)} h_{kr}^{(q)} \right\|_F^2 . \tag{4.3}$$

An important advantage of the CP decomposition in comparison to matrix decompositions, such as PCA, is that it is essentially unique [89, 90] up to scale and permutation indeterminacies under mild conditions on the tensor rank, without imposing additional constraints such as orthogonality or independence. In [89, 90], the following sufficient condition for essential uniqueness has been derived:

$$k_{\mathbf{A}^{(q)}} + k_{\mathbf{H}^{(q)}} + k_{\mathbf{S}^{(q)}} \geqslant R_q + 2, \tag{4.4}$$

where, $k_{\mathbf{A}^{(q)}}$, $k_{\mathbf{H}^{(q)}}$, and $k_{\mathbf{S}^{(q)}}$ denote the Kruskal ranks of the matrices $\mathbf{A}^{(q)}$, $\mathbf{H}^{(q)}$, and $\mathbf{S}^{(q)}$, respectively. The Kruskal rank of a matrix $\mathbf{A}$ corresponds to the largest number of columns that can be chosen from $\mathbf{A}$ such that the columns are linearly independent for any chosen combination of columns. In particular, as has been shown in [16], if $\mathbf{A}^{(q)}$, $\mathbf{S}^{(q)}$, and $\mathbf{H}^{(q)}$ have full rank and $T_q \geqslant R_q$, $L_q \geqslant R_q$ (i.e., if the number of events and the number of time samples per event are larger than the number of components R_q to be extracted), then $M = 2$ sensors are enough to blindly separate R_q components.

However, errors in the decomposition are to be expected due to noise and interfering sources b_{ijk}, in particular if the source to be extracted is weak in comparison to the interfering sources. In this case, the other source signals can be considered as outliers and strongly influence the optimization of the criterion (4.3) because they prevent the decomposition algorithm to concentrate on the signal of interest. To overcome this practical problem, we propose to apply a tensor decomposition that is robust to outliers. In the following, we present two different robust decomposition schemes, which are based on modifications of the CP cost function. The different cost functions are displayed in Figure 4.2.

4.3.2 Robust Tensor Decomposition

Gaussian CP (GCP) Decomposition

The idea of the first method consists in resorting to a cost function that does not attribute tremendous errors to outliers as does the classical quadratic cost function used in (4.3). In [88],

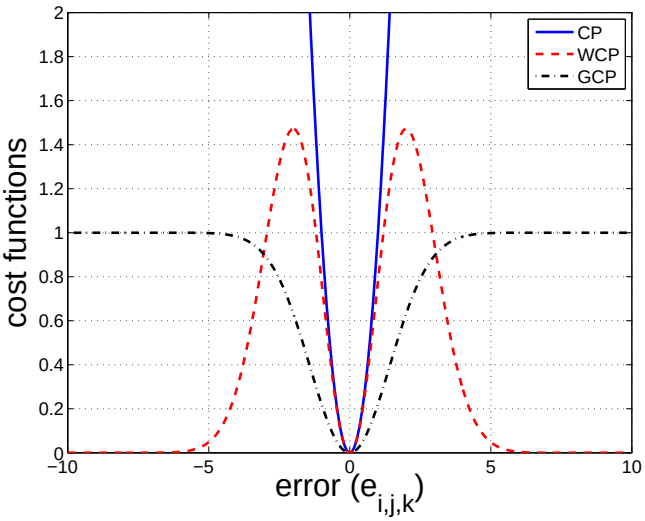

Figure 4.2: Cost functions applied to the error $e_{i,j,k}$ of each tensor element for the classical CP decomposition and the robust WCP and GCP methods.

the use of an L1-norm cost function was proposed. We go a step further and employ a cost function J_G which is based on Gaussian-like functions and limits the maximal error to 1 (see Figure 4.2). This leads to the following optimization criterion:

$$\min_{\{\mathbf{A}^{(q)},\mathbf{S}^{(q)},\mathbf{H}^{(q)}\}} \sum_{i,j,k} \psi\left(y_{ijk}^{(q)} - \sum_{r=1}^{R_q} a_{ir}^{(q)} s_{jr}^{(q)} h_{kr}^{(q)}\right), \tag{4.5}$$

with $\psi(u) = 1 - \exp\{-\frac{u^2}{2\sigma^2}\}$. In this case, an error value of about 3σ between a tensor element and the reconstructed tensor element is treated as an outlier since its effective error value $\psi(u)$ is very close to the maximum value. The parameter σ that adjusts the width of the Gaussian function thus permits to define a threshold between "normal" errors and large outliers and has a high influence on the results of the decomposition. For small σ, most of the errors will be treated as outliers, which makes the identification of the model difficult, while for large σ, outliers might not be recognized and can lead to biased estimates of the loading matrices. The optimal value for σ lies in between and should be chosen according to the data. If available, estimates of the variances of the q-th source to extract, of the noise, and of the other sources can be used to determine an appropriate value for the width of the Gaussian function.

The optimization of the cost function J_G can be accomplished using a gradient descent algorithm. Starting with initial estimates of the loading matrices $\mathbf{A}^{(0)}$, $\mathbf{S}^{(0)}$, and $\mathbf{H}^{(0)}$ (here the superscript denotes the iteration; for a better readability the superscripts referring to the sources

are left out in the following), the loading matrices at iteration l are updated according to

$$\begin{cases} \mathbf{A}^{(l+1)} = \mathbf{A}^{(l)} - \mu_{\mathbf{A}}\, \mathbf{g}_{\mathbf{A}} \\ \mathbf{S}^{(l+1)} = \mathbf{S}^{(l)} - \mu_{\mathbf{S}}\, \mathbf{g}_{\mathbf{S}} \\ \mathbf{H}^{(l+1)} = \mathbf{H}^{(l)} - \mu_{\mathbf{H}}\, \mathbf{g}_{\mathbf{H}} \end{cases} \tag{4.6}$$

until convergence. Here, $\mu_{\mathbf{A}} = \mu_{\mathbf{S}} = \mu_{\mathbf{H}} = \mu$ is a stepsize parameter and $\mathbf{g}_{\mathbf{A}} = \frac{\partial J_G}{\partial \mathbf{A}}$, $\mathbf{g}_{\mathbf{H}} = \frac{\partial J_G}{\partial \mathbf{H}}$, and $\mathbf{g}_{\mathbf{S}} = \frac{\partial J_G}{\partial \mathbf{S}}$ denote the gradients of the cost function J_G with respect to the three loading matrices, respectively. The r-th column of the matrix $\mathbf{g}_{\mathbf{A}} = \frac{\partial \mathbf{J_G}}{\partial \mathbf{A}}$ can be computed as

$$\mathbf{g}_{\mathbf{a}_r} \;=\; -[(\mathbf{h}_r \otimes \mathbf{s}_r) \otimes \mathbf{I}_M]^{\mathrm{T}} \left[\frac{\mathbf{e}_1}{\sigma} \boxdot \exp\left\{ \frac{\mathbf{e}_1 \boxdot \mathbf{e}_1}{2\sigma^2} \right\} \right], \tag{4.7}$$

with $\mathbf{e}_1 = \mathrm{vec}\left\{ [\boldsymbol{Y}]_{(1)} \right\} - [(\mathbf{H} \odot \mathbf{S}) \otimes \mathbf{I}_M] \mathrm{vec}\{\mathbf{A}\}$. Here,

$$\mathbf{A} \otimes \mathbf{B} = \begin{bmatrix} a_{11}\mathbf{B} & \cdots & a_{1R}\mathbf{B} \\ \vdots & \ddots & \vdots \\ a_{M1}\mathbf{B} & \cdots & a_{MR}\mathbf{B} \end{bmatrix}$$

denotes the Kronecker product of matrices $\mathbf{A} \in \mathbb{R}^{M \times R}$ and $\mathbf{B}$, $\odot$ denotes the Khatri-Rao column-wise Kronecker product, $\boxdot$ is the Hadamard element-wise product, $\mathrm{vec}\{\mathbf{A}\}$ is the vector obtained by concatenating the columns of the matrix $\mathbf{A}$, and $\mathbf{I}_M$ is the identity matrix of size $M \times M$. Furthermore, $[\boldsymbol{Y}]_{(1)} \in \mathbb{R}^{M \times (L_q T_q)}$ denotes the first unfolding matrix of the tensor $\boldsymbol{Y}$, which is composed of all mode-1 vectors of the tensor (a mode-1 vector is obtained by fixing the second and third index of the tensor elements and varying the first index from 1 to M) with an ordering such that the second index is varied faster than the third one (for more details and illustrations of operations on tensors see e.g., [91]). The other two gradient matrices are determined in an analogous way.

Since it does not require any information about the data except for an estimate for the threshold between noise and outliers, this robust decomposition method is rather general. It is therefore applicable to a large range of applications. However, to obtain accurate results, a good initialization is required (see Section 4.4.1). This is especially mandatory if the difference between the values of outliers and the values of the signal of interest is in the same range as the amplitude of the signal of interest.

Weighted CP (WCP) Decomposition

The second proposed robust tensor decomposition method is based on the weighted cost function (see the red dashed curve in Figure 4.2):

$$\min_{\{\mathbf{A}^{(q)}, \mathbf{S}^{(q)}, \mathbf{H}^{(q)}\}} \sum_{i,j,k} \left\| w_{ijk}^{(q)} \left(y_{ijk}^{(q)} - \sum_{r=1}^{R_q} a_{ir}^{(q)} s_{jr}^{(q)} h_{kr}^{(q)} \right) \right\|_F^2, \tag{4.8}$$

and exploits the particular structure of the data at hand to determine suitable weights $w_{ijk}^{(q)}$. In fact, for applications with a small variability of the amplitudes, one can exploit the desynchronization of noise and interference which manifests itself by a high variance σ_{ij}^2 over different event-synchronized windows compared to the signal of interest to identify the outliers. The influence of the outliers can then be attenuated by the attribution of low weights while weights close to 1 are assigned to the tensor elements that exhibit a small variance over event-synchronized windows. The weights are thus computed depending on the variance σ_{ij}^2 as

$$w_{ijk}^{(q)} = \exp\left\{-\frac{(y_{ijk}^{(q)} - \mu_{ij})^2}{\sigma_{ij}^2}\right\}, \quad q = 1, \ldots, Q, \tag{4.9}$$

where μ_{ij} is the mean of the tensor elements over all event-synchronized windows, and can be stored into a nonnegative weight tensor, which is of the same dimensions as $\boldsymbol{Y}^{(q)}$. In order to obtain robust estimates for the variances σ_{ij}^2, we use the median absolute deviation (MAD) estimator [92] for their determination.

The optimization of (4.8) can, for example, be performed using a weighted Alternating Least Squares algorithm (see [87]). As for ECG, MCG and EEG signals, the amplitudes for different event-synchronized windows are approximately the same, the WCP decomposition is especially adapted to these applications even if the desired source is much weaker compared with the interfering sources. The reason is that the WCP decomposition exploits the structure of the data to compute weights that discriminate values of the undesired signals in the tensor related to the desired signal. Moreover, contrary to the GCP decomposition, which requires the manual selection of the parameter σ, all the parameters are determined automatically from the data and the technique is robust to initialization. Please note, though, that in the general case, the pattern amplitudes may change considerably from one event-synchronized window to another, which prevents the accurate estimation of the weights using the method described above.

The robust tensor decomposition methods subsequently described can be used to estimate the mixing matrix and to extract the temporal patterns and the amplitudes of the event-related sources. This is already an advantage over a matrix decomposition using the SVD, where one only obtains an estimate of the subspace spanned by the mixing matrix and no information about individual pattern amplitudes, because the temporal structure of the event-related sources is not exploited.

4.4 Results

Both synthetic and actual data have been used to study the performance of the proposed method. In the first subsection, quantitative results coming from simulations have been studied. In this subsection, the robustness of the proposed tensor decomposition methods to amplitude variations, quantity of outliers, initialization, and synchronization errors is examined based on simulations for both arbitrary tensors and tensors constructed from data of event-related sources. In the second subsection, the performance of the proposed method in fetal cardiac

signal extraction on two sets of actual data including ECG and MCG has been assessed.

4.4.1 Simulated Data

Robust Decomposition of Arbitrary Trilinear Tensors in the Presence of Outliers

First of all, we analyzed the performance of the proposed robust tensor decomposition methods for arbitrary tensors containing outliers. To this end, we generated a set of arbitrary loading matrices $\mathbf{A} \in \mathbb{R}^{5\times 2}$, $\mathbf{S} \in \mathbb{R}^{10\times 2}$, and $\mathbf{H} \in \mathbb{R}^{10\times 2}$. The elements of $\mathbf{A}$ and $\mathbf{H}$ were random variables chosen from a uniform distribution between -1 and 1. The elements of $\mathbf{S}$ were chosen from a Gaussian distribution with mean 1 and variance $\sigma_S^2 = 0.04$. The tensor was then constructed from the matrices $\mathbf{A}$, $\mathbf{S}$ and $\mathbf{H}$ according to (4.2). To simulate outliers, we falsified a certain percentage p of randomly selected tensor values by adding or subtracting 2. The value 2 has been chosen arbitrarily such that it is large enough to be considered as an outlier, but close enough to the values of other tensor elements to remain realistic. Furthermore, we added white Gaussian noise according to an SNR of 20dB. The resulting tensor was then decomposed using the CP, WCP and GCP decompositions. For initialization, we took the original loading matrices and added zero-mean Gaussian noise with variance σ_i^2. We computed each decomposition three times for different initializations and retained the estimated loading matrices that were obtained for the minimal value of the cost function. The accuracy of the estimated loading matrices $\hat{\mathbf{A}}$, $\hat{\mathbf{S}}$, and $\hat{\mathbf{H}}$ was evaluated using the following measure:

$$E_{\mathrm{LM}} = \frac{1}{3R} \min_{\mathbf{P}} \{ ||\mathbf{A}' - \hat{\mathbf{A}}'\mathbf{D_A}\mathbf{P}||_{\mathrm{F}} + ||\mathbf{S}' - \hat{\mathbf{S}}'\mathbf{D_S}\mathbf{P}||_{\mathrm{F}} + ||\mathbf{H}' - \hat{\mathbf{H}}'\mathbf{D_H}\mathbf{P}||_{\mathrm{F}} \}, \tag{4.10}$$

where R denotes the number of components, $\mathbf{P}$ is a permutation matrix and the matrices $\mathbf{A}'$, $\mathbf{S}'$, $\mathbf{H}'$, $\hat{\mathbf{A}}'$, $\hat{\mathbf{S}}'$, and $\hat{\mathbf{H}}'$ correspond to the original and estimated loading matrices normalized to unit column norm. Furthermore, $\mathbf{D_A}$, $\mathbf{D_S}$, and $\mathbf{D_H}$ are diagonal matrices whose elements correspond the signs of the elements on the diagonal of the correlation matrices $(\mathbf{A}')^{\mathrm{T}}\hat{\mathbf{A}}'$, $(\mathbf{S}')^{\mathrm{T}}\hat{\mathbf{S}}'$, and $(\mathbf{H}')^{\mathrm{T}}\hat{\mathbf{H}}'$ and which are introduced to compensate for the sign ambiguity. Subsequently, we analyzed the influence of different parameters on this error for 100 Monte Carlo trials.

Influence of Percentage of Outliers Figure 4.3 shows the error of the loading matrices, E_{LM}, as a function of the percentage of outliers p for $\sigma_i = 0.5$. It can be seen that the error of the GCP decomposition is very small (< 0.1) over a large range of values of p ranging from 1 to 50% before the high percentage of outliers leads to an increasing error. This means that this method is very robust to even a large amount of randomly distributed outliers in the tensor. With an error that is slightly smaller than that of the GCP decomposition and which has a smaller variance, the WCP decomposition achieves a slightly better performance for small percentages of outliers ($p < 10\%$). Yet for $p > 10\%$, the error increases significantly with p, showing that the WCP is only robust to a limited number of outliers. This sensitivity of the WCP decomposition method is due to the estimation of the weights, which is not robust to a large number of outliers. However, for all examined percentages of outliers, both WCP and GCP methods show a much

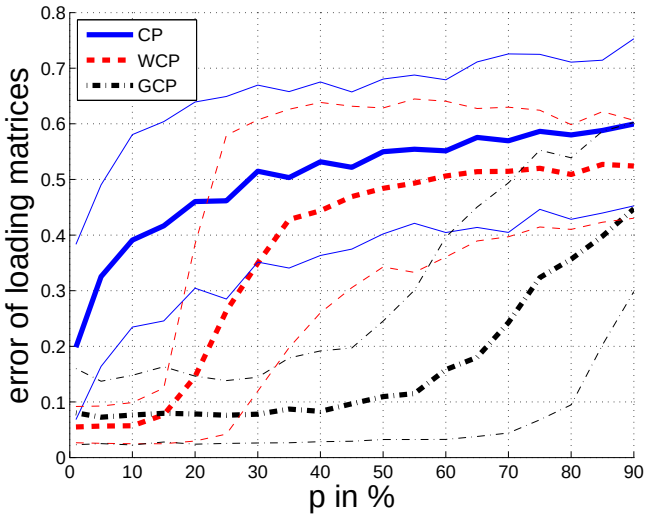

Figure 4.3: Error of the loading matrices as a function of the percentage of outliers. The bold curves show the results averaged over 100 trials while the 10% and 90% quantiles are represented by the thin curves.

better performance than the classical CP decomposition, which is not robust to outliers and already exhibits a large error of 0.2 for only 1% of outliers.

Influence of Initialization To analyze the influence of the initialization on the decomposition results, we varied the variance σ_i^2 of the Gaussian noise that is added to the original loading matrices to obtain a set of initial loading matrices. The percentage of outliers was fixed to 10%. Figure 4.4 shows that the results of the WCP decomposition and the classical CP decomposition hardly change for different initializations, with an average error increasing only slightly from 0.04 to 0.1 for the WCP decomposition and from 0.37 to 0.4 for the CP decomposition. With 80% of the errors lying between 0.23 and 0.6, the variance of the error is high for the CP decomposition and is independent of the initialization. On the other hand, the variance of the error of the WCP decomposition increases with σ_i, attaining very small values for $\sigma_i < 0.5$ and moderate values for bad initializations. On the whole, the WCP and CP decompositions can be said to be robust to initialization. On the contrary, the GCP decomposition features a strong increase of the error for rising σ_i, in particular between $\sigma_i = 1$ and $\sigma_i = 3$. In this interval, the mean error increases from 0.1 to 0.7. For small $\sigma_i < 1$, i.e., if the initial loading matrices are close to the exact loading matrices, the GCP decomposition yields good results with a very small variance, outperforming the WCP decomposition when σ_i becomes very small, while for $\sigma_i > 2$, its results are even worse than those of the classical CP decomposition. As the Gaussian cost function assumes values close to 1 for all errors exceeding a certain threshold (see Section 4.3.2), the optimization criterion of the GCP decomposition can be expected to exhibit an increased number of local minima. If the initialization is not close to the true solution, the GCP decomposition algorithm is prone to find a local minimum. This explains the strong dependence of the results of the GCP decomposition on the initialization.

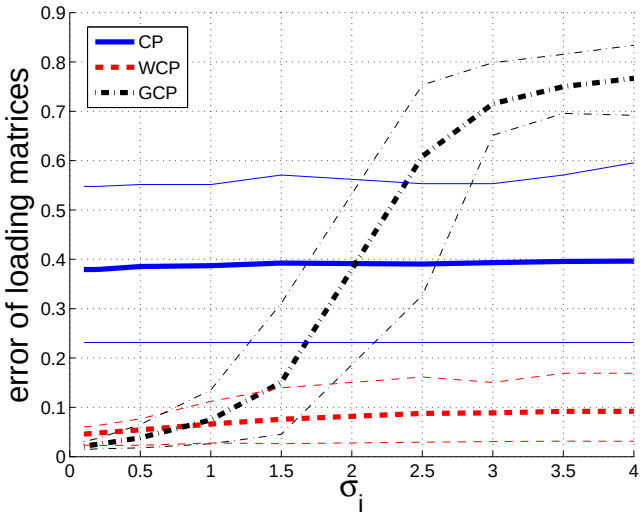

Figure 4.4: Error of the loading matrices as a function of the variance of the Gaussian noise added to the true loading matrices to obtain the initial loading matrices. The bold curves show the results averaged over 100 trials while the 10% and 90% quantiles are represented by the thin curves.

Robust Decomposition of Tensors of Event-Related Data

In the present chapter, we focus on event-related sources. Therefore, we consider in the following tensors constructed from data containing a mixture of two event-related sources with one component per source. The elements of the mixing matrices $\mathbf{A}^{(q)} \in \mathbb{R}^{5\times 1}$, $q = 1, 2$, were chosen from a uniform distribution between -1 and 1 and the amplitudes $\mathbf{S}^{(q)}$ were chosen from a Gaussian distribution with mean 1 and variance σ_S^2. The temporal patterns of the first and second sources, stored in matrices $\mathbf{H}^{(q)}$, were given by $\exp\{-\frac{(x_1-0.5T_1)^2}{2\alpha_1^2}\}$ with $\alpha_1 = 0.1$ and $\exp\{-\frac{(x_2-0.5T_2)^2}{2\alpha_2^2}\}$ with $\alpha_2 = 0.15$ where x_1 and x_2 are the indices of the time samples and $T_1 = 101$ and $T_2 = 59$ correspond to the lengths of the patterns of the first and second source, respectively. On the whole, we considered 2020 time samples of data, containing 20 periods of the first source and 34 periods of the second source, in the presence of white Gaussian noise for an SNR of 20dB. The tensors were then constructed as described in Section 4.3.1 for 100 different trials. For the decomposition, the loading matrices were initialized as described in the previous section with $\sigma_i = 0.2$.

Influence of Amplitude Variability The objective of the first simulation consisted in evaluating the influence of the variance of the amplitudes $\mathbf{S}^{(q)}$. To this end, σ_S was varied between 0.1 and 4 for both sources such that the variances of their amplitudes were equal. Figure 4.5 shows the error of the loading matrices of the two tensors as a function of the standard deviation σ_S of the amplitudes. For the classical CP and GCP decompositions, the errors of the loading matrices decrease with increasing σ_S. This can be explained by the fact that for small σ_S, the tensors are close to the degenerate case, while a higher amplitude variability facilitates the tensor

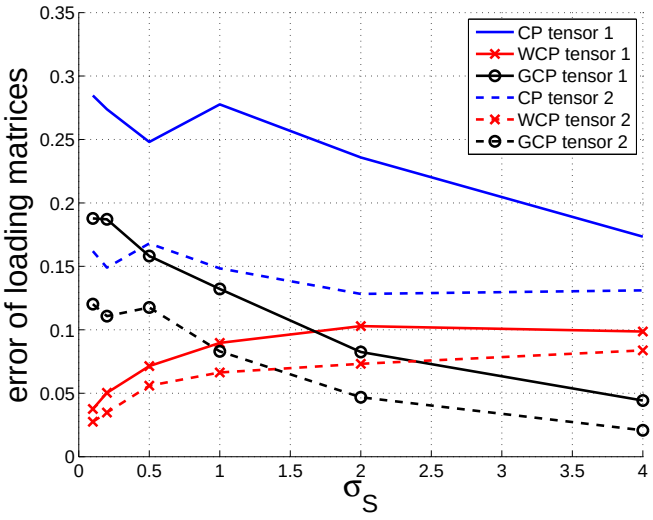

Figure 4.5: Error of the loading matrices as a function of the amplitude standard deviation σ_S for the tensor of the first source (tensor 1) and the tensor of the second source (tensor 2).

decomposition and the separation of different components. For the WCP decomposition, the best performance is achieved for small σ_S. In this case, the amplitude variation is small enough so that the peaks of the second source in the tensor of the first source and vice versa are outlying values and do not influence the computation of the weights. However, for increasing σ_S, the amplitudes become high enough for the peaks of the interfering sources to lie within the range of amplitudes that are attained by the source to be extracted. In this case, the interfering sources do not enter as outliers in the computation of the weights, which will corrupt the estimation of the weights. This leads to an increase of the errors of the loading matrices with rising σ_S.

Influence of Synchronization Errors To analyze the influence of synchronization errors (after the tensor construction, which was accomplished with perfect synchronization), we introduced artificial delays for each event period to model synchronization errors. The delays were uniformly distributed between $-\tau_{max}$ and τ_{max}, with τ_{max} chosen between 0 and $T_q\alpha_q$ samples, where α_q determines the width of the Gaussian function that characterizes the temporal pattern of the q-th source, $q = 1, 2$. The standard deviation of the amplitudes was fixed to $\sigma_S = 0.2$. Figure 4.6 shows that the error of the loading matrices increases rapidly with rising maximal delay. This means that the good synchronization of the signals in each tensor is crucial for the accuracy of the proposed method.

4.4.2 Actual Data

Fetal ECG Extraction

The ECG data used in this subsection is the DaISy fetal ECG database [71], which has been described in Appendix A, Section A.1.

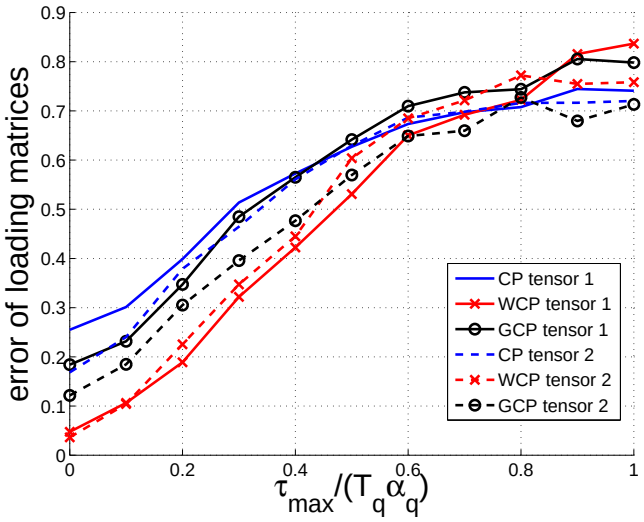

Figure 4.6: Error of the loading matrices as a function of the maximal relative synchronization error (right) for the tensor of the first source (tensor 1) and the tensor of the second source (tensor 2).

The first and second channels of this dataset used in this section and their stacked mECG beats arranged in the tensor are shown in the first and second rows of Figure 4.7. In order to construct the tensor, one can first detect mECG R-peaks to identify different beats, then the data of the mECG beats comprising a fixed number of time samples around each R-peak are stacked into the tensor. The constructed mECG tensor is of size $2 \times 12 \times 184$. As it is seen, fECG interference does not have a strong contribution in the maternal tensor. Therefore, this tensor can be decomposed via classical CP in equation (4.3). However, as seen in the third row of this Figure, although the two extracted components satisfy the optimization problem in equation (4.3), they are highly correlated and do not correspond to two different projections of mECG. In order to obtain two uncorrelated components, PCA has been applied to the extracted components. As it is seen in the fourth row of Figure 4.7, this results in two less-correlated components, which correspond to two different projections of mECG.

The first row of Figure 4.8 shows the stacked fECG beats from the channels 1 and 2 arranged in the tensor. The constructed fECG tensor is of size $2 \times 22 \times 113$. In contrast to the maternal tensor that was not highly affected by the fECG interference, the fetal tensor is significantly impacted by the interfering mECG.

Since the fetal ECG has a weak contribution in the mixture of mECG, fECG and noise, only one component is considered for this signal. The second row of Figure 4.8 shows the extracted fetal ECG component via classical CP. Since classical CP searches for the concentration of power in the constructed tensor, the extracted component has a peak between 60 to 80 samples, which corresponds to the dense interference of maternal ECG. Classical CP is therefore unable to recover the weak traces of the fetal signal and the extracted component does not correspond to the fECG. The third row of Figure 4.8 shows the extracted fetal ECG component via WCP. The

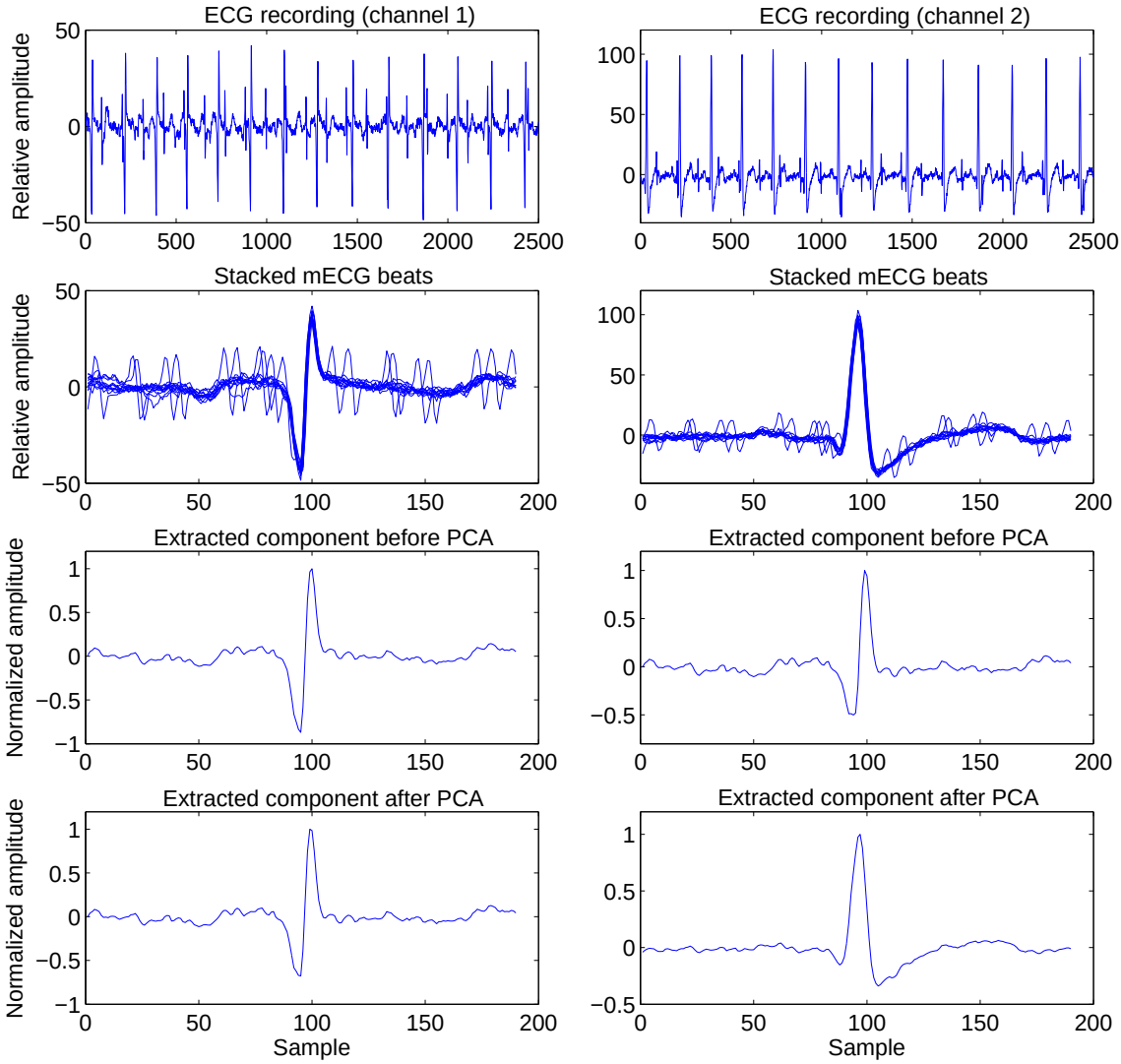

Figure 4.7: Maternal components extraction via classical CP on DaISy dataset. Top to bottom: recorded mixed ECG signals on the channels 1 and 2; stacked maternal ECG beats arranged in the maternal tensor; normalized extracted maternal ECG components before PCA; normalized extracted maternal ECG components after PCA.

WCP decomposition exploits the structure of the data to compute weights for discriminating values of the fetal signal in the constructed tensor related to the fECG. Therefore, it attributes low weight values for high-amplitude mECG interference for efficiently recovering the weak traces of fetal ECG. As it is seen in the fourth row of Figure 4.8, GCP is also able to cancel out strong interfering mECG for fetal component extraction.

Figure 4.9 shows maternal and fetal ECG estimates via tensor decomposition method from the channels 1 and 2 of DaISy dataset. As it is seen, interfering ECG has been efficiently canceled out in the estimate of desired ECG. This is seen for both maternal and fetal ECG estimates. As the drawback of the proposed method, it should be noted that the inter-beat dynamics of mECG and fECG are lost in tensor decomposition method, because all beats of the reconstructed ECGs have exactly the same temporal pattern up to their amplitudes. Moreover, starting and ending incomplete ECG beats cannot be recovered in this case. It is also observed that when mECG and fECG waves fully overlap in time, the reconstructed fECG has relatively low amplitude in the corresponding beat, especially in the GCP estimate. Therefore, WCP outperforms GCP in this experiment.

Twin MCG Extraction

In this subsection, twin fetal cardiac magnetic signals are extracted. The dataset used in this subsection has been described in Appendix A, Section A.3. Two sensors are used in this test. The presented results have been achieved for a typical couple of channels (indexed 92 and 116) of one of the available datasets, namely the q00002252 dataset.

To extract sources by the proposed tensor decomposition, they must have different pattern rates. As long as two sources are not exactly synchronous, they can be separated even if their pattern rates are approximately the same. This enables the method to separate twin cardiac signals even if heart rates are approximately equal. However, in this case, the interference of the second source in the tensor of the first source might be concentrated within a certain interval of the temporal pattern. This happens especially if the tensor is built from a small number of events. In this case, the correct decomposition of the tensor is particularly difficult and cannot be achieved by the classical CP decomposition. The introduction of the weights in the WCP method permits us to overcome this problem and to focus on the signal of interest. This discrimination is also provided by the Gaussian function in the first approach (GCP).

There are three sources to be extracted, one maternal MCG and two fetal MCGs, while two channels are to be utilized. Nevertheless, since the proposed method is applicable to underdetermined mixtures, two sensors can be sufficient for extracting these three sources. The maternal and fetal MCG ranks considered in the proposed method are 2 and 1, respectively. Figure 4.10 shows mixed MCG recordings on channels 92 and 116 and the corresponding stacked fetal MCG beats from these channels. The maternal and twin tensors are constructed with parameters $L_1 = 15$, $T_1 = 619$, $L_2 = 22$, $T_2 = 440$, $L_3 = 23$, and $T_3 = 408$, respectively. As seen, in the fourth and fifth rows of Figure 4.10, WCP and GCP could track the desired MCG in presence of the strong interfering maternal MCG and the other fetal MCG which has a close pattern

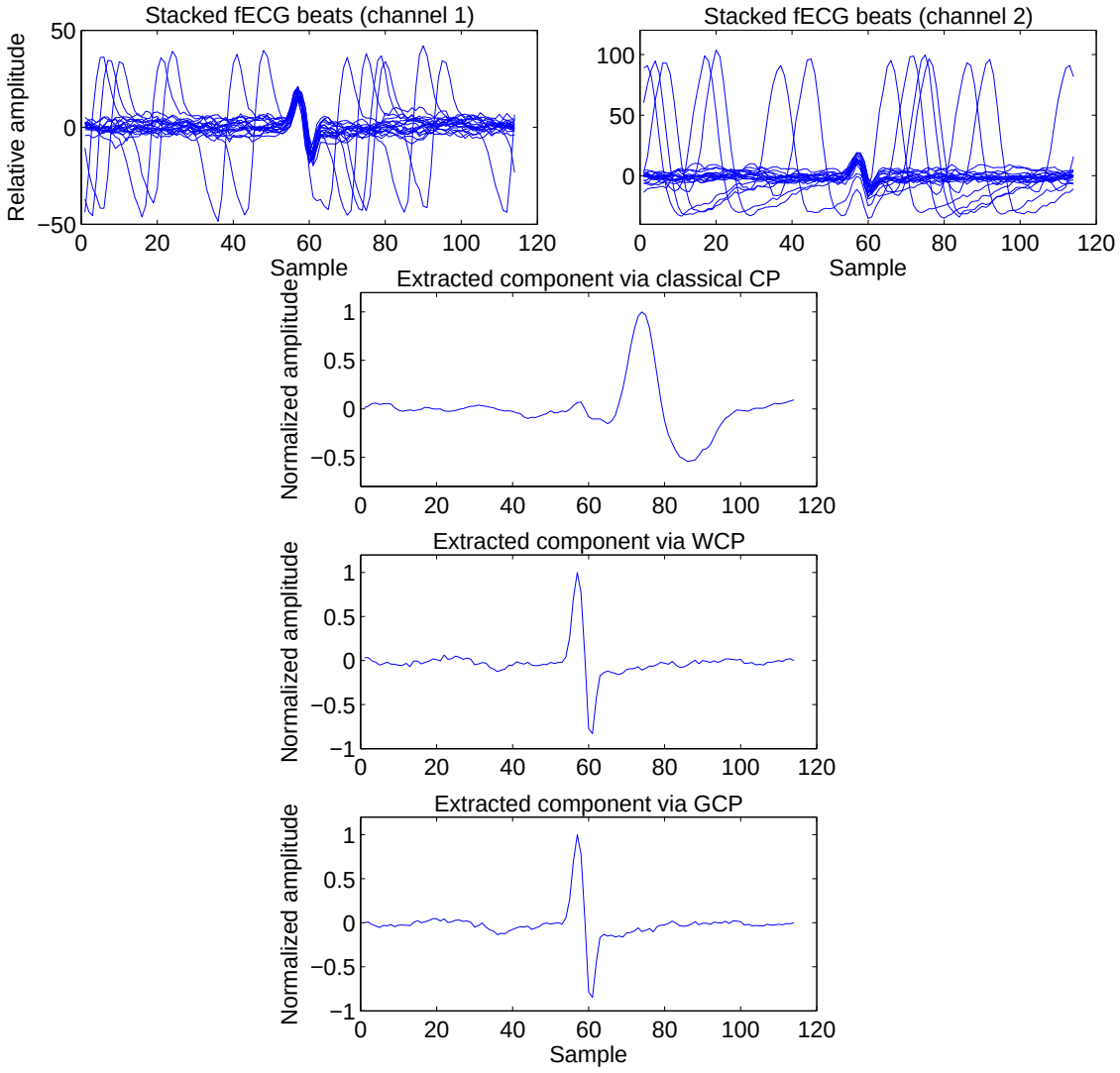

Figure 4.8: Fetal component extraction via classical CP, WCP and GCP on DaISy dataset. Top to bottom: stacked fetal ECG beats arranged in the fetal tensor from the channels 1 and 2, normalized extracted fetal ECG component via classical CP, normalized extracted fetal ECG component via WCP, normalized extracted fetal ECG component via GCP.

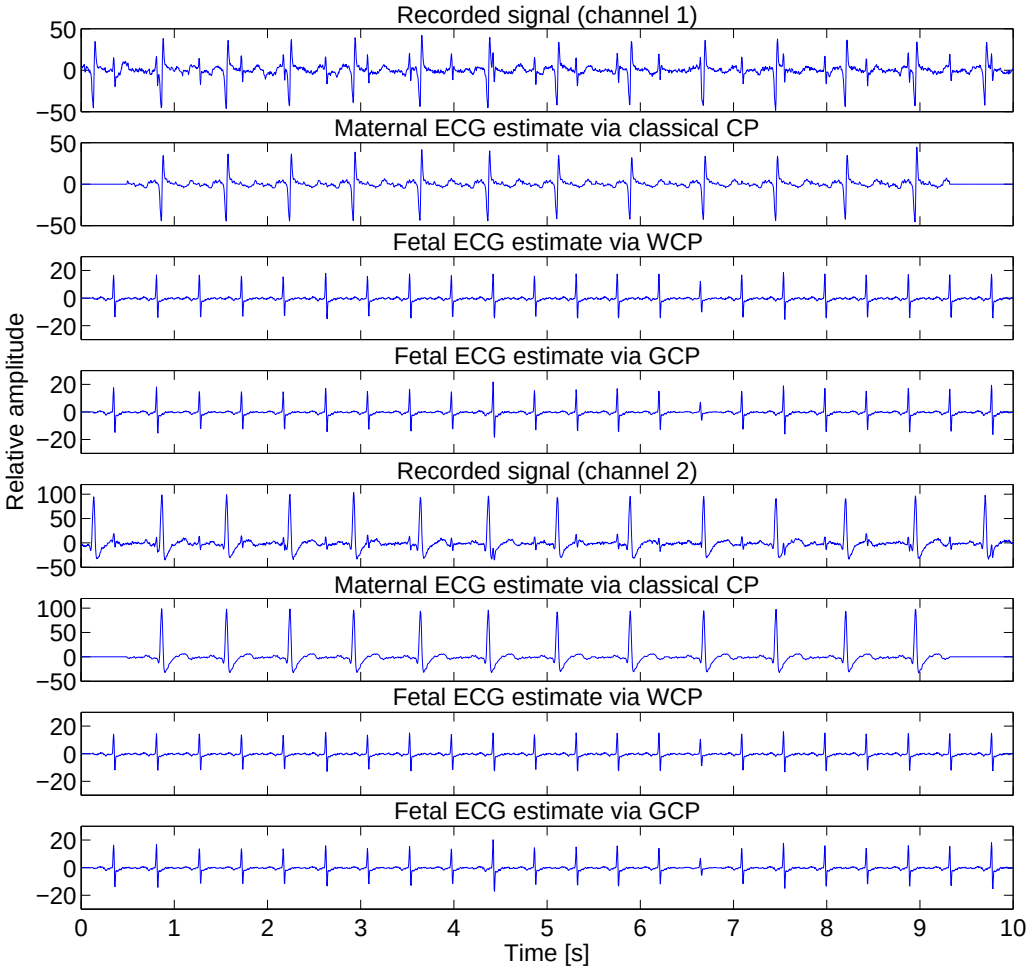

Figure 4.9: Maternal and fetal ECG extraction via tensor decomposition. Top to bottom: Mixed ECG recording, reconstructed mECG via classical CP, reconstructed fECG via WCP, and reconstructed fECG via GCP on the channels 1 and 2 of DaISy dataset.

rate. To suppress the large amount of noise that is present in the data, we also used the WCP decomposition for the maternal MCG tensor.

Figure 4.11 presents the extracted maternal and two fetal MCG signals from channel 92 using channels 92 and 116. In this experiment, WCP method significantly outperforms GCP, especially when maternal and fetal MCG waves overlap in time. In contrast to WCP method, in which interfering MCGs are efficiently canceled out in the estimate of desired MCG, the interfering maternal MCG and noise significantly prevented GCP method in providing true amplitude values for certain fetal MCG beats.

Here again, the starting and ending incomplete MCG beats cannot be recovered and the inter-beat dynamics of maternal and fetal MCGs are lost in tensor decomposition method. Therefore, another method is of interest as the next step for recovering the valuable inter-beat dynamics of ECG and MCG signals (see the next chapter).

4.5 Application to Fully Automatic Fetal R-peak Detection

Detection of fetal R-peaks is a key step in many fetal ECG extraction methods in which quasi-periodic nature of ECG signal is exploited (e.g. πCA [30], EKF framework in [13] and Chapter 3). In these methods, it is assumed that the fetal R-peaks are either already provided using another modality (e.g. using a sound sensor) or directly estimated from ECG mixture. As it has been explained in Section 3.4.2, the latter can be done by using the seq-EKF algorithm. In this case, maternal R-peaks are easily detectable from the mixture by an automatic peak search algorithm, while detection of fetal R-peaks is not fully automatic. In this method, because of low amplitude of fetal ECG, maternal ECG is first eliminated from the mixture by the EKF framework and then the residual signal is used for fetal R-peaks detection. However, efficient elimination of maternal ECG requires careful selection of the center of Gaussian functions, which is done manually by visual inspection of maternal ECG mean. The simplest way to automatize mECG elimination is to reconstruct mECG by concatenating maternal ECG mean at maternal R-peaks. However, in this case all mECG beats are assumed to have exactly the same amplitude. This assumption can significantly impact the performance of maternal ECG elimination.

The method proposed in this chapter, which is fully automatic, can be used to recover amplitudes of different beats of mECG to efficiently eliminate mECG. First, maternal R-peaks are directly detected from the mixture to identify maternal beats as the ECG pattern. Then the maternal ECG beats are stacked into a three-dimensional array. Decomposition of this tensor yields three loading matrices including the mixing matrix, the matrix of mECG beat amplitudes, and the matrix containing the temporal pattern of mECG beat. Using these matrices mECG is reconstructed and projected back to the sensor domain to be subtracted from the mixture. The residue of the subtraction, i.e. rough fECG estimate, is then used to detect fetal R-peaks using an automatic peak search algorithm.

Figure 4.12 illustrates the performance of the proposed method on ten seconds of the first channel of the recording a22 of the PhysioNet Challenge 2013 dataset [93], which has been described in Appendix A Section A.4 As it is seen, the proposed method is favorably able to

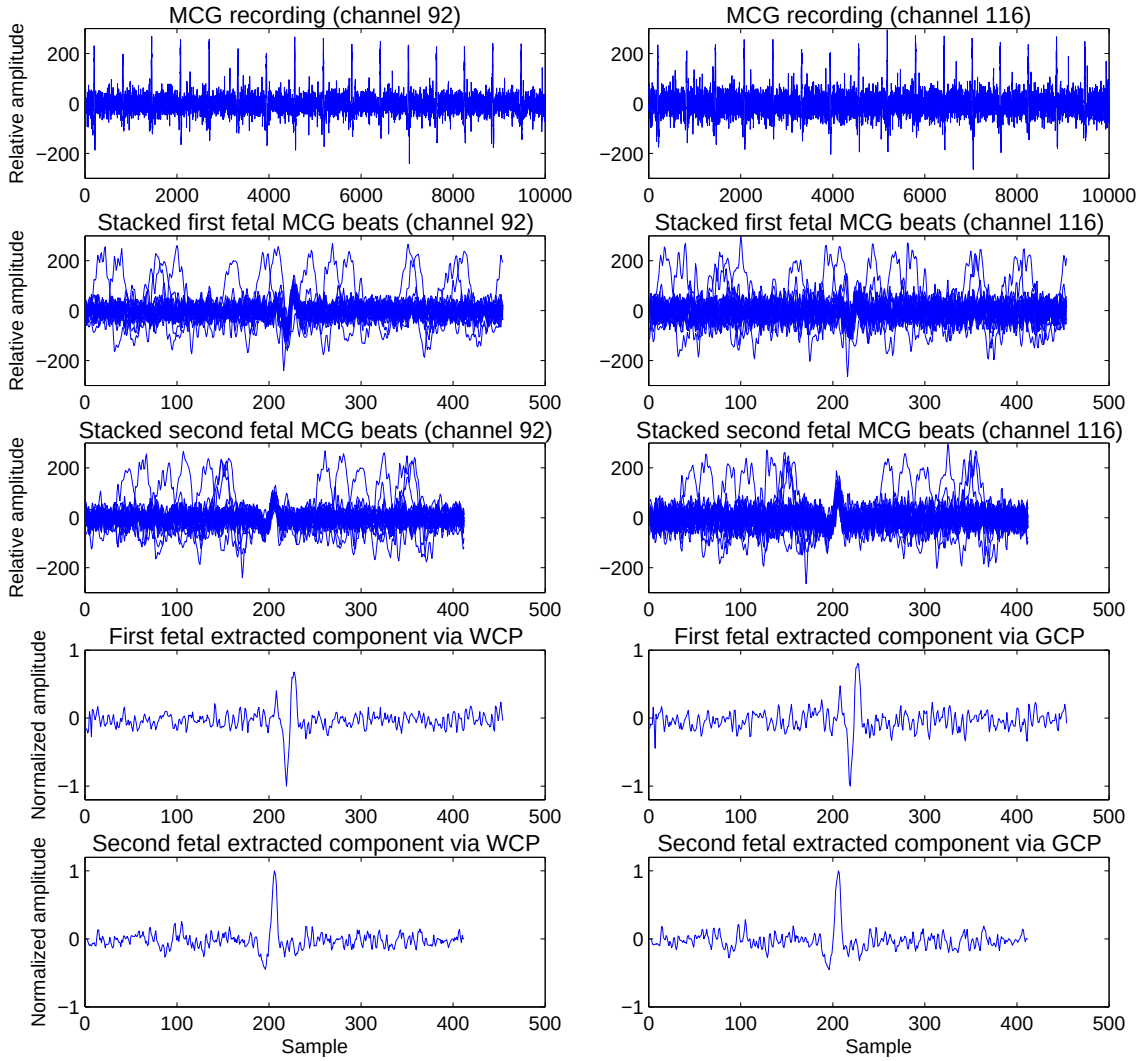

Figure 4.10: Fetal component extraction via WCP and GCP on twin MCG dataset. Top to bottom: recorded mixed MCG signals on the channels 92 and 116, stacked first fetal MCG beats arranged in the fetal tensor from the channels 92 and 116, stacked second fetal MCG beats arranged in the fetal tensor from the channels 92 and 116, normalized extracted first fetal MCG component via WCP and GCP, normalized extracted second fetal MCG component via WCP and GCP.

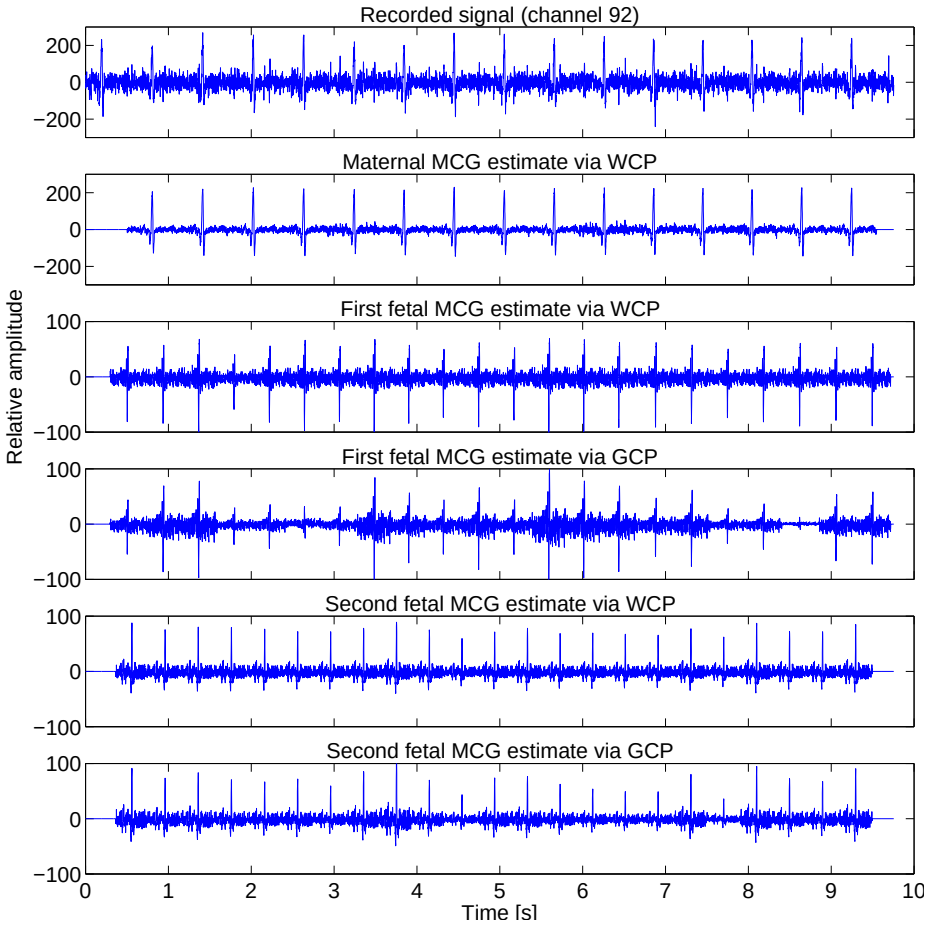

Figure 4.11: Maternal and fetal MCG extraction via tensor decomposition. Top to bottom: Mixed MCG recording, maternal MCG reconstructed via WCP, first fetal MCG reconstructed via WCP, first fetal MCG reconstructed via GCP, second fetal MCG reconstructed via WCP, and second fetal MCG reconstructed via GCP.

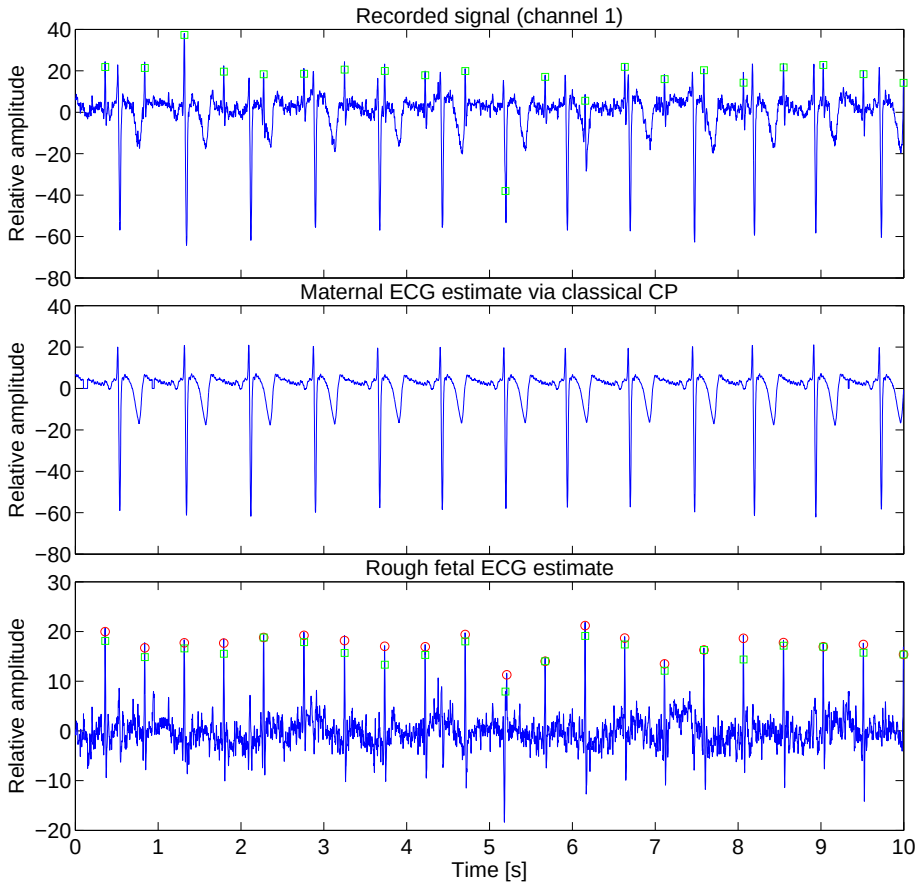

Figure 4.12: Fetal R-peaks detection via tensor decomposition on the recording a22 of the PhysioNet Challenge 2013. Top to bottom: mixed ECGs on channel 1, reconstructed maternal ECG via classical CP, residue of subtraction of reconstructed mECG from the mixture, i.e. rough fECG estimate. Given fetal R-peaks are shown in green squares and estimated fetal R-peaks are shown in red circles.

detect fetal R-peaks even in coinciding epochs, in which maternal and fetal ECG waves fully overlap in time. This is particularly noticed between t = 5s and t = 6s, where some parts of fECG signal have been corrupted after mECG subtraction.

The obtained average scores of event 4 and 5 on the set B of PhysioNet Challenge 2013 data, reported by the challenge organizers, are 1514.59 and 57.01, respectively. As a reference, the scores from the sample submission physionet2013.m (available at PhysioNet) on set B for event 4 and 5 are 3258.56 and 102.75, respectively, where the lower the scores the better. The method used in the sample submission physionet2013.m for mECG removal is based on the reconstruction of the mECG signal by concatenating maternal ECG mean at maternal R-peaks, as explained above.

4.6 Summary and Conclusions

In this chapter, we presented two robust tensor decompositions for separation of event-related sources with focus on fetal cardiac signal extraction. The robust criteria used in this chapter aim at capturing the desired event-related sources even if their powers are much lower compared with other sources.

This method is also applicable to underdetermined mixtures and this is its main interest. It allows us to utilize a minimal number of electrodes (down to two), if needed. This is a crucial feature for a monitoring system since it can highly affect the system's price, convenience and portability. Although good synchronization of events of the desired source in its tensor format is crucial for the functioning of the proposed method, application on actual fetal cardiac data shows its capability in capturing weak traces of fetal components mixed with strong maternal components and noise. Nonetheless, the main drawback of the proposed method is that it is not able to recover valuable inter-event dynamics of the desired sources. Thereby, the next chapter is devoted to develop such a method that recovers these important inter-event dynamics.

Chapter 5

Multichannel Kalman Filtering Framework for Extraction of Event-Related Sources

5.1 Introduction

Linear multichannel fECG extraction methods aim at exploiting the redundancy of the multichannel ECG recordings to reduce mECG and other interference sources. Nonetheless, the main drawback of these methods is that they are not able to totally remove exogenous noise [49]. Moreover, they demand several channels to track weak traces of fetal signal. In the previous chapter, a robust tensor decomposition method was proposed to address the above-mentioned obstacles. However, as the tensor decomposition model assumes identical temporal patterns for all events of each source, the dynamics of the sources, i.e., slight variations from one event to another, are lost. In order to recover these dynamics, a nonlinear state-space model is developed to extract N event-related sources (or components) from M observations. This model is used within a Kalman filtering framework, whose mixing matrix and state parameters are obtained from the loading matrices of the tensor decomposition. The proposed method, which is a combination of linear (tensor decomposition) and nonlinear (extended Kalman filter) methods, simultaneously extracts and denoises fECG signal and is applicable to as few as two channels.

Although we will mainly focus on the application of the proposed method on fetal cardiac signal extraction, the method is fairly general and may be applied to many applications. As an example for other applications, the proposed method is also applied to extract ERPs.

The rest of this chapter is organized as follows. In Section 5.2, a general EKF framework for extraction of event-related sources from multichannel recordings is presented. The mixing matrix and the filter parameters are estimated using the loading matrices provided by the robust tensor decomposition method, presented in the previous chapter. This framework is then customized to ECG signals for extracting N ECG components from M observations. The performance of the proposed method is investigated in Section 5.3. Qualitative results of the proposed method is compared with those of three multichannel BSS methods on fetal ECG and MCG datasets.

Then, the method is applied to extract ERPs to show its applicability to other kinds of event-related data. The multichannel method proposed in this chapter is also compared with the single-channel method in Chapter 3 to check if adding an extra channel recording could improve the performance of fECG extraction. This comparison is quantitative and is performed by means of synthetic data. Section 5.4 is devoted to propose a new approach for estimating the phase state of ECG signal. This approach aims at simultaneously filtering normal and abnormal ECG segments. Finally, a summary of this chapter and the conclusions are stated in Section 5.5.

5.2 Methods

5.2.1 EKF Framework for Extraction of Event-Related Sources

Assuming a single event-related source recorded on a unique channel, the associated state vector can be defined by the phase θ_k and amplitude z_k of the source. The phase θ_k is, in fact, a means of modeling the event-related behavior of the source. Then, each period of the source is modeled using θ_k to obtain z_k. By inspiration of the ECG model in Chapter 3, the state model of the event-related source, in its discrete form with a small sampling period δ, can be expressed as:

$$\begin{cases} \theta_{k+1} = (\theta_k + \omega\delta) \mathrm{mod}(2\pi) \\ z_{k+1} = g(\theta_k, k) + z_k + \eta_k \end{cases} \tag{5.1}$$

where θ and z are the state variables in polar coordinates and k denotes the discrete time index. ω is the phase increment, η_k is a random additive noise, and $g(.)$ models the temporal pattern and amplitude of the source. In addition to the noisy recording of the source, s_k, an observed phase ϕ_k is obtained by a linear time warping of each event interval into $[0, 2\pi)$, leading to the following system:

$$\begin{bmatrix} \phi_k \\ s_k \end{bmatrix} = \begin{pmatrix} 1 & 0 \\ 0 & 1 \end{pmatrix} \begin{bmatrix} \theta_k \\ z_k \end{bmatrix} + \begin{bmatrix} u_k \\ v_k \end{bmatrix}, \tag{5.2}$$

in which, u_k and v_k are the corresponding observation noises with zero-mean random variable entries.

With several event-related sources in multichannel recordings, redundancy of each event-related source can be exploited to estimate the information of the desired source mixed with the other sources and background noise. In order to do so, a linear transform is assumed to decompose M mixed event-related signals into N components. In other words, we assume that all event-related sources have N components in total, which are observed in M signals. For N

mixed components, the dynamic equations may be written as:

$$\begin{cases} \theta_{k+1}^{(1)} = (\theta_k^{(1)} + \omega^{(1)}\delta)\text{mod}(2\pi) \\ z_{k+1}^{(1)} = g^{(1)}(\theta_k^{(1)}, k) + z_k^{(1)} + \eta_k^{(1)} \\ \vdots \\ \theta_{k+1}^{(N)} = (\theta_k^{(N)} + \omega^{(N)}\delta)\text{mod}(2\pi) \\ z_{k+1}^{(N)} = g^{(N)}(\theta_k^{(N)}, k) + z_k^{(N)} + \eta_k^{(N)} \end{cases} \tag{5.3}$$

The phase observations of the N components, $\mathbf{\Phi} = [\phi^{(1)},...,\phi^{(N)}]^T$, and the M noisy mixtures of the N components, $\mathbf{s} = [s^{(1)},...,s^{(M)}]^T$, are related to the state vectors $\mathbf{\Theta} = [\theta^{(1)},...,\theta^{(N)}]^T$ and $\mathbf{z} = [z^{(1)},...,z^{(N)}]^T$ at time k as follows:

$$\begin{bmatrix} \mathbf{\Phi}_k \\ \mathbf{s}_k \end{bmatrix} = \begin{pmatrix} \mathbf{I} & \mathbf{0} \\ \mathbf{0} & \mathbf{A} \end{pmatrix} \begin{bmatrix} \mathbf{\Theta}_k \\ \mathbf{z}_k \end{bmatrix} + \begin{bmatrix} \mathbf{u}_k \\ \mathbf{v}_k \end{bmatrix}, \tag{5.4}$$

where $\mathbf{u}_k$ and $\mathbf{v}_k$ are the corresponding observation noises.

The key step prior to the implementation of the filter is the estimation of $g^{(n)}(.)$ for the n-th component as well as the mixing matrix $\mathbf{A}$:

$$\mathbf{A} = \begin{bmatrix} a_{11} & \dots & a_{1N} \\ \vdots & \ddots & \vdots \\ a_{M1} & \dots & a_{MN} \end{bmatrix}. \tag{5.5}$$

In order to do so, the loading matrices provided by GCP or WCP in the previous chapter, Section 4.2.2 are used:

- The mixing matrix is directly defined as the concatenation of the loading matrices $\mathbf{A}^{(n)}$ related to all the event-related source components.
- The temporal pattern of $g^{(n)}(.)$ for the n-th component is provided by the loading matrix $\mathbf{H}^{(n)}$. For example if the $n-th$ components is modeled by a few Gaussian functions, similar to Chapter 3, the parameters of $i-th$ Gaussian function $(\alpha_i^{(n)}, b_i^{(n)}, \psi_i^{(n)})$ can be estimated by using a nonlinear least-squares approach [68] to fit to the extracted component.
- The amplitude of $g^{(n)}(.)$ for the n-th component at each period is obtained by the loading matrix $\mathbf{S}^{(n)}$. By assuming that $\eta_k^{(1)},..,\eta_k^{(N)}$ are uncorrelated, a ratio (e.g. 0.1) of standard deviation of $\mathbf{S}^{(n)}$ can be used as the estimate of $\eta_k^{(n)}$ for initializing the state covariance matrix Q_k.

For multichannel recordings of maternal and fetal ECG signals, the extended EKF model presented in Chapter 3 for modeling several ECGs in a single-channel recording, can be further extended to M channels. In this case, the same system state as in Section 3.4.1 can be used:

$$
\begin{cases}
\theta_{k+1}^{(1)} &= (\theta_k^{(1)} + \omega^{(1)}\delta)\mathrm{mod}(2\pi) \\
z_{k+1}^{(1)} &= -\sum_{i\in\mathscr{W}^{(1)}} \delta \frac{\alpha_{i,k}^{(1)}\omega^{(1)}}{b_{i,k}^{(1)^2}} \Delta\theta_{i,k}^{(1)} \exp\left(-\frac{\Delta\theta_{i,k}^{(1)^2}}{2b_{i,k}^{(1)^2}}\right) + z_k^{(1)} + \eta_k^{z^{(1)}} \\
\alpha_{i,k+1}^{(1)} &= \alpha_{i,k}^{(1)} + \eta_k^{\alpha_i^{(1)}} \\
b_{i,k+1}^{(1)} &= b_{i,k}^{(1)} + \eta_k^{b_i^{(1)}} \\
\psi_{i,k+1}^{(1)} &= \psi_{i,k}^{(1)} + \eta_k^{\psi_i^{(1)}} \\
&\vdots \\
\theta_{k+1}^{(N)} &= (\theta_k^{(N)} + \omega^{(N)}\delta)\mathrm{mod}(2\pi) \\
z_{k+1}^{(N)} &= -\sum_{i\in\mathscr{W}^{(N)}} \delta \frac{\alpha_{i,k}^{(N)}\omega^{(N)}}{b_{i,k}^{(N)^2}} \Delta\theta_{i,k}^{(N)} \exp\left(-\frac{\Delta\theta_{i,k}^{(N)^2}}{2b_{i,k}^{(N)^2}}\right) + z_k^{(N)} + \eta_k^{z^{(N)}} \\
\alpha_{i,k+1}^{(N)} &= \alpha_{i,k}^{(N)} + \eta_k^{\alpha_i^{(N)}} \\
b_{i,k+1}^{(N)} &= b_{i,k}^{(N)} + \eta_k^{b_i^{(N)}} \\
\psi_{i,k+1}^{(N)} &= \psi_{i,k}^{(N)} + \eta_k^{\psi_i^{(N)}}
\end{cases}
\tag{5.6}
$$

but the observation vector would be different. In Chapter 3 only one observation was available, while in this chapter we assume that M observations are available. Therefore, the amplitude part of the state vector is related to the M ECG observations using the mixing matrix $\mathbf{A}$:

$$
\begin{bmatrix} \phi_k^{(1)} \\ \phi_k^{(2)} \\ \vdots \\ \phi_k^{(N)} \\ s_k^{(1)} \\ s_k^{(2)} \\ \vdots \\ s_k^{(M)} \end{bmatrix}
=
\left[\begin{array}{cccc:ccc}
1 & 0 & \dots & 0 & 0 & \dots & 0 \\
0 & 1 & \dots & 0 & 0 & \dots & 0 \\
\vdots & \vdots & \ddots & 0 & 0 & \dots & 0 \\
0 & 0 & \dots & 1 & 0 & \dots & 0 \\ \hdashline
0 & 0 & \dots & 0 & a_{11} & \dots & a_{1N} \\
\vdots & \vdots & \ddots & \vdots & \vdots & \ddots & \vdots \\
0 & 0 & \dots & 0 & a_{M1} & \dots & a_{MN}
\end{array}\right]
\cdot
\begin{bmatrix} \theta_k^{(1)} \\ \theta_k^{(2)} \\ \vdots \\ \theta_k^{(N)} \\ z_k^{(1)} \\ z_k^{(2)} \\ \vdots \\ z_k^{(N)} \end{bmatrix}
+
\begin{bmatrix} u_k^{(1)} \\ u_k^{(2)} \\ \vdots \\ u_k^{(N)} \\ v_k^{(1)} \\ v_k^{(2)} \\ \vdots \\ v_k^{(M)} \end{bmatrix},
\tag{5.7}
$$

where maternal and fetal ECGs have N components in total. It should be noted that it does not necessarily mean that there are N different ECGs in the mixtures. For example in the case of one mECG and one fECG ($Q = 2$), depending on data, N can be for example equal to 3 to consider 2 components for mECG and 1 component for fECG.

5.3 Results

In this section, we first qualitatively evaluate the performance of the proposed method on three sets of actual data including ECG, MCG, and ERP. The results on ECG and MCG data have been compared with the results of FastICA [64], πCA [30] and a deflation procedure for subspace decomposition [31]. The block diagram of the latter is depicted in Figure 5.1. In the case of

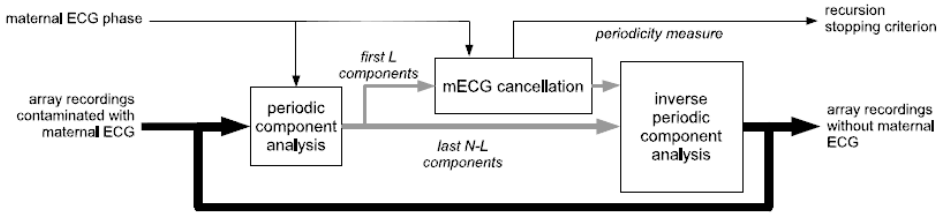

Figure 5.1: The overall iterative procedure for maternal ECG cancellation [31].

fECG extraction, the πCA method is first applied to the multichannel recording to extract L components related to the mECG. These components are then filtered via the EKF framework in [14] to obtain a clean mECG estimate from each of the L components. At the next step, the clean mECG estimates are subtracted from the L extracted components to reduce mECG. Finally, the inverse πCA is applied to project back to the sensor domain. This procedure is iterative and is repeated until no mECG component is observed in the output.

The GCP and WCP labels denote results of the first and second proposed approaches for tensor decomposition, presented in the previous chapter, without the Kalman filtering stage. GCP+EKS and WCP+EKS show the results based on GCP and WCP decompositions with the Kalman filtering stage, presented in this chapter. Then, in the second subsection, quantitative results coming from simulations are evaluated. In this subsection the results of WCP+EKS in fetal ECG extraction are quantitatively compared with the results of the single-channel EKS, proposed in Chapter 3.

5.3.1 Actual Data

Fetal ECG Extraction

The first ECG data used in this subsection is the DaISy fetal ECG database [71], as described in Appendix A, Section A.1.

The extracted maternal ECG and fetal ECG using the first and second channels of this database is shown in Figure 5.2. The mECG data was considered to be composed of 2 components, while we used only one component for the fECG data. The mixture of the first channel and extracted mECG and fECG signals using FastICA, πCA, and the proposed GCP+EKS and WCP+EKS are plotted, respectively. The fECG extracted via the deflation procedure is plotted too. These results can be also compared with the results of GCP and WCP in Figure 4.9 of Chapter 4.

As it is seen, FastICA and πCA methods fail to extract fECG when only two electrodes are available, since the mixtures are underdetermined and they demand several channels to recover the weak features of fECG. The deflation procedure provides significantly better results compared with FastICA and πCA methods. However, some parts of fECG have been distorted in the iterative algorithm of this method. This is particularly noticed between t = 0s and t = 1s, and between t = 8s and t = 9s. This phenomenon is not observed in the estimates of the proposed

Table 5.1: Maternal and fetal R-peak values on fECG estimate of DaISY dataset (mean ± standard deviation (SD)).

	Maternal R-peak value	Fetal R-peak value
Original mixture	43.66±2.38	17.68±2.37
FastICA	**31.30±2.29**	13.09±1.91
πCA	**41.39±2.68**	19.21±2.17
Deflation procedure	-1.13±0.48	15.96±2.97
GCP	-0.90±0.91	16.04±2.72
WCP	-0.88±0.83	16.65±1.26
GCP+EKS	0.17±1.46	16.19±1.11
WCP+EKS	0.29±1.40	17.54±0.99

method. There is neither ground truth nor golden standard on actual fetal ECG recordings to be used as a reference for comparing the performance of the different methods. Nevertheless, in order to quantify the performance of each method on actual data, the mean values of the contaminating and desired ECGs have been measured at their R-peak positions in the estimated ECG. This can provide an estimate for the residual of the contaminating mECG in the estimated fECG. If the contaminating mECG has been successfully removed, the values of this measure should be low; meanwhile, the values of the estimated fECG at its R-peak positions should be close to values of the corresponding points in the original mixture. Table 5.1 reports values of this measure on the fECG estimated by the different methods. The results show that the deflation procedure and the proposed GCP, WCP, GCP+EKS, and WCP+EKS significantly outperform FastICA and πCA. Although GCP and WCP provided close quantitative results compared with GCP+EKS and WCP+EKS, it should be noted that the valuable inter-beat dynamics of mECG and fECG are lost in the GCP and WCP estimates, because as it was explained in the Chapter 4 all beats of the reconstructed ECGs have exactly the same temporal pattern up to their amplitudes. Nonetheless, these valuable inter-beat dynamics of ECG signals are recovered using GCP+EKS and WCP+EKS. Moreover, in contrast to GCP and WCP, starting and ending incomplete ECG beats are also recovered via GCP+EKS and WCP+EKS.

The PhysioNet noninvasive fetal electrocardiogram database [72] described in Appendix A, Section A.2 has also been used to show the capability of the method in extracting the fECG at different periods of pregnancy, and from different channel locations. This database consists of a series of 55 multichannel abdominal fECG recordings, taken from a single subject between 21 to 40 weeks of pregnancy. Figure 5.3 shows the WCP+EKS outputs of the datasets ecgca192 using channels 3 and 5, ecgca444 using channels 3 and 6, and ecgca811 using channels 3 and 4, respectively. For each dataset, one channel of the first 20s of the mixtures and the fECG estimate are plotted. As it is seen, although visual inspection of the data shows that the fetal ECG is very weak in the mixtures, the proposed method could favorably recover the fECG signal from different channel locations.

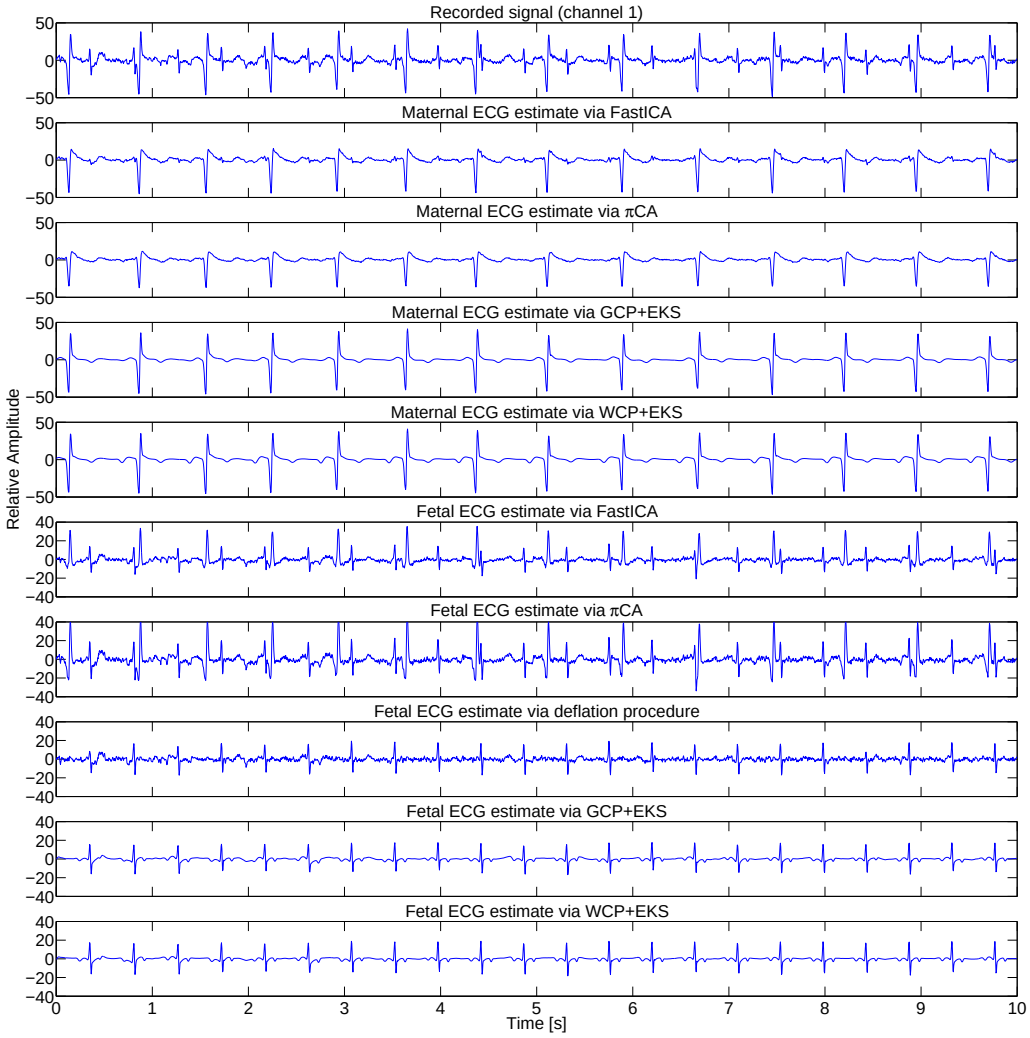

Figure 5.2: Extracted ECGs by FastICA, πCA, the deflation procedure, GCP+EKS and WCP+EKS, on the first channel of DaISy data using the first and second channels.

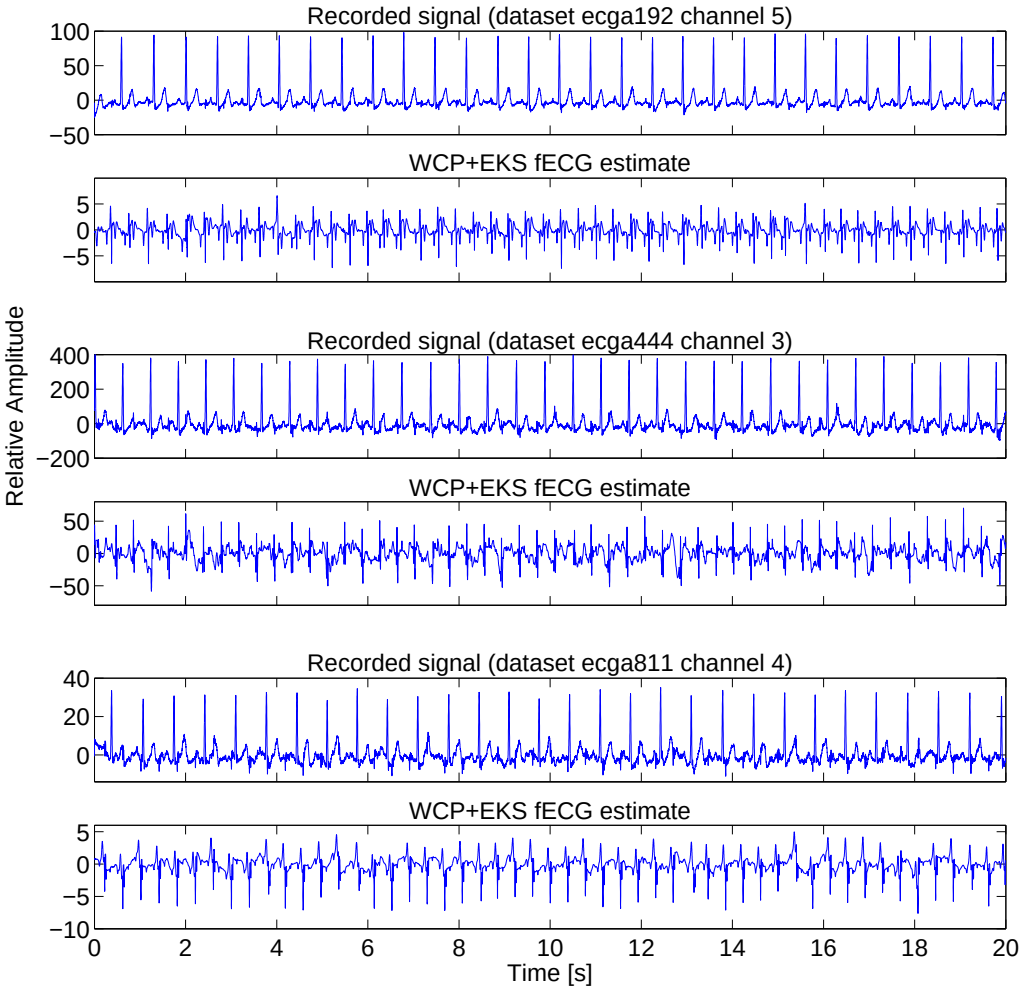

Figure 5.3: ECG mixtures of the datasets ecgca192 channel 5, ecgca444 channel 3, and ecgca811 channel 4 and their fetal WCP+EKS outputs.

Twin MCG Extraction

In this subsection, twin fetal MCG signals are extracted. The dataset used in this subsection has been described in Section 3.5.2. Two sensors are used in this experiment. In order to better compare the performance of the methods, the results have been based on the same data as in Section 4.4.2, i.e., channels 92 and 116 of the q00002252 dataset.

Since there are three sources (one maternal MCG and two fetal MCGs) to be extracted and two sensors are to be utilized, the adopted method must be applicable to underdetermined mixtures. FastICA and πCA methods are only applicable to (over)determined mixtures. Nevertheless, since in the πCA algorithms, the desired source is already selected, it is possible to apply πCA algorithm three times so that each time the covariance matrix is calculated according to the source of interest. This way, all three sources can be estimated. For the deflation procedure, since there are two fetal signals to be extracted in this experiment, first the maternal signal is removed then for each fetus the signal of the other fetus is also canceled using the same procedure as the maternal signal. The number of maternal and fetal MCG components considered in the proposed method are 2 and 1, respectively.

Figure 5.4 presents the results of πCA, the deflation procedure and the proposed GCP+EKS and WCP+EKS methods in extraction of the maternal and two fetal MCG signals from two channels. The πCA method fails to track periodic patterns related to the fetal components due to their low power and insufficient number of the utilized sensors. The deflation procedure provides better results. Yet, the sources of interferences and noises are not completely suppressed using this method. Nevertheless, the proposed GCP+EKS and WCP+EKS methods could suppress these sources and recover weak traces of fetal MCG features. These results can be also compared with the obtained results by GCP and WCP in Figure 4.10 of Chapter 4 without the Kalman filtering stage. As mentioned in Section 4.4.2, WCP significantly outperforms GCP on this data. However, as expected in comparison between WCP and WCP+EKS (or GCP+EKS), WCP method does not completely cancel out the exogenous noise, while WCP+EKS does, thanks to Kalman filter. Moreover, inter-beat dynamics of MCG signals are lost and starting and ending incomplete beats are not recovered by WCP.

The maternal and fetal R-peak values on the first fetal MCG estimate, are presented in Table 5.2. In this experiment, a perfect estimate should give very low value at maternal R-peak and the second fetal R-peak positions and a close value to those of the original mixture at the first fetal R-peak positions.

Event-Related Potentials Extraction

The proposed method is not limited to cardiac signals and may be applied to various applications. In this subsection, as a case study, the proposed WCP and WCP+EKS are employed to extract ERPs.

ERPs are the responses to brain stimulation measured by the scalp EEG. The measured responses are induced by multiple brain generators active in association with the eliciting event. However, they are mixed with background activity of the brain that is not related to the stimulus

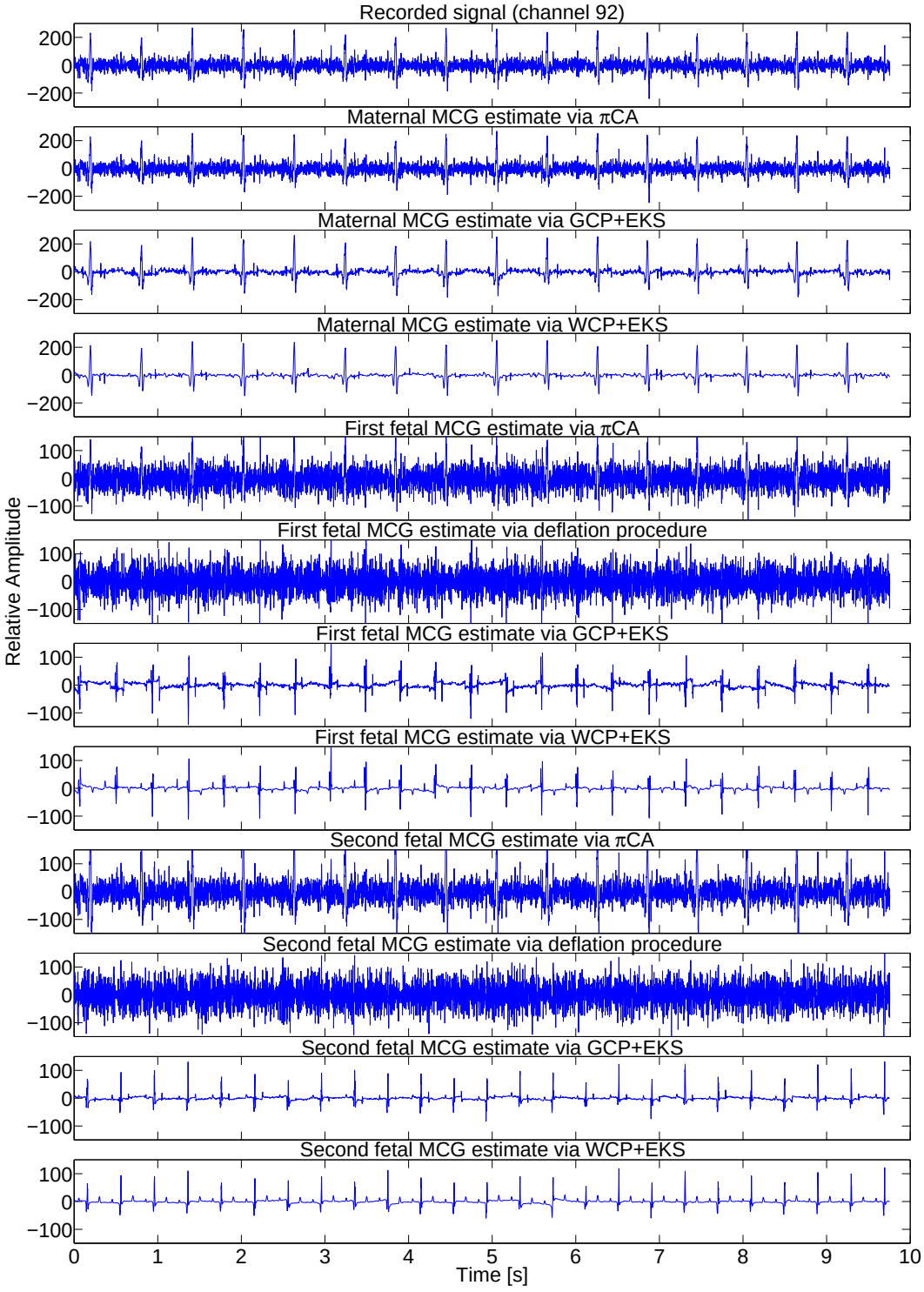

Figure 5.4: MCG extraction by πCA, the deflation procedure, GCP+EKS and WCP+EKS on the 92th channel of of twin MCG data using the 92th and 116th channels.

Table 5.2: Maternal and fetal R-peak values on the **first** fetal MCG estimate of twin MCG dataset (mean + SD).

	Maternal R-peak value	First fetal R-peak value	Second fetal R-peak value
Original mixture	210.08±31.42	66.04±40.74	74.97±29.27
πCA	**159.72±25.79**	63.15±36.77	**21.28±24.39**
Deflation procedure	-6.85±19.33	**94.14±50.98**	-3.15±9.51
GCP	-3.74±7.00	46.79±29.92	-3.08±9.55
WCP	-3.44±10.86	55.85±13.98	-2.57±8.37
GCP+EKS	1.94±8.10	65.48±33.29	1.06±8.85
WCP+EKS	1.39±6.77	71.22±28.12	0.20±6.75

and also other interferences from non-neural sources, such as eye blinks [94] and muscle artifacts. Due to the much lower power of ERPs compared with background EEG, it is difficult to estimate them even though they are dominant in lower frequencies. The most common way to extract ERPs involves averaging time-locked sections of the EEG signal over many trials. This method assumes a simple model for ERPs that consists of the sum of an invariant signal and a random process that will be attenuated by averaging over trials [95]. However, there is evidence that ERP waves may vary considerably over time [96]. Furthermore, in [97], it has been shown in the context of neonatal seizure activity that tensor-based methods that exploit the repetitive nature of EEG signals exhibit an improved performance compared to time-locked averaging. In the past, tensor-based techniques have already been applied to space-time-realization EEG data (see [98, 99]). However, the proposed method makes the decomposition more robust to noise. Furthermore, contrary to the previous tensor-based approaches, it permits to extract the original time courses of the signals, which are not identical for all realizations, using Kalman filtering.

The ERP database used in this subsection consists of EEG signals recorded during a P300 speller brain-computer interface (BCI) experiment [100]. In such a BCI, the paradigm, which consists of visual stimuli divided between target and non-target stimuli, suggests that a positive deviation about 300ms is elicited after a target stimulus, while non-target stimuli do not elicit specific brain response. The EEG signals have been sampled at 1200Hz using 16 scalps electrodes. First, a three-way tensor is built by stacking the data of sixteen channels windowed from 1 second before the stimuli and 2 seconds after the stimuli. In this experiment, The ERP data was considered to be composed of 2 components. Decomposition of this tensor yields estimates of the temporal patterns of ERPs along with their amplitudes and the mixing matrix (i.e., the spatial projection on scalp). Then, the ERP estimates are improved by the proposed KF to preserve dynamics of ERPs over time. The extracted temporal patterns of ERPs via WCP, and single-trial estimates of WCP and WCP+EKS from namely the S6 dataset are shown in Figure 5.5. As it is seen, WCP+EKS outperforms WCP because it better preserves the dynamics of ERPs which can vary from a trial to another. GCP and GCP+EKS also provide rather equivalent

results to those of WCP and WCP+EKS. The extraction procedure has been performed offline in this experiment, so that the whole data of the windowed stimuli were used in constructing the tensor. Then, the Kalman filtering stage was performed window by window using the loading matrices of the tensor decomposition stage. Nevertheless, if the procedure should be performed with less delay, one can utilize a smaller number of windows for constructing the tensor and run the Kalman filtering stage afterward.

5.3.2 Synthetic Data

Experimental Performance Analysis on Multichannel Synthetic Data

In the previous subsection, we showed on various actual data the good behavior of the proposed method in efficiently extracting event-related sources from a multichannel recording, and compared the obtained results with the results of the classical multichannel BSS methods. In this subsection, a quantitative comparison between the multichannel method proposed in this chapter and the single-channel method proposed in Chapter 3 is provided. The method in Chapter 3 aims at parallel extraction of several ECGs by simultaneously modeling them in a single-channel recording. The objective of this subsection is therefore to check if possible improvements of single-channel EKS performance can be achieved by adding another extra channel.

In order to perform a quantitative comparison, synthetic dual-channel mixtures of mECG and fECG are generated based on the three-dimensional canonical model of the single dipole vector of the heart, proposed in [69] and inspired by the single-channel ECG dynamic model presented in [66]. Then, in order to have more realistic mixtures, noise has been added to the mixtures. The noise consists of white Gaussian noise and colored noises which are band limited to 30 Hz and 60 Hz. The power of the mixed noise is adjusted to provide a 20 dB SNR. The sampling frequency is set to 500 Hz and signals include 3,000 samples. Since the basic problem of fECG extraction is to estimate the fECG signal where the interfering mECG is a stronger signal, the performance of the methods has been compared for ratios of the power of fECG to the power of mECG ranging from 0.01 to 1. [1]

In this chapter, we introduce a more general procedure for computing the output SNR, which differs from the defined output SNR in Chapter 3. The difference is that in Section 3.5.1 the estimated fECG signal, $\hat{\mathbf{s}}_f$, is assumed to be the sum of true generated mECG, true generated fECG and true generated noise, whereas in this chapter it is assumed to be the sum of true generated fECG and a noise, such that:

$$\hat{\mathbf{s}}_f = \tilde{\mathbf{s}}_f + \tilde{\mathbf{n}}, \tag{5.8}$$

where $\tilde{\mathbf{s}}_f$ and $\tilde{\mathbf{n}}$ are defined as:

$$\begin{aligned} \tilde{\mathbf{s}}_f &= \alpha \mathbf{s}_f, \\ \tilde{\mathbf{n}} &= \hat{\mathbf{s}}_f - \tilde{\mathbf{s}}_f = \hat{\mathbf{s}}_f - \alpha \mathbf{s}_f, \end{aligned} \tag{5.9}$$

[1] The large range of tested ratio values does not only include usual ratios encountered between fetal and maternal signals, but also ratio values encountered between two fetal signals.

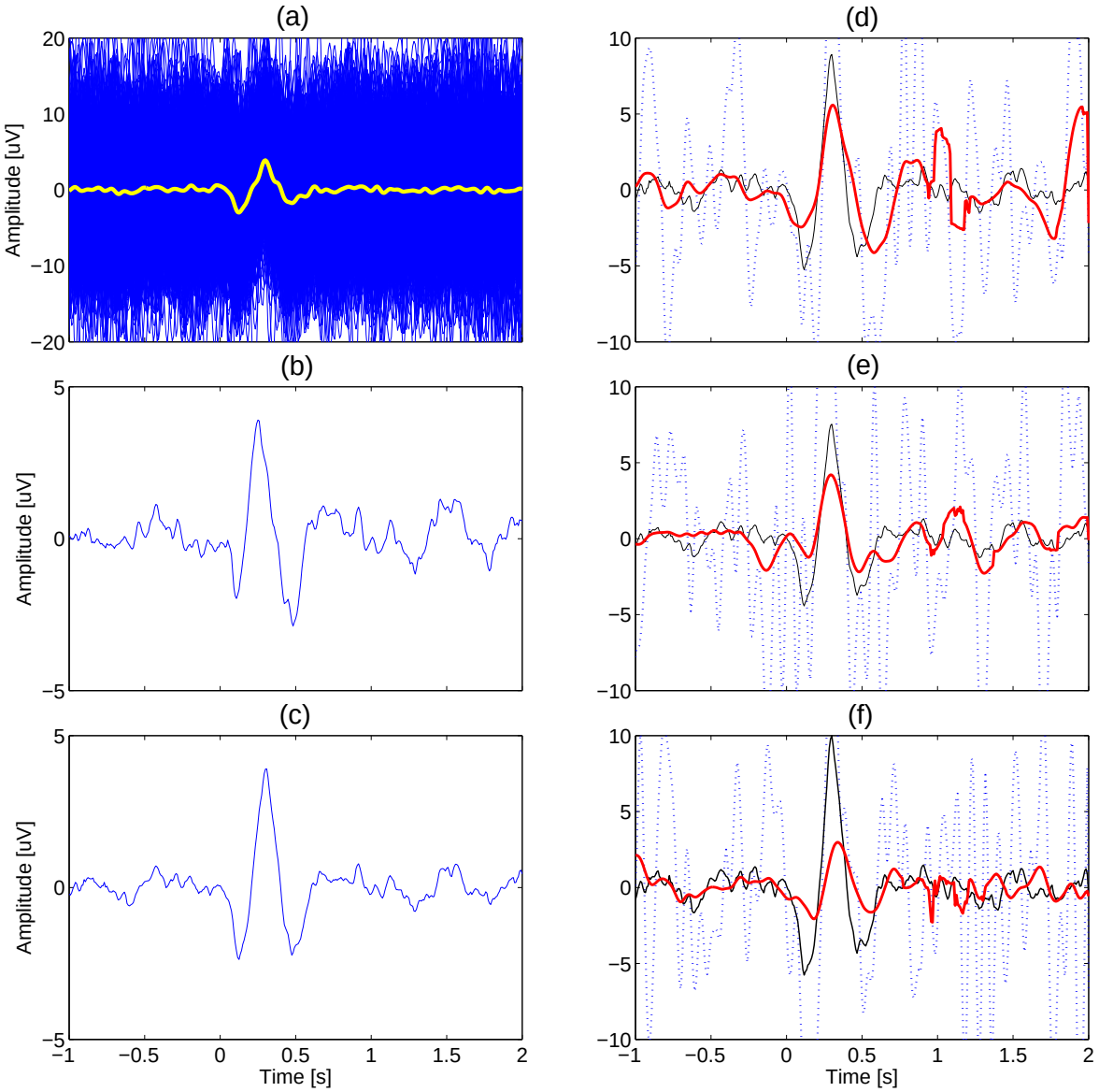

Figure 5.5: ERP extraction by WCP and WCP+EKS from namely the S6 dataset. (a): all the 500 measurements on channel 1 and the average in one plot; (b): the first temporal pattern extracted via WCP; (c): the second temporal pattern extracted via WCP; (d), (e), and (f): three examples of single-trial ERP extraction. Dotted lines represent the measurements, solid thin lines the estimates via WCP, and thick lines the estimates via WCP+EKS.

In order to estimate the coefficient α, it is assumed that $\mathbf{s}_f$, and $\tilde{\mathbf{n}}$ are orthogonal, i.e., decorrelated, which leads to:

$$\hat{\alpha} = \frac{E(\hat{\mathbf{s}}_f^T \tilde{\mathbf{n}})}{E(\mathbf{s}_f^T \tilde{\mathbf{n}})}. \tag{5.10}$$

In a successful estimation, the contribution of fECG to the output should be much more than the contribution of noise. In other words, the power of $\tilde{\mathbf{s}}_f$ should be much larger than the power of $\tilde{\mathbf{n}}$, which means the contribution of mECG, $\mathbf{s}_m$, and input noise, $\mathbf{n}$, is very low in the fECG estimate. In order to quantify the contribution of the fECG in the output, the output SNR is defined as:

$$SNR_{out} = \frac{\hat{\alpha}^2 P_{\mathbf{s}_f}}{P_{\tilde{\mathbf{n}}}} \tag{5.11}$$

where $P_{\mathbf{x}}$ denotes power of $\mathbf{x}$. The output SNR is now compared with the input SNR to investigate the performance of the fECG extraction. The input SNR is defined as:

$$SNR_{in} = \frac{P_{\mathbf{s}_f}}{P_{\mathbf{s}_m} + P_{\mathbf{n}}}. \tag{5.12}$$

Figure 5.6 shows SNR improvement results of the single-channel EKS and the proposed multichannel EKS using WCP (i.e. WCP+EKS) for different values of power ratios. For each value of power ratios, one hundred trials have been carried out. In order to have more realistic signals, mECG and fECG are allowed to have slight random variations (1%) in position of PQRST waves and also duration of each ECG beat. The power of the mECG signals is normalized to 1 (0 dB), and the average maternal and fetal heart rates are 1.1 Hz and 2 Hz, respectively. To compare the methods, single-channel EKS is first applied on both channels. Then its best result has been compared with the results of multichannel EKS on the corresponding channel. As it is seen in Figure 5.6, although the fetal SIR improvements of both single and multichannel EKS remain over 20 dB for all ranges of the power ratios, multichannel EKS led to superior results. This superiority has been obtained for all ranges of the power ratios, especially for the low values of powers ratio the difference is higher.

5.4 Phase Enhancement Using Dynamic Time Warping

So far, we have only focused on improving the estimation of amplitude of ECG signal, z_k, in the following model of ECG:

$$\begin{cases} \theta_{k+1} = (\theta_k + \omega\delta) \mathrm{mod}(2\pi) \\ z_{k+1} = -\sum\limits_{i \in \mathscr{W}} \delta \frac{\alpha_{i,k}\omega}{b_{i,k}^2} \Delta\theta_{i,k} \exp(-\frac{\Delta\theta_{i,k}^2}{2b_{i,k}^2}) + z_k + \eta_k^z \\ \alpha_{i,k+1} = \alpha_{i,k} + \eta_k^{\alpha_i} \\ b_{i,k+1} = b_{i,k} + \eta_k^{b_i} \\ \psi_{i,k+1} = \psi_{i,k} + \eta_k^{\psi_i} \end{cases} \tag{5.13}$$

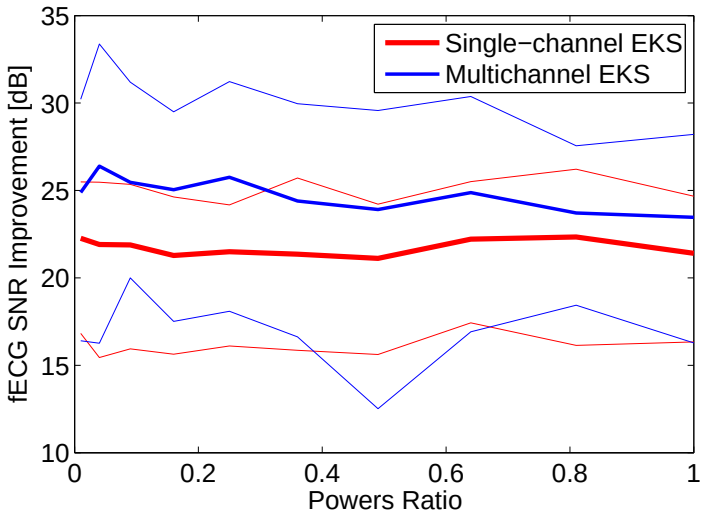

Figure 5.6: Mean SNR improvement results of the single-channel and multichannel EKS against powers ratio (bold lines). Upper and lower borders (thin lines) present maximum and minimum, respectively.

in which, a 'strictly' linear phase has been assumed in the state equation of the model. This means that all ECG beats are similar and no beat differs much from the others. The model uses information of only one channel and is therefore applicable to single-channel recordings. Moreover, it is practical and straightforward when the desired ECG is mixed with strong interferences and noises. The reason is that it simply assigns a linearly-increasing value between 0 and 2π to the intermediate samples of R-R intervals, so it is robust and other sources cannot impact it. However, there are applications in which multichannel recording is available and the desired ECG is not highly contaminated by other sources. In addition, the ECG is pathological and linear phase is not a valid assumption because a few ECG beats are significantly different. This is especially seen in some heart defects such as the premature ventricular contraction (PVC), where the abnormal wave only appears in certain cycles of the ECG. Therefore, some modifications in the state equations are necessary to simultaneously filter the normal and abnormal segments.

5.4.1 Proposed Modifications

The first modification of the phase state can be to add a random additive noise, η^{θ}, to the phase state equation (we refer to it as 'flexible' linear). Therefore, the phase model would no longer be 'strictly' linear and slight fluctuations around linear phase are allowed. Hence, state equations

are:

$$\begin{cases} \theta_{k+1} = (\theta_k + \omega\delta)\text{mod}(2\pi) + \eta^{\theta} \\ z_{k+1} = -\sum_{i \in \mathscr{W}} \delta \frac{\alpha_{i,k}\omega}{b_{i,k}^2} \Delta\theta_{i,k} \exp(-\frac{\Delta\theta_{i,k}^2}{2b_{i,k}^2}) + z_k + \eta_k^z \\ \alpha_{i,k+1} = \alpha_{i,k} + \eta_k^{\alpha_i} \\ b_{i,k+1} = b_{i,k} + \eta_k^{b_i} \\ \psi_{i,k+1} = \psi_{i,k} + \eta_k^{\psi_i} \end{cases} \tag{5.14}$$

Although this modification may improve the performance of the filter, it still assumes that all beats are almost similar and no beat differs much from others. Moreover, it also uses information of only one channel to make the ECG phase.

The second modification, which benefits from information of all channels, is to use dynamic time warping (DTW) [101] for the phase state calculation. DTW is a method for measuring similarity between two sequences or matrices, which may vary in time or speed. This method is widely used in speech recognition to recognize a unique word when it is pronounced fast or slowly. In this method an optimal match between two given sequences or matrices with certain restrictions is found [101]. For our problem of interest, a multichannel ECG beat reference $\underline{E}(l) \in \mathbb{R}^M$ is firstly selected and a linear phase is assigned to it, then the current multichannel ECG beat $\underline{s}(k) \in \mathbb{R}^M$ and the reference ECG beat are nonlinearly warped to optimize the similarity of their nonlinear variations. Finally, as it is illustrated in Figure 5.7, the phase observation of the current ECG beat is achieved by aligning the linear phase of the reference ECG beat, according to the optimal match of the reference and the current ECG beat. The computational cost of the method is low and the DTW algorithm can be implemented easily. This model of phase state can also be further modified by adding a random additive noise to make it more flexible (we refer to it as 'flexible' DTW).

Estimation of phase state based on DTW methods is especially valuable when in some beats one or more ECG waves (P, Q, R, S and T) appear sooner or later than normal ones. In those cases, since DTW methods search for optimal match between reference and current beats, premature or delayed occurrence of the ECG waves are compensated in the phase state. Thereby, the EKF can better follow premature or delayed ECG waves. Another parameter that may also affect filtering performance is expansion or contraction of each ECG wave in some dissimilar beats. Here again, it is possible to compensate the deviation from linear phase using DTW methods.

5.4.2 Evaluation on Actual and Synthetic Data

Actual Data

Figure 5.8 shows the results of the proposed methods on a part of the record 116 of the MIT-BIH Arrhythmia Database [72, 102]. This database consists of dual-channel ambulatory ECG recordings, in which some beats significantly differ from other beats. The mean ECG, which is calculated by taking average over all ECG beats, has been adopted as the reference ECG beat

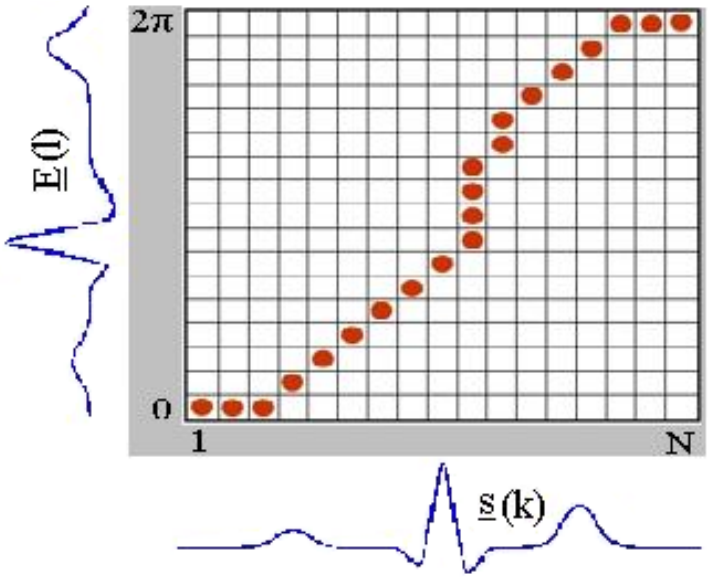

Figure 5.7: A typical example of DTW method for finding optimal match between reference ECG beat and current ECG beat.

of DTW methods. As it is seen in Figure 5.8, the best result is provided by 'flexible' DTW. Although 'flexible-linear' phase is allowed to have some variations around the linear phase, it is still unable to follow a beat, which is dissimilar to other beats. In order to have a better comparison, the residual results which are the subtraction of the original signal from the filtered signals are plotted on the right column of Figure 5.8. As it is seen, some ECG parts are distorted by 'strict' and 'flexible-linear' phases, while, DTW methods are able to follow the signal in these scenarios. We should point out that one might use the resulting errors by linear methods as a practical means to detect this kind of abnormality. Nevertheless, if the objective is to filter the abnormal ECG with highest possible fidelity, DTW methods significantly outperform linear ones.

Synthetic Data

In order to study the performance of the methods in different situations, synthetic ECG data have been generated to model these dissimilarities. In equation (5.13) ψ_i denotes location of Gaussian functions, so premature and delayed occurrence of the ECG waves can be modeled by varying ψ_i around their values. Expansion and contraction of the ECG waves can also be modeled by varying b_i. Figure 5.9 shows the results of different methods for different range of ψ_i variations, where 100% corresponds to 2π. The synthetic data consist of eight channels and input SNR is equal to 15 dB. For each value of ψ_i variations, fifty trials have been carried out to have statistically reliable results. As it is seen, when ψ_i variations are very low and all beats are very similar, linear methods provide better results, since noise cannot affect them. However, DTW methods are affected by the noise; nevertheless, they did not deteriorate the input signals, because their output SNRs are still more than 15 dB. As ψ_i variations become

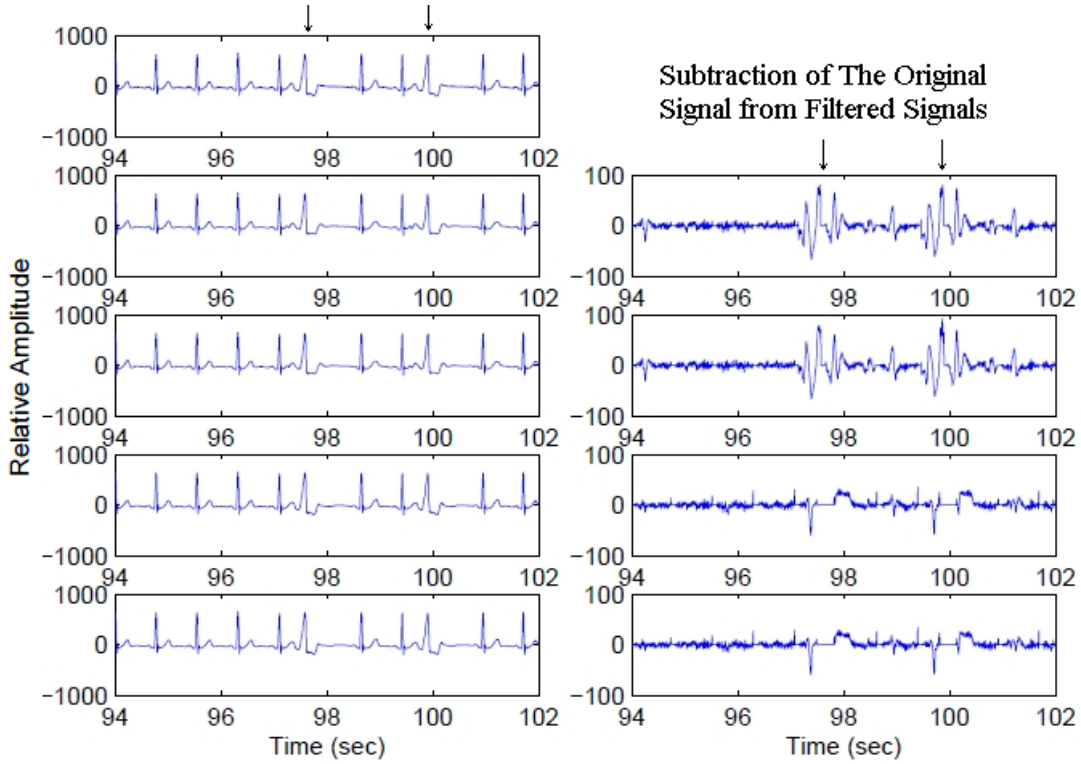

Figure 5.8: Results of proposed method on actual data. Left, Top to Bottom: Original record 116 of the MIT-BIH Arrhythmia Database, 'strict' linear, 'flexible' linear, DTW, 'flexible' DTW outputs. Right, Top to Bottom: Subtraction of the original ECG from 'strict' linear, 'flexible' linear, DTW, 'flexible' DTW outputs.

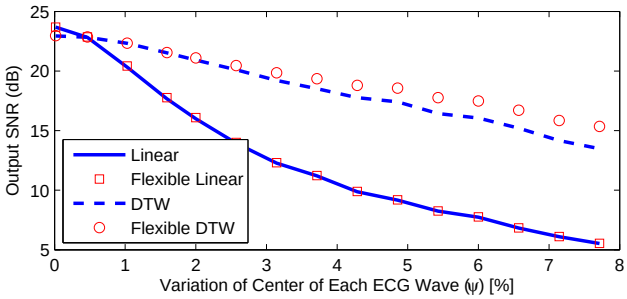

Figure 5.9: Mean value of EKF output SNR for different range of ψ variations.

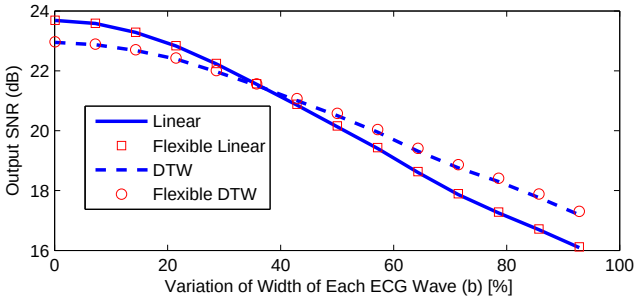

Figure 5.10: Mean value of EKF output SNR for different range of b variations.

larger, the difference between performance of the linear and DTW methods become lower. For variation equal to 0.5%, same performance is achieved and from this point, the DTW methods dramatically outperform linear ones.

Similar trials have been carried out for variations of b_i, width of Gaussian functions. As it can be seen in Figure 5.10, for low values of b_i variations, the linear methods outperform the DTW methods. However, as b_i variations become larger, the DTW methods significantly outperform the linear methods.

Figures 5.9 and 5.10 show that adding noise to the phase state equation can lead to improve the results of DTW methods for large signal distortions. Practically, for very slight variations of ψ_i or b_i, linear methods provide better results, while, for larger values of ψ_i or b_i variations, 'flexible' DTW method outperforms the other methods.

In this section, we presented the results on ECG signals, but the method is more general and can be applied to other quasi-periodic signals. It is also applicable to signals with synchronized stimuli (as described in Section 4.1). However, the method is not expected to provide good results in applications such as fetal ECG extraction where the interfering source is very strong and can highly interfere the DTW algorithm. Nevertheless, results on actual and synthetic data show that in absence of strong interfering sources, the DTW methods provide a more reliable phase state when dissimilarity between current beat and other beats is large, because this dissimilarity is compensated in the phase state. This method may therefore serve as an effective tool for simultaneously filtering normal and abnormal ECG segments. Moreover, optimal match between reference and current beats, provided by DTW method, may be used in future works

as a feature to classify normal and abnormal beats.

5.5 Summary and Conclusions

The number of utilized channels is a key feature of a monitoring system that sets a tradeoff between the system's price, convenience, and portability and its performance. Classical multichannel methods for fECG extraction need several sensors to recover the weak fECG signal. In order to utilize a minimal number of electrodes, a nonlinear Bayesian filtering framework has been extended and used within a Kalman filter to improve the fECG and mECG estimates, provided by previously proposed tensor decomposition method. The proposed method, which needs only two sensors to successfully recover several components of ECG signals, performs significantly better than the classical methods. Moreover, in contrast to the tensor decomposition method, which ignores the inter-beat dynamics of ECG signal, the proposed method is able to recover these dynamics that might be valuable for diagnosing heart diseases. The proposed method is not limited to ECG signals. The presented result of the application of the proposed method on ERPs is an example of its efficiency in recovering other kinds of event-related signals.

In this chapter, we also proposed a new approach for estimating the phase state of ECG signal. The new approach that exploits information of all channels for phase state estimation was shown to be efficient in simultaneously filtering normal and abnormal ECG segments.

Chapter 6

Nonparametric Modeling of ECG Signal for Denosing and Fetal ECG Extraction

6.1 Introduction

In this chapter, we present a novel nonparametric method based on Gaussian processes for the separation of fECG from a noisy single-channel recording of maternal and fetal ECG. The presented method in Chapter 3, which has been shown to be efficient in extraction of fECG signal is based on Kalman filtering. However, Kalman filtering relies on a strong assumption: the state equation, which models the dynamical evolution of the unobserved state. As a consequence, Kalman filtering needs reliable prior about the state to be performed accurately. To overcome the potential lack of prior information about the system, we propose to model the second order statistics of the signal instead of the signal itself, thanks to Gaussian processes.

A Gaussian process (GP) is a stochastic process $x(t)$, $t \in T$, for which any finite linear combination of samples has a joint Gaussian distribution. Therefore, any linear functional applied to the sample function $x(t)$ will give a normally distributed result. Notation-wise, one can write $\mathbf{x} \sim \mathscr{GP}(\mathbf{m}, \mathbf{K})$, meaning the random function $x(t)$ is distributed as a GP with mean function $\mathbf{m}$ and covariance function $\mathbf{K}$ [103]. Gaussian processes are widely used in statistical modeling because of properties inherited from the normal (Gaussian) distribution. Among these properties, a key fact of a Gaussian process is that it can be fully defined by its second-order statistics [104]. Thus, if a Gaussian process is assumed to be zero-mean, defining the covariance function completely defines the behavior of the process. In this chapter, considering the statistical behavior of ECG signal, we will present suitable covariance functions for maternal and fetal ECGs for ECG denoising and fetal ECG extraction.

The rest of this chapter is organized as follows. In Section 6.2, after recalling parametric modeling of ECG signal, considering ECG signal as a Gaussian process, a nonparametric modeling of this signal is proposed. The proposed covariance function used in this modeling, is defined according to the characteristics of different waves of ECG signal. This covariance function is

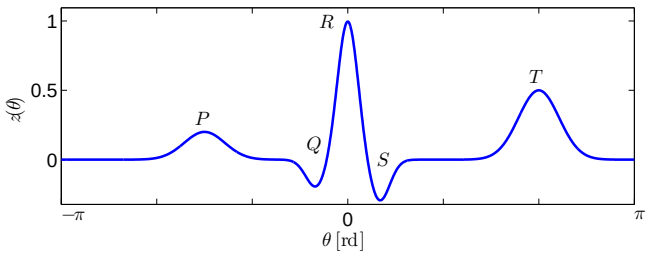

Figure 6.1: Typical waveform of one ECG beat.

then adopted in Section 6.3 for ECG denoising and fetal ECG extraction from a single-channel recording. Since the covariance function introduced in Section 6.2 is very complicated and thus leads to a complex optimization problem, in Section 6.4 a simplified version of this covariance function is proposed, which results in a simpler and faster method. Section 6.5 is devoted to presenting the results of the proposed method on both synthetic data and actual recordings. First, using synthetic data, the performance of the proposed method is quantitatively compared with the performance of the EKF framework on ECG denoising. Then, the proposed method is applied on fetal ECG and MCG recordings and its results are qualitatively compared with those of EKF framework. Finally, the summary and the conclusions of the chapter are stated in Section 6.6.

6.2 Nonparametric Modeling of ECG

As it has been mentioned in Section 3.3, it is possible to consider a parametric model for ECG signal so that each ECG beat is modeled as the summation of 5 Gaussian-shaped functions. Each of these 5 Gaussian-shaped functions models one of the P, Q, R, S and T waves (see Figure 6.1):

$$z(\theta) = \sum_{i\in\{P,Q,R,S,T\}} \alpha_i \exp\left(-\frac{(\theta-\psi_i)^2}{2b_i^2}\right). \tag{6.1}$$

This model can then be used in an extended Kalman filtering to denoise a single ECG or extract fECG from a mixture of mECG, fECG and noise. This method is thus a parametric method since the unknown amplitude $z(\theta)$ is explicitly parameterized.

On the other hand, nonparametric methods perform estimation, prediction or denoising without explicitly parameterizing the unknown amplitude $z(\theta)$. The well-known spline smoothing approach [105] is an example of such methods. In this case, if the amplitude of an ECG beat, $z(\theta)$, is considered as a statistical process, it can be fully described at the second order by its mean function $m(\theta) = \mathbb{E}[z(\theta)]$ and covariance function $k(\theta_1, \theta_2) = \mathbb{E}[(z(\theta_1) - m(\theta_1))(z(\theta_2) - m(\theta_2))]$ [106]. Consequently, the ECG beat, $z(\theta)$, is considered as a Gaussian process $\mathscr{GP}(m(\theta), k(\theta_1, \theta_2))$. In this case, the statistical latent process, $z(\theta)$, is not directly parameterized as in a parametric

model, but its statistics are, thanks to hyper-parameters. This means that by assuming a zero-mean process, a class of semidefinite positive functions $k(\theta_1, \theta_2)$ is chosen to fully describe the expected second order properties of the latent process.

As seen in Figure 6.1, an ECG beat can be decomposed into three parts: the P wave, the QRS complex and the T wave, which have different characteristics (e.g., temporal correlation and power). The P and T waves share similar kinds of second order statistics: a larger length scale and a lower power than the QRS complex. Thereby, a possible non-stationary covariance function that suits ECG signal can be proposed as:

$$k(\theta_1, \theta_2) = \sigma(\theta_1)\sigma(\theta_2)\sqrt{\frac{2l_d(\theta_1)l_d(\theta_2)}{l_d(\theta_1)^2 + l_d(\theta_2)^2}} \times \exp\left(-\frac{\left(\theta_1 - \theta_2\right)^2}{l_d(\theta_1)^2 + l_d(\theta_2)^2}\right), \tag{6.2}$$

with

$$\sigma(\theta) = a_m + (a_M - a_m)\exp\left(-\frac{(\theta - \theta_0)^2}{2\sigma_T^2}\right), \tag{6.3}$$

$$l_d(\theta) = l_M - (l_M - l_m)\exp\left(-\frac{(\theta - \theta_0)^2}{2\sigma_l^2}\right), \tag{6.4}$$

where $\sigma(\theta)$ and $l_d(\theta)$ allow to have a time-varying amplitude (between a_m and a_M) and a time-varying length scale (between l_m and l_M), respectively.

Figure 6.2 shows two functions drawn at random from the zero-mean GP prior with covariance function (6.2). This figure illustrates the flexibility of such a representation compared to model (6.1), since with the same prior, $\mathscr{GP}(0, k(\theta_1, \theta_2))$, it can generate a multitude of different shapes.

Finally, the full ECG is modeled as the succession of beats and is thus also a Gaussian process, whose covariance function is given by:

$$k_s\big(t, t'\big) = \sum_{n=1}^{N}\sum_{n'=1}^{N} k\big(t - \tau_n, t' - \tau_{n'}\big), \tag{6.5}$$

where $\{\tau_n\}_{1\leqslant n\leqslant N}$ is the set of R-peak instants that are detected from the mixture.

6.3 ECG Denoising and Fetal ECG Extraction from a Single-Channel Recording

Suppose that the single channel observed signal $x(t)$ is the superposition of the ECG signal $s(t)$ and an additive noise $n(t)$:

$$x(t) = s(t) + n(t). \tag{6.6}$$

Moreover, assume that the ECG signal and noise are uncorrelated. Based on the proposed modeling of ECG signals (Section 6.2), the full ECG signal is modeled as a zero-mean GP

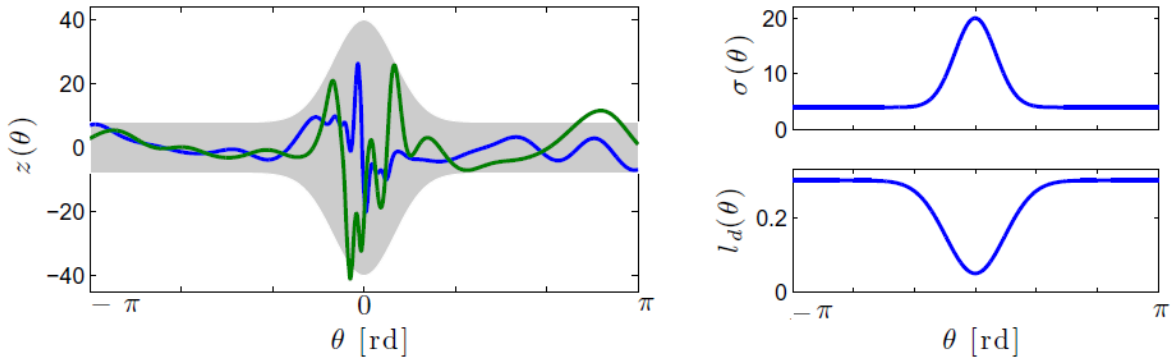

Figure 6.2: Two functions drawn at random from a zero-mean GP with covariance function (6.2). The shaded area represents plus and minus two times the standard deviation of the prior. On the right, the corresponding $\sigma(\theta)$ and $l_d(\theta)$ functions.

denoted as $\mathscr{GP}(0, k_s(t,t'))$ where the covariance function is defined as (6.5). The additive noise is also modeled as a zero-mean GP, whose covariance function $k_n(t,t')$ is given by:

$$k_n(t,t') = \sigma_n^2 \exp\left(-\frac{(t-t')^2}{2l_n^2}\right) + \sigma_w^2 \delta(t-t'), \tag{6.7}$$

where $\delta(\cdot)$ is the delta Dirac function. In the first term of this expression, σ_n^2 and l_n are used to model the baseline variation of the noisy ECG as a stationary process for which the correlation is almost unit between close samples and decreases as their distance increases compared to the length scale l_n. The second term models a white Gaussian noise of power σ_w^2.

The set of hyper-parameters $\boldsymbol{\phi} = \{a_m, a_M, \sigma_T, l_m, l_M, \sigma_l, \sigma_n, l_n, \sigma_w\}$ are estimated by maximizing the evidence (log marginal likelihood) given by [107]:

$$\log p\big(\mathbf{x}|\{T_k\}_k, \boldsymbol{\phi}\big) = -\frac{1}{2}\mathbf{x}^T\big(\mathbf{K}_s + \mathbf{K}_n\big)^{-1}\mathbf{x} - \frac{1}{2}\log\Big|\mathbf{K}_s + \mathbf{K}_n\Big| - \frac{M}{2}\log(2\pi), \tag{6.8}$$

where $\{T_k\}_k$ is the set of recording times, $\mathbf{K}_.$ is the covariance matrix whose (p,q)-th entry is $k_.(T_p, T_q)$, $\mathbf{x} = [x(T_1), \cdots, x(T_M)]^T$ and M is the number of recorded samples. The optimization of the latter equation is obtained thanks to a gradient ascent method, assuming that the initial parameter values are not too far from the actual values.

With GP modeling, $\mathbf{s}$ and $\mathbf{x}$ are jointly Gaussian distributed [107]:

$$\begin{bmatrix}\mathbf{x}\\ \mathbf{s}\end{bmatrix} \sim \mathscr{N}\left(\mathbf{0}, \begin{bmatrix}\mathbf{K}_s + \mathbf{K}_n & \mathbf{K}_s\\ \mathbf{K}_s & \mathbf{K}_s\end{bmatrix}\right). \tag{6.9}$$

The conditional distribution of $\mathbf{s}$ given $\mathbf{x}$ is itself Gaussian-distributed, so some matrix algebra

leads us to [107]:

$$\mathbf{s} \mid \mathbf{x} \sim \mathscr{N}\left(\mathbf{K}_s(\mathbf{K}_s+\mathbf{K}_n)^{-1}\mathbf{x}, \mathbf{K}_s - \mathbf{K}_s(\mathbf{K}_s+\mathbf{K}_n)^{-1}\mathbf{K}_s\right). \tag{6.10}$$

Therefore, the estimation of the ECG, which maximizes the posterior distribution of the given recording, $\mathbf{x}$, is given by:

$$\hat{s}(t) = \mathbf{k}_s{}^T\Big(\mathbf{K}_s+\mathbf{K}_n\Big)^{-1}\mathbf{x}, \tag{6.11}$$

where $\mathbf{k}_s = [k_s(t,T_1),\cdots,k_s(t,T_M)]^T$.

Fetal ECG extraction from a single abdominal sensor is then a direct extension of the proposed method by modeling the recorded signal $x(t)$ as:

$$x(t) = s_m(t) + s_f(t) + n(t), \tag{6.12}$$

where $s_m(t)$ is the maternal ECG signal, $s_f(t)$ is the fetal ECG signal, and $n(t)$ is the additive noise. All these signals are modeled as zero-mean GPs with covariance functions $k_m(\cdot,\cdot)$ and $k_f(\cdot,\cdot)$ defined by (6.5) and $k_n(\cdot,\cdot)$ obtained from (6.7), respectively.

In this case, the estimates of $s_m(t)$ and $s_f(t)$ are given by:

$$\begin{cases} \hat{s}_m(t) = \mathbf{k}_m^T\Big(\mathbf{K}_m+\mathbf{K}_f+\mathbf{K}_n\Big)^{-1}\mathbf{x} \\ \hat{s}_f(t) = \mathbf{k}_f^T\Big(\mathbf{K}_m+\mathbf{K}_f+\mathbf{K}_n\Big)^{-1}\mathbf{x} \end{cases} \tag{6.13}$$

where $\mathbf{k}_m = [k_m(t,T_1),\cdots,k_m(t,T_M)]^T$ and $\mathbf{k}_f = [k_f(t,T_1),\cdots,k_f(t,T_M)]^T$.

This procedure can also be further extended for the case in which maternal ECG and noise are mixed with more than one fetal ECG (e.g. twins).

6.4 Simplified Covariance Function

Although the proposed method based on the covariance function in (6.2) has been shown to be efficient for ECG denoising and fetal ECG extraction (see Section (6.5)), it suffers from several drawbacks. Indeed, it requires many parameters to fit well the characteristics of an ECG beat. For each ECG, a_m, a_M and σ_T form a time-varying amplitude, $\sigma(\theta)$, and l_m, l_M and σ_l form a time-varying length scale, $l_d(\theta)$, in (6.3) and (6.4), respectively. This thus leads to a quite complicated model and therefore it is tricky to optimize all the hyperparameters. Moreover, from a computational point of view, the double summation in (6.5) is quite CPU intensive.

The model is modified in two ways. Firstly, the ECG recordings are decomposed into a few sub-bands thanks to a filter bank to avoid a time-varying correlation length scale in (6.4): in each sub-band, the correlation length scale is considered as a constant. Secondly, to avoid too large computational cost, similar to Chapter 3, the R-peak detection is used to warp the time into a linear phase from 0 to 2π for each heartbeat: $\theta(t)$ is defined such that each interval $[\tau_k, \tau_{k+1})$ is mapped into interval $[2(k-1)\pi, 2k\pi)$ (Figure 6.3).

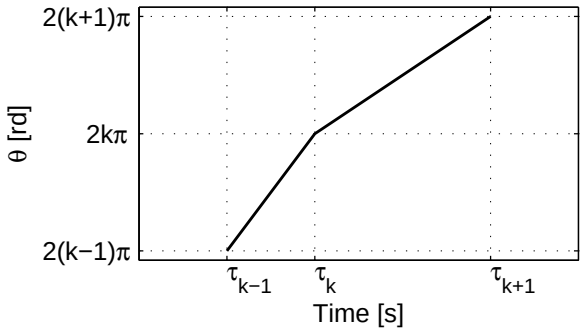

Figure 6.3: Illustration of the time warping: each heartbeat is linearly warped into a 2π interval.

The ECG signal $s(t)$ is decomposed via a filter bank into a few signals $s_i(t)$, each of them can then be warped to 2π quasi-periodic signals $z_i(\theta)$ thanks to $\theta(t)$. In each sub-band, i, this warping allows us to use the periodic covariance function defined by the following expression:

$$k_s^{(i)}(t,t') = \sigma^2(i)\exp\left(-\frac{\sin^2\Big(\big(\theta(t)-\theta(t')\big)/2\Big)}{l_d^2(i)}\right), \tag{6.14}$$

where i refers to the i-th sub-band, $\sigma^2(i)$ and $l_d(i)$ are the power, and the correlation length scale of the sub-signal $s_i(t)$, respectively. This covariance function has been proposed by inspiration of the periodic covariance function in [108]:

$$k(t,t') = \exp\left(-\frac{2\sin^2\Big(\big(t-t'\big)/2\Big)}{l^2}\right). \tag{6.15}$$

It is worth noting that the proposed covariance function allows to fit well quasi-periodic signals such as ECG thanks to the linear warping $\theta(t)$, which maps each period into interval $[0, 2\pi)$. Moreover, using such a nonparametric model, no assumption is made about the shape of the ECG signals but its (quasi-) periodicity and its smoothness which are defined by $\theta(t)$ and $l_d(i)$, respectively.

Thereby, maternal and fetal ECGs are modeled as GPs denoted as $\mathscr{GP}(0, k_m^{(i)}(t,t'))$ and $\mathscr{GP}(0, k_m^{(i)}(t,t'))$ in each subband, i, respectively, where covariance functions are defined by (6.14). The additive noise is also modeled as a zero-mean GP, whose covariance function $k_n^{(i)}(t,t')$ is given by (6.7) in each sub-band. Consequently, the estimation of mECG in the i-th sub-band, which maximizes the posterior distribution of the i-th sub-band of the given recording, $\mathbf{x}_i$, is then given by:

$$\hat{s}_{m,i}(t) = \mathbf{k}_m^{(i)^T}\Big(\mathbf{K}_m^{(i)} + \mathbf{K}_f^{(i)} + \mathbf{K}_n^{(i)}\Big)^{-1}\mathbf{x}_i. \tag{6.16}$$

In the same way, fECG in the i-th sub-band is estimated by:

$$\hat{s}_{f,i}(t) = \mathbf{k}_f^{(i)^T} \left(\mathbf{K}_m^{(i)} + \mathbf{K}_f^{(i)} + \mathbf{K}_n^{(i)} \right)^{-1} \mathbf{x}_i. \tag{6.17}$$

Finally, the full estimation of signals is given by the summation over I sub-bands:

$$\begin{cases} \hat{s}_m(t) & = \sum_{i=1}^{I} \hat{s}_{m,i}(t) \\ \hat{s}_f(t) & = \sum_{i=1}^{I} \hat{s}_{f,i}(t) \end{cases} \tag{6.18}$$

A few notes should be added here to have a better view on how the simplified covariance function reduces the complexity of the optimization problem. The covariance function in (6.2) includes 6 parameters $(a_m, a_M, \sigma_T, l_m, l_M, \sigma_l)$ to model each ECG signal and 3 parameters $(\sigma_n, l_n, \sigma_w)$ to model noise. The simplified covariance function in (6.14) includes 2 parameters (σ, l_d) to model each ECG signal and 3 parameters $(\sigma_n, l_n, \sigma_w)$ to model noise, in each sub-band. Therefore, by assuming two ECGs mixed in a recording, the first covariance function leads to an optimization problem with 15 parameters, whereas if we decompose the mixture to 3 sub-bands, we will have 3 independent parallel optimization problems each having 7 parameters. Although in the simplified version there are 3 optimization problems to be solved, this significant reduction of number of parameters and avoiding the double summation in (6.5) (thanks to linear time warping) dramatically reduce the computational cost and the memory required for processing.

6.5 Results

In this section we first investigate the performance of the proposed method on synthetic data to denoise ECG (Subsection 6.5.1). Then, the results of the proposed method on actual data are presented (Subsection 6.5.2).

6.5.1 Synthetic Data: ECG Denoising

The performance of the proposed algorithm based on the covariance function in (6.2) to denoise ECG signal is assessed in this subsection. In the first experiment, each beat of the ECG signal is generated by model (6.1). In order to mimic the variability presented in an actual ECG, the waves amplitudes and P-R and R-T intervals are randomly changed (3%) around their mean values. The ECG signal is then obtained as the concatenation of several beats with random global amplitudes and random R-R intervals. To ensure the consistency of the results, the whole procedure has been repeated one thousand times by regenerating all random parameters of the signal and noise samples. In this experiment, 1500 samples are used with 15 heartbeats simulated at 100 Hz sampled frequency. It is worth noting that the proposed method does not assume that the maxima of the R peaks are located at observed samples but can also appear in between samples. The proposed method is compared to the EKF and EKS [14]. The state

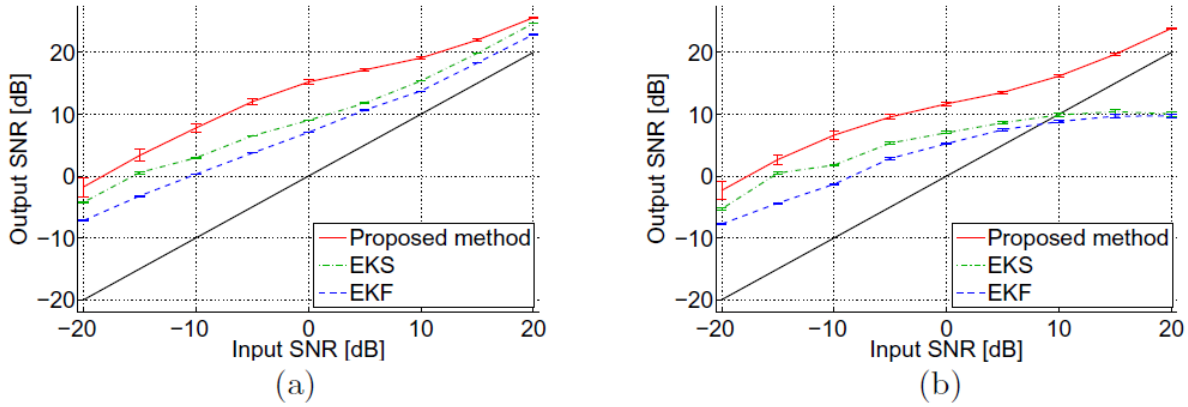

Figure 6.4: ECG denoising: output SNRs vs. the input SNR without (a) and with (b) 3% parameters variability. In both figures, the black line corresponds to the same input and output SNRs. In each case, the median value of each method is plotted, as well as the first and last quartiles as error bars.

model is chosen equal to (3.4):

$$\begin{cases} \theta_{k+1} = (\theta_k + \omega\delta)\mathrm{mod}(2\pi) \\ z_{k+1} = -\sum\limits_{i\in\mathscr{W}} \delta\dfrac{\alpha_{i,k}\omega}{b_{i,k}^2}\Delta\theta_{i,k}\exp(-\dfrac{\Delta\theta_{i,k}^2}{2b_{i,k}^2}) + z_k + \eta_k^z \\ \alpha_{i,k+1} = \alpha_{i,k} + \eta_k^{\alpha_i} \\ b_{i,k+1} = b_{i,k} + \eta_k^{b_i} \\ \psi_{i,k+1} = \psi_{i,k} + \eta_k^{\psi_i} \end{cases} \tag{6.19}$$

(i.e. the same model as the one used to generate data) whose parameters are equal to average values.

Quantitative results are shown in Figure 6.4 which compares the output SNR achieved after denoising against different input SNRs. As it is seen in Figure 6.4(b), the proposed method increases the SNR with a gain between 3 dB to 18 dB. Contrary to extended Kalman filtering, the proposed method always improves the SNR. Indeed, in the case of high input SNR, EKS and EKF deteriorate the SNR: this can be explained by the variability of the simulated ECG as confirmed by Figure 6.4(a), since this phenomenon is only observed with variability. Moreover, one can see that increasing variability decreases the overall performance, but the proposed method keeps the best performance compared with EKS or EKF.

6.5.2 Actual Data: Fetal ECG and MCG Extraction

Figure 6.5 shows efficiency of the proposed method based on the covariance function in (6.2) in extraction of maternal and fetal ECGs from the first sensor on the well-known DaISy fetal ECG database [71], as described in Appendix A, Section A.1.

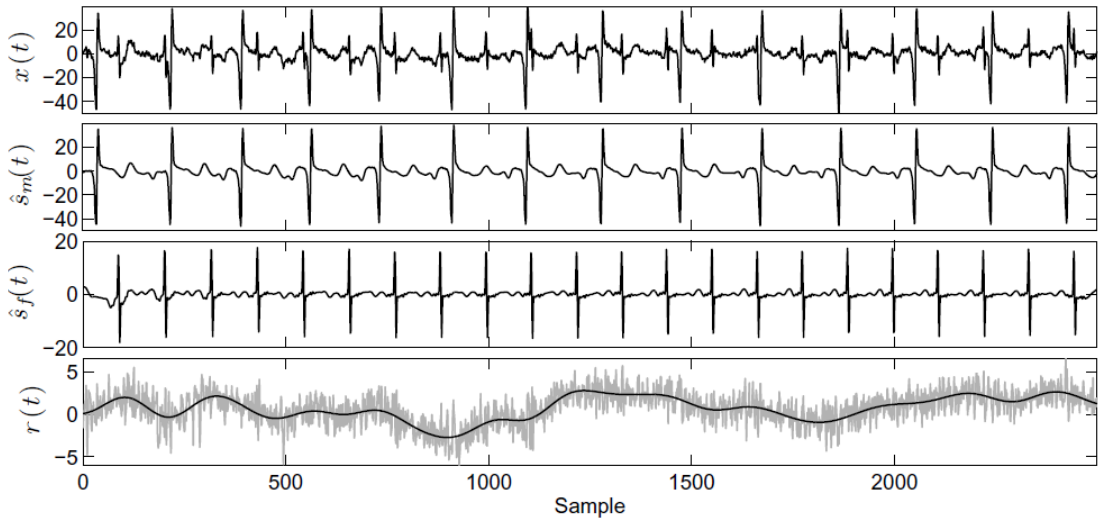

Figure 6.5: Fetal ECG extraction via the proposed method based on the covariance function in (6.2) on DaISy fetal ECG database. Top to bottom: recorded signal $x(t)$, estimated maternal ECG $\hat{s}_m(t)$, estimated fetal ECG $\hat{s}_f(t)$ and residual noise $r(t)$ (light gray curve) with estimated baseline (thick dark curve), respectively.

As it is seen, the proposed method provides suitable estimations for both maternal and fetal ECGs even when maternal and fetal R-peaks are concomitant (e.g., the fourth, seventh and tenth maternal beats). Moreover, a visual inspection of the residual noise $r(t) = x(t) - \hat{s}_m(t) - \hat{s}_f(t)$ confirms the validity of the assumed modeling (6.12). Indeed, this residual noise is effectively composed of a smooth-varying baseline (thick dark curve) related to the first term of covariance function (6.7) and a quasi white noise (validated by its covariance function empirical estimation). Moreover, both contributions are decorrelated with the maternal and fetal ECG signals.

The proposed method based on the simplified covariance function in (6.14) was also applied on the DaISy dataset. The first channel of this dataset with the sampling rate of 250 Hz is used and decomposed into 0-30 Hz, 30-60 Hz and 60-125 Hz sub-bands to apply proposed method. Figure 6.6 shows results of the sequential Kalman filtering method [13, Ch. 5, p. 50] and the proposed method for mECG and fECG extraction on this dataset. In the sequential Kalman filtering method, a synthetic dynamic ECG model within an EKF framework is used. This framework is applied in two steps on the mixture of mECG and fECG to extract fECG. The first step is extraction of mECG, considering fECG and other noises as a unique Gaussian noise and the second step is subtraction of mECG from original signal and extraction of fECG from the residual signal.

As it is seen in Figure 6.6, unlike sequential Kalman filtering method, proposed method does not fail when mECG and fECG waves fully overlap in time. It can be seen in Figure 6.6(a) that between t = 6s and t = 7s, sequential Kalman filtering method is unable to discriminate between maternal and fetal ECG signals. Therefore, some fECG features have been corrupted during mECG extraction. This temporal overlapping between maternal and fetal ECG waves did not lead to corrupting desired signals in the proposed method, because unlike the Kalman filtering

method which directly parameterizes the ECG signals, in the proposed method statistics of ECG signals are parameterized.

The results of the proposed methods based on the covariance function in (6.2) and the simplified one could be also compared. One may notice that visual inspection of these results does not show a significant difference between the performances of the two.

In order to show the capability of the proposed method in extraction of the fECG at different periods of pregnancy, and from different channel locations, the PhysioNet noninvasive fetal electrocardiogram database [72] described in Appendix A Section A.2 was used. The signals are first resampled from 1 kHz to 250 Hz using *resample* MATLAB function, then decomposed into 0-30 Hz, 30-60 Hz and 60-125 Hz sub-bands. Figure 6.7 shows the first 20s of the mixtures and fetal ECG estimates using the simplified covariance function in (6.14) from the datasets ecgca771 channel 3 ecgca274 channel 5, ecgca748 channel 4, and ecgca997 channel 3.

The twin fetal cardiac magnetic signal dataset described in Appendix A, Section A.3 was also employed to investigate the performance of the proposed method based on the simplified covariance function in (6.14). The signal is first resampled from 1025 Hz to 256 Hz, then decomposed into 0-30 Hz, 30-60 Hz and 60-128 Hz sub-bands. Figure 6.8 shows results of the parallel Kalman filtering method in Chapter 3 and the proposed nonparametric method in this chapter. Comparison between Figure 6.8(a) and Figure 6.8(b) shows that the nonparametric method is more successful in recovering the temporal pattern of MCG signals, while the parallel Kalman filtering can better cancel the severe noise of this data. Nevertheless, there might be some applications, in which parameterization of the signal of interest can be very difficult. In those situations, the nonparametric model can be more efficient, since it is more flexible and does not need to model the latent process itself, but its statistical characteristics.

6.6 Summary and Conclusions

In this chapter, a nonparametric modeling for ECG signals was derived. By considering them as second order processes, which are fully defined by their mean and covariance functions, one can model a large class of signals with a few hyper-parameters. From this modeling, denoising or extraction methods are directly obtained as the maximization of the posterior distribution. Numerical experiments showed that the proposed method outperforms an extended Kalman filtering especially in presence of slightly random state parameters. Indeed, Gaussian processes realize a tradeoff between the suitable description of the signal by its second order statistics and its intrinsic variabilities.

As the second step, the proposed method was simplified by adopting a quasi-periodic covariance function whose parameters are optimized for each sub-band of ECG signal. This leads to a less complex optimization problem with less number of hyperparameters. Therefore, it is computationally faster and easier to implement.

Finally, this nonparametric method models the second order statistics of the signal instead of the signal itself. In other words, since the statistical latent process is not directly parameterized, there is no assumption about shape of desired signals. Therefore, it is more flexible and it can

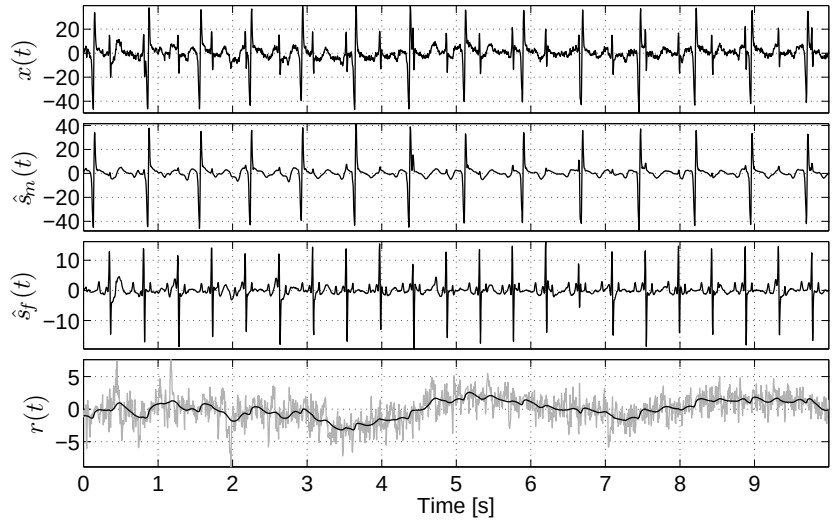

(a) Sequential Kalman filtering

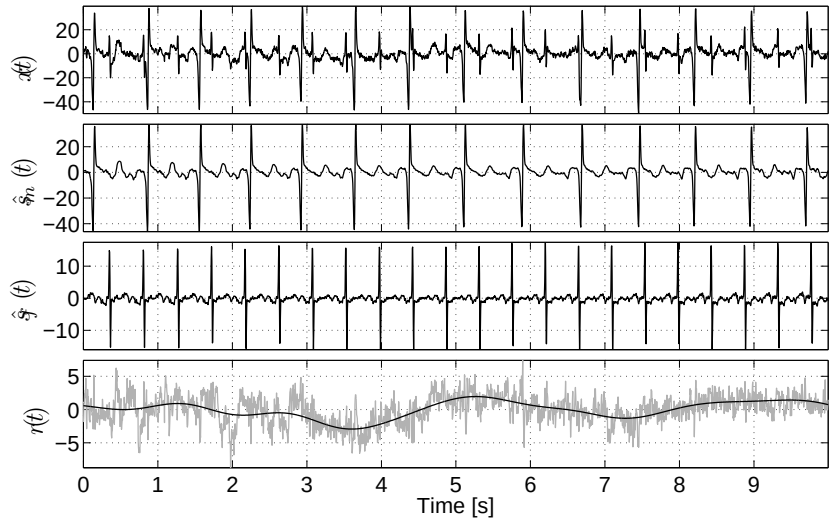

(b) Nonparametric modeling

Figure 6.6: Fetal ECG extraction from a single sensor of DaISy fetal ECG database. Top to bottom: recorded signal $x(t)$, estimated maternal ECG $\hat{s}_m(t)$, estimated fetal ECG $\hat{s}_f(t)$, and residual noise $r(t)$ (light gray curve) with estimated baseline (thick dark curve), respectively. (a): Sequential Kalman filtering, (b): the proposed method based on the simplified covariance function in (6.14)

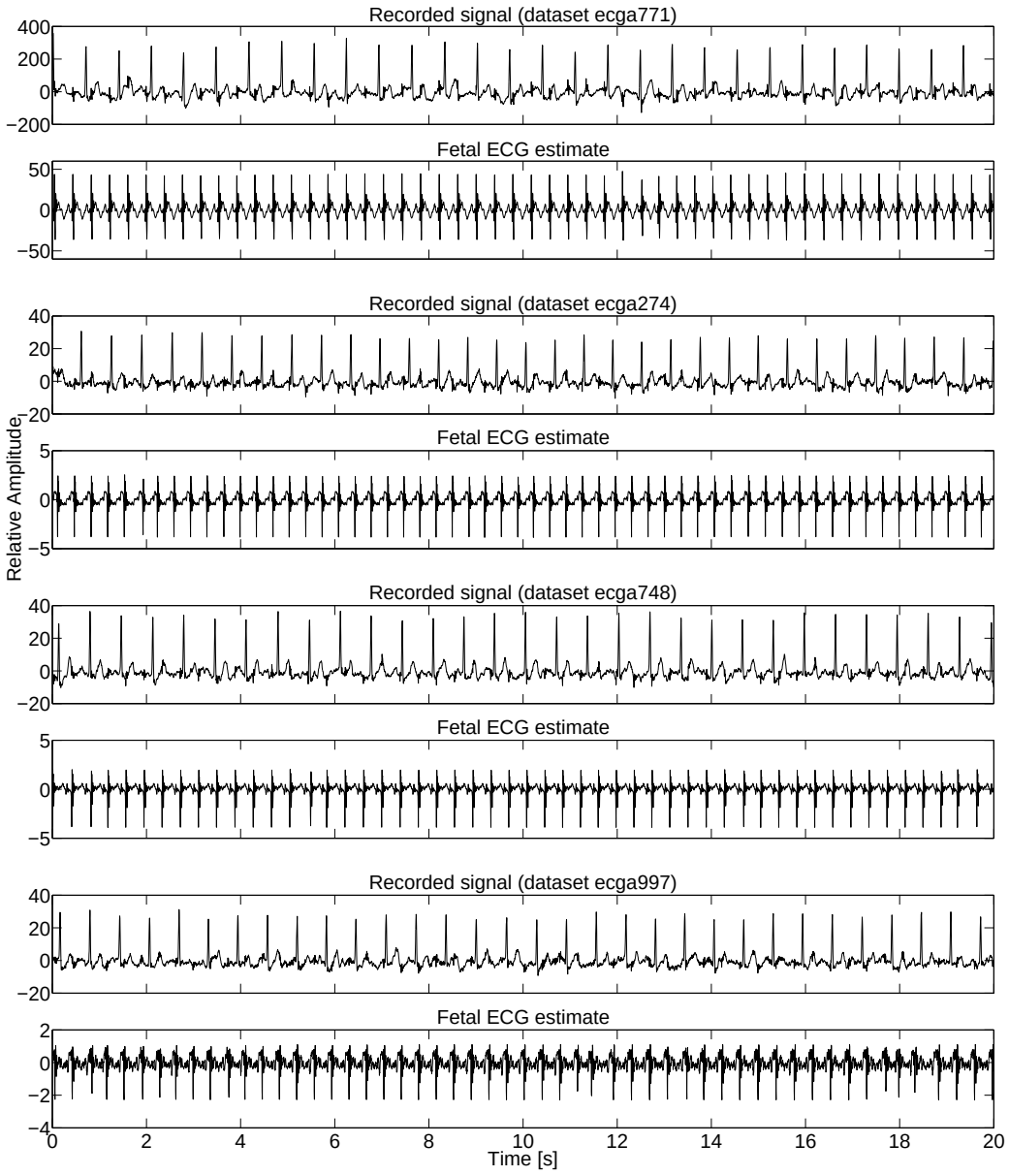

Figure 6.7: ECG mixtures from the PhysioNet noninvasive fetal electrocardiogram database. The datasets ecgca771 channel 3, ecgca274 channel 5, ecgca748 channel 4, and ecgca997 channel 3 and their fetal ECG estimates.

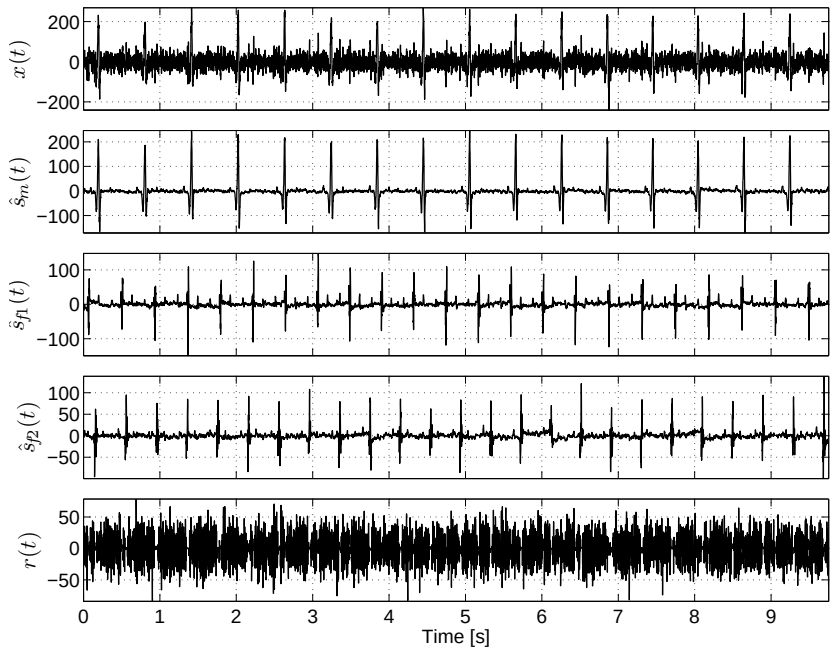

(a) Parallel Kalman filtering

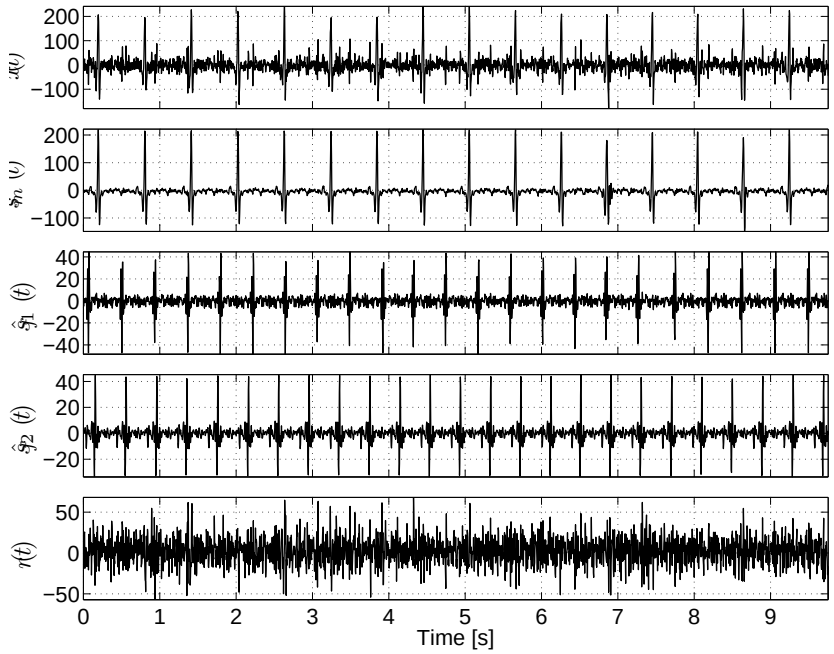

(b) Nonparametric modeling

Figure 6.8: Fetal MCG extraction from a single sensor of the twin MCG database. Top to bottom: recorded signal $x(t)$, estimated maternal MCG $\hat{s}_m(t)$, estimated fetal MCGs $\hat{s}_{f1}(t)$ and $\hat{s}_{f2}(t)$, and residual noise $r(t)$ (light gray curve) with estimated baseline (thick dark curve), respectively. (a): Parallel Kalman filtering, (b): the proposed method based on the simplified covariance function in (6.14).

be efficiently used when parameterization is difficult or when waves of signals overlap in time.

Chapter 7

Conclusions and Future Works

7.1 Conclusions

The problem of extracting and denoising of fetal cardiac signals from an array of electrodes placed on maternal abdomen was studied in this research. The various methods proposed in this study to address this problem were evaluated on actual cardiac recordings and synthetic mixtures generated according to a realistic ECG model to cover many possible scenarios. Regarding the very low SNR of fetal cardiac signals, the main contribution of this work was to develop signal-processing methods that utilize a minimal number of electrodes (down to two) to capture the weak traces of fetal cardiac signals mixed with strong maternal cardiac signals and background noise.

The method developed in Chapter 3 is in fact a refinement of a currently existing Bayesian filtering framework for fetal ECG extraction for single-channel recordings. In single-channel recordings, where less information is available for tracking fetal ECG, we showed that the refinement of the framework is essential to recover full pattern of fetal ECG. The fetal ECG is already the much weaker signal, so if each signal composing the mixture is not accurately modeled, some fetal features will be confused with those of other sources during filtering.

The main idea of Chapter 4 is based on a generally known fact: semi-blind source separation methods that utilize a priori information can be more effective than completely blind source separation methods. Quasi-periodicity is among such a priori information for an ECG signal. In this chapter, considering maternal and fetal ECGs as quasi-periodic signals that are not exactly synchronous with the same period, a tensor decomposition-based method was proposed to separate maternal and fetal ECGs. It was also shown that due to the small amplitude of fetal ECG and less information available using only two channels, robust decompositions significantly outperform the classical decomposition. However, the developed method in this chapter extracts the average signals and is not able to recover the dynamics of ECG signals. Moreover, since this method is categorized as a linear decomposition technique, it is not expected to give good results when noise is mixed in nonlinear manner. The multichannel Kalman filtering framework developed in Chapter 5, is a nonlinear method that can be considered as the second step of the proposed method in Chapter 4. This combination allows us to benefit from the

simplicity of a linear method and the power of a nonlinear method at the same time. This combined multichannel method, which is a general signal-processing tool for extracting event-related sources, including fECG, is able to simultaneously extract and denoise a desired source using a minimal number of electrodes, without losing the valuable inter-event dynamics of the source.

Finally, Chapter 6 was dedicated to develop a nonparametric method based on modeling second-order statistics of ECG signals considered as Gaussian processes. This single-channel method was shown to be more efficient in ECG denoising and fECG extraction, compared with the currently existing KF methods that are parametric. This method also provides roughly the same performance as the KF method in Chapter 3. The main merit of this method is its generic nature, while high computational cost is its main drawback.

In order to have a better view on the contributions of this thesis, Table 2.1 of Chapter 2 is recalled here in Table 7.1. The difference between the two tables is that the blank cells in Chapter 2 are filled by the proposed methods in this thesis. Of course, the proposed methods in this thesis also have their own limitations and drawbacks. According to Table 7.1, the first contribution of this thesis on single-channel methods was to extend the existing Bayesian filter to avoid failing when mECG and fECG waves overlap. However, the proposed method still needs a good state estimate. To overcome this problem, a nonparametric modeling method based on Gaussian processes was developed that does not need a state estimate. Nonetheless, this method is computationally intensive due to its complex optimization problem. For the multichannel methods, the first attempt in this thesis was made on developing a non-iterative method that is applicable to a few channels, and also has a good noise cancellation performance. The robust tensor decomposition method proposed in this thesis addresses this issue. However, as mentioned before, it is not able to recover inter-beat dynamics of the ECG signal. Therefore, the next step in this thesis was to develop a method that recovers these dynamics. Nevertheless, since the proposed multichannel Bayesian filter relies on state equations, a good state estimate is required.

The chapters of this thesis could have been arranged in another way. As depicted in Figure 7.1, the fundamental assumption behind all the proposed methods is the quasi-periodic nature of ECG signal. In the alternative arrangement, we could first begin with the tensor decomposition method, which is deterministic and a multichannel method. Then, to recover inter-beat dynamics of ECG signal, the multichannel Kalman filtering method, which relies on state modeling, would be presented. At the next chapter, the multichannel Kalman filtering method would be reformulated to be applied on single-channel recordings. In this case, although the performance of fECG extraction decreases, the single-channel Kalman filter is still able to preserve inter-beat dynamics of fECG signal and recover the fECG waves even if they fully overlap with the mECG ones. Finally, in order to avoid state estimation, the nonparametric modeling of ECG signal, which is based on Gaussian processes and is categorized as a statistical approach, would be presented.

We should here point out that no one-for-all universal filtering can be currently expected. This is partly due to the various fetal conditions, gestational ages, SNR, etc., and in part due to

Table 7.1: Comparison of the existing and proposed methods for fetal ECG extraction.

	Method	Benefit	Drawback
Single-channel	Wavelet filtering	Suitable for mixtures having different scales	Limited performance in nonlinear mixtures
	SVD-based filtering	Robust to low SNR mixtures	Limited performance in nonlinear mixtures
	Nonlinear filtering	Applicable to nonlinear or degenerate mixtures	Lose inter-beat dynamics, computationally massive
	Bayesian filtering	Preserve inter-beat dynamics	Failure when ECG waves overlap, require good state estimate
	Extended Bayesian filtering	Preserve inter-beat dynamics, not fail when ECG waves overlap	Require good state estimate
	Gaussian process modeling	Preserve inter-beat dynamics, not fail when ECG waves overlap, not require good state estimate	Computationally intensive
Multichannel	SVD/PCA	Applicable to noisy high dimensional data	Limited performance in nonlinear mixtures
	ICA	Generality	Limited separation performance, require several channels
	πCA	Adapted to ECG	Limited noise cancellation, require several channels
	Deflation procedure	Adapted to ECG, applicable to a few channels	Limited noise cancellation, iterative, lose fECG features during mECG cancellation
	Robust tensor decomposition	Adapted to ECG, good noise cancellation, applicable to a few channels	Lose inter-beat dynamics
	Multichannel extended Bayesian filtering	Adapted to ECG, good noise cancellation, applicable to a few channels, preserve fECG features and dynamics during filtering	Require good state estimate

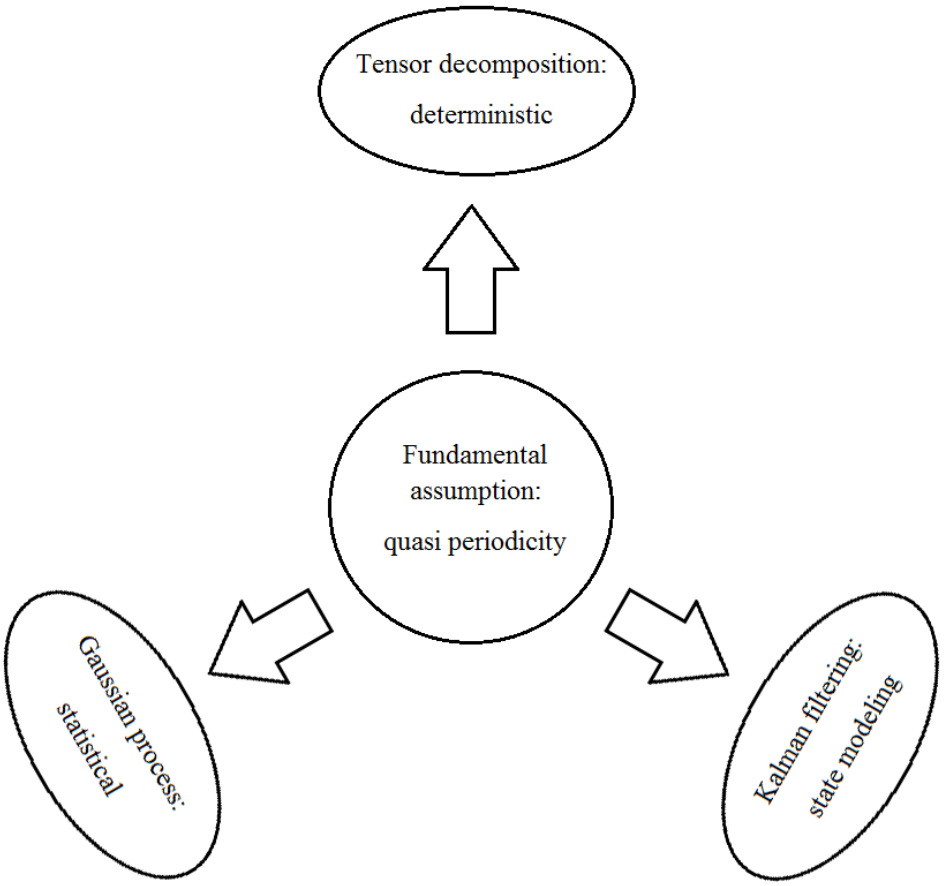

Figure 7.1: Approaches of the proposed methods.

the different objectives and measurement setups. For example, if we are only interested in fetal heart rate variability analysis and at least two channels are available, the fetal R-peak detection method in Chapter 4 could be satisfying, because it is simple, fast and more importantly fully automatic. Nonetheless, for a precise morphological analysis, a more sophisticated algorithm might be required. Accordingly, each method has its own merits and limitations and is applicable for specific scenarios.

7.2 Future Works

Among infinite number of possible questions to answer and researches on fetal cardiac signal extraction and analysis, the results of this dissertation may point to the following directions for future works:

- In this thesis a widely used Bayesian filtering framework based on a realistic model of ECG was adopted and extended in Chapter 3 and Chapter 5. This framework, which is used within Kalman filter, has not been fully automatized yet. The parameter selection procedure of this framework requires manual selection of the center of the Gaussian functions. It is therefore interesting to work on automatization of this procedure. This is especially challenging for fetal ECG parameters, due to the strong interfering maternal ECG. The extracted fetal ECG temporal pattern provided by tensor decomposition in Chapter 4 might be helpful in automatic segmentation of fetal ECG beat. Moreover, this framework can be extended to more advanced filter types such as the particle filter in future research.

- Tensor decomposition methods serve as a powerful and automatic tool for tracking fetal ECG signals. Although two robust criteria proposed in this study were shown to be efficient in capturing desired signal, they need good synchronization of events. In the field of fetal ECG extraction, this means that they require accurate fetal R-peak detection, which is not always easy especially for twins. Therefore, the development of more robust tensor decomposition methods that can handle synchronization errors can be of high interest.

- In Chapter 6 an attempt was made to model ECG signal in nonparametric manner, i.e. statistical characteristics of ECG signal were modeled instead of ECG signal itself. We believe that this approach is very promising due to its generic nature. Although we tried to simplify the primary model to avoid high computational cost and complexity, this method still needs further improvements. The hyperparameter estimation procedure of the proposed method is iterative, so the first step forward might be developing a noniterative procedure for hyperparameter estimation. This can lead to a more robust method. Moreover, other kinds of covariance functions can be also introduced for modeling ECG signal.

- All proposed methods in this thesis and most of the other promising existing methods need fetal R-peak positions as a key prior information for extraction of fetal ECG. Using R-peak positions, the quasi-periodic nature of ECG signal can be exploited. Therefore, a reliable procedure for fetal R-peaks detection is of great interest in fetal ECG extraction

studies. In such a context, the proposed methods should be robust to the variability of the projections of mixed maternal and fetal ECGs. In addition, they should not fail when fECG has very low amplitude or the background noise is very powerful. Fetal R-peak detection in twins (or more) is much more difficult and there are also mixtures in which even visual inspection of the mixture cannot help to reliably detect R-peaks. Therefore, a practical solution in these cases can be obtaining fetal R-peak positions from another modality such as echocardiography.

- The current fECG extraction methods assume that the ECG is normal. Although the resulting errors of these methods in processing of abnormal fECG might be used for abnormality detection, extraction of abnormal fetal ECG signal with highest possible fidelity could be an issue of interest. In this research, a method was developed to simultaneously filter normal and abnormal ECG beats. Cardiac abnormalities usually appear as occasional different beats between a set of normal ones. Although the proposed method addresses this smooth transition between normal and abnormal beats when there is only one ECG in the measurement, it is not currently applicable to abnormal fetal ECG mixed with maternal ECG.

- An essential step that should be taken before using any of the proposed methods in commercial clinical monitoring systems is the clinical validation of the methods over recordings of hundreds of normal and abnormal fetuses for several stages of pregnancy and different conditions. The proposed methods in this thesis were presented as general fetal ECG extraction tools and were validated on realistic simulated data and different actual datasets, each having a different recording protocol. Nevertheless, public gold standard fetal ECG databases are required, such as those for adult ECGs. These datasets should include clinical annotations such as fetal position, QRS complex locations, position of P and T waves, and clinical events.

Finally, although the fetal ECG extraction field is old enough, there are still many considerations that require attention before we can claim that a specific algorithm can be used in commercial devices. Nonetheless, recent advances and developments in this field are promising and they have the potential to positively impact the area of fetal cardiac activity monitoring in a not too distant future.

List of Related Publications

Journals

1. M. Niknazar, B. Rivet, and C. Jutten, "Fetal ECG Extraction by Extended State Kalman Filtering Based on Single-Channel Recordings," *Biomedical Engineering, IEEE Transactions on,* vol. 60, no. 5, pp. 1345-1352, 2013. **(Chapter 3)**

2. M. Niknazar, H. Becker, B. Rivet, C. Jutten, and P. Comon, "Blind Source Separation of Underdetermined Mixtures of Event-Related Sources," accepted for publication in *Signal Processing, Elsevier,* 2014. **(Chapter 4, Chapter 5)**

Conferences

1. M. Niknazar, B. Rivet, and C. Jutten, "Fetal QRS Complex Detection Based on Three-way Tensor Decomposition," Accepted in *Computing in Cardiology Conference (CinC) 2013, Spain,* 2013. **(Chapter 4)**

2. M. Akhbari, M. Niknazar, C Jutten, M. B. Shamsollahi, and B. Rivet, "Fetal Electrocardiogram R-peak Detection Using Robust Tensor Decomposition and Extended Kalman Filtering," Accepted in *Computing in Cardiology Conference (CinC) 2013, Spain,* 2013. **(Chapter 4)**

3. M. Niknazar, H. Becker, B. Rivet, C. Jutten, and P. Comon, "Robust 3-way Tensor Decomposition and Extended State Kalman Filtering to Extract Fetal ECG," Accepted in *21th European Signal Processing Conference (EUSIPCO-2013), Morocco,* 2013. **(Chapter 4, Chapter 5)**

4. M. Niknazar, B. Rivet, and C. Jutten, "Fetal ECG Extraction from a Single Sensor by a Non-parametric Modeling," *20th European Signal Processing Conference (EUSIPCO-2012), Romania,* pp. 949-953, 2012. **(Chapter 6)**

5. M. Niknazar, B. Rivet, and C. Jutten, "Application of Dynamic Time Warping on Kalman Filtering Framework for Abnormal ECG Filtering," *European Symposium on Artificial Neural Networks (ESANN), Belgium,* pp. 139-144, 2012. **(Chapter 5)**

6. B. Rivet, M. Niknazar, and C. Jutten, "Non Parametric Modelling of ECG: Applications to Denoising and Single Sensor Fetal ECG Extraction," *International Conference of Latent*

Variable Analysis and Signal Separation (LVA/ICA), Israel, pp. 470-477, 2012. **(Chapter 6)**

Appendix A

Actual Datasets Description

In this appendix, the datasets used in this thesis to evaluate the proposed methods on actual cardiac recordings are described. These datasets include three noninvasive fetal ECG recordings and one fetal MCG recording data.

A.1 DaISy Fetal ECG

The DaISy dataset includes several kinds of data including biomedical recordings for system identification [71]. The DaISy fetal ECG database [29] consists of a single dataset of cutaneous potential recording of a pregnant woman. A total of 8 channels (5 abdominal and 3 thoracic) are available, sampled at 250 Hz and lasting 10 seconds. The fetal ECG dataset has been provided by Lieven De Lathauwer. Figure A.1 shows this dataset.

A.2 PhysioNet Noninvasive Fetal Electrocardiogram

This database contains a series of 55 multichannel abdominal noninvasive fetal electrocardiogram recordings, taken from a single subject between 21 to 40 weeks of pregnancy [72]. The records have variable durations, and were taken weekly (two or more records were acquired during some weeks). The fECG recordings in this collection were amplified using a g.BSamp Biosignal Amplifier. The data have been stored in EDF/EDF+ format.

Recording information:

- 2 thoracic signals
- 3 or 4 abdominal signals (most records include 4).
- Electrode positioning was varied in order to improve SNR.
- The analog amplifier also includes a 50Hz notch filter switched ON.
- Ag-AgCl transducer.
- Bandwidth: 0.01Hz-100Hz (synchronous sampling of all signals)

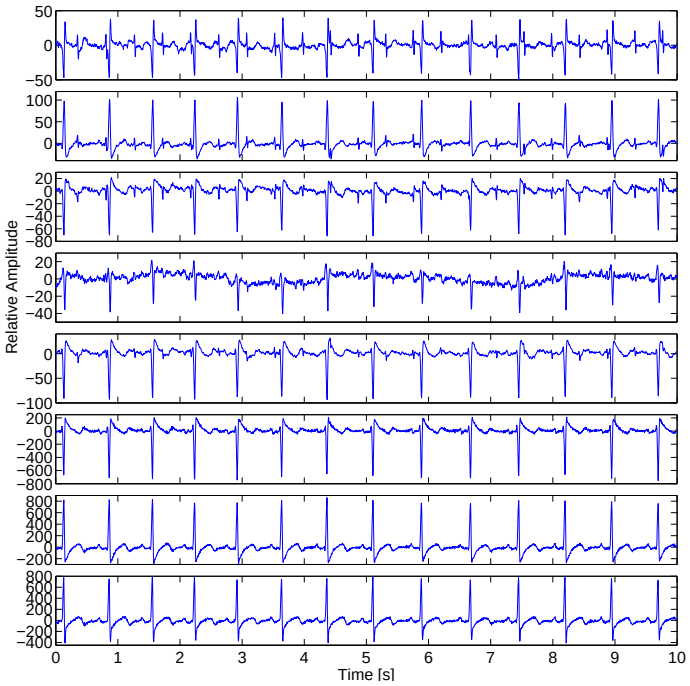

Figure A.1: DaISy Fetal ECG dataset. The first five rows are abdominal channels and the next three rows are thoracic channels.

- Sampling rate: 1kHz.
- Resolution: 16 bits.
- Gains and input ranges are included in the records in EDF format.
- Patient Identification contains the gestational age. The format is week+day.

The database has been prepared for PhysioNet by Marcelino Martinez Sober and Jorge Granado Marco, Digital Signal Processing Group (GPDS), Electronics Engineering Department, ETSE Escuela Técnica Superior de Ingeniería, Universitat de València, Spain. Figure A.2 shows the first ten seconds of one of the available datasets, namely the ecgca711 dataset.

A.3 Twin Fetal MCG

The dataset has been recorded by Dr. Dirk Hoyer in the Biomagnetic Center of the Department of Neurology, in Friedrich Schiller University, Jena, Germany. It consists of several sets of MCG and other signals from mother and twin fetuses, in arrays of 208 channels recorded over 30 minutes, with a sampling rate of 1025Hz. The description of the recorded channels are summarized in Table A.1 [13]. This data has been recorded using a SQUID Biomagnetometer system. The pregnant women were positioned supine, i.e., with a slight twist to either side, to prevent compression of the inferior vena cava by the pregnant uterus. The dewar was positioned

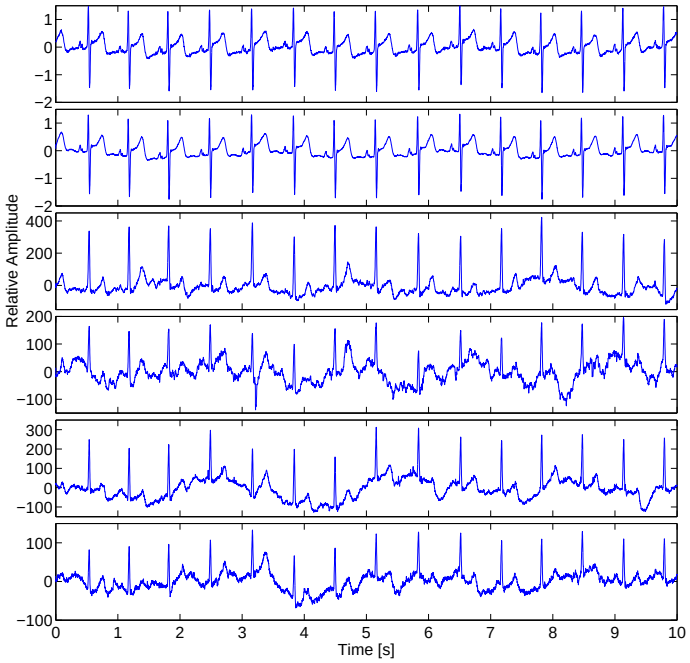

Figure A.2: The first ten seconds of namely the ecgca711 dataset of PhysioNet noninvasive fetal electrocardiogram dataset. The first two rows are thoracic channels and the next four rows are abdominal channels.

Table A.1: Description of the recorded channels [13].

Channels	Description
1-168	magnetic channels
169-195	magnetic reference channels
196-199	electric channels (mother's ECG)
200-208	others

with its curvature above the fetuses after sonographic localization as close to the maternal abdominal wall without contact as possible [109]. Figure A.3 shows the first ten seconds of channels 90 to 95 of one of the available datasets, namely the q00002252 dataset. Please note that visual inspection of the original data shows that the data are highly contaminated with baseline wander. Therefore, the baseline has been removed [13] before plotting.

A.4 PhysioNet/Computing in Cardiology Challenge 2013

The aim of PhysioNet/Computing in Cardiology Challenge 2013 was to encourage development of accurate algorithms for locating QRS complexes and estimating the QT interval in noninvasive fECG signals using carefully reviewed reference QRS annotations and QT intervals as a gold standard, based on simultaneous direct fECG when possible [93]. Data for the challenge consist

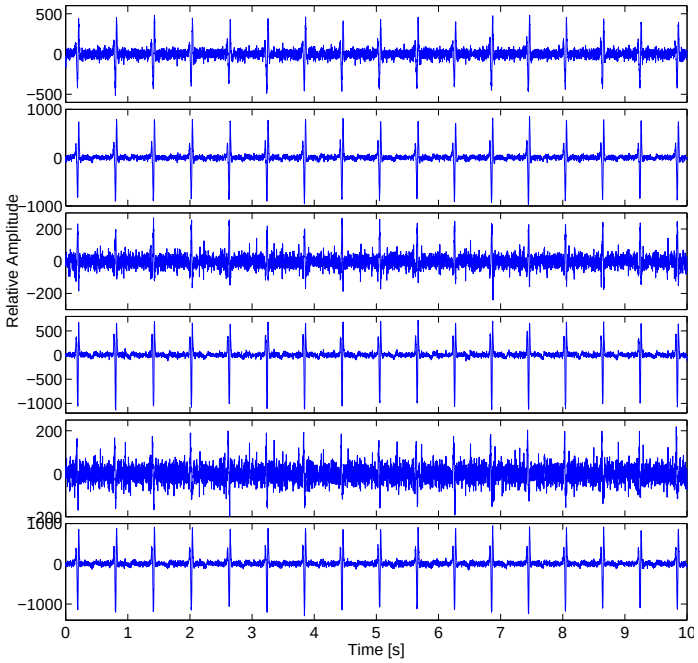

Figure A.3: Twin fetal MCG dataset. The first ten seconds of the channels 90 to 95 of namely the q00002252 dataset after baseline wander removal.

of a collection of one-minute fetal ECG recordings. Each recording includes four noninvasive abdominal signals. The data were obtained from multiple sources using a variety of instrumentation with differing frequency response, resolution, and configuration; although in all cases they are presented as 1000 samples per signal per second. In each case, reference annotations marking the locations of each fetal QRS complex were produced, usually with reference to a direct fECG signal, acquired from a fetal scalp electrode. The direct signals are not included in the challenge datasets, however. Figure A.4 shows the first ten seconds of one of the available datasets, namely the a22 dataset. This dataset is also highly contaminated with baseline wander. Therefore, the baseline has been removed before plotting.

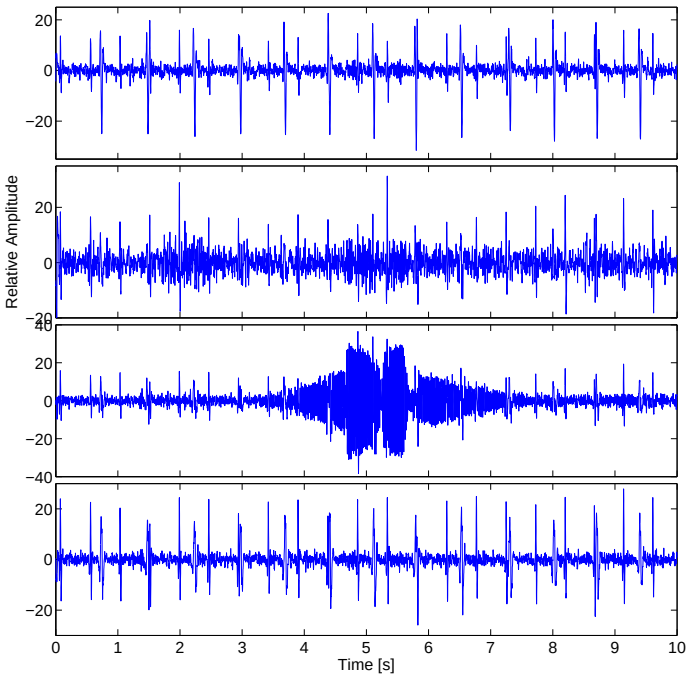

Figure A.4: PhysioNet/Computing in Cardiology Challenge 2013 fetal ECG dataset. The first ten seconds of namely the a22 dataset after baseline wander removal.

Appendix B

Résumé Etendu en Français (Extended Abstract in French)

B.1 Contexte et Objectifs

Les maladies et malformations cardiaques congénitales sont les pathologies natales les plus communes [1] et les principales causes de décès à la naissance [2]. Chaque année, environ un bébé sur 125, présente une forme de malformations cardiaques congénitales [3]. Certains de ces défauts sont tellement légers que le bébé semble en bonne santé pendant de nombreuses années après la naissance et d'autres peuvent conduire à des décès très rapides après la naissance [4]. Les malformations cardiaques apparaissent dans les premières semaines de grossesse lorsque le cœur se forme [3], le suivi régulier de la fréquence cardiaque fœtale et la détection précoce des anomalies cardiaques peut aider l'obstétricien et le cardio-pédiatre à prescrire les médicaments appropriés pendant la grossesse ou à prendre des précautions adaptées lors de l'accouchement.

L'électrocardiogramme (ECG) peut fournir des informations utiles sur le fonctionnement du cœur du fœtus et détecter le fœtus à risque. Bien que l'échocardiographie fœtale puisse être utilisée pour détecter les pics R et de surveiller l'état cardiaque, l'ECG du fœtus (ECGf) peut fournir plus d'informations au médecin, parce que la plupart des anomalies cardiaques est visible sur le signal ECG [11].

L'ECGf peut être mesuré en plaçant des électrodes sur l'abdomen de la mère (Figure B.1). Cependant, ce signal a une très faible puissance et il est mélangé avec plusieurs sources de bruit et d'interférence. Il s'agit notamment de l'activité fœtale cérébrale, des électromyogrammes (EMG) de la mère et du fœtus, de l'activité respiratoire, et des perturbations (50 et 100 Hz) dues au secteur. En outre, sa variabilité dépend de l'âge gestationnel, de la position des électrodes, de l'impédance de la peau, etc. Néanmoins, la contamination principale est l'ECG de la mère (ECGm) [12], dont l'amplitude est très supérieure à celle du fœtus [12]. En conséquence, le problème de base consiste à extraire l'ECGf à partir du mélange des signaux ECG de la mère et du fœtus, dans lequel l'ECGm est un signal de puissance beaucoup plus forte.

En dépit de l'abondante littérature consacrée au filtrage de signaux cardiaques du fœtus, ce problème est complexe et il existe encore de nombreuses questions ouvertes qui justifient

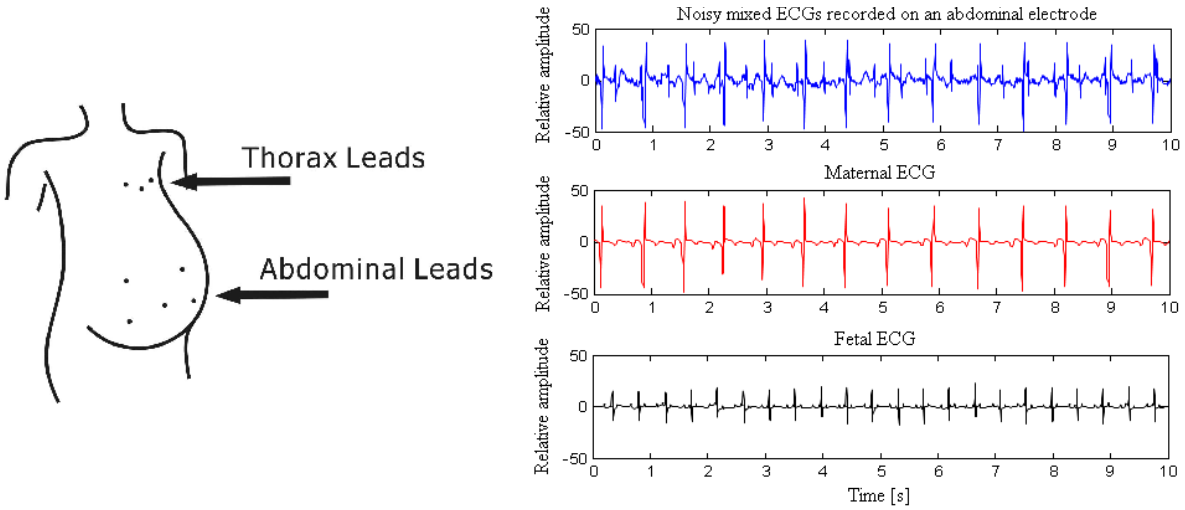

Figure B.1: Exemple typique du signal bruité composite (mélange) enregistré sur une électrode abdominale et des ECGs de la mère et du fœtus.

des recherches en traitement du signal. Un des difficultés, du point de vue de traitement de signal, est qu'il n'y a pas de domaine spécifique (par exemple, temps, espace, ou fréquence), dans laquelle l'ECGf peut être totalement séparé des signaux parasites [13]. Par conséquent, des techniques sophistiquées de traitement du signal sont nécessaires pour résoudre ce problème.

B.1.1 Méthodologies d'Extraction de l'ECG du Fœtus

Depuis la première démonstration de l'ECGf réalisée en 1906 par Cremer [22], diverses méthodes de surveillance de l'ECGf ont été proposées pour obtenir des informations sur l'état du cœur. Selon la synthèse [10], les approches d'extraction de l'ECGf dans la littérature peuvent être classées selon leurs méthodes, qui comprennent la décomposition linéaire ou non linéaire et le filtrage adaptatif.

Les méthodes de décomposition linéaire ou non linéaire sont des approches communes dans lesquelles, des enregistrements uniques ou multicanaux sont décomposés en différents composantes à l'aide des fonctions de base appropriées. Les fonctions de base peuvent être choisies en fonction de la cohérence avec les caractéristiques des composantes de l'ECG du fœtus. Les méthodes de décomposition linéaire utilisent soit des fonctions fixes de base (par exemple, les ondelettes [23]), soit des fonctions de base pilotées par les données (par exemple, des vecteurs singuliers [25]) ont des performances limitées si les mélanges sont non linéaires ou dégénérés [10]. Les méthodes de séparation aveugle ou semi-aveugle de sources, qui peuvent être classées dans les méthodes de décomposition linéaire, ont également été utilisées pour l'extraction de l'ECGf [63, 110]. Ces méthodes sont fondées sur l'hypothèse d'indépendance statistique des signaux ECG maternels et fœtaux, ou de l'existence d'un modèle temporel des signaux [26–28]. Néanmoins, la plupart des méthodes existantes est plutôt générique et n'est pas entièrement adaptée aux caractéristiques du signal ECG. Dans [30], la nature quasi-périodique de l'ECG a été exploitée pour extraire un sous-espace indépendant, basé sur la périodicité des signaux

ECGf. Cette méthode a ensuite été combinée avec un outil de traitement du signal basé sur un modèle afin de mieux éliminer l'ECGm selon une procédure de déflation [31]. Une autre tentative pour adapter les méthodes génériques existantes au signal ECG était d'utiliser l'analyse multidimensionnelle en composantes indépendantes (MICA[1]) pour séparer l'ECGf de l'ECGm et des interférences [32,33]. MICA est une extension de l'analyse en composantes indépendantes (ICA[2]), basé sur un modèle linéaire tel que celui utilisé dans l'ICA. Cependant, à la différence de l'ICA, les composantes ne sont pas supposées être toutes mutuellement indépendantes. Au lieu de cela, il est supposé que les composants peuvent être divisées en groupes, qui sont statistiquement indépendants entre eux, mais les composantes appartenant à un même groupe peuvent être dépendantes. Cette méthode a ensuite été affinée dans [34] pour fonctionner efficacement dans un grand nombre de scénarios. Dans [35,36], décomposition en ondelettes a également été associée à la séparation aveugle de sources pour l'extraction et le débruitage des signaux ECGf. Dans un travail récent, une nouvelle technique a été proposée pour accélérer la méthode ICA traditionnelle utilisée dans l'extraction de l'ECGf [46]. Dans les méthodes de séparation aveugle de sources, il est généralement supposé que les signaux et les bruits sont mélangés d'une manière stationnaire et linéaire. Cependant, ces hypothèses ne sont pas toujours vérifiées [13].

Les transformations non linéaires ont été également utilisées pour l'élimination de l'ECGm et l'extraction de l'ECGf. Dans ces méthodes, on construit l'espace de phase d'un signal bruité et de ses versions retardées, lissé à l'aide de l'analyse en composantes principales (PCA[3]) ou d'autres lisseurs classiques [48–50]. Les échantillons sont ensuite transférés à la représentation dans le domaine temporel. Bien que ces méthodes soient intéressantes car applicables à une mesure réduite à un seul canal maternel abdominal, la sélection des décalages temporels requis pour la construction de la représentation de l'espace des phases est empirique et les variations interbattements importantes des signaux cardiaques peuvent être perdues par le lissage. En outre, ces méthodes présentent une complexité de calcul plus élevée que les méthodes linéaires [10].

Le filtrage adaptatif est une autre approche classique pour la suppression de l'ECGm et l'extraction de l'ECGf [51]. Le filtrage adaptatif classique est basé sur la conception d'un filtre adaptatif pour enlever l'ECGm en utilisant un ou plusieurs canaux de référence maternelle [51, 52], ou pour extraire directement les ondes QRS du fœtus [53, 54]. Cependant, les méthodes de filtrage adaptatif pour la suppression de l'artefact ECGm, nécessitent soit un canal de référence ECGm qui est morphologiquement similaire à la forme d'onde contaminante, soit plusieurs canaux linéairement indépendants pour grossièrement reconstruire toute forme morphologique des références [51]. Ces deux approches sont peu pratiques et ont des performances limitées, car la morphologie des contaminants ECGm dépend fortement de l'emplacement des électrodes, et il n'est pas toujours possible de bien reconstruire l'ECGm à partir d'une combinaison linéaire des électrodes de référence [10]. Par conséquent, un filtre adaptatif qui ne nécessite pas d'électrodes de référence ou tout au plus une seule référence, sans contrainte de similarité morphologique, est d'un grand intérêt. Le cadre du filtrage de Kalman, qui peut être considéré comme un

[1] Acronyme anglais de multidimensional independent component analysis
[2] Acronyme anglais de independent component analysis
[3] Acronyme anglais de principal component analysis

exemple de filtres adaptatifs, est une approche prometteuse qui utilise uniquement des références ECGm et ECGf arbitraires pour supprimer l'ECGm et extraire l'ECGf. Dans [14], un ensemble d'équations d'état a été utilisé pour modéliser la dynamique temporelle des signaux ECG, et pour concevoir un filtre bayésien pour le débruitage de l'ECG. Ce cadre de filtrage bayésien a ensuite été utilisé dans [13] pour extraire l'ECGf dans le mélange d'ECGm et d'ECGf mesuré sur un canal unique. Cependant, comme il est mentionné dans [13], le filtre ne parvient pas à distinguer les composantes maternelles et fœtales quand les battements de l'ECGm et de l'ECGf se superposent entièrement. En pratique, il a été démontré que pour l'extraction de l'ECGf, les méthodes de séparation aveugle de sources surpassent les filtres adaptatifs [45]. Un avantage important du filtrage spatial sur les filtres adaptatifs classiques est leur capacité à séparer des battements ECGm et ECGf qui se superposent, mais au prix d'une acquisition sur plus de deux capteurs.

B.1.2 Défis Actuels

Au-delà de l'électrocardiographie, le cœur du fœtus peut être surveillé à l'aide d'autres modalités [11], y compris l'échocardiographie [56], la phonocardiographie [57, 58], l'oxymétrie de pouls [59], la cardiotocographie [60], et la magnétocardiographie [61, 62]. Parmi ces modalités, l'échocardiographie, qui est fondée sur des techniques classiques d'échographie, est le moyen le plus simple pour la surveillance cardiaque du fœtus [10]. Néanmoins, l'électrocardiographie et la magnétocardiographie peuvent fournir plus d'informations sur l'état de cœur de fœtus, puisque la plupart des anomalies cardiaques se manifestent sur la morphologie de l'ECG ou le magnétocardiogramme (MCG) ou simplement dans les variations de l'intervalle R-R [11]. En raison de la similarité morphologique de l'ECG et de son homologue magnétique, le MCG, les méthodes fondées sur l'ECG sont également applicables à des signaux MCG. En fait, bien qu'utilisant la technologie SQUID, le rapport signal sur bruit (RSB) du MCG du fœtus est habituellement plus élevé que celui de l'ECG, mais les dispositifs d'enregistrement d'ECG sont plus simples et a plus abordables par rapport aux systèmes MCG [10]. Ainsi, la présente étude se concentre sur des mesures électriques (ou magnétiques) de l'activité cardiaque pour récupérer la forme de l'ECG (ou du MCG) du fœtus avec la meilleure fidélité.

Dans un tel contexte, les méthodes proposées rencontrent un certain nombre de facteurs limitants et posent des questions difficiles de traitement du signal. En plus du faible RSB de signal cardiaque fœtal notamment par rapport au ECGm, les mouvements possibles du fœtus et la variation de la fréquence cardiaque fœtale doivent être également considérés. En effet, le rapport entre les rythmes cardiaques fœtaux et maternels, le rapport des puissances des ECG fœtaux et maternels, le bruit et la position du fœtus peut changer la configuration des mélanges. Les méthodes doivent donc être suffisamment robustes à la variation de ces facteurs. En outre, les méthodes doivent être aussi automatiques que possibles pour être appliquées à de longues séries de données avec une interaction minimale avec un opérateur, expert ou non.

Un autre facteur important dans ce contexte est le nombre de capteurs utilisés pour la mesure des signaux. Les méthodes actuelles utilisant un unique capteur ne parviennent pas à récupérer

les variations inter-battements de l'ECGf (par exemple, la méthode moyenne et les méthodes non linéaires) ou sont incapables de distinguer les composantes maternelles et fœtales quand l'ECGf et l'ECGm (en particulier les complexes QRS) se superposent dans le temps. La Figure B.2 montre un exemple de ce type de défaillance sur un enregistrement réel traité par filtrage bayésien [13]. Les méthodes actuelles d'extraction de l'ECGf utilisant plusieurs capteurs (par exemple, la séparation aveugle de sources [29], la séparation semi-aveugle de sources [63], le filtrage adaptatif [51, 53], et l'analyse en composantes périodiques (πCA[4]) [30]) exploitent la redondance des enregistrements multicanaux de l'ECG pour éliminer l'ECGm et les autres sources d'interférence. Néanmoins, même si cette réduction a été couronnée de succès, le bruit exogène peut ne pas être totalement éliminé de cette manière [49]. En outre, ces méthodes nécessitent plusieurs canaux pour récupérer les faibles traces des signaux fœtaux. La Figure B.3 montre un exemple de performance de deux méthodes classiques dans l'extraction des ECG maternels et fœtaux, avec seulement deux électrodes. Comme on peut le voir, à la fois les algorithmes FastICA [64] et πCA échouent complètement à extraire l'ECGf. Ceci peut être expliqué par les limites inhérentes à ces méthodes. Si les ECG maternels et fœtaux sont pas linéairement mélangés, les méthodes linéaires ne sont pas en mesure de les séparer. En outre, les signaux cardiaques sont multidimensionnels [13], de sorte que ces méthodes ne sont pas applicables aux mélanges sous-déterminés (c'est-à-dire avec un trop petit nombre de capteurs) ou lorsque les composantes du fœtus sont dominées par le signal de la mère et le bruit.

Ainsi, un premier défi est le développement de méthodes monocanal, capables de discriminer sans erreur les battements cardiaques maternels et fœtaux (même s'ils se superposent) et de préserver les dynamiques inter-battements de l'ECGf. La performance de ces méthodes doit être évaluée sur différents scénarios et configurations possibles des mélanges. Une seconde étape consiste à développer des méthodes multicanales, qui surpassent les monocanales pour l'extraction et le débruitage de signaux ECGf. Dans ce cas, le second défi est de concevoir des méthodes qui utilisent un nombre minimal d'électrodes. En effet, ceci conduirait à des dispositifs plus économiques, plus pratiques et portables, faciles à utiliser pour la surveillance de l'activité cardiaque du fœtus sur de longues durées, en routine à l'hôpital ou même à domicile.

B.2 Méthodes Proposées

Visuellement, la première caractéristique d'un signal ECG est son caractère quasi-périodique (voir Figure B.4). Dans ce travail, cette propriété de signaux ECG sera l'hypothèse fondamentale de toutes nos méthodes proposées. Nous proposerons trois approches exploitant cette propriété : modélisation de l'état dans un filtre de Kalman, une approche déterministe et une approche statistique. Dans un tel contexte, dans la présente étude, nous nous concentrerons d'abord sur un modèle amélioré du signal enregistré sur une électrode unique afin d'évaluer les performances qui peuvent être obtenues avec une seule électrode par filtrage de Kalman. Ensuite, nous étudierons l'amélioration de performance que l'on peut obtenir avec cette approche en util-

[4]Acronyme anglais de periodic component analysis

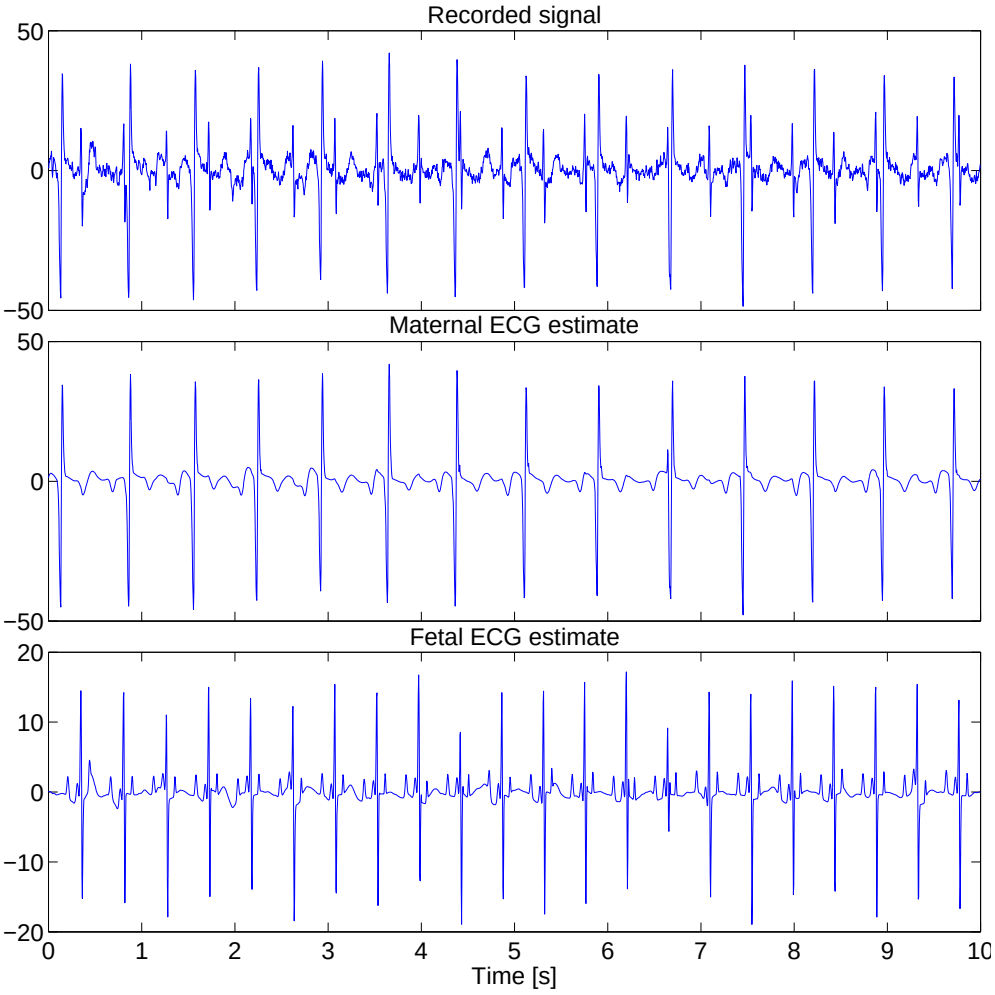

Figure B.2: Exemple typique d'échec de la méthode [13] pour la discrimination des composantes cardiaques de la mère et du fœtus lorsque les complexes QRS de l'ECGm et de l'ECGf se chevauchent entièrement, par exemple entre t = 6s et t = 7s.

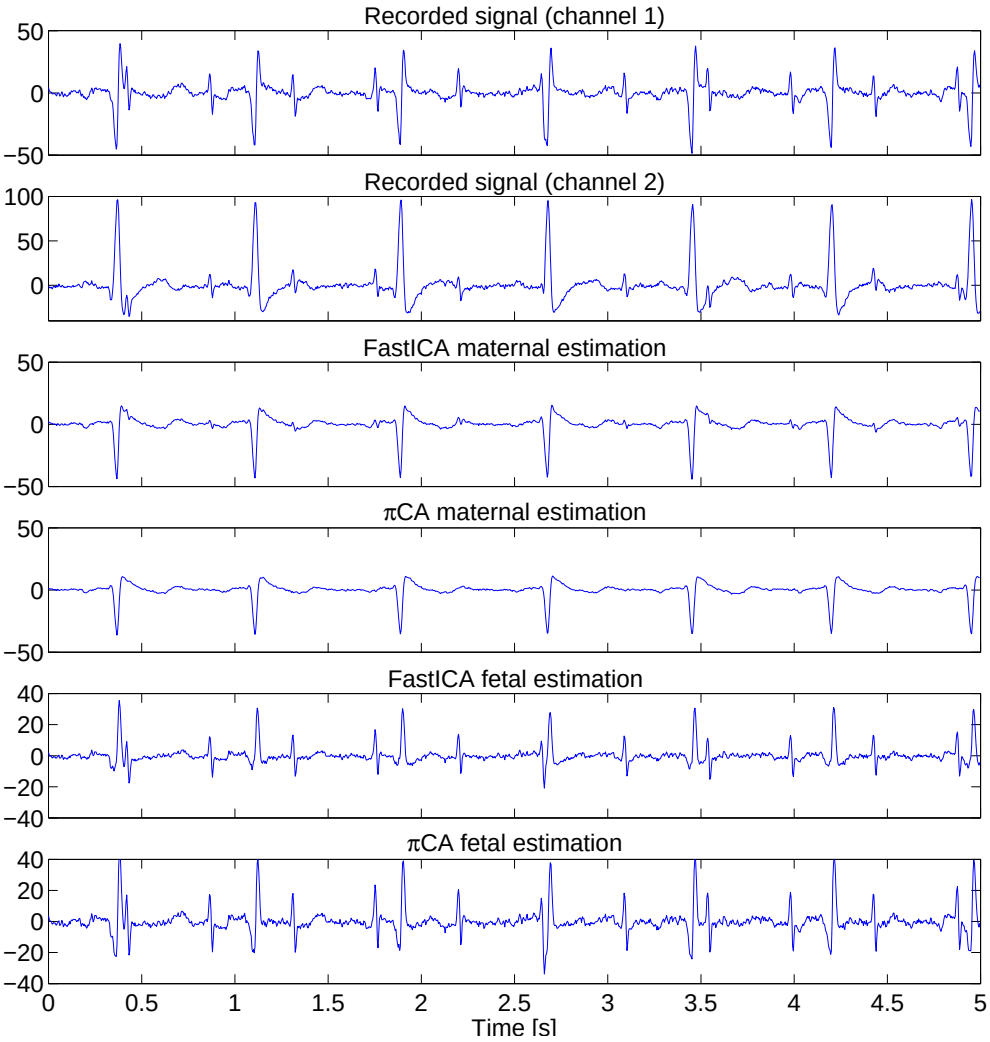

Figure B.3: Exemple typique d'échec des méthodes multicanales actuelles pour l'extraction de l'ECGf à partir d'un mélange d'ECGs maternels et fœtaux utilisant uniquement deux électrodes. Les deux méthodes FastICA et πCA ne parviennent pas à extraire correctement l'ECGf.

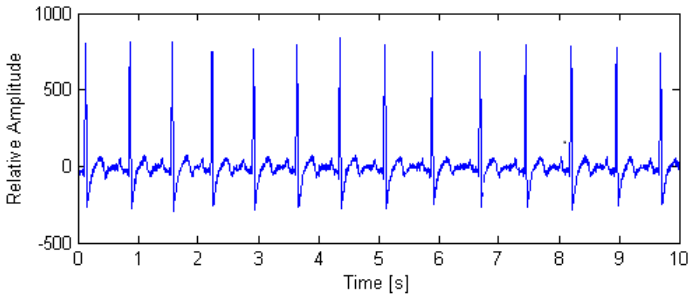

Figure B.4: Signal ECG typique.

isant des enregistrements multicanaux, mais en nous limitant à un nombre minimal d'électrodes (généralement seulement deux). Enfin, nous développerons une méthode non paramétrique (fondée sur les propriétés des statistiques d'ordre 2 d'un signal quasi-périodique), applicable à des enregistrements à canal unique.

B.2.1 Filtrage de Kalman (Approche de Modélisation d'Etat)

Dans cette approche, nous supposons que l'enregistrement est réalisé sur un seul canal. Notre objectif est d'extraire l'ECG du fœtus, considéré comme une variable d'état, et associé à une équation d'état dans un filtre de Kalman. Dans [14], les filtres bayésiens comme le filtre de Kalman étendu (EKF[5]) et le lisseur de Kalman étendu (EKS[6]) ont été proposés pour débruiter les signaux mesurés sur un seul canal. L'équation d'état utilisée pour ces filtres est inspirée de [66], et utilise un mélange de gaussiennes pour modéliser des ECG synthétiques réalistes. L'idée de base est d'approximer le complexe PQRST par la somme pondérée de 5 fonctions gaussiennes dont les paramètres doivent être ajustés. Dans [14], le générateur d'ECG synthétique, initialement proposé dans [66] en coordonnées cartésiennes, a été réécrit en coordonnées polaires. Cette modification permet une interprétation plus simple et claire des signaux [14]. Ce modèle modifié a aussi été développé dans [67]. L'équation d'état associée à d'un signal d'ECG, dans sa forme discrète avec une petite période d'échantillonnage δ, est la suivante :

$$\begin{cases} \theta_{k+1} = (\theta_k + \omega\delta) \mathrm{mod}(2\pi) \\ z_{k+1} = -\sum\limits_{i \in \mathscr{W}} \delta \dfrac{\alpha_{i,k}\omega}{b_{i,k}^2} \Delta\theta_{i,k} \exp(-\dfrac{\Delta\theta_{i,k}^2}{2b_{i,k}^2}) + z_k + \eta_k^z \\ \alpha_{i,k+1} = \alpha_{i,k} + \eta_k^{\alpha_i} \\ b_{i,k+1} = b_{i,k} + \eta_k^{b_i} \\ \psi_{i,k+1} = \psi_{i,k} + \eta_k^{\psi_i} \end{cases} \tag{B.1}$$

où θ, z, α_i, b_i, et ψ_i sont les variables d'état en coordonnées polaires et k désigne l'indice de temps discret. $\mathscr{W} = \{P, Q, R, S, T\}$ est l'ensemble des ondes du complexe PQRST. α_i et

[5] Acronyme anglais de extended Kalman filter
[6] Acronyme anglais de extended Kalman smoother

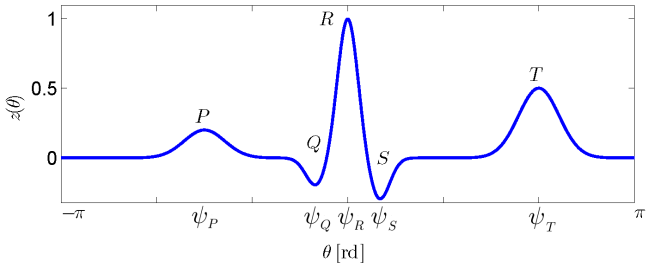

Figure B.5: Illustration de la ψ_i, ce qui correspond au centre de la $i^{\text{ème}}$ fonction gaussienne.

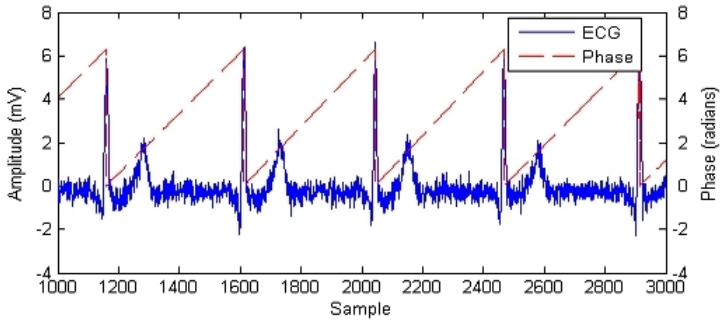

Figure B.6: Illustration de l'interpolation linéaire de phase entre deux intervalles R-R successifs.

b_i correspondent aux paramètres d'amplitude et de largeur des fonctions gaussiennes utilisées pour la modélisation de chacunes des ondes du battement cardiaque. Nous définissons $\Delta\theta_{i,k} = (\theta_k - \psi_i)\text{mod}(2\pi)$, où ψ_i correspond à la phase du maximum de la $i^{\text{ème}}$ fonction gaussienne (voir Figure B.5). Enfin, ω est l'incrément de phase et η_k^z, $\eta_k^{\alpha_i}$, $\eta_k^{b_i}$, et $\eta_k^{\psi_i}$ sont des bruits additifs aléatoires.

Le vecteur d'état du système et le vecteur de bruit du processus sont définis comme suit :

$$\begin{cases} \boldsymbol{x}_k = & [\theta_k, z_k, \alpha_{P,k}, ..., \alpha_{T,k}, b_{P,k}, ..., b_{T,k}, \psi_{P,k}, ..., \psi_{T,k}]^T \\ \boldsymbol{w}_k = & [\omega_k, \eta_k^z, \eta_k^{\alpha_P}, ..., \eta_k^{\alpha_T}, \eta_k^{b_P}, ..., \eta_k^{b_T}, \eta_k^{\psi_P}, ..., \eta_k^{\psi_T}]^T \end{cases} \tag{B.2}$$

et on note $\mathbf{Q}_k = E\left\{\boldsymbol{w}_k \boldsymbol{w}_k^T\right\}$ la matrice de variance-covariance de bruit du processus.

Le vecteur d'état associé à ce signal ECG est donc défini par sa phase θ_k, son amplitude z_k et les paramètres des fonctions gaussiennes, α_i, b_i, et ψ_i. En plus de la mesure de l'ECG bruité, noté s_k, une phase observée, ϕ_k, est obtenue par une interpolation linéaire dans $[0, 2\pi[$ entre deux intervalles R-R successifs (Figure B.6), conduisant au système suivant :

$$\begin{bmatrix} \phi_k \\ s_k \end{bmatrix} = \begin{bmatrix} 1 & 0 \\ 0 & 1 \end{bmatrix} . \begin{bmatrix} \theta_k \\ z_k \end{bmatrix} + \begin{bmatrix} u_k \\ v_k \end{bmatrix}, \tag{B.3}$$

où u_k et v_k sont les bruits d'observation supposés de moyenne nulle et de matrice de variance-covariance notée $\mathbf{R}_k = E\left\{[u_k, v_k]^T [u_k, v_k]\right\}$.

Les ECGs composants le mélange observé peuvent être estimés en appliquant l'EKF de manière récursive : à chaque étape, un ECG est extrait selon une procédure de déflation [13]. Dans le cas d'un mélange d'ECGm et d'ECGf, la première étape extrait, à partir de l'enregistrement brut, l'ECG dominant (souvent l'ECGm) en considérant la somme de l'ECGf et des autres bruits comme un bruit gaussien unique. Après la soustraction de l'ECG dominant à partir du signal original, la deuxième étape est l'extraction de l'ECGf à partir de ce signal résiduel. Cette procédure est appelée EKF séquentiel ou EKS séquentiel (EKF-seq ou EKS-seq). Dans la première étape de cette procédure de déflation, l'ECGf et les autres bruits sont modélisés par des bruits gaussiens $\mathbf{v}_k$ et $\mathbf{w}_k$, qui n'est pas une hypothèse pertinente. De plus, les ECGf peuvent être confondus avec l'ECG dominant - et éliminés lors de la soustraction - lorsque leurs ondes (en particulier le complexe QRS) se chevauchent. Enfin, les erreurs de chaque étape de déflation, s'accumulent au cours de la procédure, limitant les performances.

Méthodes

Pour résoudre ce problème, nous proposons d'étendre le cadre EKF pour l'extraction d'un ECG à l'extraction de plusieurs ECGs. Pour cela, chaque ECG présent dans le signal observé sera modélisé par une équation d'état. Les nouvelles équations d'état sont associées à des équations d'observation étendues de sorte que chaque ECG possède une observation indépendante de la phase. Enfin, l'observation sur le capteur unique est le mélange de tous les ECGs et du bruit.

Les équations d'état (B.1) sont ainsi généralisées pour modéliser simultanément N ECGs mélangés dans une seule observation. Dans ce cas, les équations d'état peuvent être écrites :

$$
\begin{cases}
\theta_{k+1}^{(1)} &= (\theta_k^{(1)} + \omega^{(1)}\delta)\mathrm{mod}(2\pi) \\
z_{k+1}^{(1)} &= -\sum_{i\in\mathscr{W}^{(1)}} \delta \frac{\alpha_{i,k}^{(1)}\omega^{(1)}}{b_{i,k}^{(1)^2}} \Delta\theta_{i,k}^{(1)} \exp\left(-\frac{\Delta\theta_{i,k}^{(1)^2}}{2b_{i,k}^{(1)^2}}\right) + z_k^{(1)} + \eta_k^{z^{(1)}} \\
\alpha_{i,k+1}^{(1)} &= \alpha_{i,k}^{(1)} + \eta_k^{\alpha_i^{(1)}} \\
b_{i,k+1}^{(1)} &= b_{i,k}^{(1)} + \eta_k^{b_i^{(1)}} \\
\psi_{i,k+1}^{(1)} &= \psi_{i,k}^{(1)} + \eta_k^{\psi_i^{(1)}} \\
&\vdots \\
\theta_{k+1}^{(N)} &= (\theta_k^{(N)} + \omega^{(N)}\delta)\mathrm{mod}(2\pi) \\
z_{k+1}^{(N)} &= -\sum_{i\in\mathscr{W}^{(N)}} \delta \frac{\alpha_{i,k}^{(N)}\omega^{(N)}}{b_{i,k}^{(N)^2}} \Delta\theta_{i,k}^{(N)} \exp\left(-\frac{\Delta\theta_{i,k}^{(N)^2}}{2b_{i,k}^{(N)^2}}\right) + z_k^{(N)} + \eta_k^{z^{(N)}} \\
\alpha_{i,k+1}^{(N)} &= \alpha_{i,k}^{(N)} + \eta_k^{\alpha_i^{(N)}} \\
b_{i,k+1}^{(N)} &= b_{i,k}^{(N)} + \eta_k^{b_i^{(N)}} \\
\psi_{i,k+1}^{(N)} &= \psi_{i,k}^{(N)} + \eta_k^{\psi_i^{(N)}}
\end{cases}
\tag{B.4}
$$

Par conséquent, les vecteurs d'état et de bruit du nouveau modèle sont :

$$\begin{cases} \boldsymbol{x}_k = & [\theta_k^{(1)}, z_k^{(1)}, \alpha_{P,k}^{(1)}, ..., \alpha_{T,k}^{(1)}, b_{P,k}^{(1)}, ..., b_{T,k}^{(1)}, \psi_{P,k}^{(1)}, ..., \psi_{T,k}^{(1)}, \dots, \\ & \theta_k^{(N)}, z_k^{(N)}, \alpha_{P,k}^{(N)}, ..., \alpha_{T,k}^{(N)}, b_{P,k}^{(N)}, ..., b_{T,k}^{(N)}, \psi_{P,k}^{(N)}, ..., \psi_{T,k}^{(N)}]^T \\ \boldsymbol{w}_k = & [\omega_k^{(1)}, \eta_k^{z^{(1)}}, \eta_k^{\alpha_P^{(1)}}, ..., \eta_k^{\alpha_T^{(1)}}, \eta_k^{b_P^{(1)}}, ..., \eta_k^{b_T^{(1)}}, \eta_k^{\psi_P^{(1)}}, ..., \eta_k^{\psi_T^{(1)}}, \dots, \\ & \omega_k^{(N)}, \eta_k^{z^{(N)}}, \eta_k^{\alpha_P^{(N)}}, ..., \eta_k^{\alpha_T^{(N)}}, \eta_k^{b_P^{(N)}}, ..., \eta_k^{b_T^{(N)}}, \eta_k^{\psi_P^{(N)}}, ..., \eta_k^{\psi_T^{(N)}}]^T \end{cases} \tag{B.5}$$

et on note $\mathbf{Q}_k = E\left\{\boldsymbol{w}_k \boldsymbol{w}_k^T\right\}$ la matrice de variance-covariance du bruit de modèle.

Dans ce modèle, chaque jeu de paramètres $[\theta_k^{(n)}, z_k^{(n)}, \alpha_{P,k}^{(n)}, ..., \alpha_{T,k}^{(n)}, b_{P,k}^{(n)}, ..., b_{T,k}^{(n)}, \psi_{P,k}^{(n)}, ..., \psi_{T,k}^{(n)}]^T$ $\forall n \in \{1, \dots, N\}$ est liée à l'un des ECGs. Ici aussi, en détectant les pics R des N ECGs, N observations de phase supplémentaires sont obtenues. Pour ce faire, une valeur de phase comprise entre 0 et 2π est attribuée aux échantillons intermédiaires des intervalles R-R, pour chacun des N ECGs, séparément. Ces observations de phase supplémentaires sont utilisées pour synchroniser les trajectoires dynamiques du filtre de Kalman avec les signaux bruités de référence, sans nécessiter de synchronisation manuelle. De cette façon, la nature quasi-périodique de chaque signal ECG est exploitée. Ainsi, les observations de phase des N ECGs, $\phi^{(1)}$,...,$\phi^{(N)}$, et le mélange bruité (mesuré sur un seul canal) des N ECGs, s, sont liés au vecteur d'état à l'instant k comme suit :

$$\begin{bmatrix} \phi_k^{(1)} \\ \phi_k^{(2)} \\ \vdots \\ \phi_k^{(N)} \\ s_k \end{bmatrix} = \left[\begin{array}{ccc:ccc} 1 & 0 & \dots & 0 & \dots & 0 \\ 0 & 1 & \dots & 0 & \dots & 0 \\ \vdots & \vdots & \ddots & 0 & \dots & 0 \\ \hdashline 0 & 0 & \dots & 1 & \dots & 1 \end{array}\right] \cdot \begin{bmatrix} \theta_k^{(1)} \\ \theta_k^{(2)} \\ \vdots \\ \theta_k^{(N)} \\ z_k^{(1)} \\ z_k^{(2)} \\ \vdots \\ z_k^{(N)} \end{bmatrix} + \begin{bmatrix} u_k^{(1)} \\ u_k^{(2)} \\ \vdots \\ u_k^{(N)} \\ v_k \end{bmatrix} \tag{B.6}$$

où $u_k^{(1)}$,...,$u_k^{(N)}$ et v_k sont les bruits d'observation supposés de moyenne nulle, et la matrice de variance-covariance du bruit d'observation est $\mathbf{R}_k = E\left\{[u_k^{(1)}, ..., u_k^{(N)}, v_k]^T [u_k^{(1)}, ..., u_k^{(N)}, v_k]\right\}$.

Ce modèle d'état étendu de filtre de Kalman est appelé EKF parallèle ou EKS parallèle (EKF-par, ou EKS-par), respectivement. L'EKF-par, ou l'EKS-par sont plus précis pour extraire l'ECGf à partir de capteurs abdominaux que l'EKF-seq ou l'EKS-seq. En effet, dans la méthode proposée tous les ECGs sont modélisés conjointement par les équations d'états de sorte que seuls les vecteurs de bruit de l'état et de la mesure sont supposés être distribués normalement, ce qui est réaliste. De plus, les équations d'état de l'EKF-par modélisent correctement la superposition possible des ondes de plusieurs ECGs. Enfin, les bruits d'état et d'observation permettent l'adaptation à des variabilités des formes de l'ECG. Bien sûr, ce modèle ne peut pas modéliser de trop grandes variations (par exemple des arythmies), mais l'existence d'un résidu important permettrait de détecter des battements anormaux.

L'EKF-par et l'EKS-par nécessitent plusieurs paramètres d'état, notamment $\{\alpha_i^{(n)}, b_i^{(n)}, \psi_i^{(n)}, \omega^{(n)}\}_{i \in \mathscr{W}_n}$. La procédure d'estimation des paramètres décrits dans [14] pour un seul ECG peut être facilement étendue pour estimer les paramètres d'état de N ECGs.

Résultats

La Figure B.7 présente les résultats de l'EKS-par et de l'EKS-seq en utilisant un seul (le premier) canal des données DaISy [71]. La méthode πCA [30], utilisant tous les huit canaux, est utilisée comme référence (*golden standard*). Contrairement à l'EKS-seq, l'EKS-par extrait correctement les ECGf, même lorsque les complexes QRS des ECGf et l'ECGm se superposent.

Cette méthode est capable d'extraire l'ECGf à différentes périodes de la grossesse et sur tous les capteurs, quelle que soit la position du capteur sur l'abdomen de la mère. Pour le montrer, nous avons utilisé des enregistrements issus de la base de données non invasive d'ECGf PhysioNet [72]. Les premières 20 secondes des mélanges et les ECGf estimés par l'EKS-par sur les données ecgca274 canal 5, ecgca748 canal 4, et ecgca997 canal 3 sont montrées à la Figure B.8.

La méthode proposée a été principalement conçue pour les signaux d'ECG. Néanmoins, en raison de la similarité morphologique entre l'ECG et le MCG, elle est applicable directement à des enregistrements MCG. Un ensemble d'enregistrements MCG de fœtus jumeaux a été utilisé pour évaluer les performances de la méthode proposée dans l'extraction de signaux cardiaques de jumeaux. La Figure B.9 présente les résultats de l'EKS-par pour extraire les deux signaux MCG fœtaux à partir d'un unique capteur. Même si la méthode multicanal πCA (utilisant 168 capteurs !) donne de meilleurs résultats que les méthodes de canal unique (EKF-par ou EKS-seq), l'algorithme EKS-par réussit à extraire les deux MCG fœtal alors que l'EKS-seq n'est pas capable de discriminer correctement les deux MCG fœtaux quand ils se chevauchent (voir parties de signaux encadrées, dans la Figure B.9).

En considérant différents scénarios possibles dans le problème de l'extraction de l'ECGf, nous avons évalué les performances de la méthode proposée sur des données synthétiques, en faisant notamment varier la puissance de bruit d'entrée, le rapport entre les amplitudes de l'ECGf et de l'ECGm, et le rapport entre les rythmes cardiaques du fœtus et de la mère. Les résultats montrent la robustesse de l'algorithme dans une large gamme de variation de tous ces paramètres, ce qui atteste de son intérêt sur un large éventail des configurations réelles.

B.2.2 Décomposition Tensorielle (Approche Déterministe)

Dans cette approche, nous supposons que les données ont été enregistrées par plusieurs capteurs, l'objectif restant de n'en utiliser qu'un nombre réduit (généralement deux). Chaque signal ECG pouvant être considéré comme multidimensionnel [13], les signaux enregistrés sont donc des mélanges sous-déterminés (i.e. plus de sources que de capteurs) car issus du mélange de l'ECG de la mère et de celui ou ceux du ou des fœtus. Les méthodes classiques de séparation aveugle de sources telles que l'ICA ou la πCA ne peuvent être utilisées. Dans ce travail, nous utilisons la décomposition tensorielle qui peut être appliquée aux mélanges sous-déterminés.

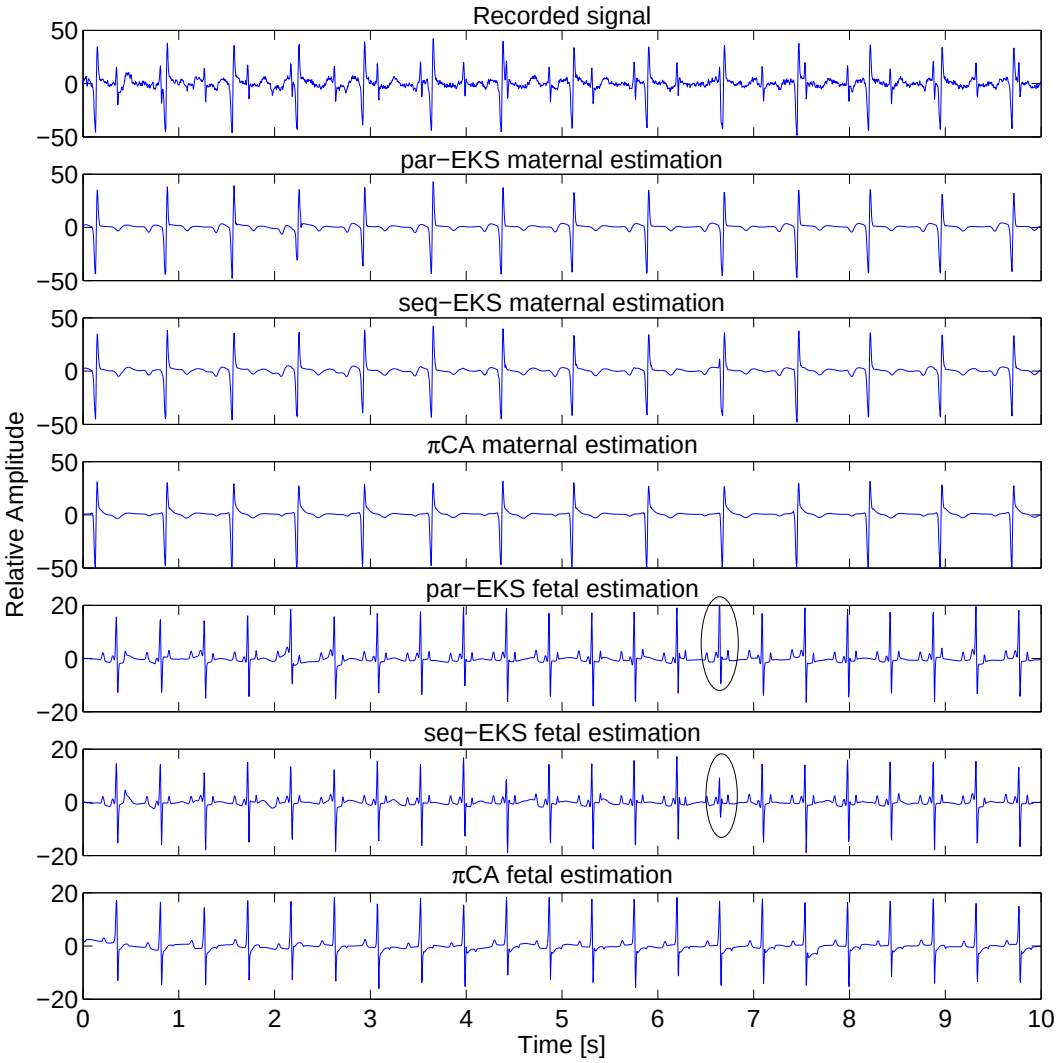

Figure B.7: Comparaison de l'extraction de l'ECGf par les méthodes EKS-par, EKS-seq et πCA sur un seul canal des données DaISy. Contrairement à l'EKS-seq, l'EKS-par extrait correctement l'ECGf même quand l'ECGm et l'ECGf se superposent. Ceci est particulièrement visible entre t = 6s et t = 7s.

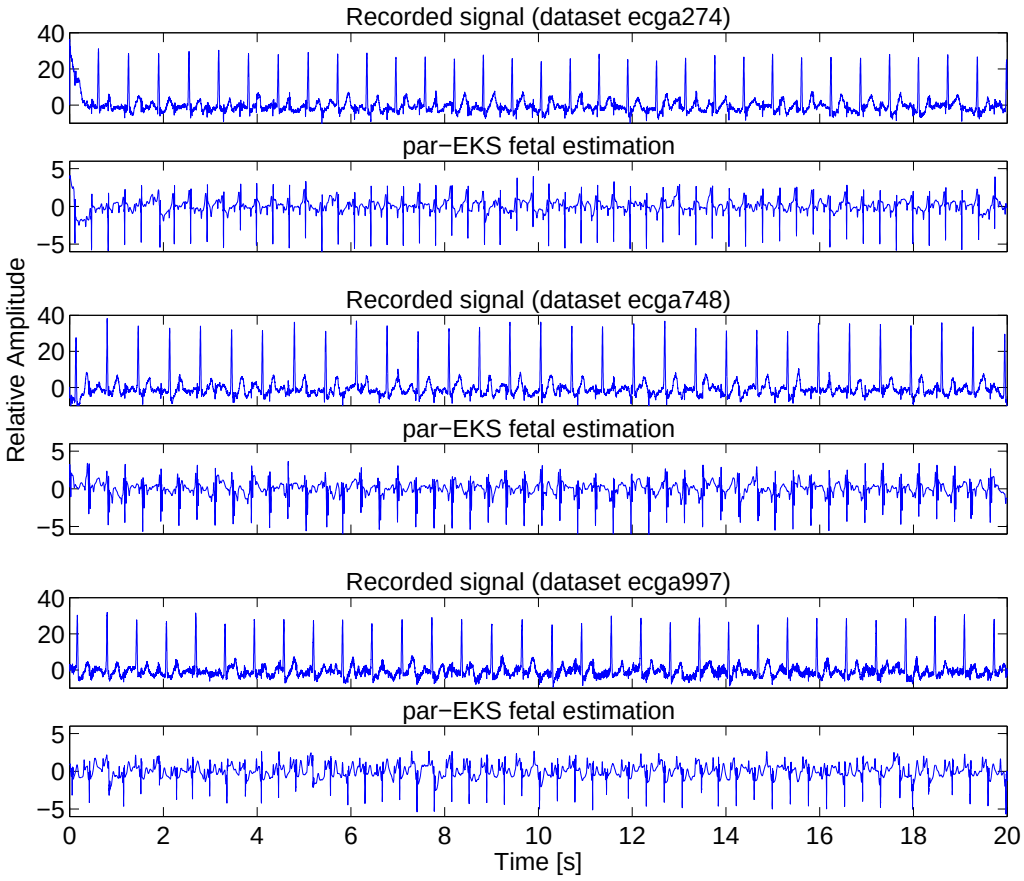

Figure B.8: Mélanges ECG (base de données ECGf PhysioNet) : données ecgca274 canal 5, ecgca748 canal 4, et ecgca997 canal 3, et les ECGf estimés par EKS-par.

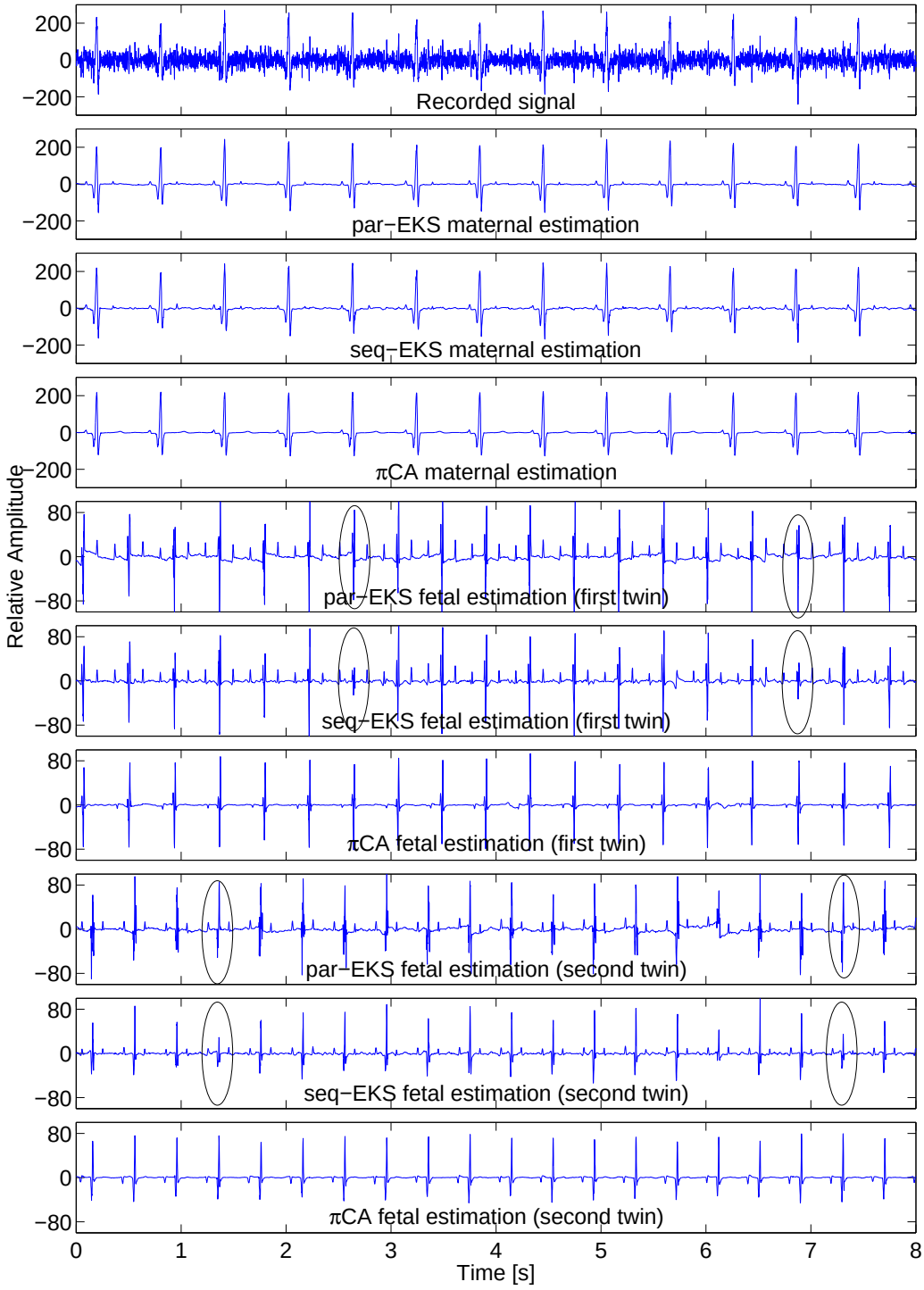

Figure B.9: Résultats des EKS-par, EKS-seq, et πCA sur les données MCG de jumeaux. Contrairement à l'EKS-seq, l'EKS-par extrait correctement le MCG du fœtus même quand le MCG maternel et le MCG fœtal se chevauchent entièrement dans le temps. Ceci est particulièrement visible entre t = 2s et t = 3s et entre t = 6s et t = 7s pour le premier fœtus et entre t = 1s et t = 2s et entre t = 7s et t = 8s pour le second fœtus.

La première étape consiste à construire un tenseur en réarrangeant les données bi-dimensionnelles (temps × capteurs) originelles dans un tenseur tri-dimensionnel. Pour cela, la quasi-périodicité des signaux ECG est exploitée comme hypothèse de base comme dans le cas des signaux de télécommunication [16]. Cette méthode peut s'appliquer aux mélanges sous-déterminés tant que les Q sources d'intérêt sont composées de symboles périodiques dès lors que ces périodes sont différentes d'une source à l'autre. A cette fin, pour chacune des sources à extraire, un tenseur tri-dimensionnel (capteurs × période du symbole × motif temporel) est construit. Ainsi pour la $q^{\text{ème}}$ source, les L_q périodes composées chacune de T_q échantillons temporels enregistrées sur M capteurs permettent de construire le tenseur $\mathbf{Y}^{(q)} \in \mathbb{R}^{M \times L_q \times T_q}$.

Dans le contexte de l'extraction de l'ECG, en raison de la nature quasi-périodique du signal ECG, on peut dans un premier temps détecter les pics R de l'ECG pour identifier les différents battements (symboles). Ensuite, le tenseur $\mathbf{Y}^{(1)}$ est construit en se synchronisant sur les battements de la mère puis un autre tenseur $\mathbf{Y}^{(2)}$ est construit de la même façon à partir des pics R relatifs au fœtus. Ces tenseurs $\mathbf{Y}^{(q)}$ peuvent donc être décomposés en matrices de facteurs $\mathbf{A}^{(q)} \in \mathbb{R}^{M \times R_q}$, $\mathbf{S}^{(q)} \in \mathbb{R}^{L_q \times R_q}$ et $\mathbf{H}^{(q)} \in \mathbb{R}^{T_q \times R_q}$ qui fournissent des estimations de la matrice de mélange, de l'amplitude des battements de l'ECG et la structure temporelle de ceux-ci. Ces matrices sont obtenues par la décomposition canonique polyadique (CP) selon le critère :

$$\min_{\{\mathbf{A}^{(q)},\mathbf{S}^{(q)},\mathbf{H}^{(q)}\}} \sum_{i,j,k} \left\| y_{ijk}^{(q)} - \sum_{r=1}^{R_q} a_{ir}^{(q)} s_{jr}^{(q)} h_{kr}^{(q)} \right\|_F^2, \tag{B.7}$$

où $y_{ijk}^{(q)}$ sont les éléments de $\mathbf{Y}^{(q)}$ et R_q est le rang supposé pour la $q^{\text{ème}}$ source correspondant au nombre de composantes de cet ECG. Si $T_q \geqslant R_q$ et $L_q \geqslant R_q$ alors $M = 2$ capteurs suffisent à séparer R_q composantes [16]. Ceci démontre que l'on peut extraire les ECG de la mère et du fœtus à partir de seulement 2 capteurs. Dans ce cas, un algorithme classique, basé sur la décomposition en valeurs propres [111], peut être utilisé pour calculer la décomposition (CP[7]).

Cependant, le critère classique (B.7) ne permet pas de retrouver le signal ECG du fœtus. Ceci est du au fait que le signal ECG du fœtus ECGf est bien moins puissant que celui de la mère ECGm. Pour surmonter ce problème, une décomposition tensorielle robuste est proposée en modifiant la fonction de coût de la CP.

Méthodes

Le premier critère robuste est fondé sur une pondération du critère originel CP (WCP[8]) qui applique un poids sur chacun des éléments du tenseur pour mieux se concentrer sur le signal d'intérêt. En conséquence, le nouveau critère est :

$$\min_{\{\mathbf{A}^{(q)},\mathbf{S}^{(q)},\mathbf{H}^{(q)}\}} \sum_{i,j,k} \left\| w_{ijk}^{(q)} \left(y_{ijk}^{(q)} - \sum_{r=1}^{R_q} a_{ir}^{(q)} s_{jr}^{(q)} h_{kr}^{(q)} \right) \right\|_F^2, \tag{B.8}$$

[7] Acronyme anglais de canonical polyadic
[8] Acronyme anglais de weighted CP

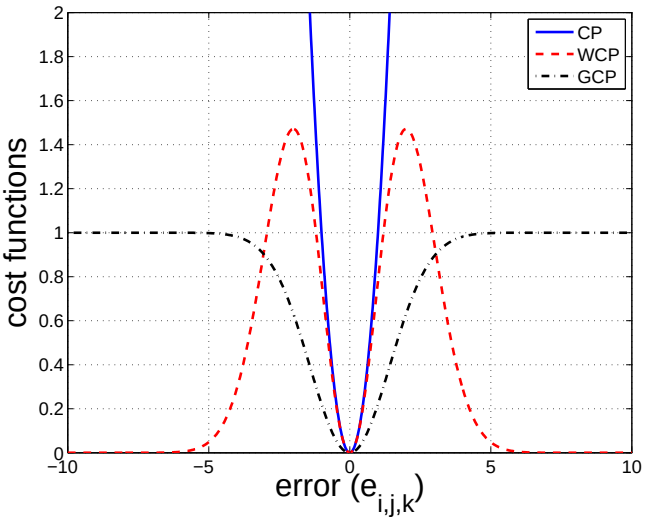

Figure B.10: Fonctions de coûts appliquées à l'erreur de reconstruction du tenseur pour les critères CP, WCP et GCP.

où

$$w_{ijk}^{(q)} = \exp\left\{-\frac{(y_{ijk}^{(q)} - \mu_{ij})^2}{\sigma_{ij}^2}\right\}, \quad q = 1, \ldots, Q, \tag{B.9}$$

sont les éléments d'un tenseur de poids non négatif qui a la même dimension que $\mathbf{Y}^{(q)}$. Ici, μ_{ik} est la moyenne de $\mathbf{Y}^{(q)}$ par rapport à la $j^{\text{ème}}$ dimension et σ_{ik} est l'écart type de $\mathbf{Y}^{(q)}$ selon la même dimension. En pratique, des poids de petites valeurs sont attribués aux valeurs fortement différentes de la valeur moyenne.

Une deuxième solution plus générale, qui peut également présenter un intérêt pour d'autres applications, consiste à remplacer la fonction de coût quadratique de la décomposition CP classique par une fonction de coût saturante. On obtient alors le critère suivant :

$$\min_{\{\mathbf{A}^{(q)},\mathbf{S}^{(q)},\mathbf{H}^{(q)}\}} \sum_{i,j,k} \psi\left(y_{ijk}^{(q)} - \sum_{r=1}^{R_q} a_{ir}^{(q)} s_{jr}^{(q)} h_{kr}^{(q)}\right), \tag{B.10}$$

avec $\psi(u) = 1 - \exp\{-\frac{u^2}{2\sigma^2}\}$. La décomposition résultante est appelée décomposition CP gaussienne (GCP[9]). Dans ce cas, une erreur de reconstruction supérieure à 3σ est limitée à une valeur proche de 1 dans le critère. Le paramètre σ, qui ajuste la forme de la fonction de pondération, permet ainsi de définir un seuil entre les erreurs considérées comme normales et celles aberrantes. La valeur optimale de σ doit donc être choisie en fonction des données. Ce critère peut être optimisé en utilisant un algorithme de descente du gradient.

Les différentes fonctions de coûts utilisées sont représentées à la Figure B.10.

Ces deux nouvelles méthodes peuvent être utilisées pour extraire directement l'ECG fœtal.

[9] Acronyme anglais de Gaussian CP

Cependant, dans ce cas, le principal inconvénient est de perdre la dynamique des sources (i.e. le fait que les battements ont des allures temporelles proches mais différentes d'un battement à l'autre). En effet, une extraction directe de l'ECGf fournit des battements ayant exactement le même motif temporel à l'amplitude près. Dans le but d'estimer les ECGf les plus réalistes possibles, un filtrage de Kalman est appliqué aux données. Pour se faire, l'approche précédente (filtrage de Kalman appliqué à un seul capteur) est étendue pour extraire plusieurs ECGs à partir d'un enregistrement multi-capteurs. Dans ce cas, les équations d'état peuvent être conservées, mais le vecteur d'observation est lié au vecteur d'état à l'instant k par :

$$\begin{bmatrix} \phi_k^{(1)} \\ \phi_k^{(2)} \\ \vdots \\ \phi_k^{(N)} \\ s_k^{(1)} \\ s_k^{(2)} \\ \vdots \\ s_k^{(M)} \end{bmatrix} = \left[\begin{array}{cccc:ccc} 1 & 0 & \dots & 0 & 0 & \dots & 0 \\ 0 & 1 & \dots & 0 & 0 & \dots & 0 \\ \vdots & \vdots & \ddots & 0 & 0 & \dots & 0 \\ 0 & 0 & \dots & 1 & 0 & \dots & 0 \\ \hdashline 0 & 0 & \dots & 0 & a_{11} & \dots & a_{1N} \\ \vdots & \vdots & \ddots & \vdots & \vdots & \ddots & \vdots \\ 0 & 0 & \dots & 0 & a_{M1} & \dots & a_{MN} \end{array}\right] \cdot \begin{bmatrix} \theta_k^{(1)} \\ \theta_k^{(2)} \\ \vdots \\ \theta_k^{(N)} \\ z_k^{(1)} \\ z_k^{(2)} \\ \vdots \\ z_k^{(N)} \end{bmatrix} + \begin{bmatrix} u_k^{(1)} \\ u_k^{(2)} \\ \vdots \\ u_k^{(N)} \\ v_k^{(1)} \\ v_k^{(2)} \\ \vdots \\ v_k^{(M)} \end{bmatrix}, \tag{B.11}$$

où les ECGs maternel et fœtal ont N composantes, chacun des ECG pouvant être composés de plusieurs composantes. Pour appliquer ce filtrage de Kalman, les matrices de facteurs obtenues par la décomposition du tenseur sont utilisées pour obtenir les valeurs des paramètres du modèle d'état : $\{\alpha_i^{(n)}, b_i^{(n)}, \psi_i^{(n)}\}_{i \in \mathscr{W}}$ est obtenu à partir de $\mathbf{H}^{(n)}$, la variabilité de la $n^{\text{ème}}$ composante de l'ECG obtenue par $\mathbf{S}^{(n)}$ peut être utilisée comme bruit d'état. La matrice de mélange

$$\mathbf{A} = \begin{bmatrix} a_{11} & \dots & a_{1N} \\ \vdots & \ddots & \vdots \\ a_{M1} & \dots & a_{MN} \end{bmatrix} \tag{B.12}$$

est obtenue à partir de la matrice de facteur $\mathbf{A}^{(n)}$.

Résultats

La méthode de décomposition tensorielle a été appliquée à des mélanges d'ECG et de MCG. Les résultats ont été comparés à la séparation de sources par l'algorithme Fast-ICA, ou la πCA. Les méthodes de décomposition tensorielle suivie du filtrage de Kalman sont notées WCP+EKS et GCP+EKS.

Les ECGm et ECGf extraits grâce aux deux premiers canaux de la base de données DaISy [71] sont présentés à la Figure B.11. Pour cela, le signal maternel est considéré comme étant composé de deux composantes tandis que celui du fœtus n'en ayant qu'une seule.

Comme on peut le voir, les méthodes Fast-ICA et πCA ne peuvent extraire l'ECGf avec uniquement deux capteurs car, dans ce cas, les mélanges sont sous-déterminés. La procédure de déflation fournit de meilleurs résultats par rapport à ces méthodes. Cependant, certaines

portions de l'ECGf sont déformées par cette méthode, cela est particulièrement visible pour des instants entre t = 0s et t = 1s et entre t = 8s et t = 9s. Cette distorsion n'est plus visible avec la méthode proposée.

La base de données PhysioNet [72] a été utilisée pour montrer la capacité de la méthode à extraire l'ECGf à différentes périodes de grossesse et à partir de capteurs placés à différents endroits de l'abdomen. Cette base de données se compose d'une série de 55 enregistrements multicanaux abdominaux enregistrés sur un seul sujet de 21 à 40 semaines de grossesse. La Figure B.12 montre les estimations obtenues par WCP+EKS pour trois enregistrements: signaux ecga192 en utilisant les canaux 3 et 5, ecga444 en utilisant les canaux 3 et 6, et ecga811 en utilisant les canaux 3 et 4. Pour chaque jeu de données, les 20 premières secondes sont représentées. Comme on peut le voir, bien que l'inspection visuelle des données montre que l'ECG fœtal a une amplitude très faible dans les mélanges, ceux-ci sont correctement extraits dans les différentes situations.

Les performances de la méthode proposée pour extraire les signaux cardiaques de jumeaux ont également été évaluées à l'aide de deux canaux MCG. La Figure B.13 présente les estimations obtenues par πCA, la procédure de déflation et par GCP+EKS et WCP+EKS. Comme précédemment, la méthode πCA ne parvient pas à extraire les signaux cardiaques car les mélanges sont sous-déterminés et la procédure de déflation améliore un peu les estimations. Cependant, les sources interférantes et le bruit ne sont pas complètement supprimés. Finalement, GCP+EKS et WCP+EKS proposées dans cette thèse permettent d'améliorer grandement l'extraction des signaux cardiaques des jumeaux.

La robustesse de la méthode de décomposition tensorielle proposée par rapport aux variations d'amplitude, aux valeurs aberrantes, à l'initialisation et aux erreurs de synchronisation a été quantifiée par des simulations. De plus, les comparaisons sur simulations entre la méthode multicanal et celle monocanal montrent l'apport d'un canal supplémentaire.

B.2.3 Modélisation Non Paramétrique (Approche Statistique)

Comme mentionné pour la représentation d'état, il est possible de modéliser le signal ECG par un modèle paramétrique de sorte que chaque battement est modélisé comme la somme de 5 fonctions gaussiennes. Chacune des fonctions permet de modéliser une des ondes P, Q, R, S ou T (Figure B.14) :

$$z(\theta) = \sum_{i \in \{P,Q,R,S,T\}} \alpha_i \exp\left(-\frac{(\theta - \psi_i)^2}{2b_i^2}\right). \tag{B.13}$$

Ce modèle peut alors être utilisé par un filtre de Kalman étendu pour débruiter un ECG ou pour extraire l'ECGf à partir d'un enregistrement abdominal. Cette méthode est donc paramétrique en ce sens que l'amplitude (inconnue) $z(\theta)$ est explicitement paramétrée.

D'autre part, les méthodes non-paramétriques effectuent l'estimation, la prédiction ou le débruitage sans paramétrage explicite de l'amplitude (inconnue) $z(\theta)$. L'approche par lissage à base de splines est une de ces méthodes non-paramétriques classiques [105]. Dans ce cas, l'amplitude $z(\theta)$ est considérée comme un processus statistique. En se limitant à l'ordre deux, il

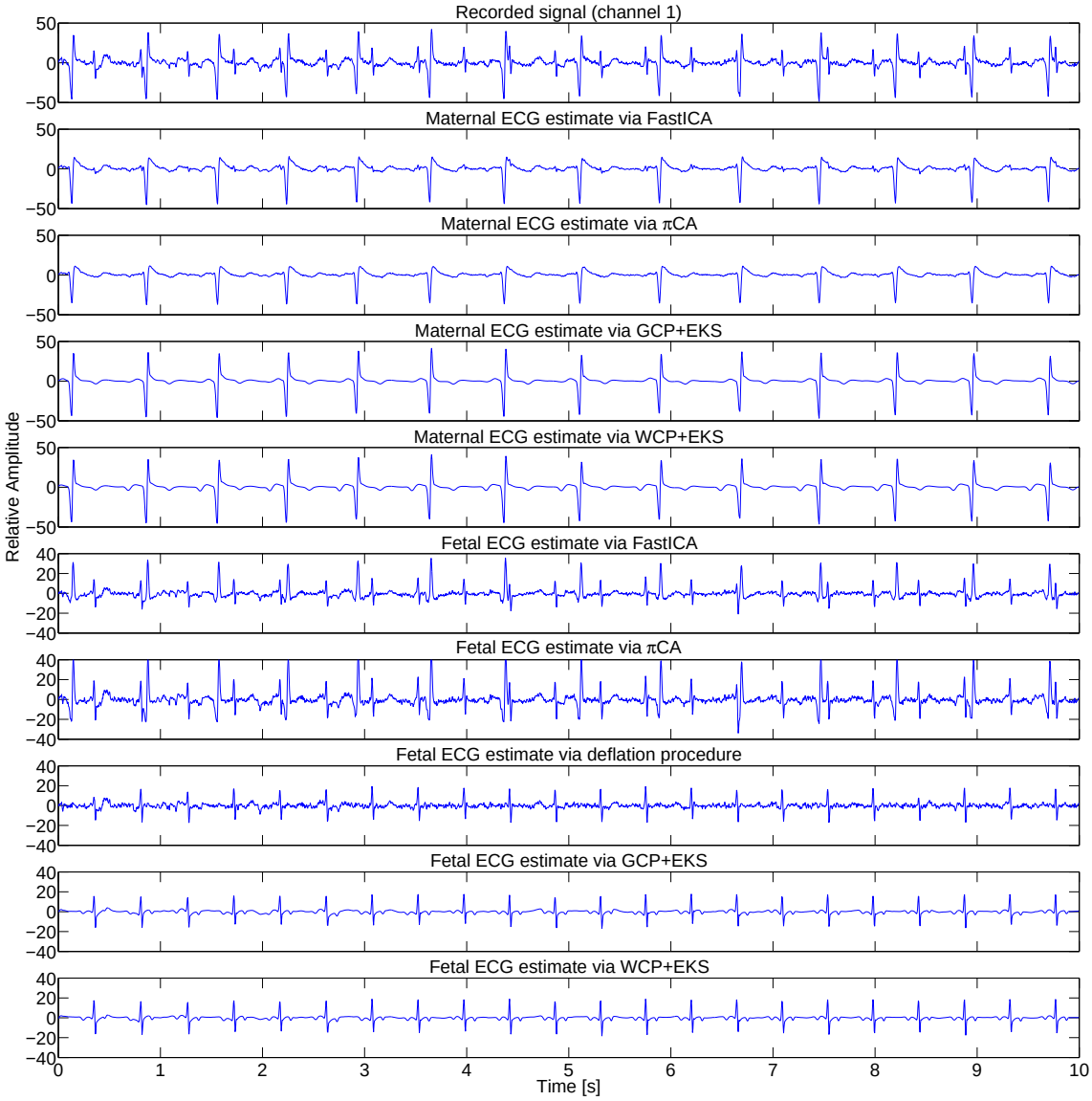

Figure B.11: ECGs extraits par Fast-ICA, πCA, la procédure de déflation, GCP+EKS, et WCP+EKS en utilisant les deux premiers canaux de la base de données DaISy.

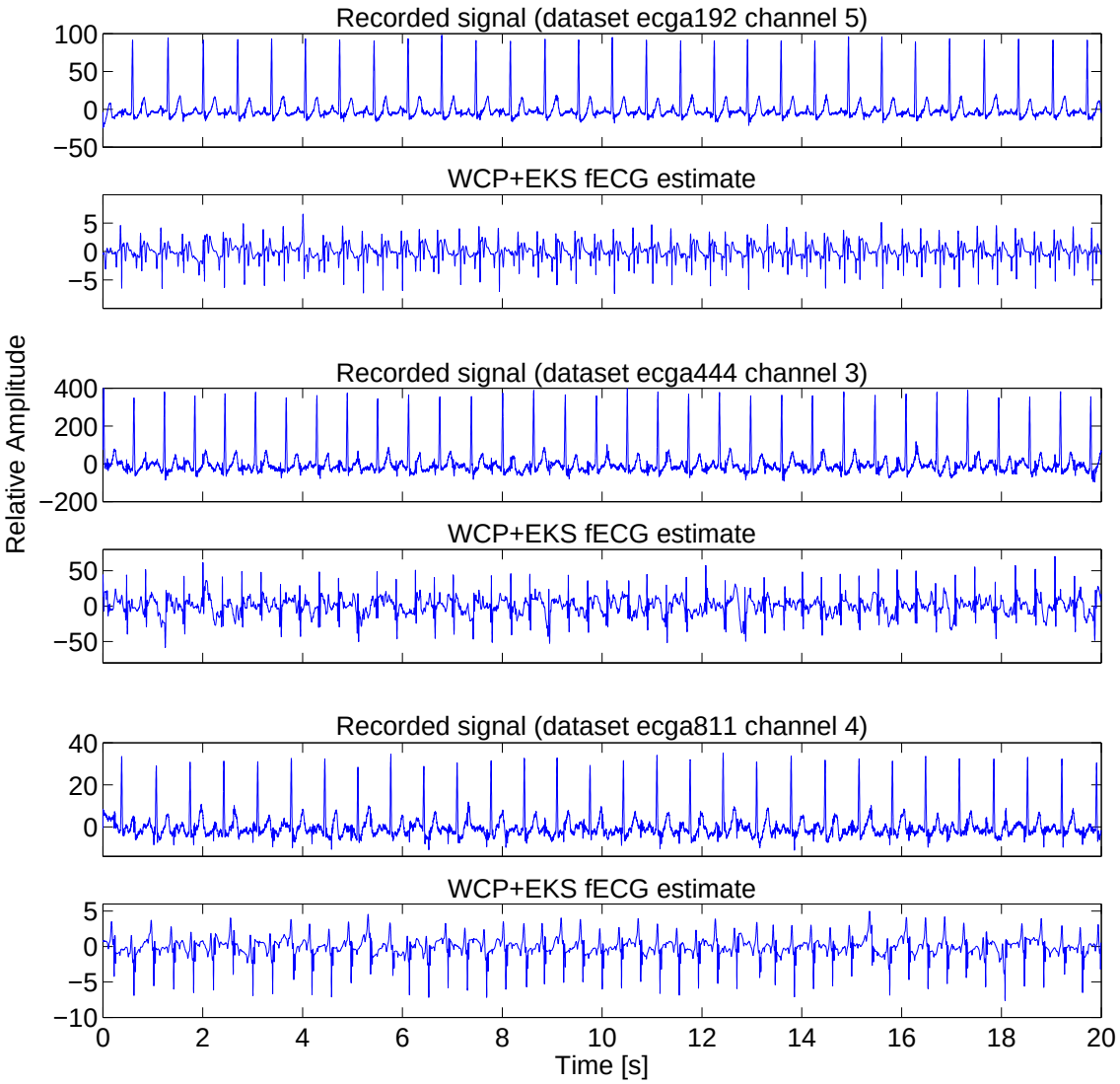

Figure B.12: Mélanges ECGs des jeux de données ecgca192 canal 5, ecgca444 canal 3, et ecgca811 canal 4 et les estimations de l'ECGf obtenues par WCP+EKS.

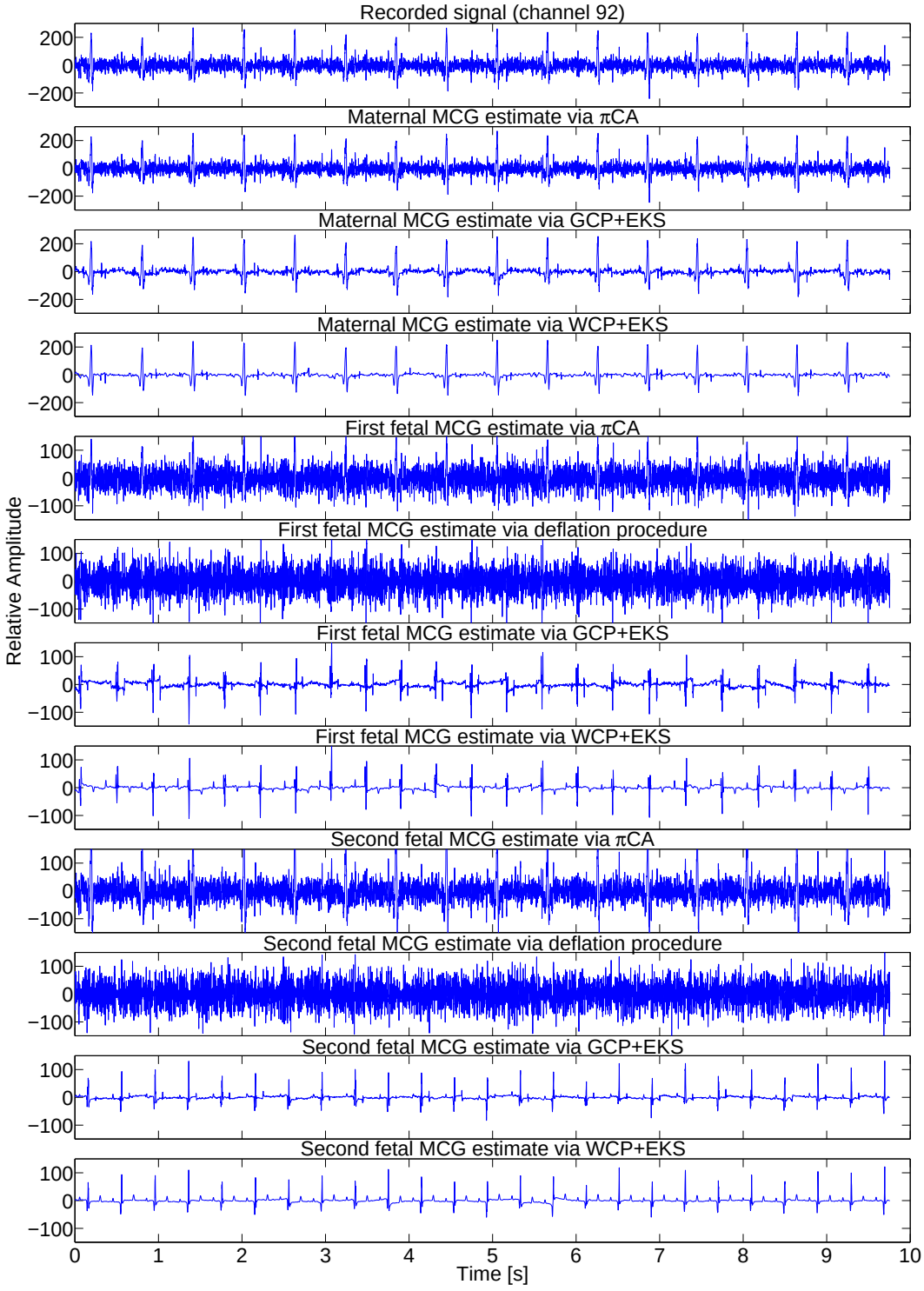

Figure B.13: Extraction du MCG de jumeaux par πCA, la procédure de déflation, GCP+EKS et WCP+EKS en utilisant deux canaux.

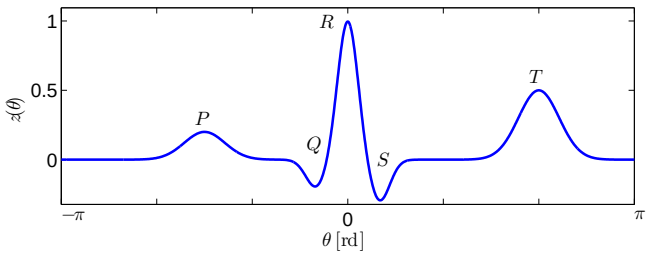

Figure B.14: Battement typique d'ECG.

est possible de la définir complètement par sa fonction moyenne $m(\theta) = \mathbb{E}[z(\theta)]$ et sa fonction de covariance $k(\theta_1, \theta_2) = \mathbb{E}[(z(\theta_1) - m(\theta_1))(z(\theta_2) - m(\theta_2))]$ [106]. En conséquence, le battement de l'ECG, $z(\theta)$ est considéré comme un processus gaussien (GP[10]) $\mathscr{GP}(m(\theta), k(\theta_1, \theta_2))$. Dans ce cas, le signal latent $z(\theta)$ n'est pas paramétré directement comme avec un modèle paramétrique, mais ce sont ses statistiques qui le sont grâce à des hyper-paramètres.

Comme illustré à la Figure B.14, un battement ECG peut être décomposé en trois parties: l'onde P, le complexe QRS et l'onde T, qui ont des caractéristiques différentes comme la corrélation temporelle et la puissance. Les ondes P et T partagent les mêmes caractéristiques différentes du complexe QRS : ainsi les variations sont plus lentes pour les ondes P et T que pour le complexe QRS et la puissance de ces ondes est plus faible que celle du complexe. De ce fait, la fonction de covariance non-stationnaire suivante peut être utilisée :

$$k(\theta_1, \theta_2) = \sigma(\theta_1)\sigma(\theta_2)\sqrt{\frac{2l_d(\theta_1)l_d(\theta_2)}{l_d(\theta_1)^2 + l_d(\theta_2)^2}} \times \exp\left(-\frac{\left(\theta_1 - \theta_2\right)^2}{l_d(\theta_1)^2 + l_d(\theta_2)^2}\right), \tag{B.14}$$

avec

$$\sigma(\theta) = a_m + (a_M - a_m)\exp\left(-\frac{(\theta - \theta_0)^2}{2\sigma_T^2}\right), \tag{B.15}$$

$$l_d(\theta) = l_M - (l_M - l_m)\exp\left(-\frac{(\theta - \theta_0)^2}{2\sigma_l^2}\right), \tag{B.16}$$

où $\sigma(\theta)$ et $l_d(\theta)$ permettent d'avoir une amplitude variant dans le temps (entre a_m et a_M) et une longueur de cohérence également variable (entre l_m et l_M).

La Figure B.15 montre deux tirages a priori d'un GP de fonction moyenne nulle et de fonction de covariance (B.14). Cette figure illustre la flexibilité d'une telle représentation par rapport au modèle (B.13) : un même a priori, permet de générer une infinité de signaux différents partageant les mêmes caractéristiques.

Enfin, pour modéliser la succession de battements, le GP associé est à fonction moyenne nulle

[10] Acronyme anglais de Gaussian process

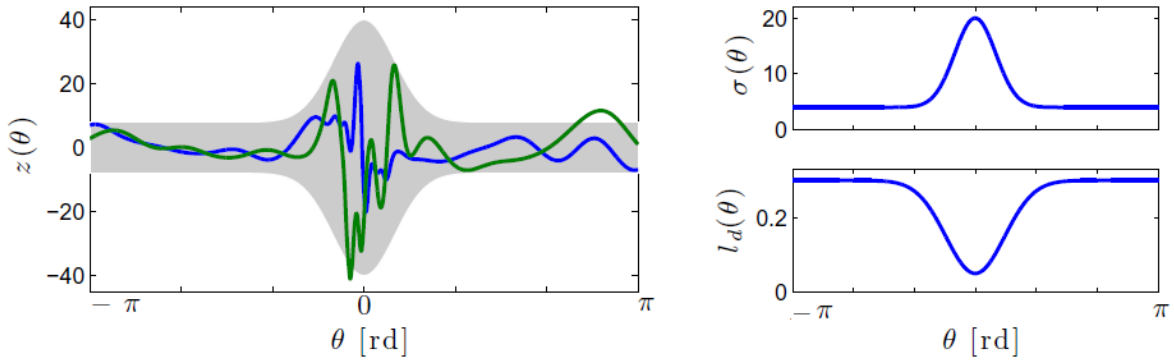

Figure B.15: Deux fonctions a priori généré par un GP de moyenne nulle et de fonction de covariance (B.14). La zone grisée représente plus et moins de deux fois l'écart type du prieur. Sur la droite, les fonctions correspondant à $\sigma(\theta)$ et $l_d(\theta)$.

et sa fonction de covariance est donnée par :

$$k_s(t,t') = \sum_{n=1}^{N}\sum_{n'=1}^{N} k(t-\tau_n, t'-\tau_{n'}), \tag{B.17}$$

où $\{\tau_n\}_{1\geqslant n\geqslant N}$ est l'ensemble des instants des pics R détectés à partir du mélange.

Le signal enregistré (monocanal) $x(t)$ est supposé être une superposition du signal ECG $s(t)$ et d'un bruit additif $n(t)$:

$$x(t) = s(t) + n(t). \tag{B.18}$$

Le bruit est également modélisé par un GP à fonction moyenne nulle et de fonction de covariance $k_n(t,t')$ donnée par :

$$k_n(t,t') = \sigma_n^2 \exp\left(-\frac{(t-t')^2}{2l_n^2}\right) + \sigma_w^2\delta(t-t'), \tag{B.19}$$

où $\delta(\cdot)$ est le Dirac. Le premier terme de cette expression permet de modéliser les variations de la ligne de base de l'ECG, le second terme correspond à un bruit blanc stationnaire de puissance σ_w^2.

L'ensemble des hyper-paramètres $\boldsymbol{\phi} = \{a_m, a_M, \sigma_T, l_m, l_M, \sigma_l, \sigma_n, l_n, \sigma_w\}$ est estimé en maximisant la log-vraisemblance marginale définie par [107] :

$$\log p\big(\mathbf{x}|\{T_k\}_k, \boldsymbol{\phi}\big) = -\frac{1}{2}\mathbf{x}^T\big(\mathbf{K}_s + \mathbf{K}_n\big)^{-1}\mathbf{x} - \frac{1}{2}\log\Big|\mathbf{K}_s + \mathbf{K}_n\Big| - \frac{M}{2}\log(2\pi), \tag{B.20}$$

où $\{T_k\}_k$ est l'ensemble des échantillons enregistrés, $\mathbf{K}_.$ est la matrice de covariance dont le $(p,q)^{\text{ème}}$ terme est $k_.(T_p, T_q)$, $\mathbf{x} = [x(T_1), \cdots, x(T_M)]^T$ et M le nombre d'échantillons temporels. Cette optimisation est obtenue par une montée de gradient avec une initialisation des paramètres choisie manuellement en fonction des informations biomédicales connues.

L'extraction de l'ECG fœtal à partir d'un seul capteur est alors une extension directe de la méthode proposée pour la modélisation d'un seul ECG :

$$x(t) = s_m(t) + s_f(t) + n(t). \tag{B.21}$$

où $s_m(t)$ est le signal ECG maternel, $s_f(t)$ le signal de l'ECG fœtal et $n(t)$ le bruit additif. Chacun de ces signaux est modélisé comme un GP de fonction moyenne nulle et dont les fonctions de covariance $k_m(\cdot,\cdot)$ et $k_f(\cdot,\cdot)$ sont définies par (B.14) et $k_n(\cdot,\cdot)$ défini par (B.19), respectivement.

Grâce à cette modélisation, les estimations de $s_m(t)$ et $s_f(t)$ sont alors données par :

$$\begin{cases} \hat{s}_m(t) = \mathbf{k}_m^T \Big(\mathbf{K}_m + \mathbf{K}_f + \mathbf{K}_n\Big)^{-1} \mathbf{x} \\ \hat{s}_f(t) = \mathbf{k}_f^T \Big(\mathbf{K}_m + \mathbf{K}_f + \mathbf{K}_n\Big)^{-1} \mathbf{x} \end{cases} \tag{B.22}$$

où $\mathbf{k}_m = [k_m(t,T_1),\cdots,k_m(t,T_M)]^T$ et $\mathbf{k}_f = [k_f(t,T_1),\cdots,k_f(t,T_M)]^T$.

Cette procédure peut également être étendue dans le cas de grossesse multiple en ajustant le nombre de GP au nombre de signaux présents.

Bien que cette méthode a montré son efficacité pour l'extraction de l'ECG fœtal, elle souffre cependant de plusieurs inconvénients. En effet, elle nécessite de nombreux hyper-paramètres pour s'ajuster correctement aux caractéristiques physiologiques d'un battement cardiaque. Ceci se traduit par un modèle assez compliqué et il en résulte des difficultés à optimiser la log-vraisemblance. En outre, la double sommation de l'équation (B.17) est assez coûteuse en temps de calcul.

Pour essayer de simplifier ce modèle, deux pistes sont envisagées. Pour cela, les enregistrements sont décomposés par un banc de filtres en sous-bandes : cette décomposition a pour intérêt de ne plus recourir à des rayons de cohérence variable pour modéliser le changement de dynamique des différentes ondes de l'ECG. En effet, pour chacune des sous-bandes, le rayon de corrélation est alors considéré comme constant, chacune des ondes appartenant principalement à une seule sous-bande. D'autre part, pour limiter le coût de calcul, la détection des pics R permet de construire une relation entre le temps et un espace des phases. A chaque battement est ainsi défini une phase linéaire de 0 à 2π : $\theta(t)$ est défini de telle sorte qu'à chaque intervalle $[\tau_k, \tau_{k+1}[$ est associé un intervalle $[2(k-1)\pi, 2k\pi[$ (Figure B.16).

Le signal ECG original dans la $i^{\text{ème}}$ sous-bande est alors modélisé à partir d'un GP 2π périodique et de la fonction définissant la phase $\theta(t)$. La fonction de covariance associée à ce GP est définie par :

$$k_s^{(i)}(t,t') = \sigma^2(i) \exp\left(-\frac{\sin^2\Big(\big(\theta(t)-\theta(t')\big)/2\Big)}{l_d^2(i)}\right), \tag{B.23}$$

$\sigma^2(i)$ et $l_d(i)$ définissant la puissance et la longueur de cohérence pour la $i^{\text{ème}}$ sous-bande.

Il est important de noter que la fonction de covariance proposée permet de s'adapter à bien des signaux quasi-périodiques tels que l'ECG grâce à la transformation $\theta(t)$ du temps en phase

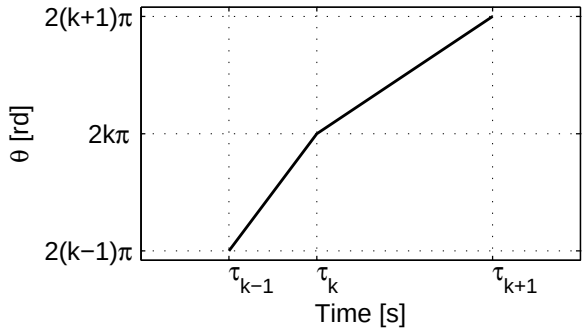

Figure B.16: Illustration de la définition de l'espace des phases : chaque battement cardiaque est linéairement déformé dans un intervalle de longueur égale à 2π.

qui associe chaque battement à l'intervalle $[0, 2\pi[$. De plus, un tel modèle non-paramétrique ne fait aucune hypothèse sur la forme des signaux mais exploite uniquement sa quasi-périodicité et sa régularité.

Ainsi, dans le signal enregistré, chaque ECG est modélisé par un GP dont les fonctions de covariances sont choisies comme (B.23). Ainsi, l'estimation de l'ECG maternel au sens du maximum a posteriori donne pour la $i^{\text{ème}}$ sous-bande :

$$\hat{s}_{m,i}(t) = \mathbf{k}_m^{(i)^T} \left(\mathbf{K}_m^{(i)} + \mathbf{K}_f^{(i)} + \mathbf{K}_n^{(i)} \right)^{-1} \mathbf{x}_i. \tag{B.24}$$

De la même manière, l'ECG fœtal est estimé par :

$$\hat{s}_{f,i}(t) = \mathbf{k}_f^{(i)^T} \left(\mathbf{K}_m^{(i)} + \mathbf{K}_f^{(i)} + \mathbf{K}_n^{(i)} \right)^{-1} \mathbf{x}_i. \tag{B.25}$$

Enfin, l'estimation complète des signaux est obtenue après sommation des I sous-bandes :

$$\begin{cases} \hat{s}_m(t) & = \sum_{i=1}^{I} \hat{s}_{m,i}(t) \\ \hat{s}_f(t) & = \sum_{i=1}^{I} \hat{s}_{f,i}(t) \end{cases} \tag{B.26}$$

Ce choix pour la fonction de covariance (B.23) ne contient que 2 paramètres (σ, l_d) par sous-bande au lieu des 6 paramètres $(a_m, a_M, \sigma_T, l_m, l_M, \sigma_l)$ pour la fonction de covariance (B.14). De ce fait, l'optimisation de la log-vraisemblance est simplifiée. Le principal avantage de la nouvelle fonction de covariance est d'éviter la double sommation présente dans (B.17) grâce à l'utilisation d'une fonction de covariance périodique combinée à la fonction phase $\theta(t)$.

Résultats

La Figure B.17 illustre les possibilités offertes par la modélisation des signaux en tant que GP avec une fonction de covariance (B.14) pour extraire les ECG maternel et fœtal en utilisant

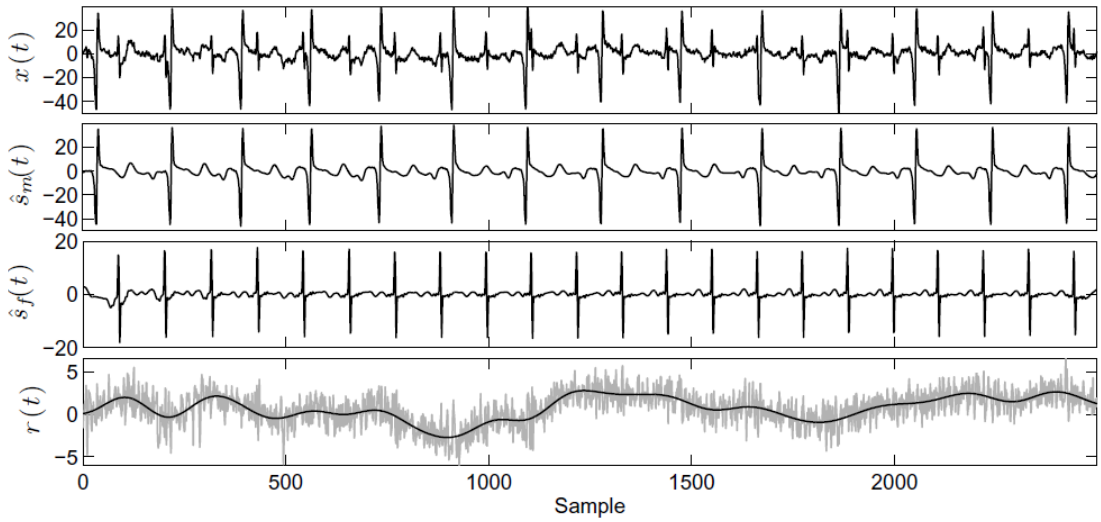

Figure B.17: Extraction de l'ECG fœtal via la modélisation par GP avec une fonction de covariance définie par (B.14). Les données proviennent de la base de données DaISy. De haut en bas : signal enregistré $x(t)$, l'estimation de l'ECG maternel $\hat{s}_m(t)$, l'estimation de l'ECG fœtal $\hat{s}_f(t)$ et du bruit résiduel $r(t)$ (courbe gris clair) avec la ligne de base estimée (courbe noire).

seulement le premier capteur de la base de données DaISy [71].

Comme on peut le voir, la méthode proposée fournit de bonnes estimations pour les ECG maternel et fœtal, même lorsque les pics R maternels et fœtaux apparaissent simultanément (par exemple, au moment des quatrième, septième et dixième battements maternels). De plus, une inspection visuelle du bruit résiduel $r(t) = x(t) - \hat{s}_m(t) - \hat{s}_f(t)$ confirme la validité de la modélisation choisie (B.21). En effet, ce bruit résiduel ne comporte qu'une ligne de base basse fréquence (courbe noire) lié au premier terme de la fonction de covariance (B.19) et un bruit quasi-blanc (validé par son estimation empirique de sa fonction de covariance). En outre, ces deux contributions sont décorrélés des signaux ECG maternel et fœtal estimés.

Afin de montrer la capacité de la méthode proposée à extraire l'ECGf à différentes périodes de la grossesse et à partir de différents capteurs, elle a aussi été appliquée sur la base de donnée PhysioNet [72]. Les signaux ont tout d'abord été rééchantillonnés à 250Hz puis décomposés en trois sous-bandes 0-30Hz, 30-60Hz et 60-125Hz. La Figure B.18 montre les 20 premières secondes des mélanges ainsi que les estimations des ECGf correspondants obtenues par une modélisation par GP avec comme fonction de covariance (B.23).

De même, cette méthode a été appliquée aux données MCG de jumeaux. Les signaux ont été rééchantillonnés à 256Hz et décomposés en sous-bandes 0-30Hz, 30-60Hz et 60-128Hz. La Figure B.19 montre les résultats obtenus par le filtrage de Kalman parallèle et la modélisation non-paramétrique. L'inspection visuelle montre que la modélisation non-paramétrique est plus efficace pour extraire les signaux MCG que la modélisation d'état.

Finalement, des mesures quantitatives pour comparer les approches non-paramétriques et celle du filtrage de Kalman ont été obtenues sur des données simulées. Les résultats montrent que la modélisation non-paramétrique surpasse le filtrage de Kalman notamment lorsque la

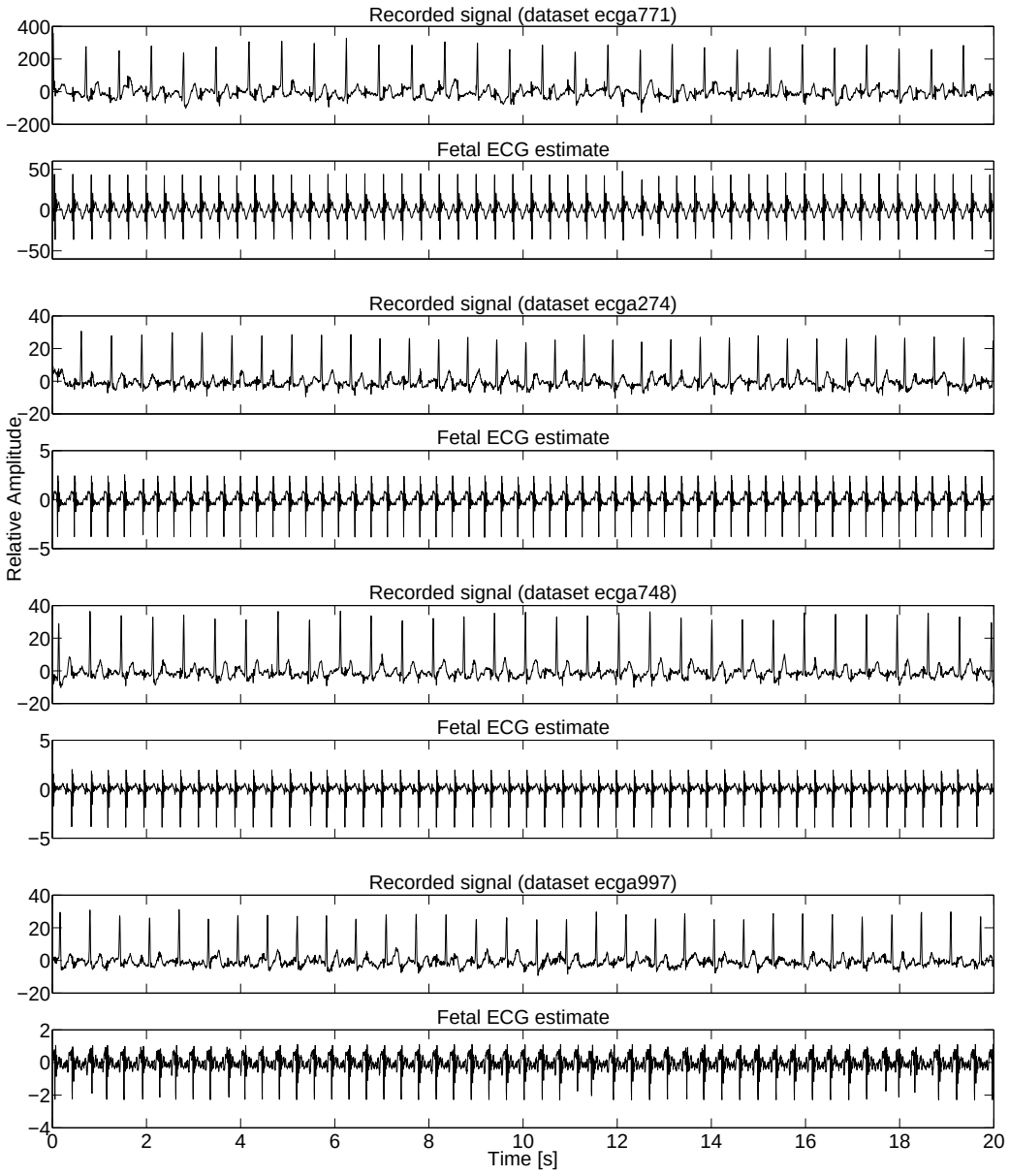

Figure B.18: Signaux de la base de données PhysioNet. Quatre signaux enregistrés (ecga771 canal 3, ecga274 canal 5, ecga748 canal 4, et ecga 997 canal 3) ainsi que les estimations de l'ECGf.

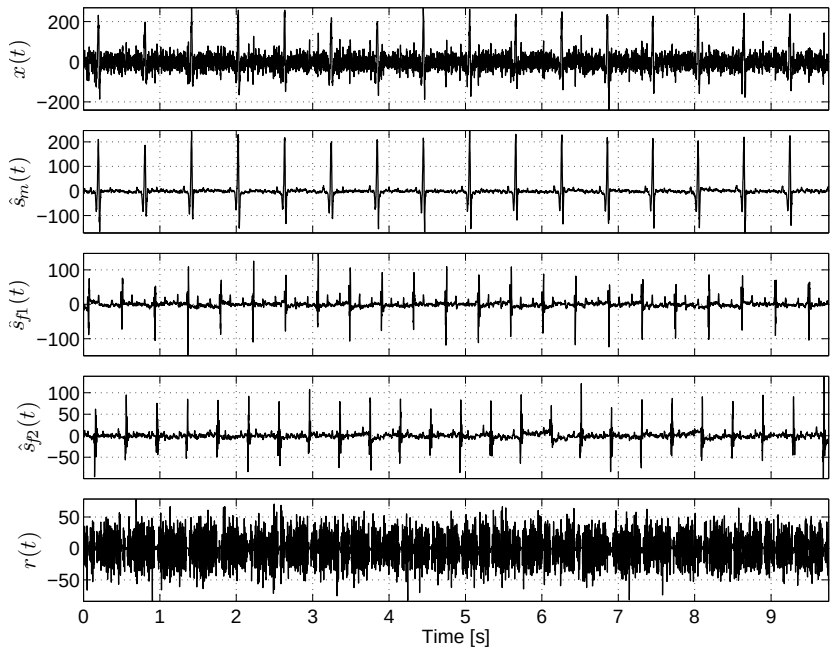

(a) Filtrage de Kalman parallèle

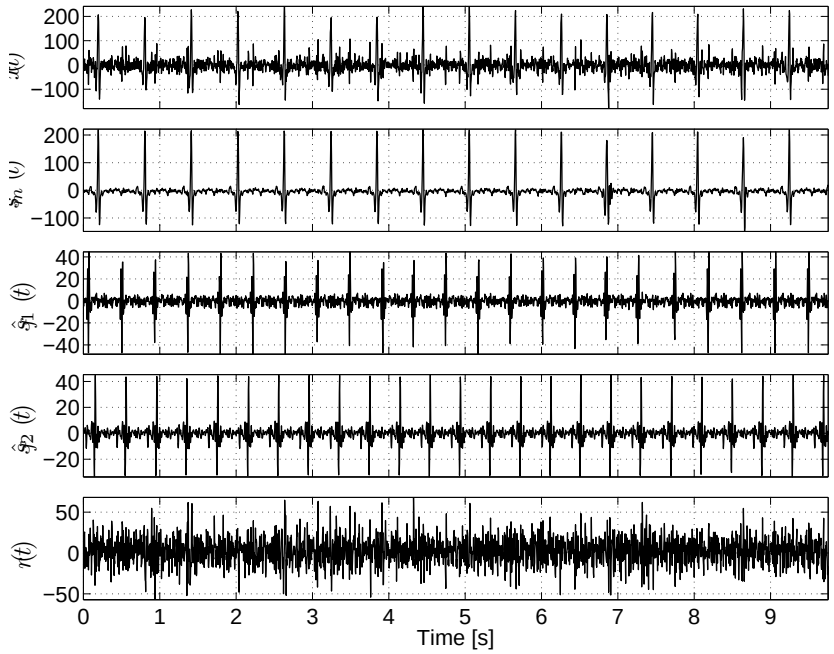

(b) Modélisation non paramétrique

Figure B.19: Extraction de MCG de jumeaux à partir d'un seul capteur. De haut en bas : le signal enregistré $x(t)$, le MCG maternel estimé $\hat{s}_m(t)$, les estimations des MCG des jumeaux $\hat{s}_{f1}(t)$ et $\hat{s}_{f2}(t)$, et le bruit résiduel $r(t)$ (courbe gris clair) avec la ligne de base estimée (courbe noire). (a): le filtrage de Kalman parallèle, (b): la méthode non paramétrique repose sur la fonction de covariance simplifiée (B.23).

variabilité des signaux ECG augmentent.

B.3 Conclusion et Perspectives

Dans ce travail, nous avons abordé le problème de l'extraction non-invasive de l'ECG fœtal. Nous avons proposé des méthodes qui utilisent un nombre minimal de capteurs entre un et deux et qui permettent même l'extraction des signaux cardiaques de jumeaux. L'hypothèse fondamentale a été la quasi-périodicité du signal ECG. Trois méthodes ont été proposées autour de celle-ci : modélisation d'état, approche déterministe et méthode statistique. Pour l'ensemble des méthodes proposées, dans un premier temps, des simulations ont été utilisées pour évaluer leurs performances dans des différentes conditions, puis dans un second temps, sur des enregistrements réels.

Les méthodes proposées dans ce travail ne se limitent pas aux signaux ECG car l'hypothèse principale de ces méthodes est très générale. Ainsi par exemple la méthode tensorielle a également été appliquée pour des potentiels évoqués issus de données de l'électroencéphalogramme (EEG).

Plusieurs perspectives peuvent être envisagées. A court terme, l'automatisation du choix du positionnement des fonctions gaussiennes dans le filtre de Kalman serait nécessaire. La méthode tensorielle proposée nécessite la synchronisation exacte des battements pour la construction du tenseur : ainsi, une méthode plus robuste aux erreurs de synchronisation serait un plus. De même, la méthode non-paramétrique est coûteuse en temps de calcul, il pourrait être intéressant d'essayer de la rendre plus rapide. A plus long terme, la détection des pics R dans l'ECG nécessaire à la synchronisation permettant l'utilisation de la quasi-périodicité des signaux pourrait être obtenue par une autre modalité telle que l'échocardiographie. Celle-ci permettrait d'obtenir les instants des pics R fœtaux ou de détecter les battements anormaux. Enfin, certains aspects cliniques devront être abordés grâce à l'utilisation des méthodes sur de nombreuses bases de données comportant tant des signaux de fœtus normaux que présentant des pathologies cardiaques et ce à plusieurs stades de la grossesse. Pour cela, des bases de données publiques sont nécessaires pour s'assurer d'une comparaison juste entre les méthodes proposées et celles de la littérature.

Bibliography

[1] A. A. Richards and V. Garg, "Genetics of congenital heart disease," *Current cardiology reviews*, vol. 6, no. 2, p. 91, 2010.

[2] M. E. Pierpont, C. T. Basson, D. W. Benson, B. D. Gelb, T. M. Giglia, E. Goldmuntz, G. McGee, C. A. Sable, D. Srivastava, and C. L. Webb, "Genetic basis for congenital heart defects: Current knowledge a scientific statement from the american heart association congenital cardiac defects committee, council on cardiovascular disease in the young: Endorsed by the american academy of pediatrics," *Circulation*, vol. 115, no. 23, pp. 3015–3038, 2007.

[3] "Congenital heart defects in children fact sheet," *American Heart Association*, 2008. [Online]. Available: http://www.americanheart.org/children

[4] A. M. Miniño, M. P. Heron, S. L. Murphy, and K. D. Kochanek, "Deaths: final data for 2004," 2007.

[5] E. Pajkrt, B. Weisz, H. V. Firth, and L. S. Chitty, "Fetal cardiac anomalies and genetic syndromes," *Prenatal diagnosis*, vol. 24, no. 13, pp. 1104–1115, 2004.

[6] "Congenital heart defects," *March of Dimes*, 2005. [Online]. Available: http://www.marchofdimes.com/baby/birthdefects_congenitalheart.html

[7] H. P. Nieminen, E. V. Jokinen, and H. I. Sairanen, "Late results of pediatric cardiac surgery in finland," *Circulation*, vol. 104, no. 5, pp. 570–575, 2001.

[8] S. Thorne and J. Deanfield, "Long-term outlook in treated congenital heart disease." *Archives of disease in childhood*, vol. 75, no. 1, pp. 6–8, 1996.

[9] A. Uebing, P. J. Steer, S. M. Yentis, and M. A. Gatzoulis, "Pregnancy and congenital heart disease," *BMJ: British Medical Journal*, vol. 332, no. 7538, p. 401, 2006.

[10] R. Sameni and G. D. Clifford, "A Review of Fetal ECG Signal Processing; Issues and Promising Directions," *The Open Pacing, Electrophysiology & Therapy Journal (TOPETJ)*, vol. 3, pp. 4–20, November 2010.

[11] M. Peters, J. Crowe, J.-F. Piéri, H. Quartero, B. Hayes-Gill, D. James, J. Stinstra, and S. Shakespeare, "Monitoring the fetal heart non-invasively: a review of methods," *Journal of perinatal medicine*, vol. 29, no. 5, pp. 408–416, 2001.

[12] G. Camps, M. Martinez, and E. Soria, "Fetal ECG extraction using an FIR neural network," in *Proc. Computers in Cardiology 2001*, 2001, pp. 249–252.

[13] R. Sameni, "Extraction of Fetal Cardiac Signals from an Array of Maternal Abdominal Recordings," Ph.D. dissertation, Sharif University of Technology – Institut National Polytechnique de Grenoble, July 2008, available Online: http://www.sameni.info/Publications/Thesis/PhDThesis.pdf.

[14] R. Sameni, M. B. Shamsollahi, C. Jutten, and G. D. Clifford, "A Nonlinear Bayesian Filtering Framework for ECG Denoising," *IEEE Trans. Biomed. Eng.*, vol. 54, no. 12, pp. 2172–2185, December 2007.

[15] M. Niknazar, B. Rivet, and C. Jutten, "Fetal ECG extraction by extended state Kalman filtering based on single-channel recordings," *Biomedical Engineering, IEEE Transactions on*, vol. 60, no. 5, pp. 1345–1352, 2013.

[16] A. Almeida, P. Comon, and X. Luciani, "Deterministic blind separation of sources having different symbol rates using tensor-based parallel deflation," in *Proceedings of the 9th international conference on Latent variable analysis and signal separation*, ser. LVA/ICA'10. Berlin, Heidelberg: Springer-Verlag, 2010, pp. 362–369. [Online]. Available: http://dl.acm.org/citation.cfm?id=1929142.1929194

[17] M. Niknazar, B. Rivet, and C. Jutten, "Fetal QRS complex detection based on three-way tensor decomposition," in *Computing in Cardiology 2013*, 2013, [accepted].

[18] M. Niknazar, H. Becker, B. Rivet, C. Jutten, and P. Comon, "Robust 3-way tensor decomposition and extended state Kalman filtering to extract fetal ECG," in *Signal Processing Conference (EUSIPCO), 2013 Proceedings of the 21th European*, 2013, [accepted].

[19] M. Niknazar, B. Rivet, and C. Jutten, "Application of dynamic time warping on Kalman filtering framework for abnormal ECG filtering," *ESANN 2012 Proceedings*, 2012.

[20] B. Rivet, M. Niknazar, and C. Jutten, "Nonparametric modelling of ECG: applications to denoising and to single sensor fetal ECG extraction," in *Latent Variable Analysis and Signal Separation*. Springer, 2012, pp. 470–477.

[21] M. Niknazar, B. Rivet, and C. Jutten, "Fetal ECG extraction from a single sensor by a non-parametric modeling," in *Signal Processing Conference (EUSIPCO), 2012 Proceedings of the 20th European*, 2012, pp. 949–953.

[22] H. M. Jenkins, "Technical progress in fetal electrocardiography–a review." *J Perinat Med*, vol. 14, no. 6, pp. 365–370, 1986.

[23] A. Khamene and S. Negahdaripour, "A new method for the extraction of fetal ECG from the composite abdominal signal," *IEEE Trans. Biomed. Eng.*, vol. 47, no. 4, pp. 507–516, 2000.

[24] S. Almagro, M. M. Elena, M. J. Bastiaans, and J. M. Quero, "A new mother wavelet for fetal electrocardiography, to achieve optimal denoising and compressing results," in *Computers in Cardiology, 2006*, 2006, pp. 157–160.

[25] P. Kanjilal, S. Palit, and G. Saha, "Fetal ECG extraction from single-channel maternal ECG using singular value decomposition," *IEEE Trans. Biomed. Eng.*, vol. 44, no. 1, pp. 51 –59, 1997.

[26] A. K. Barros and A. Cichocki, "Extraction of specific signals with temporal structure," *Neural Computation*, vol. 13, no. 9, pp. 1995–2003, Sep. 2001. [Online]. Available: http://dx.doi.org/10.1162/089976601750399272

[27] Z. Y. Z. Zhang, "Extraction of temporally correlated sources with its application to non-invasive fetal electrocardiogram extraction," *Neurocomputing*, vol. 69, no. 7-9, pp. 894–899, 2006.

[28] Y. Li and Z. Yi, "An algorithm for extracting fetal electrocardiogram," *Neurocomputing*, vol. 71, no. 7-9, pp. 1538 – 1542, 2008.

[29] L. de Lathauwer, B. de Moor, and J. Vandewalle, "Fetal electrocardiogram extraction by blind source subspace separation," *IEEE Trans. Biomed. Eng.*, vol. 47, no. 5, pp. 567 –572, may 2000.

[30] R. Sameni, C. Jutten, and M. B. Shamsollahi, "Multichannel electrocardiogram decomposition using periodic component analysis," *Biomedical Engineering, IEEE Transactions on*, vol. 55, no. 8, pp. 1935–1940, 2008.

[31] R. Sameni, C. Jutten, and M. Shamsollahi, "A deflation procedure for subspace decomposition," *Signal Processing, IEEE Transactions on*, vol. 58, no. 4, pp. 2363–2374, 2010.

[32] J.-F. Cardoso, "Multidimensional independent component analysis," in *Acoustics, Speech and Signal Processing, 1998. Proceedings of the 1998 IEEE International Conference on*, vol. 4. IEEE, 1998, pp. 1941–1944.

[33] V. Zarzoso, "Extraction of ECG characteristics using source separation techniques: exploiting statistical independence and beyond," in *Advanced Biosignal Processing.* Springer, 2009, pp. 15–47.

[34] J. Camargo-Olivares, R. Marti-Clemente, S. Hornillo-Mellado, M. Elena, and I. Roman, "The maternal abdominal ECG as input to MICA in the fetal ECG extraction problem," *Signal Processing Letters, IEEE*, vol. 18, no. 3, pp. 161 –164, 2011.

[35] M. G. Jafari and J. A. Chambers, "Fetal electrocardiogram extraction by sequential source separation in the wavelet domain," *IEEE Trans. Biomed. Eng.*, vol. 52, no. 3, pp. 390–400, 2005.

[36] V. Vigneron, A. Paraschiv-Ionescu, A. Azancot, O. Sibony, and C. Jutten, "Fetal electrocardiogram extraction based on non-stationary ICA and wavelet denoising," in *Proc. Seventh Int Signal Processing and Its Applications Symp*, vol. 2, 2003, pp. 69–72.

[37] B. Azzerboni, G. Finocchio, M. Ipsale, F. La Foresta, and F. C. Morabito, "A new approach to detection of muscle activation by independent component analysis and wavelet transform," in *Neural Nets*. Springer, 2002, pp. 109–116.

[38] B. Azzerboni, M. Carpentieri, F. La Foresta, and F. Morabito, "Neural-ICA and wavelet transform for artifacts removal in surface EMG," in *Neural Networks, 2004. Proceedings. 2004 IEEE International Joint Conference on*, vol. 4. IEEE, 2004, pp. 3223–3228.

[39] B. Azzerboni, F. La Foresta, N. Mammone, and F. C. Morabito, "A new approach based on wavelet-ICA algorithms for fetal electrocardiogram extraction." in *ESANN*, 2005, pp. 193–198.

[40] A. Cohen, I. Daubechies, and J.-C. Feauveau, "Biorthogonal bases of compactly supported wavelets," *Communications on pure and applied mathematics*, vol. 45, no. 5, pp. 485–560, 1992.

[41] J.-F. Cardoso and A. Souloumiac, "Blind heamforning for non-Gaussian signals," *Proc. IEE -F*, vol. 140, pp. 362–370, 1993.

[42] A. Hyvärinen and E. Oja, "A fast fixed-point algorithm for independent component analysis," *Neural computation*, vol. 9, no. 7, pp. 1483–1492, 1997.

[43] A. J. Bell and T. J. Sejnowski, "An information-maximization approach to blind separation and blind deconvolution," *Neural computation*, vol. 7, no. 6, pp. 1129–1159, 1995.

[44] P. Comon, "Independent component analysis, a new concept?" *Signal processing*, vol. 36, no. 3, pp. 287–314, 1994.

[45] K. Ananthanag and J. Sahambi, "Investigation of blind source separation methods for extraction of fetal ECG," in *Electrical and Computer Engineering, 2003. IEEE CCECE 2003. Canadian Conference on*, vol. 3. IEEE, 2003, pp. 2021–2024.

[46] R. Martin-Clemente, J. Camargo-Olivares, S. Hornillo-Mellado, M. Elena, and I. Roman, "Fast technique for noninvasive fetal ECG extraction," *IEEE Trans. Biomed. Eng.*, vol. 58, no. 2, pp. 227–230, 2011.

[47] D. Graupe, Y. Zhong, and M. H. Graupe, "Extracting fetal from maternal ECG for early diagnosis: Theoretical problems and solutions-BAF and ICA," in *Proceeding of the International Conference on Biomedical Engineering*, 2007, pp. 352–356.

[48] M. Kotas, "Projective filtering of time-aligned ECG beats," *IEEE Trans. Biomed. Eng.*, vol. 51, no. 7, pp. 1129–1139, 2004.

[49] M. Richter, T. Schreiber, and D. Kaplan, "Fetal ECG extraction with nonlinear state-space projections," *IEEE Trans. Biomed. Eng.*, vol. 45, no. 1, pp. 133 –137, 1998.

[50] T. Schreiber and D. T. Kaplan, "Signal separation by nonlinear projections: The fetal electrocardiogram," *Physical Review E*, vol. 53, no. 5, pp. R4326–R4329, 1996.

[51] B. Widrow, J. Glover, J.R., J. McCool, J. Kaunitz, C. Williams, R. Hearn, J. Zeidler, J. Eugene Dong, and R. Goodlin, "Adaptive noise cancelling: Principles and applications," *Proceedings of the IEEE*, vol. 63, no. 12, pp. 1692 – 1716, 1975.

[52] N. Outram, E. Ifeachor, P. Van Eetvelt, and J. Curnow, "Techniques for optimal enhancement and feature extraction of fetal electrocardiogram," *Science, Measurement and Technology, IEE Proceedings* -, vol. 142, no. 6, pp. 482 –489, 1995.

[53] A. G. Favret, "Computer matched filter location of fetal R-waves." *Med Biol Eng*, vol. 6, no. 5, pp. 467–475, Sep 1968.

[54] Y. C. Park, K. Y. Lee, D. H. Youn, N. H. Kim, W. K. Kim, and S. H. Park, "On detecting the presence of fetal R-wave using the moving averaged magnitude difference algorithm," *IEEE Trans. Biomed. Eng.*, vol. 39, no. 8, pp. 868–871, 1992.

[55] V. Zarzoso and A. K. Nandi, "Noninvasive fetal electrocardiogram extraction: blind separation versus adaptive noise cancellation," *IEEE Trans. Biomed. Eng.*, vol. 48, no. 1, pp. 12–18, 2001.

[56] J. A. Drose, *Fetal echocardiography.* WB Saunders Company, 2010.

[57] F. Kovacs, M. Torok, and I. Habermajer, "A rule-based phonocardiographic method for long-term fetal heart rate monitoring," *Biomedical Engineering, IEEE Transactions on*, vol. 47, no. 1, pp. 124–130, 2000.

[58] A. J. Zuckerwar, R. A. Pretlow, J. W. Stoughton, and D. A. Baker, "Development of a piezopolymer pressure sensor for a portable fetal heart rate monitor," *Biomedical Engineering, IEEE Transactions on*, vol. 40, no. 9, pp. 963–969, 1993.

[59] S. L. Bloom, C. Y. Spong, E. Thom, M. W. Varner, D. J. Rouse, S. Weininger, S. M. Ramin, S. N. Caritis, A. Peaceman, Y. Sorokin *et al.*, "Fetal pulse oximetry and cesarean delivery," *New England Journal of Medicine*, vol. 355, no. 21, pp. 2195–2202, 2006.

[60] M. G. Signorini, G. Magenes, S. Cerutti, and D. Arduini, "Linear and nonlinear parameters for the analysisof fetal heart rate signal from cardiotocographic recordings," *Biomedical Engineering, IEEE Transactions on*, vol. 50, no. 3, pp. 365–374, 2003.

[61] V. Kariniemi and K. Hukkinen, "Quantification of fetal heart rate variability by magnetocardiography and direct electrocardiography." *American journal of obstetrics and gynecology*, vol. 128, no. 5, p. 526, 1977.

[62] H. Ter Brake, A. Rijpma, J. Stinstra, J. Borgmann, H. Holland, H. Krooshoop, M. Peters, J. Flokstra, H. Quartero, and H. Rogalla, "Fetal magnetocardiography: clinical relevance and feasibility," *Physica C: Superconductivity*, vol. 368, no. 1, pp. 10–17, 2002.

[63] J.-F. Cardoso, "Multidimensional Independent Component Analysis," in *Proc. of the IEEE International Conference on Acoustics, Speech, and Signal Processing (ICASSP '98)*, vol. 4, May 1998, pp. 1941–1944.

[64] A. Hyvarinen, "Fast and robust fixed-point algorithms for independent component analysis," *Neural Networks, IEEE Transactions on*, vol. 10, no. 3, pp. 626–634, 1999.

[65] M. S. Grewal and A. P. Andrews, *Kalman filtering: theory and practice using MATLAB*. Wiley-IEEE press, 2011.

[66] P. McSharry, G. Clifford, L. Tarassenko, and L. Smith, "A dynamical model for generating synthetic electrocardiogram signals," *IEEE Trans. Biomed. Eng.*, vol. 50, no. 3, pp. 289 –294, 2003.

[67] O. Sayadi and M. Shamsollahi, "ECG denoising and compression using a modified extended Kalman filter structure," *IEEE Trans. Biomed. Eng.*, vol. 55, no. 9, pp. 2240 –2248, 2008.

[68] G. D. Clifford, A. Shoeb, P. E. McSharry, and B. A. Janz, "Model-based filtering, compression and classification of the ECG," *Int. J. Bioelectromag.*, vol. 7, no. 1, pp. 158–161, 2005.

[69] R. Sameni, G. D. Clifford, C. Jutten and M. B. Shamsollahi, "Multichannel ECG and Noise Modeling: Application to Maternal and Fetal ECG Signals," *EURASIP Journal on Advances in Signal Processing*, vol. 2007, p. Article ID 43407, 2007. [Online]. Available: http://www.hindawi.com/GetArticle.aspx?doi=10.1155/2007/43407

[70] T. J. DuBose, J. A. Cunyus, and L. F. Johnson, "Embryonic heart rate and age," *Journal of Diagnostic Medical Sonography*, vol. 6, no. 3, pp. 151–157, 1990. [Online]. Available: http://jdm.sagepub.com/content/6/3/151.abstract

[71] B. De Moor, P. De Gersem, B. De Schutter, and W. Favoreel, "DAISY: A database for identification of systems," *Journal A, Special Issue on CACSD (Computer Aided Control Systems Design)*, vol. 38, no. 3, pp. 4–5, Sep. 1997.

[72] A. L. Goldberger, L. A. N. Amaral, L. Glass, J. M. Hausdorff, P. C. Ivanov, R. G. Mark, J. E. Mietus, G. B. Moody, C.-K. Peng, and H. E. Stanley, "PhysioBank, PhysioToolkit, and PhysioNet: Components of a new research resource for complex physiologic signals," *Circulation*, vol. 101, no. 23, pp. e215–e220, 2000 (June 13), circulation Electronic Pages: http://circ.ahajournals.org/cgi/content/full/101/23/e215.

[73] P. Comon and C. Jutten, *Handbook of Blind Source Separation: Independent Component Analysis and Applications*. Elsevier Science, 2010.

[74] A. Ozerov and C. Févotte, "Multichannel nonnegative matrix factorization in convolutive mixtures for audio source separation," *Audio, Speech, and Language Processing, IEEE Transactions on*, vol. 18, no. 3, pp. 550–563, 2010.

[75] A. Y. Kibangou and G. Favier, "Blind equalization of nonlinear channels using a tensor decomposition with code/space/time diversities," *Signal Processing*, vol. 89, no. 2, pp. 133–143, 2009.

[76] H. Lee, Y.-D. Kim, A. Cichocki, and S. Choi, "Nonnegative tensor factorization for continuous eeg classification," *International journal of neural systems*, vol. 17, no. 04, pp. 305–317, 2007.

[77] D. Letexier, S. Bourennane, and J. Talon, "Nonorthogonal tensor matricization for hyperspectral image filtering," *Geoscience and Remote Sensing Letters, IEEE*, vol. 5, no. 1, pp. 3–7, 2008.

[78] P. Comon, "Blind identification and source separation in 2 times;3 under-determined mixtures," *Signal Processing, IEEE Transactions on*, vol. 52, no. 1, pp. 11 – 22, jan. 2004.

[79] R. Gribonval, S. Lesage *et al.*, "A survey of sparse component analysis for blind source separation: principles, perspectives, and new challenges," in *ESANN'06 proceedings-14th European Symposium on Artificial Neural Networks*, 2006, pp. 323–330.

[80] Z. He, S. Xie, S. Ding, and A. Cichocki, "Convolutive blind source separation in the frequency domain based on sparse representation," *Audio, Speech, and Language Processing, IEEE Transactions on*, vol. 15, no. 5, pp. 1551 –1563, 2007.

[81] P. Georgiev, F. Theis, and A. Cichocki, "Sparse component analysis and blind source separation of underdetermined mixtures," *Neural Networks, IEEE Transactions on*, vol. 16, no. 4, pp. 992 –996, 2005.

[82] P. Tichavsky and Z. Koldovsky, "Weight adjusted tensor method for blind separation of underdetermined mixtures of nonstationary sources," *Signal Processing, IEEE Transactions on*, vol. 59, no. 3, pp. 1037 –1047, 2011.

[83] P. Comon, "Contrasts, independent component analysis, and blind deconvolution," *International Journal of Adaptive Control and Signal Processing*, vol. 18, no. 3, pp. 225–243, 2004. [Online]. Available: http://dx.doi.org/10.1002/acs.791

[84] G. Zhou and A. Cichocki, "Canonical polyadic decomposition based on a single mode blind source separation," *Signal Processing Letters, IEEE*, vol. 19, no. 8, pp. 523 –526, 2012.

[85] P. Chevalier, A. Ferreol, and L. Albera, "On the behavior of current second order blind source separation methods for first and second order cyclostationary sources-application to CPFSK sources," in *Acoustics, Speech, and Signal Processing (ICASSP), 2002 IEEE International Conference on*, vol. 3, may 2002, pp. III–3081 –III–3084.

[86] P. Comon, L. Luciani, and A. L. F. D. Almeida, "Tensor decompositions, alternating least squares and other tales," *Journal of Chemometrics*, vol. 23, pp. 393–405, 2009.

[87] R. Bro, "Multi-way analysis in the food industry: Models, algorithms and applications," Ph.D. dissertation, University of Amsterdam (NL), 1998.

[88] S. A. Vorobyov, Y. Rong, N. C. Sidiropoulos, and A. B. Gershman, "Robust iterative fitting of multilinear models," *IEEE Transactions on Signal Processing*, vol. 53, no. 8, pp. 2678–2689, August 2005.

[89] J. B. Kruskal, "Three-way arrays: rank and uniqueness of trilinear decompositions with application to arithmetic complexity and statistics," *Linear Algebra and Applications*, vol. 18, pp. 95–138, 1977.

[90] N. D. Sidiropoulos, G. B. Giannakis, and R. Bro, "Blind PARAFAC receivers for DS-CDMA systems," *IEEE Transactions on Signal Processing*, vol. 48, no. 3, pp. 810–822, March 2000.

[91] T. G. Kolda and B. W. Bader, "Tensor decompositions and applications," *SIAM Review*, vol. 51, no. 3, pp. 455–500, 2009.

[92] P. J. Huber and E. M. Ronchetti, Eds., *Robust statistics*. Hoboken, New Jersey: John Wiley & Sons, 2009, ch. Scale Estimates, pp. 105–124.

[93] *Noninvasive Fetal ECG: the PhysioNet/Computing in Cardiology Challenge 2013*. [Online]. Available: http://www.physionet.org/challenge/2013/

[94] S. Georgiadis, P. Ranta-aho, M. Tarvainen, and P. Karjalainen, "Single-trial dynamical estimation of event-related potentials: a Kalman filter-based approach," *Biomedical Engineering, IEEE Transactions on*, vol. 52, no. 8, pp. 1397 –1406, aug. 2005.

[95] H. Mohseni, E. Wilding, and S. Sanei, "Preprocessing of event-related potential signals via Kalman filtering and smoothing," in *Digital Signal Processing, 2007 15th International Conference on*, july 2007, pp. 179 –182.

[96] M. L. Jongsma, T. Eichele, C. M. V. Rijn, A. M. Coenen, K. Hugdahl, H. Nordby, and R. Q. Quiroga, "Tracking pattern learning with single-trial event-related potentials," *Clinical Neurophysiology*, vol. 117, no. 9, pp. 1957 – 1973, 2006. [Online]. Available: http://www.sciencedirect.com/science/article/pii/S1388245706002227

[97] W. Deburchgraeve, P. J. Cherian, M. D. Vos, R. M. swarte, J. H. Blok, G. H. Visser, and P. Govaert, "Neonatal seizure localization using parafac decomposition," *Clinical Neurophysiology*, vol. 120, pp. 1787–1796, 2009.

[98] J. Möcks, "Decomposing event-related potentials: A new topographic components model," *Biological Psychology*, vol. 26, pp. 199–215, June 1988.

[99] A. Field and D. Graupe, "Topographic component (parallel factor) analysis of multichannel evoked potentials: practical issues in trilinear spatiotemporal decomposition," *Brain Topography*, vol. 3, no. 4, pp. 407–423, 1991.

[100] J. R. Wolpaw, N. Birbaumer, W. J. Heetderks, D. J. McFarland, P. H. Peckham, G. Schalk, E. Donchin, L. A. Quatrano, C. J. Robinson, T. M. Vaughan *et al.*, "Brain-computer interface technology: a review of the first international meeting," *IEEE Transactions on Rehabilitation Engineering*, vol. 8, no. 2, pp. 164–173, 2000.

[101] H. Sakoe and S. Chiba, "Dynamic programming algorithm optimization for spoken word recognition," *Acoustics, Speech and Signal Processing, IEEE Transactions on*, vol. 26, no. 1, pp. 43–49, 1978.

[102] *The MIT-BIH Arrhythmia Database*. [Online]. Available: http://www.physionet.org/physiobank/database/mitdb/

[103] C. E. Rasmussen, "Gaussian processes in machine learning," in *Advanced Lectures on Machine Learning*. Springer, 2004, pp. 63–71.

[104] C. M. Bishop *et al.*, *Pattern recognition and machine learning*. Springer New York, 2006, vol. 1.

[105] G. S. Kimeldorf and G. Wahba, "A correspondence between bayesian estimation on stochastic processes and smoothing by splines," *The Annals of Mathematical Statistics*, vol. 41, no. 2, pp. 495–502, 1970.

[106] A. Papoulis, *Probability, Random Variables, and Stochastic Processes*, 3rd ed. McGraw-Hill, 1991.

[107] C. Rasmussen and C. Williams, *Gaussian Processes for Machine Learning*, ser. Adaptive Computation and Machine Learning. Cambridge, MA, USA: MIT Press, 1 2006.

[108] D. J. MacKay, "Introduction to Gaussian processes," *NATO ASI Series F Computer and Systems Sciences*, vol. 168, pp. 133–166, 1998.

[109] B. Grimm, J. Haueisen, M. Huotilainen, S. Lange, P. V. Leeuwen, T. Menendez, M. J. Peters, E. Schleussner, and U. Schneider, "Recommended standards for fetal magnetocardiography," *Pacing Clin. Electrophysiol.*, vol. 26, pp. 2121–2126, 2003.

[110] L. de Lathauwer, B. de Moor, and J. Vandewalle, "Fetal electrocardiogram extraction by blind source subspace separation," *IEEE Trans. Biomed. Eng.*, vol. 47, no. 5, pp. 567 –572, may 2000.

[111] S. Leurgans, R. T. Ross, and R. B. Abel, "A decomposition for three-way arrays," *SIAM Jour. Matrix Anal. Appl.*, vol. 14, no. 4, pp. 1064–1083, Oct. 1993.

Abstract: Congenital heart defects are the leading cause of birth defect-related deaths. The fetal electrocardiogram (fECG), which is believed to contain much more information as compared with conventional sonographic methods, can be measured by placing electrodes on the mother's abdomen. However, it has very low power and is mixed with several sources of noise and interference, including the strong maternal ECG (mECG). In previous studies, several methods have been proposed for the extraction of fECG signals recorded from the maternal body surface. However, these methods require a large number of sensors, and are ineffective with only one or two sensors. In this study, state modeling, statistical and deterministic approaches are proposed for capturing weak traces of fetal cardiac signals. These three methods implement different models of the quasi-periodicity of the cardiac signal. In the first approach, the heart rate and its variability are modeled by a Kalman filter. In the second approach, the signal is divided into windows according to the beats. Stacking the windows constructs a tensor that is then decomposed. In a third approach, the signal is not directly modeled, but it is considered as a Gaussian process characterized by its second order statistics. In all the different proposed methods, unlike previous studies, mECG and fECG(s) are explicitly modeled. The performance of the proposed methods, which utilize a minimal number of electrodes, are assessed on synthetic data and actual recordings including twin fetal cardiac signals.
Keywords: fetal ECG extraction, Kalman filter, tensor decomposition, Gaussian process.

Résumé : Les malformations cardiaques congénitales sont la première cause de décès liés à une anomalie congénitale. L'électrocardiogramme du fœtus (ECGf), qui est censé contenir beaucoup plus d'informations par rapport aux méthodes échographiques conventionnelles, peut être mesuré par des électrodes sur l'abdomen de la mère. Cependant, il est très faible et mélangé avec plusieurs sources de bruit et interférence, y compris l'ECG de la mère (ECGm) dont le niveau est très fort. Dans les études précédentes, plusieurs méthodes ont été proposées pour l'extraction de l'ECGf à partir des signaux enregistrés par des électrodes placées à la surface du corps de la mère. Cependant, ces méthodes nécessitent un nombre de capteurs important, et s'avèrent inefficaces avec un ou deux capteurs. Dans cette étude, trois approches innovantes reposant sur une paramétrisation algébrique, statistique ou par variables d'état sont proposées. Ces trois méthodes mettent en œuvre des modélisations différentes de la quasi-périodicité du signal cardiaque. Dans la première approche, le signal cardiaque et sa variabilité sont modélisés par un filtre de Kalman. Dans la seconde approche, le signal est découpé en fenêtres selon les battements, et l'empilage constitue un tenseur dont on cherchera la décomposition. Dans la troisième approche, le signal n'est pas modélisé directement, mais il est considéré comme un processus Gaussien, caractérisé par ses statistiques à l'ordre deux. Dans les différents modèles, contrairement aux études précédentes, l'ECGm et le (ou les) ECGf(s) sont modélisés explicitement. Les performances des méthodes proposées, qui utilisent un nombre minimum de capteurs, sont évaluées sur des données synthétiques et des enregistrements réels, y compris les signaux cardiaques des fœtus jumeaux.
Mots clés : ECG fœtal extraction, filtre de Kalman, décomposition tensorielle, processus Gaussien.